Copper contamination in end-of-life steel recycling,
developing a new strategy from million-tonnes to milligrams.

Katrin E. Daehn

St Catharine's College

University of Cambridge

A thesis submitted for the degree of Doctor of Philosophy.

January 2019.

Declaration

This dissertation is the result of my own work and includes nothing which is the outcome of work done in collaboration except as declared in the Preface and specified in the text. It is not substantially the same as any that I have submitted, or, is being concurrently submitted for a degree or diploma or other qualification at the University of Cambridge or any other University or similar institution except as declared in the Preface or specified in the text. I further state that no substantial part of my dissertation has already been submitted, or, is being concurrently submitted for any such degree, diploma or other qualification at the University of Cambridge or any other University or similar institution except as declared in the Preface and specified in the text.

This dissertation contains approximately 62,500 words, 59 figures and 44 tables (including appendices). This is within limits set by the Engineering Degree Committee.

Katrin Daehn

Submitted for examination January 2019.

Title: Copper contamination in end-of-life steel recycling, developing a new strategy from million-tonnes to milligrams

Name: Katrin Daehn

Abstract

Increasing the share of scrap-based steel production is necessary to achieve CO_2 emissions targets. However, the quality of recycled steel is compromised by contaminating elements, of which copper is the most pervasive. Copper from wiring and motors entangles with steel fragments during shredding and is not completely removed by magnetic separation. Beyond hand-picking, no commercial process exists for extraction, but copper in solution with steel segregates during hot rolling, causing surface cracking and defects that are unacceptable for high-quality flat products. This thesis characterizes copper in the global steel system, evaluates the energy requirements of possible extraction processes and presents experimental results to aid in the development of an efficient extraction technique.

Copper contamination is currently managed by globally trading contaminated scrap to tolerant applications and by dilution with primary steel. An evaluation of copper in the global steel system is needed to develop long-term strategies, and this is presented in the first part of this thesis. The copper concentration of flows along the 2008 steel supply chain are estimated from a range of literature sources and compared with the maximum concentration that can be tolerated in all steel products. Quantities of final steel demand and scrap supply by sector from a global stock-saturation model are used to estimate the amount of copper in the future scrap supply, and the total amount tolerable. Assuming current scrap preparation continues, more copper will enter the steel cycle than can be tolerated by demanded products by 2050. This global constraint will set in sooner if primary production is cut to meet climate mitigation targets.

Given the upcoming constraints, improved copper control is necessary. Various techniques for copper separation have been explored in laboratory trials, but as yet no attempt has been made to provide an integrated assessment of these options. The second part of this thesis presents a framework to define the full range of separation routes and evaluate their potential to remove copper, while estimating their energy and material input requirements. The thermodynamic, kinetic and technological constraints of the various techniques are

analyzed to show that copper could be removed to below 0.1wt% (enabling the production of high-value flat products) with 5-20% of the melting energy in the electric arc furnace route.

The above analysis reveals a promising and under-explored process route: preferential melting of copper from solid steel scrap, which could be integrated into conventional scrap re-melting with little additional energy. Previous investigations show removal of liquid copper is limited by its adherence to solid scrap. In the third part of this thesis, the individual and combined effects of several parameters (steel carbon content, initial surface oxidation and applied coatings) on the wetting behavior of liquid copper are observed with a heating microscope to understand if a process window to enable separation exists. The most significant factor was carbon content. On medium carbon steel substrates, copper spread rapidly, likely due to reduction of the oxide layer by carbon. Non-wetting copper droplets were observed on low carbon substrates in an inert atmosphere. This indicates a possible process window, but further investigation considering diverse, fragmented end-of-life scrap is needed.

The scrap supply of all metals is expanding. The multi-scale, interdisciplinary method developed in this thesis could be applied to other metal systems to understand the constraints caused by contamination and identify key areas to develop efficient extraction processes, necessary to conserve resources and reduce CO_2 emissions.

Acknowledgements

This thesis, and my experience creating it, has been enriched by many people. A first and vital component to acknowledge is my funding, from the Cambridge Trust. With this funding, my supervisor, Professor Julian Allwood, saw the potential to explore new directions. He challenged me from beginning to end, and I will carry many lessons from our time working together. I am thankful for the insightful discussions with my advisor, Dr. Jonathan Cullen, and the example he provides of how to be thoughtful and creative in engineering research. Through the whole process, I worked with Dr. André Cabrera Serrenho, who provided useful ideas, planning and feedback. His calm and constructive guidance certainly kept me on track.

The third part of my PhD was particularly dependent on the help of others, and would not have been possible without the support of the Materials Processing Institute (MPI). Dr. Peter Warren facilitated this arrangement, while Dr. Adam Hunt provided training, technical support and more general guidance during my visit. I'm grateful for the spark test they performed on my samples, and for making my time there interesting – seeing pilot-scale continuous casting was a highlight. Len Howlett at Cambridge also provided essential support for this phase of my research. I used his lab to try a few initial experimental ideas, and later for sample preparation and microscopy. While there he made me feel welcome, and always kept fun and curiosity a part of the process.

Various others provided valuable insight and input. I appreciate conversations with Dr. Vasant Kumar in the Materials Science and Metallurgy Department. A meeting with Professor Mike Ashby one year into my project generated ideas that held until the end. Mick Steeper provided context on industrial practice, and I appreciate him connecting me into the UK steel network. I am thankful for contact with Tata Steel – Dr. Peter Hodgson hosted a tour of the EAF facilities at Rotherham and Gill Thornton provided me with a representative bucket of end-of-life steel scrap.

Each person in the Use Less Group and Resource Efficiency Collective has influenced me, and deserves a big thanks. José very tangibly helped me with the physical aspects of my project – lathing my samples and connecting me to resources in the department, but he also always kindly checked in with me. I could always rely on him to let me know when I wasn't making sense. Similarly, Pippa was a wonderful lab-mate to go through the process with, and learn from her on how to get things done. The additional attendees of the Novel Materials meetings – Iacopo, Chris, Johannes, Cyrille, Adam and Evros – provided helpful comments

and questions, and set a high standard for research in the group. Rick was super helpful with the uncertainty analysis in my first paper. Karin and Kirsten were positive, reliable and effective for all administrative help along the way. Iain took me on various industry and related trips with him at the beginning of my PhD, which I enjoyed and broadened my perspective. Michal, Jennifer and Brendan were fun, caring desk-mates. Simon deserves an acknowledgement for his amazing organization and can-do attitude, from the ICTP industry tours to the Liverpool adventure. I also appreciate interesting feedback and conversations with Ana, Peter and Leo.

I appreciate the support of my college. My travel expenses to the TMS Conference in Phoenix, AZ, and my visit to MPI were covered by their Travel Grants. I'm thankful for the college's support of my gardening society, and generally the warm and entertaining atmosphere I enjoyed at St Catharine's.

I met many kindred spirits during my time in Cambridge. I'm especially thankful for my Krussel-street kitchen-mates my first year, as well as the friendship of Sophie, Anni and Emma, who cooked me many dinners and coaxed me to find a little more celebration and silliness in daily life. This journey also traces back to my housemates Jacqueline and Noe, who warmly introduced me to life in Cambridge the summer before beginning my PhD (2014). Many thanks to Andrew for the fun times and coffee in Mansfield C during my write-up.

And of course, the love of my family is essential. I am ever-more aware and appreciative of the example my parents provide for me. I so admire my dad's work – he is a very direct source of inspiration, but I want my mom to know the equally-important role she plays in showing me how to be grounded, selfless and kind. My brothers kept me up to date with the latest funny stories, and unconditionally believed in me. My extended family has always been supportive, but a special acknowledgement goes to my grandpa, Ralph, who started the tradition of engineering and metallurgy in our family. My most heartfelt appreciation goes to my fiancé (and current financier), Alex, who somehow always understood me and provided love, laughs and grounded, sensical support over the phone in all kinds of circumstances. I look forward to our life chapters, after these thesis chapters.

Journal articles

K. Daehn, A. Serrenho, J. Allwood. How will copper contamination constrain future global steel recycling? *Environmental Science and Technology*. 2017 51 (11), 6599-6606.

Top Policy Paper in Environmental Science and Technology, *2017*

K. Daehn, A. Serrenho, J. Allwood. Finding the most efficient way to remove residual copper from steel scrap. *Metallurgical and Materials Transactions, B*. 2019, 50 (3), 1225-1240.

K. Daehn, A. Serrenho, J. Allwood. Preventing wetting between liquid copper and solid steel: a simple extraction technique. In press, *Metallurgical and Materials Transactions, B*. 2019.

Conference presentations

K. Daehn, A. Serrenho, J. Allwood. *Mapping and evaluating all the ways to remove copper from steel*, TMS Annual meeting, March 2018, Phoenix, AZ.

K. Daehn, A. Serrenho, J. Allwood. *An energy assessment of chemically extracting copper from steel scrap,* MRS Fall Meeting, November 2017, Boston, MA.

K. Daehn, A. Serrenho, J. Allwood. *When will copper contamination constrain global steel recycling?* ISIE Biennial conference, June 2017, Chicago, IL.

Panelist at *Future of UK Steel* Huxley debate, British Science Festival, September 2017, Swansea, Wales.

Responsible for content in *Purity in car recycling: supply, demand, the environment, strategy and society*, presented by J. Allwood as the keynote at International Automobile Recycling Congress, March 2016, Berlin, Germany.

Other

Contributed to *A bright future for UK steel*, 2016, a guiding document for UK government and industry as steelworks faced closure decisions.

Contents

Chapter 1. Managing copper in steel recycling: a climate and business necessity 1

1.1 Global warming, CO_2 and steel 1

1.2 Options to reduce steel emissions 4

1.3 Limits to steel recycling 7

1.4 Market disruptions and the need to control copper 10

1.5 Thesis structure 12

Chapter 2. Review of published literature 14

2.1 How does copper constrain steel recycling? 14

2.1.1 Metallurgical effects of tramp elements on steel 15

2.1.2 Previous work on systemic effects of copper on the steel system 18

2.1.3 The current and future global steel system 23

2.2 Can copper be extracted from steel, and what would be the energy and material requirements of potential processes? 25

2.2.1 Thermodynamic principles of separation 26

2.2.2 Scrap-based steelmaking practice 36

2.2.3 Other options for copper control 42

2.3 Is there space for further development in an extraction process? 46

2.3.1 Preferential melting as an extraction technique 46

2.3.2 Relevant wetting principles 48

2.3.3 Investigations into wetting on an oxidized iron surface 49

2.4 Gaps in the literature 52

Chapter 3. How will copper contamination constrain global steel recycling? 54

3.1 Methodology 54

3.1.1 End-of-life scrap and copper in the present global steel system 56

3.1.2 The future global steel system 64

3.1.3 End-of-life vehicles in the global steel system 67

3.2 Results 68

3.2.1 Copper in the 2008 global steel system 69

3.2.2 Copper in the future global steel system 71

3.2.3 End-of-life vehicles in the global steel system 75

3.3 Discussion 77

Chapter 4. Finding the most efficient way to extract residual copper from shredded steel scrap 81

4.1 Applying the framework to copper in steel 84

4.1.1 Step 1: finding the possible separation routes 85

4.1.2 Step 2: describing the rate of copper reduction 91

4.1.3 Step 3: defining the potential processes 95

4.1.4 Step 4: estimating specific energy and material consumption 98

4.2 Results 100

4.2.1 Specific energy consumption 101

4.2.2 Specific material consumption 103

4.3 Discussion 106

Chapter 5. Preventing wetting between liquid copper and solid steel: a simple extraction technique 109

5.1 Methodology 110

5.1.1 Test matrix 110

5.1.2 Droplet observation 112

5.1.3 Metallography 114

5.2 Results 114

5.3 Discussion 119

5.3.1 Liquid copper wetting on steel in air 119

5.3.2 Liquid copper wetting on low carbon substrates 120

5.3.3 Liquid copper wetting on medium carbon substrates 123

5.3.4 Process development 128

Chapter 6. Conclusions 130

6.1 Main contributions of thesis 130

6.2 Implications for policy, industry, researchers 132

6.3 Future work 138

6.3.1 Evaluating the effects of contamination in metal systems and prioritizing action 138

6.3.2 Preferential melting process development 142

References 144

Appendix. A1 – copper in global steel recycling 171

A2 – catalogue of copper extraction experimental work 191

A3 – energy and material consumption estimates for each process route 209

List of figures

Chapter 1
1.1 Global CO_2 emissions over the last 10,000 years, pg. 2
1.2 The average energy to produce a tonne of crude steel from 1960 to 2013, pg. 5
1.3 Share of global primary and secondary steel production from 1960 to 2050, pg. 6
1.4 Qualitative plot showing the transformation of material to a functional product, pg. 10

Chapter 2
2.1 The iron section of the "metal wheel," pg. 15
2.2 Overview of the nature and effects of residual elements in steels, pg. 16
2.3 Image of copper wiring entangled in steel scrap, pg. 18
2.4 The 2008 steel Sankey diagram by Cullen et al. (2012), tracing the mass flow of steel during the transformation from raw sources to final products, pg. 24
2.5 Variation in molar Gibbs free energy of both a heterogeneous and homogenous mixture as X_B increases, pg. 27
2.6 Activities of components A and B in a homogeneous mixture as X_A increases, pg. 28
2.7 Sherwood plot showing the prices of chemical products correlated with their degree of dilution in the raw material from which they were separated, pg. 29
2.8 Activities of copper and iron, pg. 31
2.9 Enthalpy (ΔH_f) and Gibbs free energy of formation (ΔG_f) of liquid Fe-Cu alloy, pg. 31
2.10 Vapor pressure of elements and oxygen partial pressure for metal/oxide equilibrium, pg. 33
2.11 Sequence of EAF steelmaking, pg. 40
2.12 Sequence of ladle refining, pg. 41
2.13 The Young's contact angle of a liquid droplet, pg. 48

Chapter 3
3.1 Comparison of methodologies for studying the systemic impacts of copper contamination, pg. 54
3.2 Summary of the methodology for applying copper concentration data to the current of global steel supply chain, pg. 56
3.3 Plot of measured copper concentration values collected from the literature, pg. 59
3.4 Summary of the methodology for determining the role of copper in the future global steel system, pg. 65
3.5 Summary of the methodology for end-of-life vehicles in the global steel system, pg. 68
3.6 2008 global steel flows (in Mt) with estimated copper concentrations of steel flows, pg. 70
3.7 Zoom-in of the steel Sankey diagram in 3.6 showing the likely proportion and average copper concentration of EAF steel, used in the construction sector: buildings and infrastructure, as well as the copper tolerance of products, pg. 71
3.8 Zoom-in of the steel Sankey diagram in 3.6 showing the copper concentration of end-of-life scrap, specifically that transport scrap is the most significant source of copper, pg. 71
3.9 Mass of copper in the end-of-life scrap supply and copper tolerable by demanded products from 1950 to 2100, pg. 72
3.10 Projected masses of iron sources and finished steel products in end-use, plotted by expected copper concentration for 2008, 2020, 2030, 2040 and 2050, pg. 73
3.11 Trends in projected masses (Mt) of steel categories (required primary, total scrap, products requiring <0.06% copper and >0.4% copper) from 2008-2050, pg. 75

3.12 The steel mass flows (in Mt) corresponding to the production of cars and the recycling of end-of-life vehicles isolated from the 2008 global steel system, pg. 76
3.13 Closed-loop end-of-life vehicle recycling, pg. 76
3.12 Copper tolerable by demand and copper in supply curves with the result of Monte Carlo simulations of 2000 samples, pg. 79

Chapter 4
4.1 Stakeholders along the steel supply chain and incentives for improved copper control, pg. 82
4.2 The current assessments and the proposed framework for evaluating the feasibility of removing copper from steel, pg. 85
4.3 General routes to remove an impurity attached to solid scrap, pg. 86
4.4 General routes to remove an impurity attached to solid scrap, pg. 86
4.5 Possible phase distributions for extracting copper from solid scrap, pg. 87
4.6 Possible phase distributions for extracting copper from the steel melt, pg. 87
4.7 The possible copper separation routes with the associated measure of principle feasibility for solid steel scrap, pg. 88
4.8 The possible copper separation routes with the associated measure of principle feasibility for the steel melt, pg. 89
4.9 Routes for copper separation from solid scrap, with determined rates of copper reduction in the corresponding process window, pg. 93
4.10 Routes for copper separation from the melt, with determined rates of copper reduction in the corresponding process window, pg. 94
4.11 The reactor, conditions, sources of energy consumption and secondary effects of the potential solid scrap processes, pg. 96
4.12 The reactor, conditions, sources of energy consumption and secondary effects of the melt potential processes, pg. 97
4.13 Temperature-time profile of the assumed EAF route with placement of potential processes, pg. 98
4.14 The copper concentration reduction from 0.4wt% and estimated specific energy consumption for the various processes, pg. 101
4.15 Mass of material reactants and the calculated associated embodied energy to reduce copper concentration from 0.4wt% to 0.1wt% in the various processes, pg. 104

Chapter 5
5.1 The copper/steel wetting system showing the variables at the focus of this study, pg. 111
5.2 Schematic of the Misura HSM2 heating microscope, pg. 114
5.3 Profiles of copper droplets on low carbon and medium carbon steel with different surface preparations from 1060-1080°C, pg. 116
5.4 Droplet contact angle over temperature for all preparations, pg. 117
5.5 Cross-sections of solidified copper on all substrate preparations, pg. 118
5.6 Iron oxide scale with liquid copper entrapment when low carbon steel was treated in air, pg. 119
5.7 Micrographs of the copper droplet on low carbon steel substrates in the as received, oxidized and initially polished conditions, pg. 121
5.8 Micrographs of the copper droplet on low carbon steel substrates on initially ground and initially oxidized low carbon steel substrates with an applied Na_2SO_4 coating, pg. 122
5.9 Optical micrographs of the copper droplet on initially ground and initially oxidized low carbon steel substrates with an applied Na_2SiO_3 coating, pg. 123

5.10 Optical micrographs of the copper spread on medium carbon steel substrates in the initially ground and initially oxidized condition, pg. 124
5.11 The initially oxidized medium carbon substrate with a 2% Nital etch to reveal decarburization, pg. 125
5.12 Initial oxide scales for medium and low carbon steel samples, pg. 126
5.13 Optical micrographs of the copper spread on medium carbon steel substrates in the initially ground and initially oxidized condition with the Na_2SO_4 coating, pg. 127
5.14 Optical micrographs of the copper spread on medium carbon steel substrates in the initially ground and initially oxidized condition with the Na_2SiO_3 coating, pg. 127

Appendix

A3.1: k_{Cu} values in the literature plotted by temperature and pressure regime, pg. 223

List of tables

Chapter 2
2.1 Copper limits of different steel products, pg. 17
2.2 Thermodynamic data on dilute metals and metalloids in liquid iron, pg. 30
2.3 Separation efficiencies of various processes, pg. 32
2.4 Excerpt of King's classification of separation processes, pg. 35

Chapter 3
3.1 Global end-of-life steel scrap supply in 2008 by four end-use categories, pg. 57
3.2 Reported copper concentration of scrap types, pg. 58
3.3 Range of copper concentrations of scrap source categories decided for this analysis, pg. 59
3.4 Estimated copper concentrations and quantities of inputs into the primary and secondary routes, pg. 60
3.5 Estimated percentage of EAF steel by pro-rota flow to each product, pg. 61
3.6 Estimated percentage of EAF steel by pro-rota flow to each sector, pg. 61
3.7 Copper tolerance ranges for each intermediate to end-use sector flow, pg. 63
3.8 2008 sectoral steel demand quantities, pg. 65
3.9 Identified sources of uncertainty and the resolution of each in the analysis of the future steel system, pg. 78

Chapter 5
5.1 The characteristics varied between the different steel substrates, pg. 111
5.2 Chemical composition of the low and high carbon steel substrates, pg. 112

Appendix
A1.1: References corresponding to the numbered points in Figure 3.3, pg. 171
A1.2: Reported copper concentrations of EAF steel products, pg. 174
A1.3: Reported copper tolerances of steel products, pg. 176
A1.4: Qualitative requirements of steel products, pg. 177
A1.5: Comparison of annual historic worldsteel data from 1990-2014 to production estimated by extrapolating the intermediate product to sector matrix, pg. 178
A2.1: Catalogue of studies for improved shredding and magnetic separation, pg. 179
A2.2: Catalogue for density separation to isolate copper-rich fraction, pg. 180
A2.3: Catalogue of studies for reactive gas applied to solid scrap, pg. 181
A2.4: Catalogue of studies for preferential melting, pg. 182
A2.5: Catalogue of studies for solvent extraction applied to solid scrap, pg. 183
A2.6: Catalogue of studies for matte extraction applied to solid scrap, pg. 184
A2.7: Catalogue of studies for copper embrittlement, pg. 185
A2.8: Catalogue of studies for leaching, pg. 186
A2.9: Catalogue of studies for distillation, pg. 188
A2.10: Catalogue of studies for vacuum arc re-melting, pg. 194
A2.11: Catalogue of studies for reactive gas applied to the melt, pg. 195
A2.12: Catalogue of studies for melt injection, pg. 197
A2.13: Catalogue of studies for solidification segregation, pg. 198
A2.14: Catalogue of studies for phase separation, pg. 199
A2.15: Catalogue of studies for solvent extraction applied to the melt, pg. 200
A2.16: Catalogue of studies for slagging, pg. 202
A2.17: Catalogue of studies for inclusion formation, pg. 207

A2.18: Catalogue of studies for filtration, pg. 208
A3.1: Experimental parameters, pressure (Pa) and melt additions, corresponding to the measured points in Figure A3.1 and the corresponding reference, pg. 224
A3.2: Diffusivities of copper in liquid iron found in the literature, pg. 233
A3.3: Range of variables used to calculate k_m, pg. 234
A3.4: Range of values calculated for k_m, pg. 234
A3.5: Calculated quantities of solvents and slags needed to treat one tonne of steel from 0.4 to 0.1wt% from the reported equilibrium ratios, pg. 236
A3.6: Representative operating parameters in VAR (Scholz et al.), pg. 239

Nomenclature

Bt: billion-tonnes
Mt: million-tonnes, or Megatonne
t/tonne: metric tonne
kg: kilogram
mg: milligrams
mol: mole
Pa: Pascal
m: meter
mm: millimeter
hr: hour
min: minute
s: second
MWh: Mega-Watt hour
kWh: kilo-Watt hour
^{o}K: degrees Kelvin
^{o}C: degrees Celcius
atm: atmosphere (pressure unit)
J: Joule

EoL: end-of-life, post-consumer scrap
Secondary production/route: scrap-based steelmaking
Primary production/route: iron ore-based steelmaking
ELV: end-of-life vehicle
Critical metal: technologically and geopolitically important elements subject to supply disruptions
Tramp element: element that remains in the melt during refining and has a deleterious effect on the final properties of the metal product
EAF: Electric Arc Furnace
BOF: Blast Oxygen Furnace
Rebar: reinforcing bar
HRC: hot rolled coil
CRC: cold rolled coil
galv.: galvanized (zinc-coated)
C-sat.: carbon-saturated
α-Fe: ferrite
HBI: hot briquetted iron
DRI: direct reduced iron

IPCC: Intergovernmental Panel on Climate Change
OECD: Organization for Economic Co-operation and Development
IEA: International Energy Agency
EU: European Union
UK: United Kingdom
US: United States
GDP: Gross Domestic Product

LCA: Life-cycle Assessment

MFA: Material Flow Analysis
WIO: Waste Input-Output Analysis
MPA: Material Pinch Analysis

CO_2: carbon dioxide
CO(g): carbon monoxide
G: Gibbs free energy
ΔG_{mix}: Gibbs free energy of mixing
X: molar fraction of a component
T: temperature
P: pressure
S: entropy
H: enthalpy
ΔH_{mis}: change in enthalpy of mixing
ΔS_{mix}: change in entropy of mixing
γ: activity coefficient
a: activity of a component in solution
R: universal gas constant
s: solid
l: liquid
μ: chemical potential
W: work input into a system
Q: heat exchanged between a system and surroundings at T_0
T_0: initial temperature
p_i: vapor pressure of pure element, i
p_{O2}: oxygen partial pressure
k: rate constant (m/s)
A: specific surface area, m^{-1}
L: distribution ratio of an impurity between the melt and solvent/slag
k: solidification partition coefficient
ϕ: relative volatility, to measure feasibility of vaporization
β: constant to define feasibility of removal during vacuum arc refining
wt%: weight percent concentration of a component in solution
[x]: concentration of impurity, x
ppm: parts per million

θ_Y: Young's contact angle
$\sigma_{S/L}$: surface energy, solid or liquid
σ_{SL}: solid/liquid interfacial energy

Chapter 1. Managing copper in steel recycling: a climate and business necessity

This thesis examines copper contamination in end-of-life steel recycling at multiple scales. The flow of million-tonnes of copper within the global steel system is estimated and the potential processes to remove residual copper from steel scrap are evaluated, leading to an experimental study of milligrams of liquid copper on various steel substrates. Before beginning this journey, this chapter establishes the motivation behind such an investigation. Understanding and managing copper contamination in end-of-life steel recycling is necessary for climate change mitigation, but the future viability of the steelmaking in industrialized countries also depends on a proactive strategy for controlling tramp elements. The role of steel production within global climate change, options for reducing carbon emissions, the projected surge in discarded steel and how copper limits the utilization of end-of-life scrap will be explained in this chapter.

1.1 Global warming, CO_2 and steel

The latest Intergovernmental Panel on Climate Change (IPCC) special report, SR1.5, culminates over 6,000 studies to understand what life on the planet will be like with 1.5°C warming, and evaluates whether a 1.5°C target could be achieved. Human activities have already caused an average warming of approximately 1.0°C above pre-industrial levels. At the current rate, global warming will reach 1.5°C between 2030 and 2050, well within the lifetimes of most people on the planet. This level of warming puts human life at risk, but sea-level rise, flooding, droughts, and species extinction are predicted to be assuredly less with 1.5°C warming compared to the 2+°C scenarios – Arctic ice and coral reefs are much more likely to partially survive. Thus, the report presents compelling evidence to adopt a strict 1.5°C target. However, the cut in annual carbon dioxide, CO_2, emissions must be drastic and swift: less than 25 $BtCO_2$/year must be achieved by 2030 (from the current level of roughly 42 $BtCO_2$/year), followed by a decline to net zero by 2050. Policy to enforce such a transition is absent, and present intended pathways are woefully out-of-touch. Estimates show the global emissions outcome from the stated mitigation ambitions under the 2015 Paris Agreement will be 52-58Bt CO_2/year in 2030 (IPCC, 2018). The way forward is unprecedented and uncertain, but what remains clear is the trend shown in Figure 1.1, which plots the CO_2

concentration in the atmosphere over the timespan of human life on the planet, must be reversed.

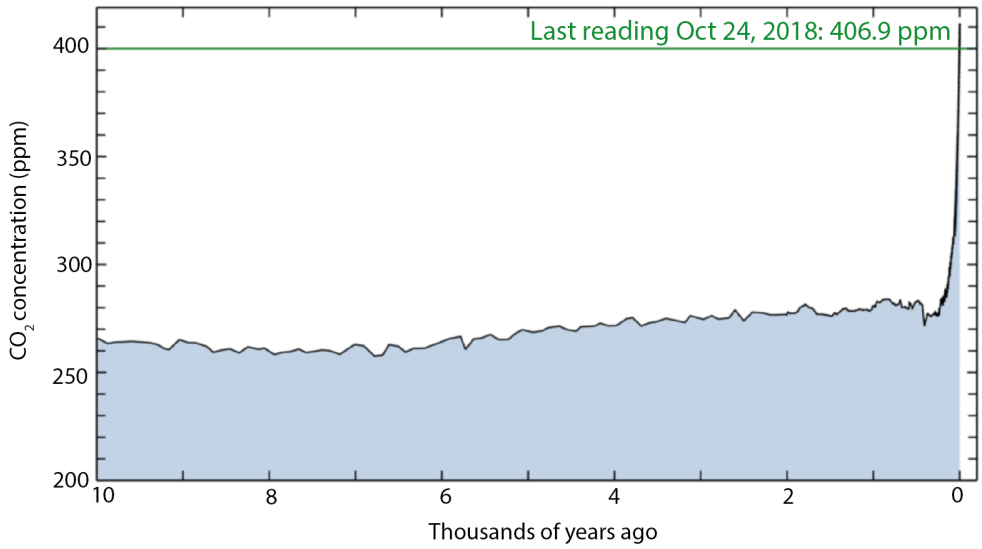

Figure 1.1: Global CO_2 emissions over the last 10,000 years. From the Scripps Institution of Oceanography. Data from before 1958 is from ice-cores by Lüthi et al. (2008), and data after is from Mauna Loa by Keeling et al. (2001).

The first step in reducing emissions is to understand the underlying sources. The International Energy Agency (IEA, 2017) estimates that industry accounts for about 38% of current global final energy use, of which 70% is attributed to five sectors, known as the heavy industries: iron and steel, aluminum, chemicals and petrochemicals, cement and pulp and paper. Although all opportunities for emissions reduction must be pursued in turn, opportunities related to bulk materials production have received considerably less research and development, as discussed by Allwood et al. (2011). Further, the heavy industries face particular challenges. Increasing the share of renewable energy will be insufficient to meet emissions targets, because CO_2 is inextricable to the current production processes of the materials listed above. Meanwhile, demand for these materials continues to grow. Stocks of these basic engineering materials are key to urbanization, industrialization and general quality of life.

Steel production is particularly deserving of attention, as it is the single largest contributor of industrial CO_2 emissions and totals 7% of energy-related global emissions (IEA, 2017). CO_2 emissions from steel production originate primarily from the reduction of iron ore. Carbon combines with oxygen in iron ore, to form CO(g) and CO_2(g) and yield metallic iron. Emissions are also generated from the electricity required to melt scrap, as well

as to supply heat and mechanical force in the various production steps: from crushing ore and shredding scrap, to refining impurities, and rolling, forging and forming.

The share of CO_2 emissions attributed to steelmaking reflects the sheer scale of steel use, because steel is a vital ingredient for modern life. The abundance of iron in the earth's crust traces back to the supernova that fused the elements that make up our planet today. In supernova nucleosynthesis, iron is the heaviest element to form in an exothermic reaction, and thus constitutes the peak in relative abundance versus atomic weight (Burbidge et al., 1957). At room temperature, iron atoms arrange in a body-centered cubic structure. Pure iron is soft and ductile. Carbon added to iron inhabits the tetrahedral interstitial sites, imparting a non-symmetric distortion to the lattice that is especially effective at impeding dislocation motion (Cottrell et al., 1949). This mix of iron (ferrite) and carbon can be further strengthened by a dispersion of cementite, Fe_3C. The morphology and distribution of cementite can be manipulated through heat treatment to vary hardness, strength and ductility. Non-equilibrium structures, bainite and martensite, controlled by quenching and tempering, unlock a yet wider property space. The intelligent use of alloying elements diversifies carbon steel further, to distinct classes, such as high-strength and stainless steels. The ubiquity of steel in society thus derives from the fact that the two main constituents, iron and carbon, are abundant and cheap, and careful processing of these elements yields material with a wide range of properties, ideal for applications from jewelry to industrial equipment. Steel is the most important engineering material, and there is no substitute for the role it plays in transportation, buildings and goods.

Recent research quantifies just how much steel is needed to build and maintain an industrialized society. Work by Müller et al. (2006) characterizes anthropogenic metal cycles, i.e. how iron flows from mines, to in-use stocks, to disposal. Pauliuk et al. (2013a) observe that steel stocks in OECD (Organization for Economic Co-operation and Development) member countries tend to plateau at 10-14 tonnes per capita. The average steel stock in non-OECD countries is 2 tonnes per capita, so per annum steel production has been rapidly increasing – nearly doubling from 2000 to 2015 (850 Mt to 1.6 Bt), driven by the developing world. Projecting the observed stock saturation patterns forward shows per annum steel production will nearly double from 2015 to the end of the century (Pauliuk et al., 2013b).

Despite increasing demand, a significant net reduction in per annum steelmaking CO_2 emissions from 2000 to 2050 is a crucial part of the global climate change mitigation effort. Softening the emissions mandates for steelmakers would require unattainable emissions

reductions in other sectors (Allwood et al., 2010). A wider range of strategies must be investigated for the steel industry to participate meaningfully in climate change mitigation.

1.2 Options to reduce steel CO_2 emissions

Current emissions from steelmaking total roughly 2.5 BtCO_2/year, but applying the IPCC fourth assessment report global emissions targets (Metz, 2007) to the steel sector means less than 1 Gt CO_2/year must be emitted by 2050 (Milford et al., 2013). CO_2 is emitted during steel production, and steel is produced to meet demanded human services. Thus, there are two main approaches to reduce CO_2 emissions, focusing either from the side of supply or demand. The supply-side approach attempts to make steel production less CO_2-intensive, while the demand-side reconsiders how much steel is needed to deliver the demanded service.

In order to make a significant difference with the supply-side approach, major shifts in current practice are required. Steel production is energy-intensive – energy is a principal cost, so steelmaking is already highly efficient. The primary (iron-ore based) steel industry has consistently achieved increased efficiency over the last several decades, but these gains are beginning to level as the thermodynamic limit is approached, as shown in Figure 1.2 (Cullen et al., 2011). Further efficiency gains will be marginal. As long as carbon is used as a reductant for iron ore, CO_2 will be produced as a by-product. To decouple steel from CO_2, a reductant other than carbon must be used, such as hydrogen or electrons. There is no thermodynamic limitation to these reactions, but the scalable design is challenging (Allanore, 2015). These production routes are proven at the laboratory-scale (Allanore et al., 2013), but are unlikely to be commercialized for widespread use in the timeline set by global warming.

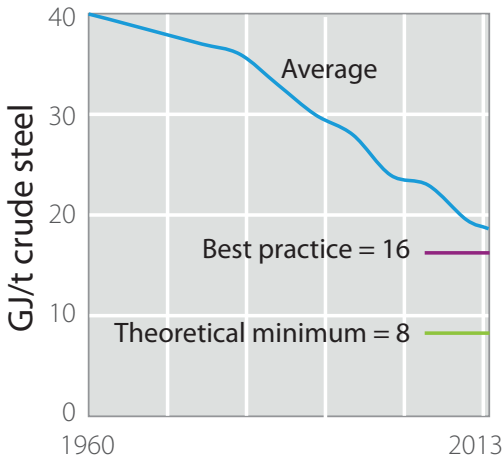

Figure 1.2: The average energy to produce a tonne of crude steel from 1960 to 2013 in the primary route, showing best practice and the thermodynamic theoretical minimum (Cullen et al., 2011).

Reducing emissions from ore-based steel production presents long-term challenges, so increasing the ratio of steel made from scrap is key. It is possible to decouple steelmaking from CO_2 with scrap-based production. To melt steel scrap, electricity and exothermic chemical reactions are used, which generate CO_2 emissions. However, the specific CO_2 emissions from scrap-based production is a fraction of the specific CO_2 emissions from ore-based production: 0.4 tonne CO_2/tonne steel in the Electric Arc Furnace (EAF) route compared to 2.3 tonne CO_2/tonne steel for Blast Oxygen Furnace (BOF) (Material Economics, 2018). Specific CO_2 emissions from EAF's could decrease further as renewable energy increases in the electricity mix. Using post-consumer scrap as a resource also offsets demand for mineral resources, and requires less energy. Producing one tonne steel from scrap instead of hot metal saves approximately 990 kg iron ore, 575 kg coal and 2.6 MWh of energy (Toulouevski et al., 2010a). It is important to clarify that these savings are only true for recycling end-of-life, post-consumer scrap. Manufacturing scrap, also known as prompt, circulation or new scrap, originates from yield losses during material production and manufacturing. This scrap circulates within the production phase, and is an inefficiency which must be minimized. This thesis focuses specifically on end-of-life scrap.

The share of scrap-based production depends firstly on the amount of scrap available, which depends on prior steel production, use and disposal. Historically, the extent of recycling has been constrained by the amount of scrap available (Oda et al., 2013). However, the amount of end-of-life scrap will increase significantly in the coming decades, as revealed by physical stock-based modelling and average product lifetimes, as presented by Pauliuk et al.

(2013b). With this projected surge of end-of-life scrap, recycling could reach unprecedented levels.

Despite the potential shifts in steel production practice, reducing steel demand remains essential to meet 2050 CO_2 mandates. If steel use continues to follow stock-saturation patterns, primary production will remain dominant until 2050. The global share of primary and secondary production is shown in Figure 1.3, assuming all available scrap is used in recycling. The global scrap supply alone will not match demand for at least a century to come. Considering the future supply of scrap, Milford et al. (2013) evaluated various scenarios of global steelmaking emissions from present to 2050. The only scenario to successfully meet the reductions recommended by the IPCC relied heavily on demand-reduction to aggressively cut primary production. Similarly, at a regional level, increased recycling is not a panacea. In the EU, if recycling increases in line with the anticipated scrap supply, and the energy supply continues to transition to clean sources as projected, emissions from steelmaking stay largely the same from today to 2050 (Material Economics, 2018). Therefore, demand-reduction is essential to change the pattern of steel-use in society. Then as steel demand reduces, scrap-based production will constitute an increased share of steelmaking.

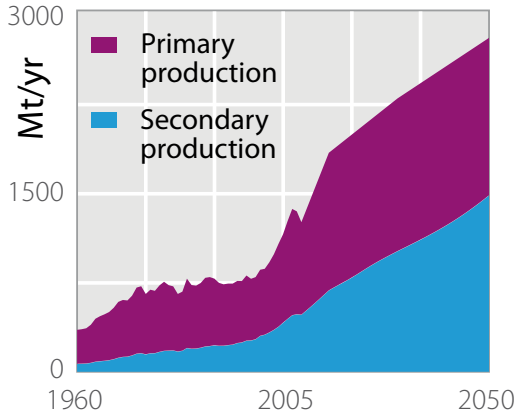

Figure 1.3: Share of global primary and secondary steel production from 1960 to 2050, if all available scrap is used for recycling and demand follows current stock-saturation patterns (Allwood, 2016a).

Reducing demand and increasing the proportion of scrap-based production make up a powerful, mutually-reinforcing strategy. A comprehensive overview of demand reduction strategies has been presented in *Sustainable Materials, with both eyes open* (Allwood and Cullen, 2012). Increased materials re-circulation and material efficiency also fit within the widely-discussed "circular economy" paradigm. The circular economy model takes inspiration from natural feedback systems, where material cycles in a closed loop, such that waste is used

as feedstock. The European Climate Foundation evaluated the potential emissions abatement from adopting circular practices (increased materials re-circulation, materials efficiency and new business models). Their analysis shows that applying these measures to the bulk materials (steel, aluminum, cement and plastics) is essential to meet emissions targets, and could cut industrial emissions by 58%, or 3.6Bt CO_2/year globally (Materials Economics, 2018).

Steel plays an especially important role in establishing the circular practices described above. There is enthusiasm for applying the circular economy model to a variety of materials (Stahel, 2016). However, in order for the circular economy to displace the current model of "take, make, dispose," an implicit requirement is that the supply of waste is sufficient to meet feedstock demand. Due to growing material demand, parity between demand and scrap supply is not close for any major industry (Cullen, 2017). However, many developed countries have leveled their steel stocks, such that new steel is only needed to replace annual stock turnover – 2-3% of the stock quantity. Steel is the first material with sufficient stocks and recyclability to possibly approach the circular economy model. By 2030, the EU steel economy could become the first to meet demand for new products by recirculating present stocks (Materials Economics, 2018).

To summarize, industrial emissions are key to climate mitigation. Industry can meet satisfactory emissions reductions only by reducing demand and increasing scrap-based production. The steel industry must be the first of the heavy industries to demonstrate the viability of these practices.

1.3 Limits to steel recycling

The implementation of demand reduction and re-circulation strategies for steel production must be investigated. Within the Allwood research group, substantial, technically-feasible opportunities for reducing steel demand have been identified. Cullen et al. (2012) mapped the global flow of steel to identify six distinct strategies for the more efficient utilization of steel. Cooper and Allwood (2012) show that approximately 30% of steel in use can be re-used. Demand for construction steel could be cut because the average utilization of structural steel beams is less than 50% of their capacity (Moynihan and Allwood, 2014). Horton and Allwood (2017) show that vehicle process scrap could be significantly reduced because yield losses account for 44% of the sheet metal produced for passenger vehicles. Incentives for these practices have been examined as well (Skelton and Allwood, 2013).

Cooper-Searle et al. (2018) show how material efficiency may be incorporated into future climate policy, and Dunant et al. (2018) present currently available options to increase steel re-use.

Comparatively, there is less research for the other key strategy, increased scrap-based production. It is well-known that steel is highly recyclable. It is the most recycled material, at a rate of 83% (worldsteel, 2010). Because it is magnetic, it can be easily separated from waste streams. The infrastructure for collecting and re-melting steel is mature. Metallic bonds do not degrade upon melting, and a new product can be cast, shaped and finished.

Although steel recycling has been effective thus far, the increase in the scrap supply means recycling must expand to unprecedented levels. In order to offset primary demand, this secondary steel must serve as a genuine substitute. In this future scenario, inefficiencies and losses in recycling will set a limit to the expansion of steel recycling. Therefore, the recycling process must be examined in greater detail.

The purpose of recycling is to impart functionality to a discarded product. A discarded product may be re-used at end-of-life, but often the components are disassembled and the base materials are separated for feedstock to be used for the next generation of products. The composition of the feedstock is key – function derives from composition. The elements present in a metal determine the evolution of microstructure and resultant properties. The wide range of steel microstructures and properties are attainable only with advanced refining.

Refining steel in the primary route has a long legacy (Burn, 1961). Refining processes have evolved to handle the mineralogy of iron ore to control impurities to parts per million precision. Investment and development in the secondary route has not reached the same level. The dedicated infrastructure for melting post-consumer scrap, EAF mini-mills, gained prominences in the 1960's (Madias, 2014). To refine steel scrap, a subset of the refining processes originally developed for the primary route are used, despite the distinct challenges scrap refining presents. Other metals combine with steel in products and during scrap preparation, which then contaminate the melt. Beyond separating non-magnetic austenitic stainless steel, the many steel grades are mixed together (Björkman and Samuelson, 2013). Thus, new elements foreign to the primary route are introduced into the scrap melt, and techniques to extract these elements have not yet been developed.

The lack of control over composition has several consequences. Valuable alloying elements may be unintentionally oxidized and effectively lost, or may not be utilized appropriately in the new product, as reviewed by Reijnders (2016). Elements which remain in

the melt during refining and have deleterious effects on the properties of the steel product are known as "tramp" elements, as identified by Nakajima et al. (2011). Katayama et al. (1997) explain that the presence of tramp elements restricts the EAF route to lower-value long products, while the primary route can produce high-value flat products. Long products (beams, bars and structural components) for construction are more tolerant of impurities in the scrap stream, so end-of-life scrap is directed to these applications. Flat products (sheets, strip) used for cars, equipment, appliances, and packaging have strict impurity allowances as discussed by Schrade et al. (2006). Overall, it is apparent that the highly-engineered individual grades of steel lose functionality and value when they are mixed and melted together.

Primary and secondary steelmakers therefore serve different markets, but the secondary market must expand. It is unclear whether this expansion is economically viable. The European Climate Foundation discusses that current barriers and market failures hinder secondary material recovery and production. To enhance economic viability, collection and production costs must be reduced, or the value of the final product must be increased (Materials Economics, 2018).

The current quality losses during steel recycling are not fundamental. Barnett and Morse (1962) state that the quality of a resource is a function of the present state of technology. Additional process steps could improve the quality of recycled steel. Figure 1.4 plots how functionality is imparted to material through a series of process steps (qualitatively). Each process step requires some energy input. Conceptually, Connelly and Koshland (1997) explain added energy is behind material cycling. Perhaps with additional energy, steel can be recycled to the same quality. However, these energy inputs must be assessed. As Allwood (2013) explains, recycling is not free of impacts. For both climate mitigation and economic feasibility, it is important to examine the causes of down-cycling and the processes required to return steel to the same quality, and when the additional energy is justified.

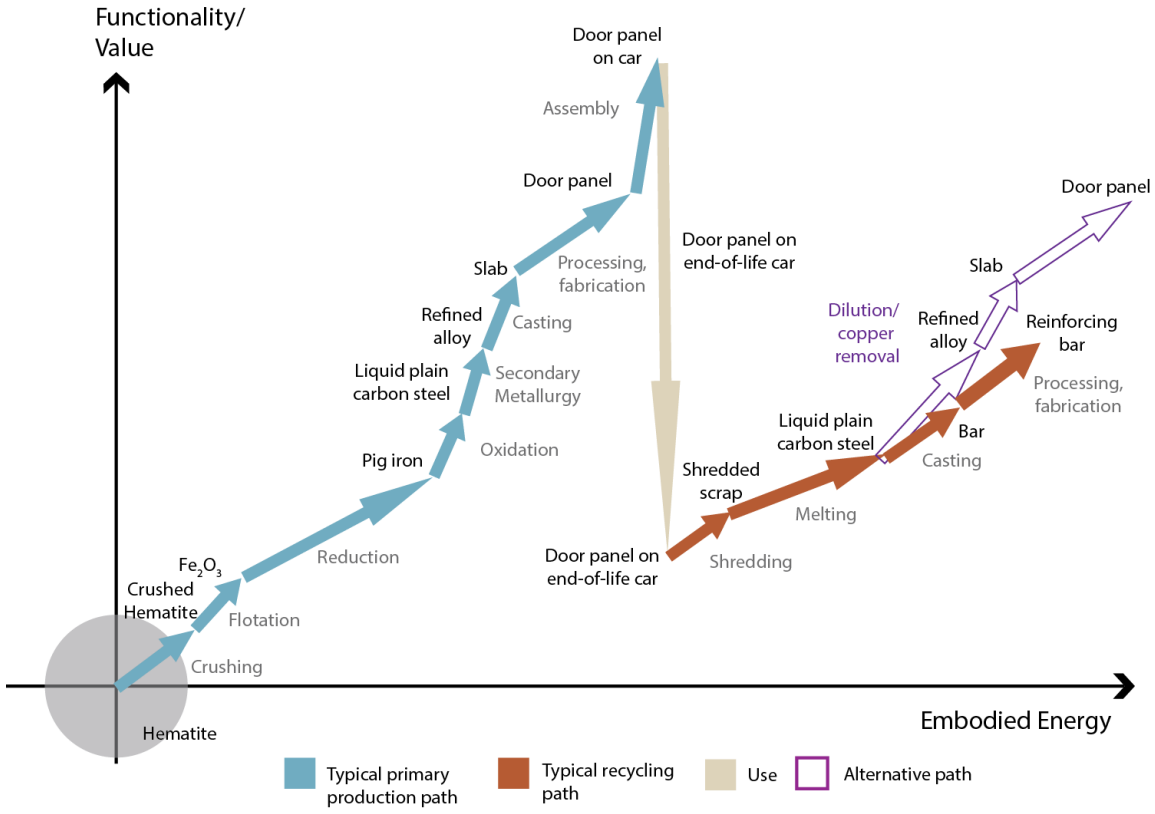

Figure 1.4: Qualitative plot showing the transformation of material to a functional product – in the primary and recycling routes.

1.4 Market disruptions and the need to control copper

In 2014-2015, the global weighted steel price fell by 26% (Seetharman et al., 2016). The effects have been especially acute in the UK. In May 2016, Tata Steel put its UK steelworks up for sale, prompting policy makers, researchers and industry to devise a strategy for the future steel industry. Although the market is constantly fluctuating and margins have always been thin, fundamental shifts underlie these disruptions.

World-wide crude steel production has nearly doubled since 2000, with 95% of growth in China (worldsteel, 2001-2018). As a result, the world is now over-capacity for iron-ore based production. Industrialized countries with a long legacy of steelmaking struggle to compete with newer facilities in China, where labor is also cheaper. Although these trends have been recognized for years, the acting strategy of UK steelmakers has been to maintain resilience through fluctuations and further innovate with primary steel to serve high-tech, niche markets. However, Allwood (2016 a, b) and Seetharaman et al. (2016) argue that this approach is unwise.

An alternative strategy is to shift production routes. Industrialized countries have

unique assets: local scrap and established high-tech industries. There is a robust manufacturing market in the UK, and domestic steel only supplies 35% of the demand from the manufacturing sector (Serrenho et al., 2016). Steelmakers could act as a crucial link between the growing scrap heap and value-added products. However, tramp elements are the main obstacle. The UK market requires mostly strip steels for automotive, construction, energy, general engineering and packaging sectors. End-of-life scrap is not suitable to meet these product specifications. Allwood et al. (2016, b) explains that upcycling scrap is the only way for the EAF-route to be competitive against ore-based production today. If steel scrap is down-cycled to reinforcing bar, the iron ore route remains attractive, because of the similar energy and raw material costs in both routes. Eventually, as ore grades deplete and scrap increases, costs will further favor EAF steelmaking.

Although the metallurgical effects of tramp elements have been long-recognized, the steel industry has largely evaded the problem. Savov et al. (2003) explain that attention to tramp elements increased in the 1980's because the introduction of continuous casting reduced the share of high-quality prompt scrap. However, primary steel production continued to increase, which could be used for applications with strict tramp element tolerances. Thus, there has yet been little incentive to improve the control of tramp elements in end-of-life steel recycling. It is interesting that growth in primary production reduced the urgency of managing tramp elements, but this period is ending – now overcapacity is turning attention back to contamination in recycling.

Several tramp elements present challenges to secondary steelmakers, but copper has been cited as the main obstacle to high-quality scrap-based production. Of the various tramp elements, copper is present at the highest concentration in end-of-life scrap, and causes serious metallurgical problems during conventional processing. Copper is used for wiring and motors in vehicles, appliances and equipment. During scrap preparation and shredding, copper entangles with steel scrap. No commercial process exists to extract copper from the steel melt, but liquid copper segregates to grain boundaries during hot rolling, causing surface cracking and defects. High-quality steel products have strict limits on the amount of copper tolerable. Therefore, end-of-life scrap can only be used for a subset of steel products for less demanding applications. Thus, the steel industry must understand how copper may constrain future steelmaking, and the changes in current practice that are required to recycle steel in a closed loop. Narrowing the focus to copper allows for the development of frameworks and principles that could then be applied to other tramp elements or metal systems in future work.

Greater recovery of copper is important for the future viability of steel recycling, but also for the copper cycle itself. Copper demand is expanding rapidly, driven by further global development and clean energy technologies. Alonso et al. (2007) explain that "while the depletion of copper is not imminent, most metrics indicate that the risk of copper disruption is significantly greater than for other major metals (e.g. iron and aluminum) and is at or near a historical high." Using secondary sources for copper production reduces energy needs by up to 85% (Rankin, 2011), and avoids the creation of toxic SO_2(g) as a by-product. There is an economic incentive for improved stewardship of copper as well. The year average price of copper is $3.4/lb (Gloser et al., 2013). An average car contains over $150 USD-worth of copper, and even more value is contained in electric vehicles. However, recovery costs of copper relatively dilute (0.4wt%) in dense, highly fragmented steel scrap may not be justified. Copper is present in ore at concentrations of 0.2-5%, and 30% in ore concentrate (USGS, 2008). As ore grades further deplete, steel scrap may be an attractive resource for pure copper.

1.5 Thesis structure

So, the steel industry must recycle end-of-life scrap to demanding applications to participate in climate change mitigation and adapt to changing market conditions. Copper contamination is the main barrier. The goal of this thesis is to inform an energy-efficient strategy for managing copper in end-of-life steel recycling. Copper in steel is a complex problem where multiple considerations converge: economic, environmental, policy, scientific and infrastructure/equipment. The scrap-based market is subject to sharp fluctuations and each region faces unique political, economic and infrastructure conditions at any point in time. To provide results that are useful and universally applicable, this thesis maintains a physical, rather than political or economic, basis. Scientific principles, from industrial ecology to materials science, are applied in an engineering approach to understand, then overcome the problem. This thesis takes the form of a 3-part investigation, beginning from a high-level to understand copper in steel and evaluate the range of possible solutions, and follows these results to a specific potential process that could enable high-quality steel recycling. This area is then experimentally investigated in greater detail.

The problem of copper contamination in steel recycling must first be investigated to understand if a new strategy is actually required. The adverse metallurgical effects of copper on steel have been known and monitored for decades, but hand-picking and dilution have

remained effective and practical at a commercial scale. Is copper contamination an urgent problem? How is copper managed in the global steel system? Does it limit the amount of steel scrap that is recycled? When will copper prevent steel scrap from being recycled to a useful application? Thus, the first question this thesis addresses is:

Q1. How does copper contamination constrain steel recycling?

With an understanding of the time-scale and magnitude of the problem of copper contamination, the solutions must be evaluated. A range of interventions along the supply chain could be applied. Which options are most beneficial? What are the incentives for controlling copper? What physical constraints limit the separation of copper from steel? The second question this thesis addresses is:

Q2. Can copper be removed, and what would be the energy and material requirements of extraction?

An analysis of the full range of possible extraction processes can then pinpoint promising, but under-explored process routes. Is there a viable process window for copper removal that also minimizes energy consumption? The last question addressed in this thesis is:

Q3. Is there space for further development of a potential extraction process?

The first step to answer these questions is to review the current literature. The literature review is presented in Chapter 2, structured by the three questions above, to establish current understanding, identify relevant methodologies and define succinct gaps in knowledge. Results to fill these gaps are presented in Chapters 3, 4, and 5 – addressing the first, second and third questions respectively. Chapter 6 takes the whole of the results in chapters 3, 4 and 5 to draw larger implications and future work for researchers, as well as for steelmakers and policy makers.

Chapter 2. Review of published literature

To develop a new strategy to manage copper contamination, the history of copper in steel recycling and existing solutions must be understood. Copper contamination of steel is not a new problem. As Melford (1980) explains, the embrittlement of iron caused by copper has been observed for centuries – since 78 A.D. An account from a metallurgist of the day, translated by Rackham (1952), notes not just the metallurgical effects, but the reduced applicability of copper-containing iron: "There are numerous varieties of iron…some lands yield a soft iron closely allied to lead, others a brittle and coppery kind that is specially to be avoided for the requirements of wheels and for nails." Considering the long history of observing copper in solution with steel, there is a rich collection of literature that can provide some answers to the three questions introduced in Section 1.5.

Subsections 2.1, 2.2, and 2.3 assemble relevant literature from materials science, industrial ecology, thermodynamics and process engineering corresponding to questions 1, 2, and 3. Remaining gaps in knowledge for each research area are summarized in 2.4. This approach is question-led, not methodology-led. The literature review therefore also focuses on relevant methodologies that can be used or modified in new analysis in Chapters 3, 4, and 5.

2.1 How does copper constrain steel recycling?

How serious is copper contamination, and does it deserve the attention of steelmakers now? Literature is reviewed to understand the metallurgical effects of copper on steel, and the implications for the greater steel system. 2.1.1 reviews the effects of various tramp elements on steel properties, to understand why copper in particular is cited as the main barrier to high-quality steel recycling. To understand the consequences of these metallurgical effects for energy consumption and recycling rates, 2.1.2 reviews previous work investigating the copper-steel system. The scope, data sources and methodologies employed in those studies are discussed as well, revealing that most studies are regional. Section 2.1.3 discusses the global trade patterns of steel scrap, and reviews current work on the global steel system that could be used for further analysis.

2.1.1 The metallurgical effects of tramp elements on steel

A number of elements cannot be refined from the steel melt in commercial practice. Nakajima et al. (2011) used thermodynamic analysis to determine the distribution of elements between the melt, slag and gas phases in the various conventional metal production routes. The "metal wheel" concisely presents these results. The iron section of the "metal wheel" is shown in Figure 2.1.

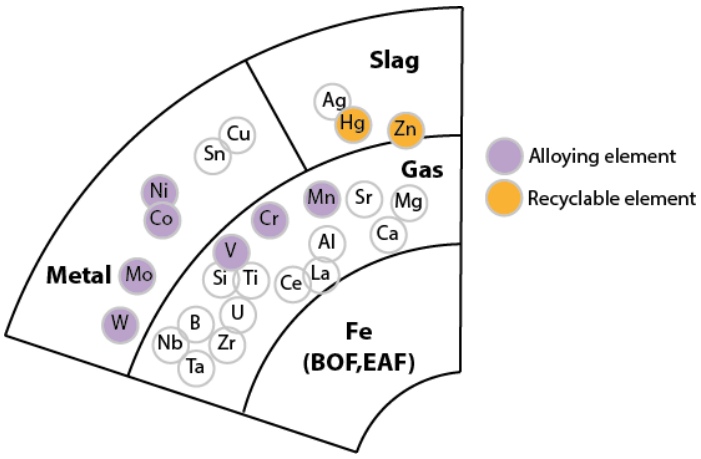

Figure 2.1: The iron section of the "metal wheel," adapted from Nakajima et al. (2011).

Elements that remain in the melt (or "metal" phase, above) receive most attention in the literature because they affect product properties. However, insufficient control over elements that distribute to the slag or gaseous phase has consequences as well. Chromium, manganese and vanadium are valuable alloying elements and are also designated "critical metals" (technologically and geopolitically important elements subject to supply disruptions, as designated by the European Commission (2012)), but they wastefully oxidize to the slag phase (Seetharaman et al., 2013). Zinc, a common coating for corrosion protection, is extremely prevalent in scrap-based steelmaking. Zinc has a high vapor pressure and vaporizes during scrap heating, creating "EAF dust," that is harmful and difficult to manage, as reviewed by de Buzin et al. (2017).

The metallurgical effects of the elements that remain in the melt are well-understood. Bell et al. (2006) and Rod et al. (2006) review the interaction of these residual elements with steel. Elements may form a solid solution with iron (substituting in the matrix or occupying interstitials), or precipitate as a distinct phase. The behavior of the different elements and the

effects on properties are summarized in Figure 2.2. All residual elements strengthen steel through solid solution and precipitation mechanisms, with an accompanying decrease in ductility and drawing properties. Some elements segregate during cooling and downstream thermos-mechanical processing, which can lead to embrittlement, cracks and surface defects.

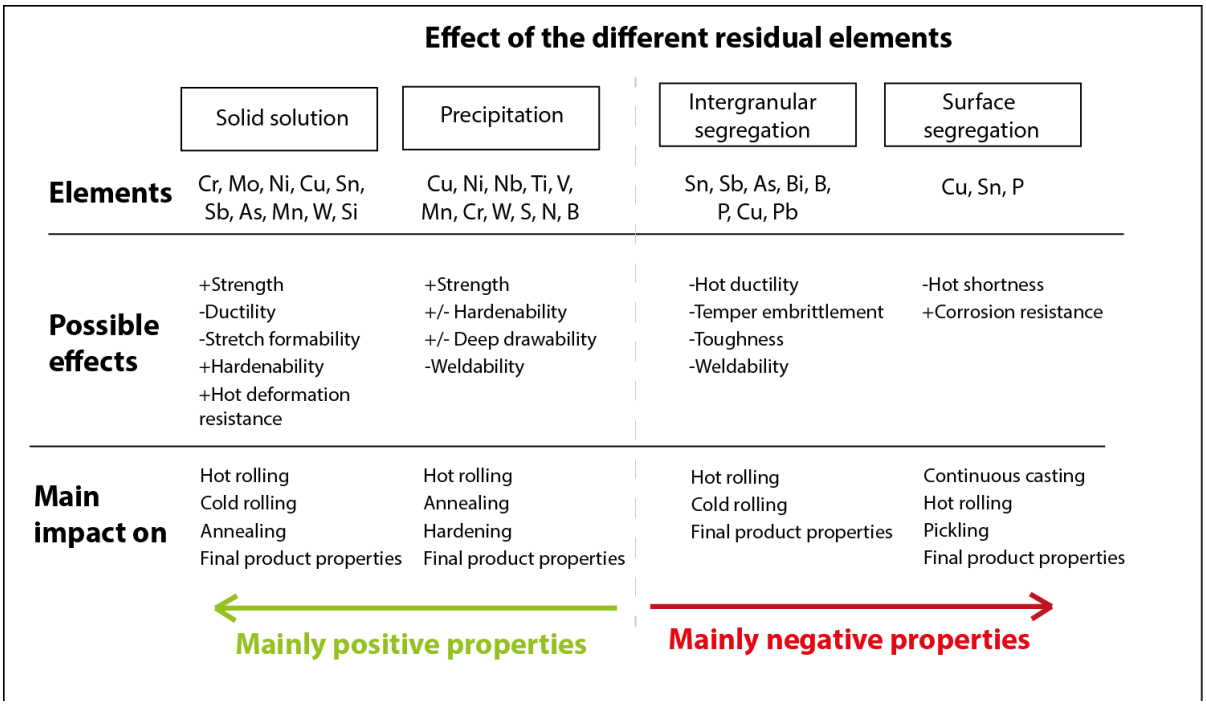

Figure 2.2: Overview of the nature of residual elements in steels and their possible effects on down-stream processes and end properties, adapted from Rod et al. (2006).

Copper, tin, chromium, nickel, molybdenum and vanadium are the main elements monitored, because they are commonly present in steel scrap. Amongst the various residual elements, copper and tin are often cited as the most problematic. Copper and tin cause a phenomenon known as "surface hot shortness," a form of liquid metal embrittlement. Traditionally, "hot shortness" refers to grain boundary melting and embrittlement as a consequence of segregation of impurities during casting, which can occur throughout the bulk of the material. For copper in steel, hot shortness emerges at the surface during hot rolling and processing, when steel is exposed to an oxidizing atmosphere at high temperature (above 1100°C). In these conditions, iron oxidizes, but copper and tin have limited solubility in austenite and are more noble than iron. Therefore, copper and tin enrich at the surface, and form a liquid film (due to their lower melting point). As rolling forces are applied, the liquid penetrates grain boundaries and opens cracking pathways. Problematic temperatures and atmospheres are difficult to avoid during hot rolling, and embrittlement can occur at any concentration of copper greater than 0.1%. Copper must be present for surface hot shortness

to develop, but additional elements such as silicon, nickel, tin, arsenic and antimony worsen the condition. Tin can be especially problematic because it further decreases the solubility of copper in austenite and lowers the melting point of the liquid film (Imai et al., 1997).

Surface hot shortness causes complications beyond the hot rolling process. This form of liquid metal embrittlement compromises surface properties, which determine the performance of a component, such as its corrosion and fatigue resistance, crucial for many applications. Certain products are more tolerant of surface defects. Reinforcing bar is embedded in concrete, so surface properties are not as critical. Final steel products have a set maximum concentration allowable, determined by their shape and application, shown in Table 2.1 (Schrade, 2006). Rods and bars have high copper tolerance because they generally require smaller reductions in thickness (i.e. less mechanical working), but also because the applications are less demanding.

Table 2.1: Copper limits of different steel products (Schrade, 2006).

Steel Grade	Interstitial Free	Deep Drawing Quality	Drawing	Commercial	Structural	Fine Wire	Rebar
Maximum Allowable Cu (wt %)	0.03	0.04	0.06	0.1	0.12	0.07	0.4

Copper is the main concern because of its prevalence in scrap. Copper originates from wiring and motors in vehicles, appliances and equipment. These products are commonly prepared for recycling by hammer shredding. This high-throughput process dispenses lighter material (shredder residue, separated by suction), and metals at the shredder outlet. The magnetic and non-magnetic metals are then separated. However, entangled copper wiring and steel-encased motors with reduced magnetic permeability may not be removed from the shredded steel scrap during magnetic separation (Aboussouan et al., 1999). Figure 2.3 shows images of copper wiring and motors entangled in fragmented steel scrap, obtained from a UK scrap yard.

Figure 2.3: Images of copper wiring entangled in steel scrap obtained from a UK scrap yard.

Steel may also contain alloyed copper. Structural steel may contain up to 0.5 wt% Cu, from previous recycling or added intentionally for corrosion resistance and strengthening (Rod et al., 2006). Engine blocks also have higher copper content: 0.7 to 1.0wt%, and steel parts made by powder metallurgy may contain up to 7.0wt% (Newell, 2017). Therefore, copper is pervasive in end-of-life scrap: 0.25 to 0.45wt% copper is common in magnetically separated steel scrap (Tee and Fray, 2006). Tin may also be present, and must be monitored, but tin-plated steel makes up a much smaller portion of steel products (<1%, as shown in the supply chain by Cullen et al. (2012)), and can be isolated more readily.

High-quality steel recycling must aim to better manage all alloying and contaminating elements. The unintentional oxidation or vaporization of elements during refining is inefficient, with an accompanied value loss. However, these elements could be replaced and do not restrict the range of products end-of-life scrap can be used for. The focus of this thesis will remain on copper, because of the prominence of copper in end-of-life scrap and the strict limitations it imposes on scrap utilization.

2.1.2 Previous work on the systemic effects of copper on the steel system

The metallurgical effects of copper have wide implications. Steelmakers must decide to either tolerate copper, or compensate with scrap diversion, dilution or modified processing. These actions determine the energy consumption of processing and recycling rates. The greater steel system must therefore be considered. These research topics fall within the field of

industrial ecology – the study of material and energy flows through industrial systems. Previous work in industrial ecology on the copper-steel system is presented below.

Each study on copper in the steel system has a different objective and scope. Here, three different types of studies are distinguished. The first considers the recycling of a product, independent from the rest of the metal system. The second traces the recycling of a specific product within the greater metal system. These studies have thus far focused on vehicles, because vehicles are the subset of the steel system most effected by copper contamination. Lastly, multiple scrap and product categories could be studied within the whole steel system. The literature is reviewed below by this categorization, while discussing the insights and limitations of the employed methods and data sources.

Product-level studies.

The isolated recycling of end-of-life vehicles (ELV's) has been studied by several authors because it exemplifies open-loop recycling. Vehicle scrap often contains copper wiring, but sheet steel for new cars has strict copper tolerances. Nakamura et al. (2012) sought to quantify these quality and dilution losses during the recycling of ELV scrap. Using a Japanese input-output table as primary data, the ratio of pig iron needed to dilute the ELV scrap was calculated. The results show that neglecting the embodied-energy of pig iron can lead to an overestimation of the emissions savings of ELV recycling of over 30%, compared to conventional life cycle assessment (LCA). LCA methodologies are used to evaluate the environmental impacts of each stage of a product's life: raw materials processing, manufacture, use and disposal or recycling, as described by Klöpffer (1997). These results from Nakamura et al. (2012) are consistent with conclusions in the industrial ecology community that quantifying emissions savings during recycling can be problematic and inconsistent, because of dynamics in primary and secondary material utilization, as discussed in a review by Johnson et al. (2013).

The losses from mixing with impurities during metal recovery and recycling can also be characterized by chemical exergy, defined as the maximum work that can be obtained when considering the system is brought into reaction substances present in the environment (Szargut, 2005). Exergy has been applied as a metric in numerous studies to quantify and evaluate energy and material efficiency, also known as resource efficiency. Gonzalez-Hernandez et al. (2018) explain that exergy can capture the quality and dissipation of material

and energy streams. Applying chemical exergy to recovery and recycling is explained by Castro et al. (2007), and this method is demonstrated with an example of steel scrap contaminated by copper. The exergy associated with the pure steel required for dilution was calculated, as well as the exergy of the materials at each stage of recycling, to show that the specific exergy content decreased from the original material to the recycled product. These studies by Nakamura et al. (2012) and Castro et al. (2007) reveal that dilution is a significant, and sometimes unaccounted, factor in steel recycling. However, these studies quantify these impacts within an isolated cycle, which does not reflect real practice.

Tracing a product within the greater steel system.

Further studies seek to trace a specific product within the greater metal system, to evaluate losses in a more realistic model. Within a greater steel system, dilution may not be required, as scrap could be directed to a more tolerant application. Additionally, the embodied energy and associated emissions of steel for dilution is only true when its production could have been avoided. Whether dilution is necessary or not, primary steel will be produced because steel demand is significantly greater than the scrap supply.

To construct these more complex models, the underlying steel system must be characterized. Two main methods exist: input-output analysis or material flow analysis. Input-output tables contain monetary flows of an entire industry or sector within a country, and thus reveal the connections in a supply chain from raw materials to final products. However, these tables do not contain data on the flow of waste and do not meet the mass balance principle, which are fundamental requirements for studying the flow of materials. These concerns are discussed by Strassert (2002), who proposed constructing input-output tables with physical units. Further, Nakamura et al. (2007) propose waste input-output (WIO) analysis, which converts monetary input-output tables into a physical input-output table. The authors argue that this method avoids the prohibitive cost associated with finding physical data. Alternatively, material flow analysis (MFA) is based on physical data in the first instance to balance the flow of materials into and out of a system, as described by Schmidt (2008). The analysis can be static, showing the flow of material at one point in time (i.e. per annum flows), or dynamic, considering multiple time periods. These models can be populated with "bottom-up" data, where steel stocks are counted directly or by proxy, or by "top-down" data, from production and trade statistics.

To understand the effects of contamination, the underlying steel system model is layered with composition data – the copper concentration of the scrap, and the tolerance of final steel products. Scenarios are devised to evaluate the utilization of scrap. The matching of scrap supply and product demand, and the consequential cascading or dilution required, can be illustrated with material pinch analysis (MPA). MPA derives from energy pinch analysis, where curves of the enthalpy and temperature of heat sources and sinks in an industrial plant are plotted together to optimize allocation. In MPA, the scrap and product quantity and quality curves are plotted together, where copper concentration is the "quality" metric (Ekvall, 2015).

These systems-level methods have been employed in several studies to understand the utilization of ELV steel scrap. Matsubae et al. (2011) used WIO to evaluate the amount of ferrous scrap utilized, the amount of copper eliminated and subsequent contamination of the steel products, under several scenarios in Japan. The authors explained that EAF steel is mainly used for construction and civil engineering projects. Contaminated ELV scrap can be utilized as long as there is enough demand in these sectors, but construction demand in Japan is expected to plateau soon. Adding to this, Nakamura et al. (2014) used input-output analysis (based on the 2005 Japanese Input-Output table) and dynamic MFA to track the open-loop recycling of ELV steel scrap over 100 years. It was found that only 7-8% of recovered car steel recycled back to automotive steel, showing the limited extent of closed-loop recycling. Hatayama et al. (2014) investigated the feasibility of closed loop recycling of automobile steel sheets using MPA and dynamic modeling, based on previous stock flow analysis (Hatayama et al., 2010). The authors found that the proportion of old sheet scrap that can be recycled into new steel sheets will decrease, because the use of shredders in scrap preparation is increasing, as well as scrap quantities. To increase the utilization of old sheet scrap, the authors tested the efficacy of several potential technologies in different scenarios: improved shredding, replacing the copper harnesses with aluminum and improving copper tolerance during sheet rolling. None of the technologies were sufficient to avoid downcycling completely, but increasing the copper tolerance of steel sheets was the most effective measure, with immediate benefits. The authors predicted that by 2030, partial cascading would be unavoidable, and by 2050 more than half of old steel sheet scrap generated would be down-cycled.

The down-cycling caused by copper affects other elements in steel, specifically alloying elements. The down-cycling of these elements has been characterized with similar systems-level methods. Ohno et al. (2014) used waste input-output material flow analysis and Japanese

data to show that passenger cars were the largest end-use for alloying elements in Japan. A following study (Ohno et al., 2015) estimated that 93% of ferrous ELV scrap recycled to carbon steel, for applications that did not utilize the functionality of these alloying elements. When alloying elements are not retained, they must be replaced, using ferroalloys (FeMn, FeCr, FeMo, etc.). The production of ferroalloys is highly energy-intensive, as discussed by Holappa (2010). An LCA study by Diener and Tillman (2015) ranked alloying element management as a top priority, claiming that replacing substances in more highly-alloyed steel grades incurred five times greater CO_2-equivalent emissions than replacing normal grades. These findings thus reinforce the importance of closing the recycling loop for automotive steel.

Whole steel system.

The recycling of many different types of steel scrap (beyond ELV's) to different products, can be evaluated in a model that captures the whole steel system. Again, an appropriate WIO or MFA model serves as the framework, but multiple scrap categories are disaggregated and assigned copper concentration values.

Previous work has used this approach to determine broad trends for scrap utilization. Noro et al. (1997) used historic data comparing the amount of steel discarded to the increase in steel stocks. The authors extrapolated historic trends to predict that the copper concentration of scrap would increase by 1.2-1.5 times from 1996 to 2015. Thus, the authors argued that technologies capable of removing copper by about 55% would be needed by 2010 to avoid the accumulation of unusable scrap. Kakudate et al. (2000) investigated the increasing urgency of copper control using a simplified macro model of steel flow in Japan. Steel was classified by virgin steel for machinery and for construction and recycled steel for machinery and construction, to calculate the recycling ratio and copper contamination that allowed for a supply of recycled steel for machinery.

The constraints projected by Noro et al. (1997) and Kakudate et al. (2000) nearly 20 years ago have not emerged, because the effects of trade were not considered. Igarashi et al. (2007) built on a dynamic model developed by Daigo et al. (2005) to analyze the change in the tramp element concentration in steel recycling under different scrap export scenarios from Japan. The authors found that the export scenario determines whether the average copper concentration increases or decreases.

In addition to these studies in Japan, the viability of future steel recycling has also been evaluated in China. Pauliuk et al. (2011) sought to evaluate the feasibility of implementing a steel circular economy in China, and used dynamic material flow analysis to forecast production, recycling and iron ore consumption in China to 2100, as driven by in-use stock per capita. The authors found that quality constraints were likely to occur once construction steel demand plateaus and the scrap supply increases. Old scrap would need to be used for transportation and equipment applications after 2030. However, the authors also noted that there would be high demand for construction steel in other regions, such as India. Thus, the authors were unsure of the extent to which exports could delay or eliminate impending quality constraints.

Few studies characterize copper in a multi-regional steel system. Pauliuk et al. (2017) investigate steel losses in a multi-regional model to 2100. Significant losses were characterized, occurring from trade patterns, recovery and re-melting, but this study did not explicitly track the effects of tramp elements. Only one global analysis of tramp elements in the global steel system was identified. Ekvall et al. (2014) applied MPA to the global steel system in a pilot study. Three categories of application were distinguished based on material quality and scrap supply was specified by copper concentration. In a hypothetical scenario where steel scrap supply was equivalent to final steel demand, at least 20% of scrap would be unrecyclable due to contamination. The study calls for a more thorough analysis, but demonstrates the potential of this approach at a global level.

In total, there is significant previous work investigating the systemic effects of copper in steel recycling. However, most of the research is regional, specifically on the Japanese steel system, and is derived from monetary data. Therefore, the applicability of the current literature is limited.

2.1.3 The current and future global steel system

Most existing studies evaluate copper in steel at a regional level, but constraints in scrap utilization cannot be revealed in studies of a regional scope. Accumulating obsolete scrap within country borders will not take place so long as there is use for it elsewhere. The trade patterns of the global steel scrap market have been investigated by economists. Söderholm et al. (2008) provide an overview of the steel scrap market, explaining that international trading ensures scrap flows to appropriate uses. Gesing (2004) explains that vehicles are recycled

within a global market, and this unrestricted flow of scrap metal between markets and geographical locations is essential for a sustainable metal system. Thus, in order to understand the severity of copper contamination, international trade must be considered with a model of global scope.

Fortunately, recent research characterizes the current and future global steel flows, which can be built upon to include the flow and impacts of copper contamination. Cullen et al. (2012) mapped the 2008 global steel supply chain from raw materials to end-products using MFA and data from a range of sources: primarily the worldsteel association, as well as regional associations, national statistics offices, trade organizations, steel companies and private media groups. The consolidated data is presented visually in a Sankey diagram, as shown in Figure 2.4, where the magnitude of the mass flows in million-tonnes is represented by the width of the lines. The structure of the supply chain, with the inputs and outputs of each transformation, is also conveyed. This work also maps intermediate products to final products used by the four main sectors: construction, transportation, infrastructure and goods.

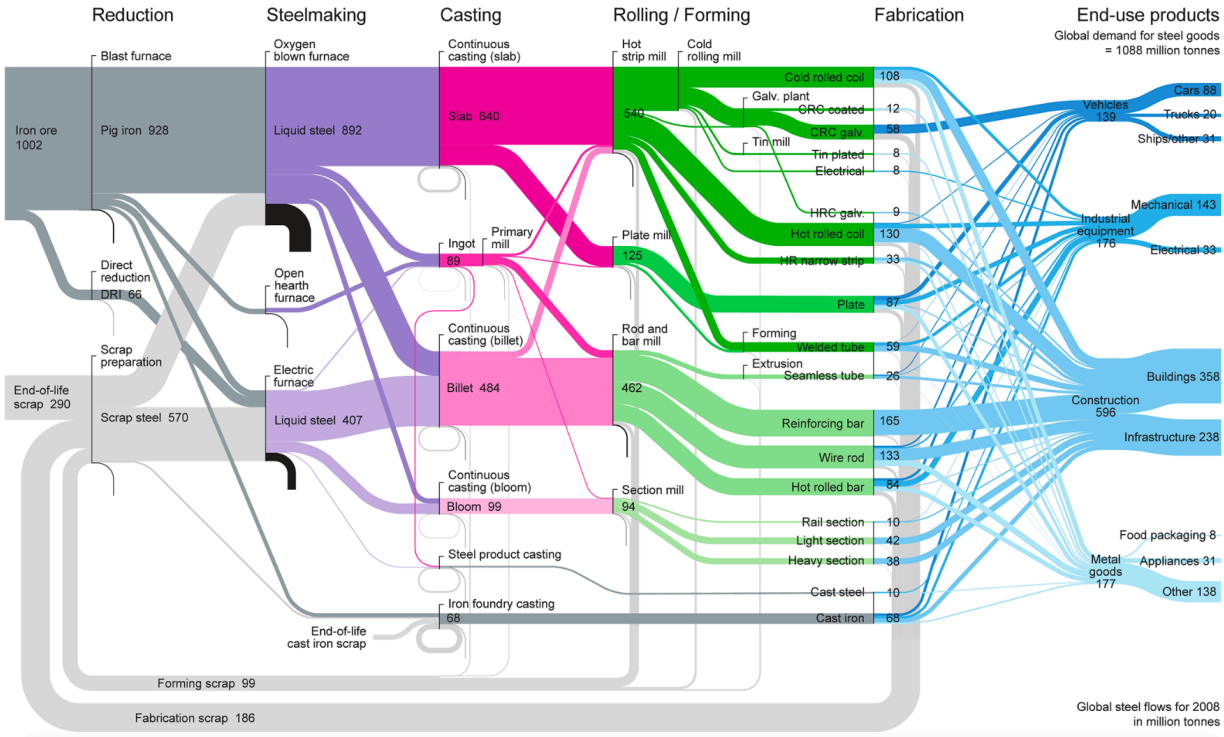

Figure 2.4: The 2008 steel Sankey diagram by Cullen et al. (2012), tracing the mass flow of steel during the transformation from raw sources to final products. The width of the lines is correlated to mass, and the mass of flows is provided on the figure in million tonnes.

Future trends in global steel demand can be characterized by extrapolating historic trends forward, as demonstrated by Wang et al. (2007) and Yellishetty et al. (2010). Gross domestic product (GDP) can be correlated with steel demand – an approach demonstrated by

the International Energy Agency (2009). However, models are more robust if the physical mechanism driving behavior is described. Pauliuk et al. (2013a) explain that steel services are provided by stocks, not GDP or annual production. The authors show that in-use steel stocks are between 6 and 16 tons per capita in most industrialized countries, and saturation tends towards 11-16 tons per capita. This trend can be extrapolated to estimate future steel demand in the "stock-driven" approach. Hatayama et al. (2010) constructed a dynamic MFA for 42 countries. The future economic growth of each country was considered to estimate future steel demand to 2050, disaggregated by three end-use sectors. Steel demand was found to increase to a peak in 2025, dominated by construction needs, and after this point demand for vehicles increases, while construction demand decreases. Noting that the work by Hatayama et al. (2010) considers only the use phase of steel, Pauliuk et al. (2013b) supplement this study by exploring how the steel industry and waste management could respond to an increasing scrap supply. Future final steel demand and old scrap supply was estimated from 1950 to 2100 by four end-use sectors: products, construction, machinery and transportation. This work is the first to characterize the surge in global end-of-life scrap: per annum old scrap will treble from 2010 (about 300 Mt/yr) to 2050 (over 950 Mt/yr). All growth in future steel demand could be met by growth in the secondary market.

Overall, the works by Cullen et al. (2012) and Pauliuk et al. (2013b) can be used as frameworks to develop an analysis of copper contamination. Such an analysis would reveal constraints in future steel recycling at a global scale. Given the global nature of scrap trading, this would be a useful contribution to the literature.

2.2 Can copper be extracted from steel, and what would be the energy and material requirements of a potential process?

Management strategies may prevent the adverse metallurgical and systemic effects described in 2.1. Specifically, a removal process would allow contaminated scrap to recycle to any application without the need for dilution. Therefore, the purpose of the literature review in Section 2.2 is to develop a richer understanding of the feasibility of copper removal, independent of the current refining infrastructure. This understanding must begin from fundamental concepts, so the principles governing separation are presented in 2.2.1. These principles reveal that there is wide scope for the development of a separation process. However, any viable process must be compatible with standard EAF steel refining, so EAF

steelmaking practice is reviewed in 2.2.2. Extraction is not the only option for improved control of copper contamination, so other options are reviewed in 2.2.3.

2.2.1 Principles of separation

Copper removal is a matter of separation – the process of converting a mixture (contaminated scrap) into its distinct components (steel and copper). The information that thermodynamics provides for evaluating the feasibility of separation is discussed. The information that thermodynamics does not provide is discussed as well – specifically how separation may be achieved in practice. In practice, a separation mechanism is required, so the identification and classification of possible mechanisms is described in this subsection as well.

Thermodynamic description of a mixture.

Thermodynamics is the branch of physical science that describes the relationships between all forms of energy. Thermodynamics can describe chemical energy, i.e. the macroscopic energy changes involved in breaking and forming bonds. The foundational concepts were introduced by Gibbs and Bumstead (1906). David and Gaskell (1995) provide a comprehensive resource for applying thermodynamics to materials. The metric used to characterize a system undergoing compositional changes is Gibbs free energy (G), measured in Joules/mole (J/mol). It is the maximum amount of non-expansion work that can be extracted from a thermodynamically closed system, and it is minimized in a system at equilibrium.

Each pure substance has an inherent chemical potential, μ (measured in J/mol), which is a form of potential energy that can be absorbed or released during a chemical reaction. The Gibbs free energy of a heterogeneous mixture with distinct phases varies linearly by the proportion of the components. When the distinct phases (A and B) are mixed into a single, homogeneous mixture, the Gibbs free energy reduces from the proportional sum of the two components, shown as a function of the molar fraction of B, X_B, in Figure 2.5 below. This reduction is the Gibbs free energy of mixing, ΔG_{mix}. To separate the phases, ΔG_{mix} must be overcome.

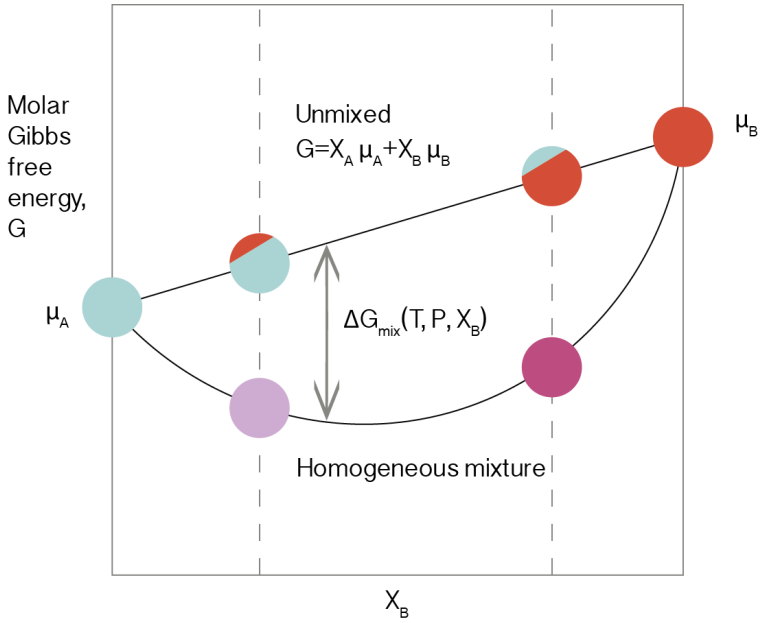

Figure 2.5: Variation in molar Gibbs free energy of both a heterogeneous and homogenous mixture as X_B increases, adapted from (David and Gaskell, 1995).

In an ideal system of non-interacting particles, ΔG_{mix} is a function of only configurational entropy, S (measured in J/°K). Entropy is a measure of disorder of the system, and the configurational entropy is the portion due to the location of the particles. However, when particles interact, there is a change in enthalpy, H (measured in J), which is a thermodynamic quantity equivalent to the total heat content of a system. To account for the bond energies of the mixing components, ΔG_{mix}, the total driving force for mixing, is defined in equation 2.1 below (David and Gaskell, 1995).

$$\Delta G_{mix} = \Delta H_{mix} - T\Delta S_{mix} \tag{2.1}$$

As described in *Chemical Metallurgy* (Moore, 1981), if ΔH_{mix} is negative, mixing is more thermodynamically favorable because an attractive force exists between the particles, and vice versa when ΔH_{mix} is positive. The deviation from ideality due to these interactions is described by the activity coefficient, γ. When $\gamma>1$, A-A and B-B bond energies are greater than the A-B bond energy, which can result in clustering and phase separation. When $\gamma<1$, A-B bonds are energetically preferred over A-A and B-B bonds, ΔH_{mix} is negative. This behavior varies with the molar fraction of the component. When X_B is low (dilute in solution), there is a greater likelihood that A will completely surround B atoms, which strongly influence the behavior of the B atoms. In this regime, γ_B can be multiplied by the molar fraction to obtain a measure of effective concentration, known as activity, a_B. When X_B is high, the interaction of

the B atoms with A atoms is not as significant and the solution approaches ideal behavior, and Raoult's law (simply $X_A=a_A$) can be used. These cases are illustrated in Figure 2.6.

$$a_B = \gamma_B X_B \tag{2.2}$$

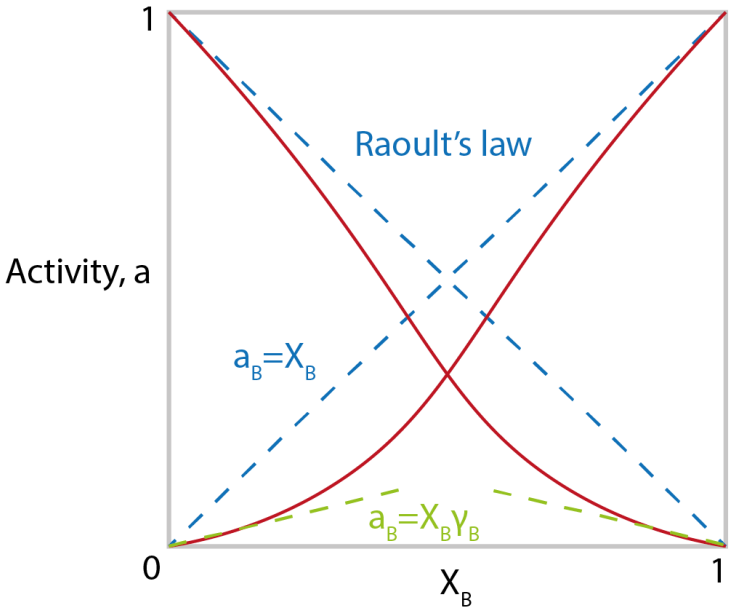

Figure 2.6: Activities of components A and B in a homogeneous mixture as X_B increases, shown as the red line – an example of negative deviation from ideality. Raoult's law is shown as the dotted line, as well as the application of activity coefficient to account for non-ideal behavior, adapted from (Moore, 1981).

Evaluating the feasibility of extraction.

The activity of a component indicates how easily it could be extracted from the mixture. When there is a negative deviation from ideal (Raoultian) behavior, as shown in Figure 2.6, the solute is more strongly held from evaporating, reacting or otherwise separating from the solution. This behavior is described in the equation below for the minimum work of extraction of B, $w_{min,B}$ (J/mol), from a mixture, where R is the universal gas constant and T is temperature (Gutowski, 2007).

$$w_{min,B} = RT\left(\ln\frac{1}{a_B}\right) \tag{2.3}$$

This thermodynamic relation has been used to describe long-standing observations in extraction and metal production. Sherwood (1959) shows that as the concentration of a

targeted substance decreases, the work and technical costs for extraction increases. This trend has been observed for a range of substances in various contexts, shown in Figure 2.7.

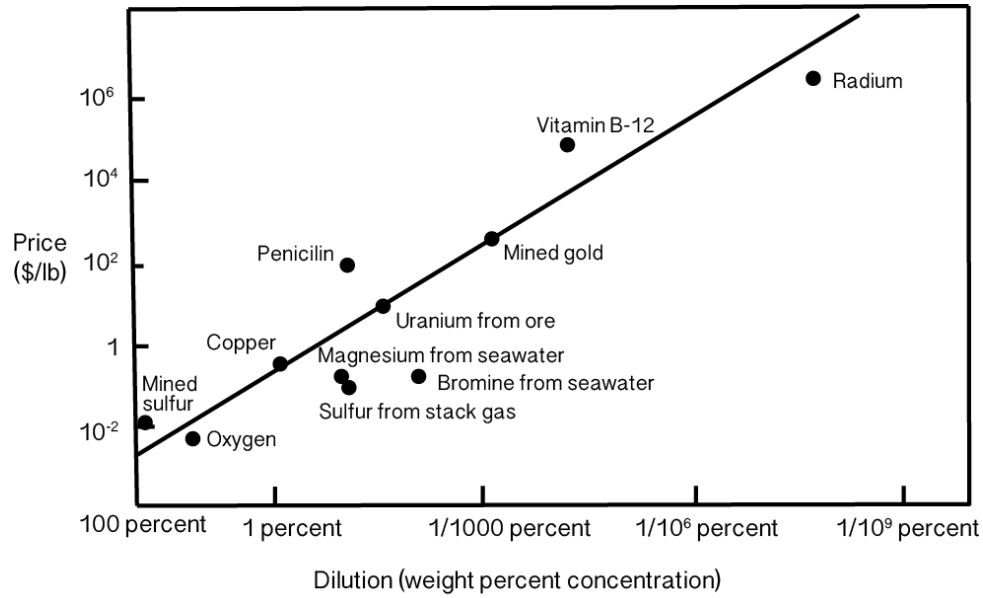

Figure 2.7: Sherwood plot showing the prices of chemical products correlated with their degree of dilution in the raw material from which they were separated. Recreated from (Prausnitz, 1994).

Thermodynamic relations also provide a physical basis for understanding metal prices. In 1976, Phillips and Edwards showed that the price of a metal derives from ore grade (a function of metal concentration) and the Gibbs free energy requirement to transform the ore, ΔG. The relation below was derived from the market prices of 22 metals, where p is metal price, g is ore grade and γ_1 and γ_2 are coefficients for the best linear correlation.

$$p = \gamma_1 \left(\frac{1}{g}\right) + \gamma_2 \Delta G \qquad (2.4)$$

Thus, these basic thermodynamic descriptions can be powerful for describing broad real-world trends, and may be useful in describing the feasibility of impurity removal in a process-independent way. However, care must be taken when using these descriptions to evaluate the feasibility of separating a specific system. Table 2.2 presents the thermodynamic data on dilute elements in liquid iron. Silicon shows the most negative deviation from ideality and the most negative molar free energy in a 1% solution. However, silicon can be readily controlled in steelmaking. Alternatively, copper shows the most positive deviation from ideality and highest molar free energy in a 1% solution, but copper is not removed from the steel melt.

Table 2.2: Thermodynamic data on dilute metals and metalloids in liquid iron (Vignes, 2011). T refers to temperature in Celsius.

Element (all in liquid state)	Raoultian activity coefficient γ at infinite dilution at 1600°C	Molar free energy in a 1% solution (cal/mol)
Al	0.029	-15,100 – 6.67T
Cr	1	4,600 – 11.18T
Cu	7-10	11,370 – 11.62T
Mn	1.48	1,450 – 9.12T
Si	0.018	-31,400 – 3.6T
Ni	0.62	-1,800 – 0.25T

The interaction between liquid iron and copper in solution is well-characterized. Thermodynamic information on iron-based iron-copper melts was compiled by Zaitsev et al. (2001), who found the activity coefficient of copper in an infinitely dilute solution is 8.8 at 1600°C. The activity of copper by molar fraction in solution with iron is compiled in Figure 2.8. Carbon additions only increase the activity coefficient of copper. Wang et al. (1991) compile values from researchers, reporting between 16 and 31 in carbon-saturated melts at 1600°C. An activity coefficient greater than 1 denotes a repulsive interaction between the components in solution. Thus, considering only this interaction, copper should be relatively easy to remove. An energy requirement of roughly 1 kWh/tonne steel to reduce copper concentration in iron from 0.4wt% to 0.1wt% copper follows from the Gibbs free energy difference reported by Zaitsev et al. (2001) at 1550°C, shown in Figure 2.9.

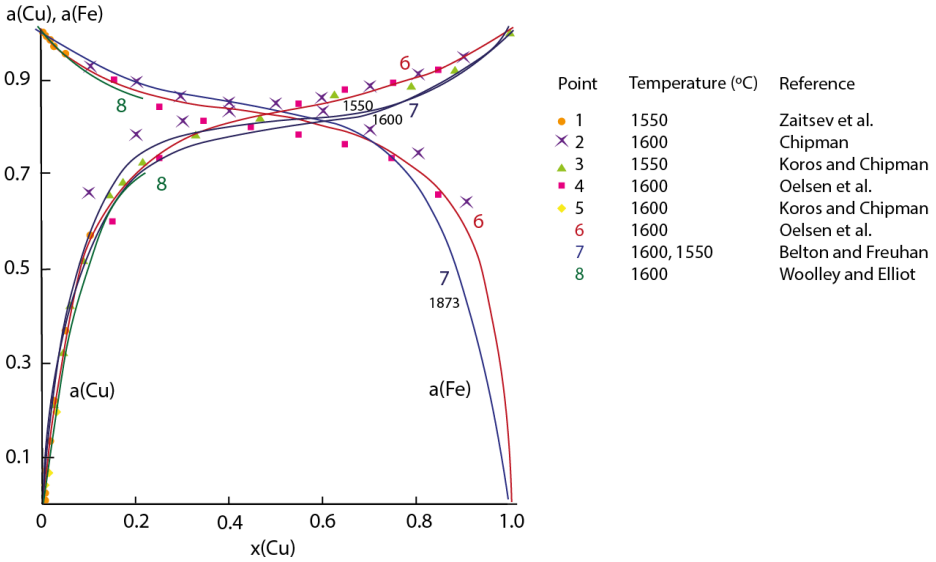

Figure 2.8: Activities of copper and iron as the molar fraction of copper, X(Cu), varies, adapted from Zaitsev et al. (2001).

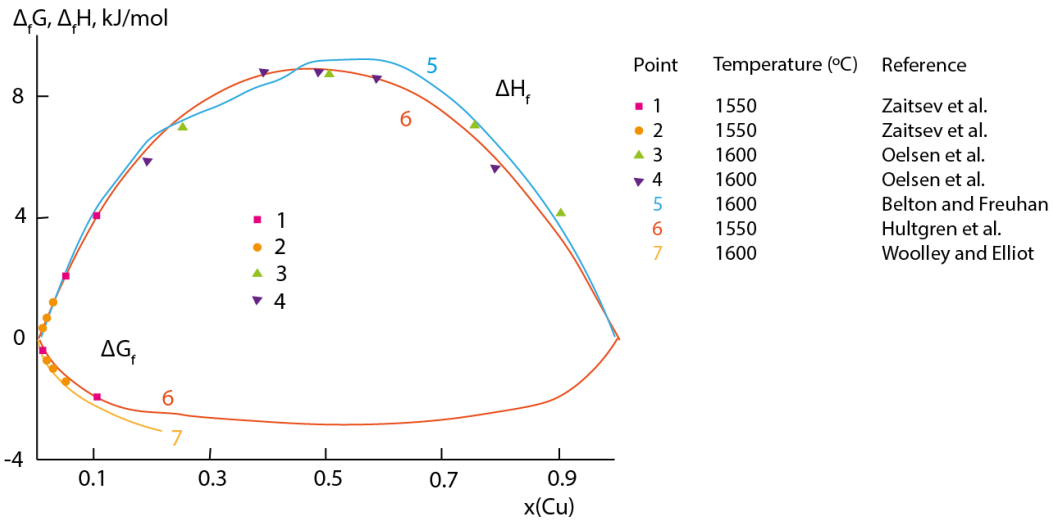

Figure 2.9: Enthalpy (ΔH_f) and Gibbs free energy of formation (ΔG_f) of liquid Fe-Cu alloy, adapted from Zaitsev et al. (2001).

This process-independent result shows copper is not fundamentally inseparable from the steel melt. However, process-independent thermodynamics alone cannot be used to estimate the amount of energy required for separation in practice. As Rousseau (2009) explains, if only the first law of thermodynamics governed separation, the thermodynamic energy requirement would correlate directly with the fuel required. However, the second law distorts this relationship. The energy flows, both quantity and quality, through a system must be considered.

In a review of the thermodynamics of recycling, Gutowski (2007) presents Table 2.3 below to show the vast difference between the theoretical (ΔG_{mix}) and a measure of the actual energy (Q, E) required to perform separation. W is the work input into the system, while Q is the heat exchanged between the system and the surroundings at an initial temperature, T_0. King (1987) estimates this difference is typically a factor of 50. The energy-intensive part of separation is not necessarily overcoming the interaction of the components, but in driving the physical transport of the component from solution.

Table 2.3: Separation efficiencies of various processes (Gutowski, 2007).

Materials	Process	Efficiency	Reference
Propane/Propylene	Distillation	2% ($-\Delta G_{mix}/Q$)	(Swaan Arons et al., 2004)
Various metallic ores	Mining and milling	0.3% ($-\Delta G_{mix}/E$)	(Chapman and Roberts, 1983)
Hexane/polybutadiene	Steam vaporization	0.1% ($-\Delta G_{mix}/Q$)	(Gutowski et al., 1983)
CO_2/combustion gas	Amine stripping	3.6% ($-\Delta G_{mix}/Q$)	(Gutowski, 2007)

Achieving separation in practice: separation mechanisms.

To achieve separation some sort of device, system or process supplies the equivalent of thermodynamic work. Thermodynamic data can be attuned to the applied mechanism for a more accurate evaluation. For steel refining, two main mechanisms are employed: vaporization and oxidation. Seetharaman (2013) presents the plot shown in Figure 2.10 below. The vapor pressure of a pure element i, p_i, and oxygen partial pressure, p_{O2}, for metal/oxide equilibrium at 1600°C are shown for each element. The elements to the right of iron can vaporize, while those below can oxidize during refining. This plot provides information on the feasibility of removal from the basis of a mechanism, and so is more applicable to practice than the thermodynamic information in Table 2.2. Silicon can be easily removed because it oxidizes before iron, but copper has only a slightly higher vapor pressure than iron.

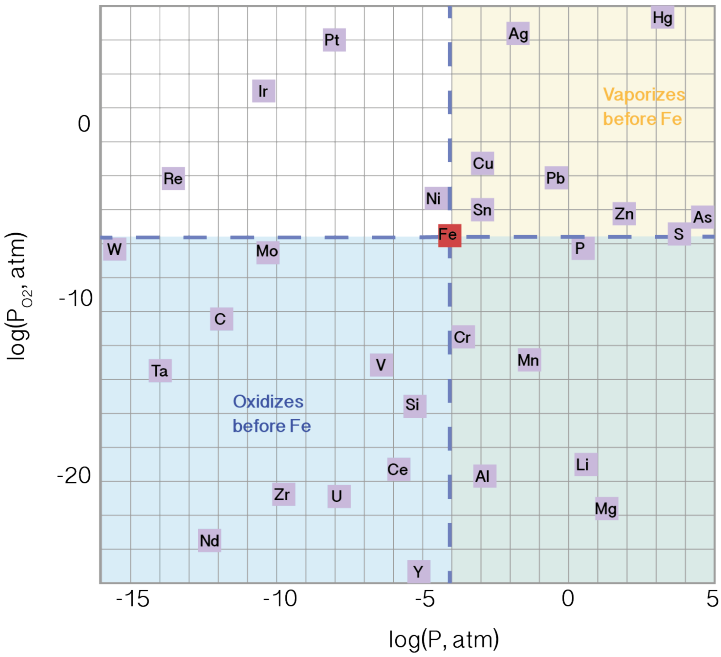

Figure 2.10: Vapor pressure of pure elements and oxygen partial pressure (atm) for metal/oxide equilibrium. Recreated from (Seetharaman, 2013).

Indeed, the Metal Wheel introduced in Figure 2.1 is based on the same principles. Castro et al. (2004) used the oxygen partial pressure and activity of the impurity in the melt to calculate its equilibrium distribution to an oxidizing slag. Later, Nakajima et al. (2010) expanded on this calculation to incorporate the effect of temperature, composition of the slag and vapor pressure. Both assessments conclude that copper cannot be removed from the melt in commercial refining, because iron oxidizes before copper.

These assessments show copper is difficult to remove in commercial refining. However, the scope of these assessments is limited, as it neglects the wider range of processes that could be developed. Hayes (1985) explains that because of the complexity of metallurgical

processing, most developments come about through evolutionary paths. It could be that there simply has not been enough time or investment for the development of a commercial copper extraction technique.

Current industrial practice evolved due to historic and economic factors, so it should not be used as fundamental basis to evaluate future possibilities. Reck and Graedel (2012) used the metal wheel to conclude that certain impurities would be "either very energy-intensive or essentially impossible," and that "elements remaining in metal phase cannot be separated." The THEMA (thermodynamic evaluation of materials combinations) model identifies metal combinations that be avoided in product design and scrap preparation (Castro et al. 2004). This scheme similarly uses current practice to evaluate metal combinations, not fundamental thermodynamics as the name suggests.

To determine the potential "removability" of copper, the range of available extraction mechanisms must be identified and evaluated. In separation, one component is selectively transported with respect to the other. Transport approaches equilibrium, so equilibrium conditions (temperature, pressure, electric potential, etc.) are established to favor the displacement. King (1987) explains almost any known physical mass transport or equilibrium phenomenon can be used.

Classification systems can help to define these various phenomena, but in *Unified Separation Science,* Giddings (1991) states there are multiple elements of similarity and differences among the methods such that it is not possible to define a set of techniques that stand uniquely at the core of separations. In describing the principles of metal refining, Engh (1992) provides the broad categorization of common techniques for impurity removal from metals:

1. *Impurity x is transferred to another phase where x has a high solubility. This second phase is not soluble in the molten metal.*
2. *X reacts with a second phase that may be solid, molten or gaseous.*
3. *X reacts with another element (added to the melt). The reaction product whether solid, liquid or gaseous, has to be removed from the melt. This removal may be produced by the effect of gravity or buoyancy forces, inertial forces or forces generated by stirring the melt.*
4. *An electric potential is applied to the melt to remove x by electrolysis.*

5. *The molten metal is allowed to solidify partially or a solid is partially melted. X is enriched either in the solid or liquid phase, and this phase is removed.*

King (1987) also provides a classification of separation processes, an excerpt of which is shown in Table 2.4. King explains that a separating agent, either a stream of matter or energy, is applied to the feed to cause the formation of a second phase of matter as a product, driven by a difference in properties.

Table 2.4: Excerpt of classification of separation processes by King (1987).

Type	Name	Feed	Separating agent	Products	Principle of separation
Diffusional: ordinary, energy-separating agent	Evaporation	Liquid	Heat	Liquid and vapor	Difference in volatilities
	Distillation	Liquid and/or vapor	Heat	Liquid and vapor	Difference in volatilities
	Crystallization	Liquid	Cooling or heating causing simultaneous evaporation	Liquid and solid	Difference in freezing tendencies, preferential participation in crystal structure
	Zone melting	Solid	Heat	Solid of non-uniform composition	Same as crystallization
Diffusional: ordinary, mass-separating agent	Extraction	Liquid	Immiscible liquid	2 liquids	Different solubilities of different species in the 2 liquid phases
	Leaching/washing	Solids	Solvent	Liquid and solid	Preferential solubility
	Precipitation	Liquid	Chemical reactant	Liquid and solid	Formation of insoluble precipitate

With an appropriate mechanism, a separation process can be defined. The driving force and equilibrium limits of a specific process can be described with thermodynamics. Thermodynamics does not provide information on the rate of chemical changes, so experimental measurements and correlations with empirical equations and approximate theories are needed, as explained by Giddings (1991). The description of a given separation process must be rooted in the area of physical science it operates within. For example, Prausnitz (1994) states that Newton's laws of gravitation and electrophoresis must be employed to describe centrifugal separation. Therefore, separation processes require careful and specific descriptions. Gutowski (2005) explains that the more detailed and attuned the model, the more accurate the estimate of energy consumption will be. In total, to determine the feasibility of extracting a component from a mixture in practice, the relevant separation mechanisms must be identified and the requirements of processes employing those mechanisms must be evaluated.

For the copper-steel system, significant experimental work exists that can be used to evaluate possible separations. Experimental investigations date from 1950 to present, and have been conducted at universities, national labs and research centers around the globe, primarily in Germany, Japan, Russia, the UK and the United States. Reviews by Jimbo et al. (1988), Savov et al. (1998 and 2003), Freuhan and Cramb (1991), Katayama et al. (1997) and

Marique (1996) summarize these efforts, but an integrated assessment is needed. Each experimental study evaluates copper removal under specific conditions. The principles and classification schemes discussed above may be used to impart structure to the dispersed experimental work, and serve as a basis to determine the feasibility of extracting copper from steel.

2.2.2 Scrap-based steelmaking practice

Steelmaking involves achieving a precise balance of many different elements through a series of processes. Any future copper removal process must be compatible with the established steel recycling refining practice. The copper removal process would affect the other elements present, and similarly the composition of the melt may affect the behavior of copper. Therefore, the conventional, established practice for producing steel from the EAF route is reviewed here. Recent developments in technology, as well as areas the steel industry and researchers seek to further improve are described as well.

Steel is produced by two main routes: the basic oxygen furnace (BOF) and the electric arc furnace (EAF). Scrap is used in both routes. The BOF is charged primarily with pig iron, and scrap is added as a coolant for the excess heat generated when carbon in pig iron reacts with oxygen (Ghosh and Chatterjee, 2008). Typically, steel scrap makes up about 20% of the charge, but the scrap typically originates from production or manufacturing processes, and thus the composition is known. Currently, end-of-life scrap is mainly used in the EAF (Pretorius et al., 2010).

Collection is the first step in scrap-based steelmaking. Processors buy scrap from a variety of sources – auto dismantlers, municipalities, demolition sites and shipyards. Steel is prepared at processing facilities by torching, baling, cutting and shredding. In developed countries, shredding is the dominant method to fragment steel components to the appropriate density. Magnets then separate ferrous and non-ferrous scrap (Aboussouan et al., 1999). Some dezincing and detinning processes and incineration may be performed on certain scrap streams (Javaid, 2003).

Brokers connect the processors to industrial scrap consumers (mills and foundries). Scrap is classified and sold by grades. Classification schemes are defined by several industry groups – such as the Institute of Scrap Recycling Industries (ISRI, 2016), EUROFER (Eurofer, 2016), and the Japanese Ferrous Raw Materials Association (Japanese Ferrous Scraps, 2008). These classifications specify the dimensions of the scrap pieces, the origin of

scrap, and define limits on impurities and residual elements. However, these limits are nominal, and composition is not typically measured until scrap has been mixed with other raw materials and melted (Noll et al., 2001). The relationship between the specific scrap dealer and steelmaker is the main assurance that residual limits are honored, and steel companies may define their own specifications as well. Scrap processors can adjust their preparation for steelmakers as needed (Brahmst, 2006). When copper control is critical, manually hand-picking copper from the line is the only technique in widespread use (Dalmijn and de Jong, 2007).

The processing of end-of-life vehicles is of particular interest, as discussed in 2.1.2. A review of vehicle recycling from a global perspective is provided by Gesing (2004). Generally, ELV's in the developed world are prepared for the EAF by some dismantling. Wheels, transmissions and engines may be removed for re-use, but wire harnesses and smaller motors are difficult to remove and are not interchangeable with other vehicles. The steel bodies are hammer shredded and copper wires become enmeshed such that magnetic separation is only partially effective (Brahmst, 2006). Though automobile hulks often make up the majority of raw material for shredders, white goods (stoves, washers, dryers, refrigerators) and industrial waste and machinery are often also shredded alongside automobiles (Manouchehri, 2006). In developing parts of the world, automobiles may still be completely dismantled by hand (Hatayama et al., 2014).

A range of materials can be charged to the EAF: hot briquetted iron (HBI), direct reduced iron (DRI), pig iron and hot metal. Madias (2014) states that on average 25% of metallics charged to the EAF are DRI/HBI, pig iron, hot metal, but in the developed world, 100% scrap is the most common charge. Steelmakers use sophisticated batch planning models to optimize the charging density and minimize the risk of exceeding impurity limits (Gaustad et al., 2007).

The primary function of the EAF is to melt the charged materials. Lime and carbon are charged in addition to the metallic inputs. To melt, electric power is provided by electrodes, and chemical energy is provided by oxy-fuel burners and exothermic reactions. During heating, organic coatings and contaminants combust. Zinc on galvanized steels volatilizes during heating, forming ZnO, known as EAF dust.

Once scrap is melted, oxygen is introduced by injectors or lances. Chemical energy is released as carbon combines with oxygen and iron oxidizes, and CO(g) bubbling aids in forming a foamy slag. The slag is critical for refining, but also helps with thermal insulation,

heat transfer, arc stability and to protect the refractory material. Slag is formed from lime, as well as oxides, gangue and ash from the charge materials. The main components are CaO, SiO_2, FeO and MgO (Madias, 2014).

Once melted, refining controls the metalloids, gases and inclusions present. The EAF is efficient for melting, but ladles are more efficient for refining, so refining is performed primarily after the EAF. In the EAF, only a few elements are of interest: phosphorus, silicon and carbon. The EAF produces a standard low carbon steel, which can be tailored in the ladle.

The first element of interest, phosphorus, originates from iron ore and can be difficult to refine in the EAF. The increasing use of DRI and pig iron means phosphorus is an increasing concern (Tayeb et al., 2014). Phosphorus is typically limited to 0.04wt% to prevent solidification cracking and inhomogeneous microstructures. Phosphorus is removed via the slag/metal reaction (2.5), but conditions must be optimized to favor this reaction. Slags with high basicity (high CaO content) are used to lower the activity of P_2O_5. The reaction favors lower temperatures, so phosphorus must be removed right after the liquid bath has been formed. Carbon will compete with oxygen so dephosphorization may not take place immediately. Repeated removal of the slag and reformation may be required (International Iron and Steel Institute, 1983).

$$2\underline{P} + 5(FeO) + n(CaO) \leftrightarrow (nCaO, P_2O_5) + 5Fe \qquad (2.5)$$

If silicon is present, it oxidizes by the exothermic reaction in 2.6. The reaction similarly progresses favorably with high basicity and low temperatures. Desiliconization is a higher priority in primary steelmaking and may not be necessary in EAF refining.

$$(SiO_2) + 2C_{saturated} \leftrightarrow \underline{Si} + 2CO(g) \qquad (2.6)$$

Carbon is refined with the injection of oxygen, to form CO(g). The steelmaker aims to sufficiently remove phosphorus and silicon before carbon reaches the final specification, usually around 0.05 wt% (Madias, 2014). Charges with 100% scrap have low carbon content, but primary steel introduces carbon contents between 1.6 and 4.5 wt%. A higher initial carbon content is often beneficial, because CO(g) provides good turbulence, reaction kinetics, and exothermic heat.

Alloying elements chromium and manganese may also oxidize in the EAF, but the rest of refining takes place in the ladle: desulfurization, deoxidation, metallic alloying, and degassing, reviewed in turn in each of the paragraphs below. The refining that takes place in

the ladle is known as "secondary metallurgy." To ensure a high temperature is maintained during these steps, the melt may be superheated by up to 100°C before tapping from the EAF. The main function of secondary metallurgy is to achieve the composition and temperature before casting, and exact processing depends on the final alloy and its application (Ghosh and Chatterjee, 2008).

Sulfur is a detrimental impurity, and must be reduced to less than 0.02wt%. It originates from iron ore, but it is still a serious concern in the EAF route. Sulfur reacts with iron to form FeS, which is completely miscible in the melt and has a low melting point. During hot working, this inclusion can melt and cause cracking. A basic slag, high melt temperature and low oxygen potential are required to remove sulfur in the reaction below (2.7). This process is typically performed in a tank degasser, with vigorous stirring and mixing between the melt and slag from argon bubbling under a vacuum envelope (steeluniversity, 2016). Sulfur may also be removed by adding reactants to form inclusions. Manganese can effectively tie up sulfur to form MnS, but these inclusions turn into "stringers" upon hot rolling, which can serve as sites for crack initiation. A calcium-aluminum alloy can alternatively be added to form hard, globular CaS inclusions (Kor and Glaws, 1998).

$$3(CaO) + 2\underline{Al} + 3\underline{S} \leftrightarrow 3(CaS) + (Al_2O_3) \qquad (2.7)$$

The ladle metallurgy steps aim to significantly reduce the concentration of oxygen. Carbon will react with remaining oxygen to form CO(g), which results in deleterious blow holes and porosity in the final product. Elements with a strong affinity for oxygen, known as deoxidizers, may be added. Silicon and manganese are often added together to form manganese silicates, which can then be removed by flotation. Aluminum is added for "killed" steels, but alumina inclusions may reduce fatigue resistance (Pretorius et al., 2010).

Metallic alloying elements are added after deoxidation. These elements may be in the form of a ferroalloy and simply melted and mixed into the steel. In Composition Adjustment by Sealed Argon Bubbling – Oxygen Blowing (CAS-OB), alloying additions are made under an inert atmosphere, to avoid oxidation losses. These additions can reduce the temperature of the melt, so aluminum is added with oxygen blowing for the exothermic reaction to Al_2O_3 (steeluniversity, 2016).

Degassing is a vital step of EAF steelmaking, typically performed at the end of refining. Nitrogen contamination is a significant concern in EAF steelmaking. The arcs from the melting electrodes ionize nitrogen in the atmosphere, so the nitrogen concentration of an

EAF melt is typically higher than a melt in the BOF route. Thus, EAF steels typically require more extensive degassing. Hydrogen is another concern (though not unique to the EAF route), entering the melt from water vapor, scrap, ferroalloys, mineral additions or the general atmosphere. Additionally, secondary metallurgy processes increase the susceptibility of the melt to gas pick-up: upon deoxidation, the equilibrium concentration of nitrogen and hydrogen increases; lime from desulfurization can introduce nitrogen; and de-slagging can expose the melt to the atmosphere. Gases remaining in the melt at the end of refining lead to porosity, which degrades mechanical properties, or hydrogen can cause catastrophic cracking. To reduce the concentration of gases, a vacuum, inert/CO(g) bubbling, or reactants may be employed. Vacuum degassing has become increasingly common as high quality steels are demanded. The lower chamber pressure displaces the equilibrium concentration of gases in the melt to lower levels. Bubbling is employed in tank and recirculation degassers. Inert gas or CO(g) bubbles have a low partial pressure of nitrogen and hydrogen, and so collect these gases. Aluminum could be added to the melt to tie up nitrogen to form aluminum nitrides, which act as grain refiners (Kor and Glaws, 1998).

The melt might be reheated at several points during refining by arc heating furnaces (in some designs, heating is simultaneous with degassing) or with oxygen injection alongside silicon and aluminum additions to maintain the correct temperature range. When the correct temperature and composition are achieved, the steel melt is cast. The EAF steelmaking process is summarized in Figure 2.11, and ladle refining in Figure 2.12.

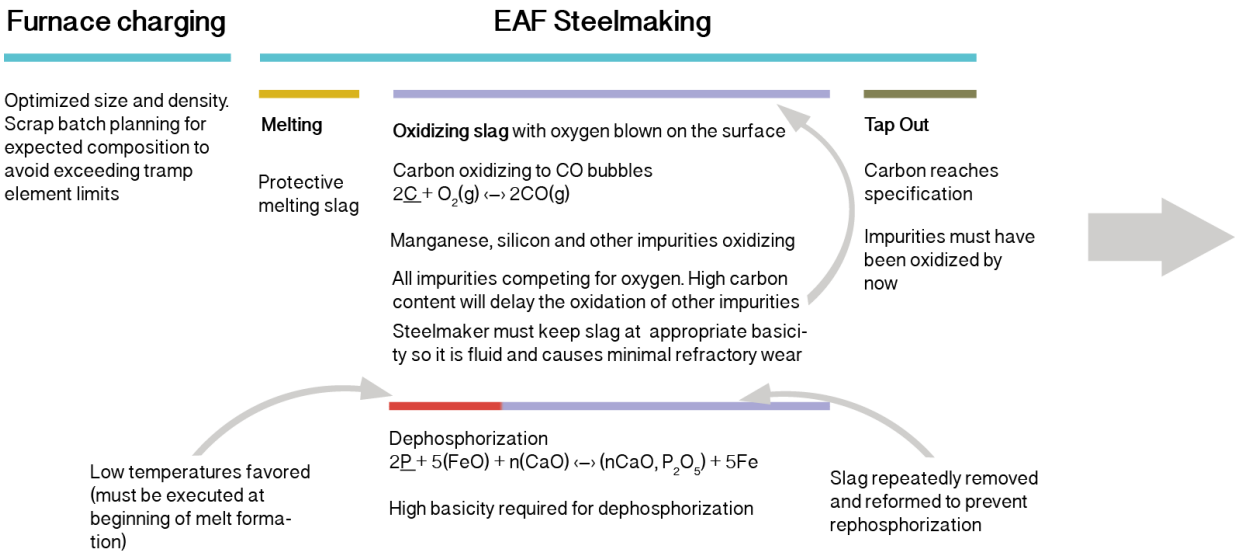

Figure 2.11: Sequence of EAF steelmaking. Information compiled from (International Iron and Steel Institute, 1983), (steeluniversity, 2016) and (Moore, 1981).

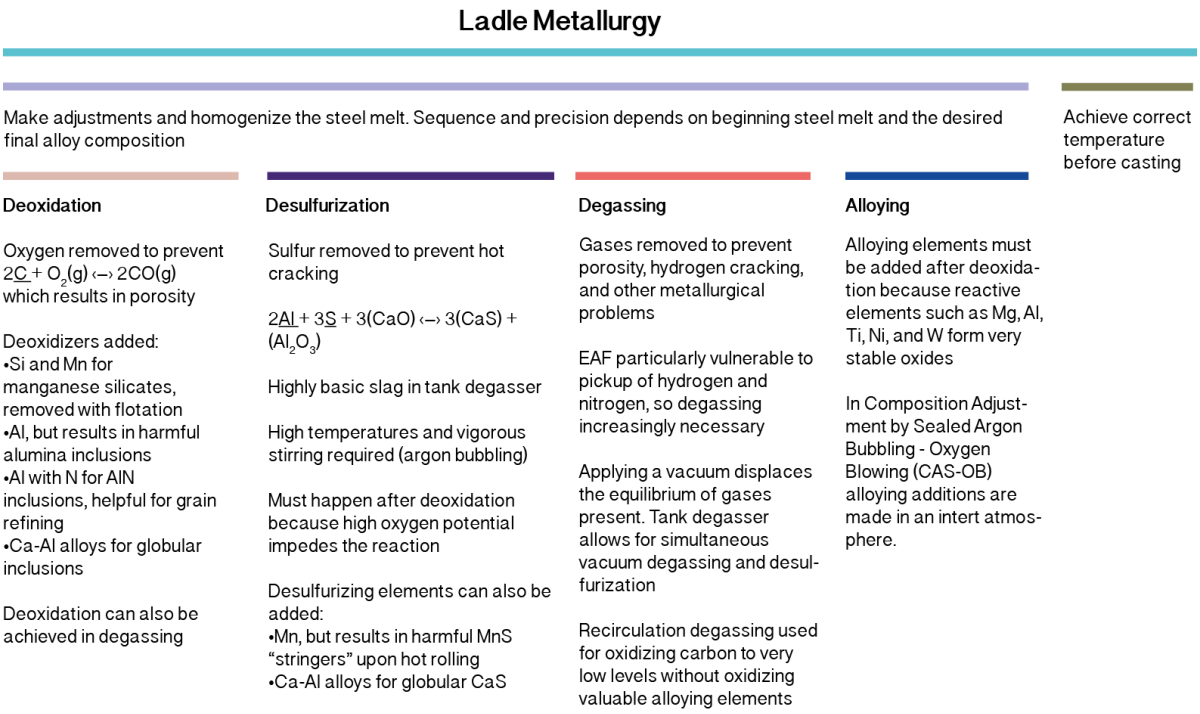

Figure 2.12: Sequence of ladle refining. Information compiled from (International Iron and Steel Institute, 1983), (steeluniversity, 2016) and (Moore, 1981).

EAF technology has advanced considerably, as reviewed by Manning and Fruehan (2001), and more recently by Toulouevski et al. (2010a) and Madias (2014). Toulouevski et al. (2010a) explain that from 1960 to present furnace productivity has increased more than 4 times, electrical energy consumption has halved, and electrode consumption reduced by 4-5 times, driven by increasing power of the EAF transformers, implementing secondary ladle metallurgy, intensive oxygen and carbon injection, slag foaming, and using hot metal in the charge. Meanwhile, melt cleanliness has generally improved, mainly due to the increasing use of vacuums to remove gases and non-metallic impurities. Steels requiring precise composition control for demanding applications, such as aircraft and aerospace, can be produced with techniques such as vacuum induction melting and electroslag refining.

Although the above innovations increase profitability and decrease inefficiencies, such as refractory wear and heat losses, these innovations have not necessarily reduced the CO_2-intensity of EAF steelmaking. The more intensive use of chemical heat, oxygen and carbon (11-18 kg additional carbon/tonne is used for the foamy slag practice) are direct sources of CO_2. However, there has been progress in greater utilization of byproducts and off-gases. Steel slag is commonly recycled to recover iron, produce cement and concrete, or may be directly applied in road construction (Yi et al., 2012). The energy in hot off-gases from the EAF can be recovered in further combustion or to pre-heat steel scrap. For example in the Consteel design (over 35 installations worldwide), scrap is continuously charged to the EAF

by a conveyor while it is preheated to 400-600°C to save 80 to 120 kWh/t (Jiemin et al., 2006). Further research seeks to treat coatings and contaminants present on end-of-life scrap, particularly zinc, during heating. Currently, these materials combust during heating, resulting in harmful dust and pollution (de Buzin et al., 2017). Porzio et al. (2016) review alternative pre-treatments, which include plastic pyrolysis and chloridizing zinc.

Overall, EAF steelmaking will remain an important and dynamic production route. It is highly flexible: the proportions of raw material inputs can be varied, and a wide range of final compositions can be achieved (Madias, 2014). Historically, EAF steel has been mainly cast as billets, which are then processed as long products, i.e. bars and rods, but the EAF product-line is diversifying. Thin slab casting and direct rolling produce sheets with high efficiency (Stubbles, 2000). The superior economics of EAF steelmaking, compared to integrated plants, will only become more obvious – the capital cost of mini-mills are 4 times less, labor costs are reduced by 3 times, and energy costs by more than 3 times (Toulouevski et al., 2010a). Steelmakers will seek to further utilize these advantages and penetrate more of the high-quality flat steel market.

2.2.3 Other options for copper control

The focus of this literature review has been on metallurgical extraction, but copper could be controlled by a range of techniques, before or after the steel melt. These options are reviewed below.

Improved liberation. An obvious method to separate copper and steel is through magnetic separation, but this technique is hindered by insufficient liberation, such that about 20% of the original copper remains (Katayama et al., 1997). Liberation could be improved through better disassembly, or better shredding. In disassembly, copper-containing parts are removed before further processing. Manual disassembly of ELV's is common in China, where the average copper concentration of EAF products is much lower (Daigo and Goto, 2015). The labor costs of this practice are thought to be too expensive in developed countries, but a study by Coates and Rahimifard (2007) assesses the economics of pre-fragmenting ELV's in the UK to find that the targeted removal of certain components is viable, especially as economic pressures and legislation shift to greater value recovery. Alternative shredding practices exist. Sawyer (1974) describes a 1964

study by General Motors that demonstrated a process that ripped an automobile hulk into eight or ten pieces, then shredded the pieces. GM concluded that copper levels of 0.12% could be achieved with this process. The density of shredded scrap determines the amount of copper that is magnetically removed. Newell (1996) describes higher-density shredding as a means for the scrap processor to attain cleaner scrap. Scrap is typically shred to 0.8 tonne/m^3, but increasing this to 1.1 tonne/m^3 or higher can ensure copper concentrations of 0.15wt% and less. Further, the distribution of copper varies with the size of the steel fragments. Aboussouan et al. (1999) used a series of sieve mesh sizes and found that most copper was removed with mesh sizes 20 to 60 mm. Simply sieving and separating this fraction would reduce copper by up to 90%. Katayama et al. (1997) describe cryogenic shredding and repeated magnetic separation to improve physical separation. At -100 to -200°C, plastic shearing changes to brittle fracture, preventing copper and steel from bonding and entangling, so 95% of copper could be removed. Simply re-iterating the magnetic separation can reduce copper concentration, to 0.15wt% with three passes. Lastly, magnetic forces could be enhanced in a ballistic separation system. Shattuck and Ramsdell (2018) describe ballistic separators, which use a fast belt and high magnetic attraction to reduce copper concentration to 0.16wt%.

Improved sorting. The human eye can easily differentiate between copper and steel pieces. Dalmjin and De Jong (2007) report that manual picking remains one of the most effective practices, and though expensive, it is performed when justified. Research aims to replace the human eye with a video camera and a computer to color analyze pictures in real time while a mechanical device diverts impurities. Sato et al. (1996) report this technique could be nearly 100% effective. Techniques such as laser-induced breakdown spectroscopy (LIBS) (as described by Gurell et al. (2012)) and X-ray fluorescence (XRF) (described by Gaustad et al., 2012) can perform rapid and precise elemental analysis, and could be applied to sort scrap by alloy type. This could be helpful when copper-rich products return for recycling, or to sort out highly alloyed steel parts. However, the technique detects composition at a single point, and cannot be applied to scan for heterogeneous impurities. To determine the total concentration of impurities in a pile of scrap, one option is to use gamma ray detection. Gamma rays bombard the scrap, and the neutrons generated from a secondary reaction are be analyzed to give a composite elemental analysis of the material. Gammatech neutron analyzers operate with at least 20 shredders in the US to measure copper, nickel, chromium, molybdenum and tin contents

of scrap pieces on a conveyor belt. Measuring the composition of a scrap source allows for directed extraction or further treatment (Russo, 2014). In a U.S. patent, Shulman (2011) describes a method to use real-time measurement of impurities, using neutron analysis, of scrap on a conveyor belt, to precisely divide the scrap into categories by copper concentration.

Scrap batching. Careful control of the input materials is key. Statistical computer-based batch-planning models are used to carefully combine a variety of scrap sources and primary materials (pig iron and DRI) for the proper charging density, as well as to avoid exceeding set tramp element limits. Gaustad et al. (2007) provide a description of current batch-planning models in the metal recycling industry and the scope for improvement. Copper-containing scrap can be directed to tolerant applications, or products that will utilize the improvement in strength and corrosion resistance. COR-TEN steel requires high copper contents, and the interaction with nickel prevents problematic hot shortness (Coburn, 1969).

Dilution. Primary steel can be added to the EAF to dilute residual elements. In the US, where the EAF route comprises 60% of production, natural gas is cheap, and DRI is widely used (Björkman and Samuelsson, 2013). However, dilution is expensive and undercuts the benefits of recycling, notably the environmental advantages. DRI melting consumes more electricity (Madias, 2017). These virgin materials also introduce other problematic impurities, primarily phosphorus and sulfur, which are difficult to control in the EAF route. These elements are becoming more prevalent as high-grade ore sources diminish (Tayeb, 2014).

Alleviate hot shortness. The evolution of hot shortness depends on the diffusion of copper and the oxidation of iron, which depends on the processing conditions of hot rolling. The processing parameters: temperature, gas composition and oxidation time, could be adjusted to ameliorate hot shortness and increase the tolerance of copper (Webler et al., 2008). Indeed, Rod et al. (2006) note that the tolerance limits of residual elements are empirical and have been set cautiously, arguing that the interactions of elements could be further studied to minimize adverse effects of residual elements. There are four main approaches to avoid hot shortness: suppress oxidation, occlude liquid copper into the scale, minimize copper diffusion/promote back-diffusion into the steel matrix, and

suppress the wettability of the liquid copper (Shibata et al., 2002). Near net shape casting and strip casting combine several of these approaches: the period in which oxidation and scale formation can occur is much shorter compared to conventional processing, a protective atmosphere is used, and in-line rolling allows for faster cooling rates (Ramadan et al., 2015). However, this casting technique restricts the thickness of steel products: 2-4mm in twin roll casting and 10-15mm in direct strip casting, compared to a conventional continuously cast slab (~25 cm thick) (Spitzer et al. 2003). Reducing oxygen in the atmosphere or the process temperature of conventional casting and rolling has been explored, but Webler (2008) notes that exposing steel products to problem temperatures and atmospheres during processing is unavoidable in practice. Sridhar (2016a) describes surface quenching for austenite decomposition and formation to disperse the copper-rich liquid within the finer grain structure. The composition of steel can also be manipulated to change oxidation and diffusion behavior. Nickel reduces the speed of copper diffusion and increases solubility in austenite (Yin et al., 2011), but it is an expensive addition. Silicon can cause copper to occlude in the oxide scale, by the formation of a liquid fayalitic slag ($FeO+2FeOSiO_2$). Sampson et al. (2013) show that between 0.1 and 0.2wt% of Si is effective to alleviate hot shortness. In another approach, Yamamoto et al. (2005) show copper can be heterogeneously nucleated at MnS precipitates in the austenite grains, and thus minimizes the formation of a surface liquid film. Understanding and accounting for the interactions of other impurities is important to manage hot shortness. Tin and arsenic decrease the solubility of copper in austenite and reduce the melting point of the liquid, so avoiding trace concentrations of these elements reduces the severity of hot shortness.

Reduce copper content in products. Upstream techniques have the potential to prevent copper from entering the scrap stream in the first instance. The use of copper in vehicles has been increasing. The Copper Development Association reports that a small car has about 15 kg copper, while a luxury car can have up to 28 kg, and electric and hybrid vehicles use twice this amount. Oba (2013) describes designs for aluminum wire harnesses for vehicles. Aluminum would be benign in steel recycling system (oxidizing to the slag), and the recommended wire harnesses could have a weight saving of up to 30%. Wire harnesses could also be designed to be easily detachable at end-of-life. Diegmann et al. (2000) describe a vehicle wiring system based on hook and loop fastening. Toyota (2015) is working on a wiring design that can be removed in one mechanical motion.

Thus, there are effective ways to control copper beyond separation. EAF mini-mills in the U.S. do not employ significantly improved scrap preparation practices, yet can produce automotive sheet steel, mainly through the use of DRI and amelioration processing techniques.

In total, the review in 2.2 has shown that there are many ways to improve current scrap practice. Copper could theoretically be removed with little energy from the steel melt, but the energy consumption in practice must be carefully evaluated. Options for copper control beyond extraction are viable, and must be considered as well.

2.3 Is there space for further development in an extraction process?

The third part (Q3) of this thesis further investigates opportunities revealed from the analysis in Chapter 4 (Q2). Chapter 4 identifies the process routes for copper removal that require significantly less specific energy. These process routes can then be further investigated to find specific areas for development. From this investigation, preferential melting was estimated to be particularly energy-efficient, if integrated into scrap heating. Further, an under-explored idea to improve the removal of liquid copper from solid steel was identified: to control the surface oxide on solid steel to minimize contact between liquid copper and solid steel.

Therefore, the review in 2.3 investigates the literature for preferential melting as an extraction technique. The first subsection, 2.3.1, seeks to understand when preferential melting is used as an extraction technique, and why it has not been used to separate copper from steel. The other metal systems that are commonly treated by preferential melting are discussed, and two main limitations for applying this technique to the copper-steel system are identified. The adherence, or wetting, behavior of liquid copper to solid steel must be understood, so relevant wetting principles are reviewed in 2.3.2. The oxide layer on the surface of the substrate determines wetting behavior, so subsection 2.3.3 reviews previous wetting observations of liquid metals on an oxidized iron surface.

2.3.1 Preferential melting as an extraction technique

Separating lower-melting point metals have from a base metal by melting is a long-established technique, known as sweating or preferential melting. There are many variations,

but the basic process is to heat the mixture above the melting point of the lower-melting metal, and then collect it. Designs are detailed in a range of patents, dating back to at least 1936 (Lindner).

Sweating is used most prominently in the aluminum industry. As reviewed by Gaustad et al. (2012), a reverberatory or rotary furnace is used, within which the temperature is stepped and held at different intervals to tap out contaminating metals with lower melting temperatures than aluminum, typically tin (232°C), lead (327°C) and zinc (419°C). Alternatively, aluminum could be melted and separated from solid metal pieces such as iron. For example, in aluminum can recycling, sweating furnaces periodically tap liquid aluminum to separate from other solid metals. A key part of the process is the use of a melting salt or flux, which promotes the coalescence of the liquid metals and limits oxidation (U.S. Environmental Protection Agency). In the aluminum industry, chloride and fluoride molten salts are used. These fluxes act to weaken the oxide layer during cleaning and promote metal/oxide separation by favoring coalescence of metallic droplets within the dross (Afshar et al., 2004). The liquid metal is also protected from the atmosphere to limit oxidation.

Researchers have long considered applying preferential melting to copper and steel. Brown and Block (1968) from the U.S. Bureau of Mines first investigated the process by statically holding samples of copper winding on steel in oxidizing, inert and reducing atmospheres at temperatures above the melting point of copper. The authors observed entrapment of the liquid copper between the oxide scale and substrate in an oxidizing atmosphere, but observed direct brazing of copper to steel in a reducing atmosphere. Elger et al. (1968) attempted to remove copper from steel scrap, but used a rotary kiln in different atmospheres. Again, copper entrapment under the oxide was observed and the authors concluded copper separation in this process route is poor. More recently, a patent by Bratina et al. (2013) proposes a design to remove "copper meatballs" from automobile scrap using a tunnel kiln furnace where liquid copper is collected through apertures at the bottom of the furnace. The temperatures and atmospheres employed by the design are not detailed, but a shield to prevent iron from heavy oxidation is noted.

In practice, there are two main limitations to applying the preferential melting technique to copper and steel: the irregular shape of end-of-life scrap, and the adherence of liquid copper to the surface of solid steel. Liquid copper could flow into the crevices of fragmented pieces, undermining separation, as described by Katayama et al. (1997). However, process design could overcome this limitation by applying mechanical force, such as shaking

and agitation. Adherence behavior determines the force that must be applied to achieve separation, and thus overall feasibility. Therefore, adherence of liquid copper to the solid steel surface must be investigated first.

2.3.2 Relevant wetting principles

The adherence behavior of a liquid metal to a solid substrate can be studied using methods and theory established in surface sciences. The aptitude of a liquid metal to wet a solid surface is a property intrinsic to the particular liquid-solid-vapor system, and is characterized by the shape of the liquid droplet. The sessile drop technique is a standard experimental method to observe wetting behavior and measure the droplet shape – most commonly Young's contact angle, θ_Y, shown on the droplet in Figure 2.13.

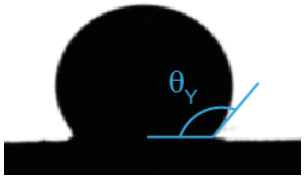

Figure 2.13: The Young's contact angle of a liquid droplet.

The Young's contact angle derives from the surface energies of the system (below). γ_S and γ_L refer to the surface energy of the solid and liquid respectively, and γ_{SL} the solid/liquid interface energy (Young, 1805).

$$cos\theta_Y = \frac{\gamma_S - \gamma_{SL}}{\gamma_L} \tag{2.8}$$

The condition for wetting is typically defined by θ_Y<90, also defined in the equation below.

$$\gamma_S > \gamma_L cos\theta + \gamma_{SL} \tag{2.9}$$

The wetting behavior of many metal/metal systems has been studied, and the determined trends provide useful context. Generally, a liquid metal will wet to another metal, and the system could be reactive or non-reactive. In a reactive system, the spreading of the liquid metal is driven by the formation of an intermetallic or diffusing into solution. In these systems, the liquid metal initially spreads and wetting can be rapid. In the absence of

interfacial reactions, wetting of the liquid metal over a solid metal substrate is still favorable, driven by a reduction in surface energy (Eustanthopolus, 2015). Formation of intermetallic compounds and solid solutions by two phases always leads to at least initial spreading.

The iron-copper system is one of the most prevalent mixtures used in the powder metallurgy industry, and the wetting of copper to iron has been extensively studied (Froschauer et al., 1975). Researchers have shown that liquid copper will spread across iron – diffusing through grains and penetrating grain boundaries until the maximum solubility of copper is reached, as characterized by Fredriksson et al. (2001). The iron-copper system does not form intermetallics. In a reducing atmosphere, the contact angle is 0° (Whalen et al., 1967), and the surface energy quantities have been measured for the pure Cu-Fe system, as reported by Burke (1968).

Most metal substrates are not metallic at the surface, but have a native oxide layer from exposure to air. Oxides have a lower surface energy than the metallic state so the above criterion ($\sigma_S > \sigma_L$) is not met, and non-wetting is observed (Eustathopulus et al., 1999). However, the liquid metal will interact with the oxide. At high temperature, a liquid metal may dissolve the oxide, but the extent depends on the favorability of the dissolution reaction. From this reaction, oxygen in solution with the liquid metal increases and oxygen clusters with partially ionic character may form. These clusters then develop Coulombian interactions with the ionocovalent surface and adsorb strongly at the metal/oxide interface to promote wetting. The Cu-Fe_3O_4 system exhibits this behavior, as shown by Eustanthopolus and Drevet (1994). Fe-O clusters adsorb at the interface, to promote wetting for an equilibrium contact angle of 60-100°. Systems exhibiting this type of behavior are particularly sensitive to oxygen in the atmosphere, which changes the surface tension of the liquid metal and increases the concentration of adsorbing clusters at the interface.

2.3.3 Investigations into wetting on oxidized iron surface

As shown above, the wetting behavior of liquid copper on iron, and liquid copper on Fe_3O_4 are well-understood. However, the system becomes more complicated when iron oxide is present as a layer between the liquid copper and steel substrate. Bondi (1953) states that "thin layers – monolayers – of oxide or sulfide and organic contamination is sufficient to prevent wetting by most liquid metals." However, the oxide layer does not assure permanent non-wetting. Many liquid metals will in due course lift the oxide layer, or migrate to the base

metal-oxide interface from a hole or defect in the oxide layer. Experimental examination of any given pair of materials is therefore required to understand these behaviors.

Steel forms a complex surface scale of three oxides in air at high temperature. The oxidation of iron has been studied extensively, as reviewed by Chen and Yuen (2002). The thickness, composition and mechanical properties of the iron oxide scale can vary widely, depending on the process history and composition of the steel, present heating conditions, atmosphere and reductants. At temperatures below 570°C, iron forms a two-layer scale of Fe_3O_4 and Fe_2O_3 (Fe_3O_4 is next to the metal). Above 570°C, FeO, wüstite, grows rapidly at the substrate/scale interface and has a porous structure, while more compact Fe_3O_4, magnetite, and Fe_2O_3, hematite, are present in much smaller proportions (4% and 1%, respectively, at 1000°C) at the outer surface of the scale. The mobility of cations and electrons in wüstite is extremely high, so thick scales develop rapidly at high temperatures. The partial pressure of oxygen for iron oxide formation is extremely low. Iron oxide forms nearly instantaneously after exposure to air, as Nelson (1937) shows a 1nm thick layer develops after seconds at room temperature.

Existing experimental work investigates the wetting behavior of the copper/steel system, considering the intervening oxide layer. As stated earlier, Brown and Block (1968) observed entrapment of the liquid copper between the oxide scale and substrate in an oxidizing atmosphere, but direct brazing in a reducing atmosphere. To further investigate the interaction of copper with the iron scale, Hara (1996) varied CO/CO_2(g) to promote scales with different phases dominant: FeO, Fe_2O_3 and Fe_3O_4. The work of adhesion of copper was greatest when FeO was dominant. The authors hypothesized that copper wetted due to the porous structure, and copper could be melted away from steel when compact Fe_2O_3 and Fe_3O_4 were present.

Later studies explore not just the influence of the type of iron oxide, but the evolution of wetting behavior as the oxide scale is reduced or otherwise disrupted. Bernardo et al. (2016) varied the compositions of copper alloys and Fe-based substrates in inert and reducing atmospheres with the goal to improve wetting for sintering applications. Non-wetting was observed with copper on a pure Fe substrate in an argon atmosphere, but when any reductants were present in the system, including carbon in 0.5wt%C steel, the oxide layer was reduced to allow complete wetting within 60 seconds. Takahira et al. (2005) observed “unusual” wetting behavior of liquid copper as a pre-oxidized iron sample was heated in a reducing atmosphere. The liquid metal rapidly proliferated through the porous structure. Studies of similar systems

show the iron oxide scale may be susceptible to penetration of liquid metal. In a study by Protsenko et al. (2005) droplets of Pb and Pb-Bi alloys (which do not form intermetallics or exhibit solubility with iron), were formed on thin oxide layers present on Fe and steel substrates in low pO_2 environments. Contact angles were close to or lower than 90°. Liquid metal penetrated defects in the oxide film (pores, microcracks) and established direct contact with the solid. Shen et al. (2015) observed liquid tin wetting on iron and found that the iron oxide film was tenacious, even at low pO_2, but disruption of the oxide allowed for wetting and interfacial reactions.

Findings from copper hot shortness investigations are also relevant to understand the interaction of copper with iron oxide. In hot shortness, liquid copper collects at the interface between the steel substrate and iron oxide layer. Researchers have studied the interaction of copper with the oxide scale, finding that the behavior of copper is determined by the morphology and structure of the scale layer. Kondo (2011) observed the distribution of copper during the oxidation of copper-containing steels, and found copper in solid solution with the upper magnetite (Fe_3O_4) layer and along the grain boundaries of the wüstite layer as a metal, showing that liquid copper can migrate within the scale.

As can be seen above, the iron oxide layer is not universally protective. Wetting behavior is highly sensitive to the system conditions (temperature, atmosphere, surface roughness, substrate composition as reviewed by Komolafe et al. (2014)), but substances can be applied to the substrate surface to control behavior and reduce sensitivity. Fluxes are commonly applied in a wide range of systems, and act to dissolve the oxides present to promote wetting. To promote non-wetting, coatings may provide a barrier. Leak and Fine (1973) applied a range of coatings, organic and inorganic pre-dips and braze inhibitors, to promote sweating of liquid copper from steel. The most successful were sodium metasilicate (Na_2SiO_3), which is chemically inert, and sodium sulphate (Na_2SO_4), which modifies the oxidation reaction of steel. The authors submerged motor armatures in a neutral molten salt medium and found nearly complete separation of copper from steel when the specified coatings were first applied. However, multiple variables could have contributed to this result. The composition of the steel was not stated. The proportion of copper present was high, which promotes liquation, and the motors were shaken and dropped to further remove copper. Therefore, the role these coatings played in achieving non-wetting is not directly known, but is worth further investigation.

2.4 Gaps in the literature

The existing literature provides partial answers to the three leading questions. Here, the remaining "gaps" in knowledge are defined. The analyses in Chapters 3, 4, and 5 then aim to address the questions that cannot be answered with the current literature, but that are key to developing a strategy to manage copper contamination in end-of-life steel recycling.

Q1. How does copper constrain steel recycling?

The effect copper has on the properties of an individual steel product are generally well-understood, but the impacts of these metallurgical effects on the greater steel system are less clear. Systemic impacts have been explored in studies with different contexts and scope, but a significant gap remains: copper contamination has not been modeled and evaluated at a global scale. Since steel scrap is globally traded, understanding copper contamination at this level is essential. For how long can the current practice of dilution, scrap mixing, and international trade be used to manage copper, considering the tolerance of demanded products? In addition to evaluating how copper contamination constrains the overall steel system, the constraints on product-loops must be considered as well. Vehicle recycling is particularly effected by copper contamination, and closed-loop recycling of vehicle steel would be beneficial to retain alloying elements. What would be required to allow a closed-loop or "circular economy" approach to car production, with new car bodies made from steel recycled from old cars?

Q2. Can copper be extracted from steel, and what would be the energy and material requirements of a potential process?

The review in 2.2 finds that there are a range of approaches that could be employed to reduce the copper content of scrap, or alleviate the effects of hot shortness. The implementation of these options must be considered. In regards to separation, copper extraction from an iron melt is theoretically feasible. However, to estimate the energy requirements of a separation process in practice, the relevant mechanisms must be identified, and process models constructed. Further, EAF steelmaking is a mature industry, and any new process must consider the overall compositional balance achieved in the series of refining steps. Overall, there has been no integrated assessment of the energy and material inputs required to remove copper from steel. An evaluation of the energy and material inputs required to extract copper from steel would inform the feasibility of recycling end-of-life steel

in a closed loop. The results would also serve as a guide for further development of viable copper extraction processes.

Q3. Is there space for further development in an extraction process?

The key question remaining from the review in 2.3 is whether a process window exists to minimize the wetting of liquid copper to solid steel. A surface oxide layer, or non-metallic coating would provide a barrier to metallic contact, but this surface layer could be compromised. Diffusion of liquid copper into the steel substrate, as well as chemical dissolution, reduction, and mechanical disruption of the oxide are known mechanisms to promote wetting. Carbon content, initial surface oxidation and coatings determine the operation of these mechanisms. The individual and combined effects of these variables on the wetting behavior of copper on steel has not yet been systematically studied, but such an investigation would provide a basis for defining a viable process window for preferentially melting liquid copper away from solid steel scrap.

Chapter 3. How will copper contamination constrain global steel recycling?

The content of this chapter has been published in Environmental Science and Technology as "How will copper contamination constrain global steel recycling?" My co-authors contributed comments on draft versions of this paper. Dr. Rick Lupton, a post-doc in the group, provided guidance on the uncertainty analysis, and performed the Monte Carlo simulations for varying the range of values for copper content in scrap and copper tolerance across all products.

In the overall global steel system, primary production has expanded rapidly over the last 20 years. Björkman et al. (2013) report that the average copper content of secondary steel has actually decreased. An informed strategy for future steel recycling must account for these dynamics, and question whether and when copper may limit the amount of steel that can be recycled. This chapter presents the methodology (3.1), results (3.2) and discussion (3.3) to understand how copper contamination constrains global steel recycling.

3.1 Methodology

A model of copper in the global steel system, which can account for all the possible applications for scrap, as well as the availability of primary steel, must be constructed to determine when scrap allocation and dilution will no longer be viable strategies. A number of methodologies exist, as discussed in 2.1.2, and the corresponding advantages and limitations are summarized in Figure 3.1.

Method	Scope	Reveals	Limitations
LCA, exergetic LCA	Isolated product loop	Dilution/mixing losses, extent of closed loop recycling	Wider scrap uses not considered Savings from avoiding dilution may not be true, as recycling would not prevent this demand
WIO/MFA, dynamic or static, with scrap/product categories by copper concentration	Whole system	Scrap destinations, maximum recycling rates	Model assumptions: Regional boundaries Time scale Resolution of scrap/product categories Data quality Validity of scenarios
with Material Pinch Analysis		Scrap/demanded product allocation	Scrap categories mix in practice

Figure 3.1: Comparison of methodologies for studying the systemic impacts of copper contamination.

This analysis aims to characterize copper in the whole steel system from physical data. Most previous studies described in 2.1.2 use input-output tables as the primary data source, but metal tonnages do not translate directly from monetary flows, and double counting is possible due to trade in multiple regions (Cooper and Allwood, 2012). The recent work by Pauliuk et al. (2013b) and Cullen et al. (2012) provide steel quantity estimates, based on physical data. This work provides the basis for a global model, covering the time period from 1950 to 2100, and with sufficient category resolution: by four end-use sectors.

Data on copper concentration must be layered with the model of the steel system, but this is limited and scattered. Reported values in the literature will be used to estimate a range. A visual representation of how copper distributes from raw materials to final products has not been presented in previous studies. The Sankey diagram by Cullen et al. (2012) will be used to illustrate how copper may distribute through the supply chain. This process is described in 3.1.1.

Once copper is characterized in the current steel system, the future steel system can be investigated, described in 3.1.2. Available data of copper contamination arising from current scrap preparation practices will be projected forward to understand when current practice will no longer be viable. The total amount of copper in the scrap supply and the amount that can be tolerated by demand provides a succinct limit to the extent copper can be managed by dilution and globally trading scrap. Sensitivity analysis will be used to show the effect of changing variables, given the uncertainty of estimating future steel quantity and composition. Sensitivity analysis is performed instead of scenario analysis, because scenarios combine multiple variables to obscure the effect of any one action. A version of material pinch analysis will also be presented for the baseline case to show possible destinies of scrap sources by copper concentration, and demanded products by copper tolerance, and the extent of dilution that would be required.

The above analysis assumes that scrap can distribute to any tolerant application, but product loops are important to understand. The retention of alloying elements would be beneficial, and examining a subset of the system more clearly elucidates the supply chain and possible interventions. Therefore, vehicles within the system will be also traced, as described in 3.1.3.

In sum, presenting the results of copper in the steel system in different ways (visually as copper flows through the steel system, as a comparison between the total amount of copper entering the steel system and the amount of copper tolerable by demanded products, as

material pinch analysis and tracing vehicles as an isolated product group) evaluates the multiple ways copper constrains steel recycling.

3.1.1 End-of-life scrap and copper in the present global steel system

To develop an analysis of copper concentration, the 2008 Sankey diagram by Cullen et al. (2012) is used as a framework. The quantity and composition of scrap must first be estimated, followed by tracing the distribution of scrap to final products, and estimating the copper tolerance of all products, as summarized in Figure 3.2. Limited data are available, but all available data were catalogued and collated to inform the present estimates.

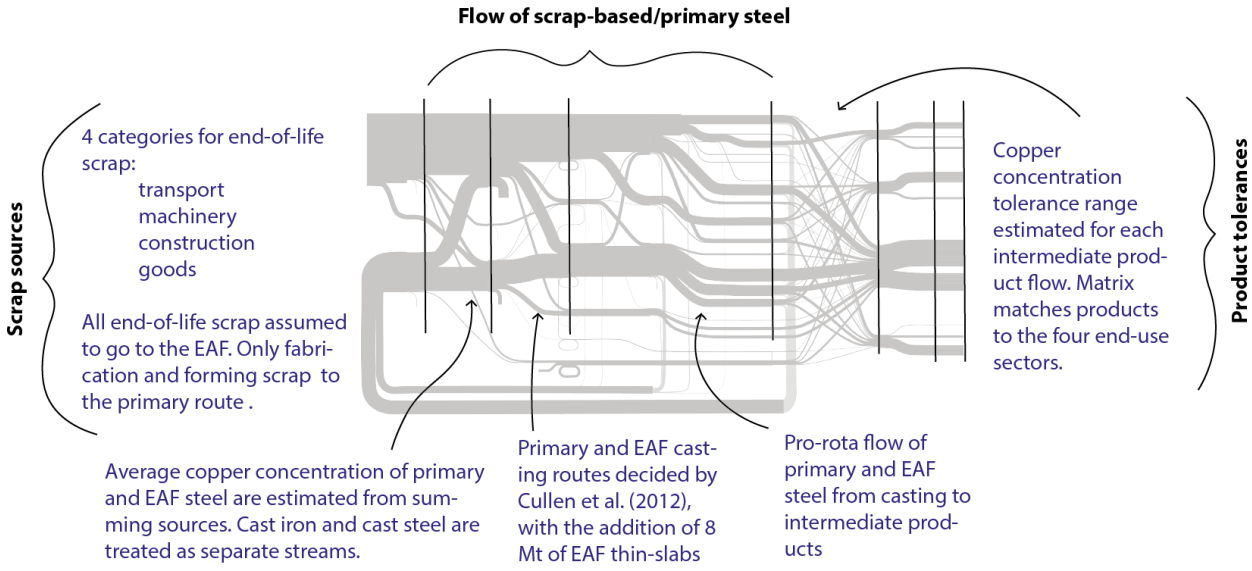

Figure 3.2: Summary of methodology for applying copper concentration data to the current global steel supply chain.

Scrap sources.

The total end-of-life steel scrap supply (~298 Mt) must be disaggregated into several categories to estimate the copper content of the scrap. Data on world steel discards by category are not available, but Pauliuk et al. (2013b) and Hatayama et al. (2010) provide modeled estimates of past and future global steel discards. Pauliuk et al. (2013b) disaggregates the global old scrap supply by four end-use sectors from 1950-2100. Hatayama et al. (2010) provide figures of global discard of steel by eight end-use categories from 1980-2005 determined by their dynamic MFA model. To compare the estimates by Hatayama et al. (2010) to Pauliuk et al. (2013b), the categories of civil and building were consolidated to construction, electrical appliances and machinery to machinery, vehicles, ships and half of

other to transportation and containers and packaging and half of other to goods. The discards were also multiplied by an assumed end-of-life discard recovery rate of 80% (worldsteel, 2010) to yield the quantities in Table 3.1. Table 3.1 shows both sources are largely in agreement. As the construction, machinery, transport and goods category match with the end-use mapping used by Cullen et al. (2012), the scrap category quantities by Pauliuk et al. (2013b) are used for the remainder of the analysis. These quantities are for available scrap supply, so scrap recovery losses are already accounted for.

Table 3.1: Global end-of-life steel scrap supply in 2008 by four end-use categories from Hatayama et al. (2010) and Pauliuk et al. (2013b).

Source	Total	Construction	Machinery	Transport	Goods
Wang et al.	296	59	86	95	55
Pauliuk et al.	298	68	81	107	42

Next, the copper concentration of the above scrap categories (construction, machinery, transport and goods) must be estimated. Scrap composition may be reported by scrap grades, or scrap type (shredded, ELV, general obsolete). Data on copper concentration has been measured at different times, places and with different sampling procedures. Table 3.2 presents available copper concentration data for different scrap types. The copper content of shredded scrap is often reported, which combines transport, machinery and goods scrap. The USGS (2010) and Brahmst (2006) report that cars make up the majority of shredded scrap in the US and Canada. Manouchehri (2006) reports the make-up of shredded scrap in a Swedish plant, where cars make up about 20%, industrial wastes 40-50%, and household/municipal waste 30%. Klempner (1999) surveyed eight shredding companies and found that shredded scrap is made up of 15-50% appliances, 5-15% other, and 45-80% automobiles.

Table 3.2: Reported copper concentration of scrap types used to inform copper content of scrap categories.

Relevant category	Scrap type	Reported wt% Cu	Reference
Transport	Shredded autos	0.4 (converter route), 0.68 (EAF route)	Daigo et al., 2005
		0.7	Ginsel et al., 2011
		0.23	Schrade et al., 2006
		0.28	Igarashi et al., 2007
Industrial equipment	Machine scrap	0.4 (converter route), 0.68 (EAF route)	Ginsel et al., 2011
		0.49	Igarashi et al., 2007
Construction	Construction	0.01 (converter route), time-dependent (EAF route)	Daigo et al., 2005
	Plate and structural	0.365	Pretorius et al., 2010
	Demolition	0.1	Internal industry presentation
Goods	Containers	0.005 (converter route), 0.287 (EAF route)	Daigo et al., 2005
	Other	0.017 (converter route), 0.275 (EAF route)	Daigo et al., 2005
	Can scrap	0.05	Schrade et al., 2006
	Shredded scrap from municipal waste incinerators	<0.5	EUROFER, 2016
	Waste electronic equipment	2.3	Ginsel et al., 2011
	Incineration bottom ash	1	Ginsel et al., 2011
Transport, Machinery, Goods	Shredded	<0.25	EUROFER, 2016
		0.28	Hatayama, 2014
		0.31	Savov et al., 2003
		0.22	Pretorius et al., 2010
All	E3 (obsolete scrap)	<0.25	EUROFER, 2016
	E1 (obsolete scrap)	<0.4	EUROFER, 2016
	1 and 2 heavy melting scrap	0.25	ISRI, 2016
	Obsolete scrap	0.17	Savov et al., 2003
	Low quality scrap for EAF	0.49	Igarashi et al., 2007

Figure 3.3 plots all of the measured copper concentration values found in the literature. The description and reference for each point can be found in the Appendix, Table A1.1. The values that fall directly into the construction, industrial equipment, transport and goods scrap categories are plotted, as well as values for scrap types (shredder, bundelings, home, heavy and busheling) that combine these categories. The overall values for EAF/obsolete scrap and the copper concentration in the primary route are plotted as well.

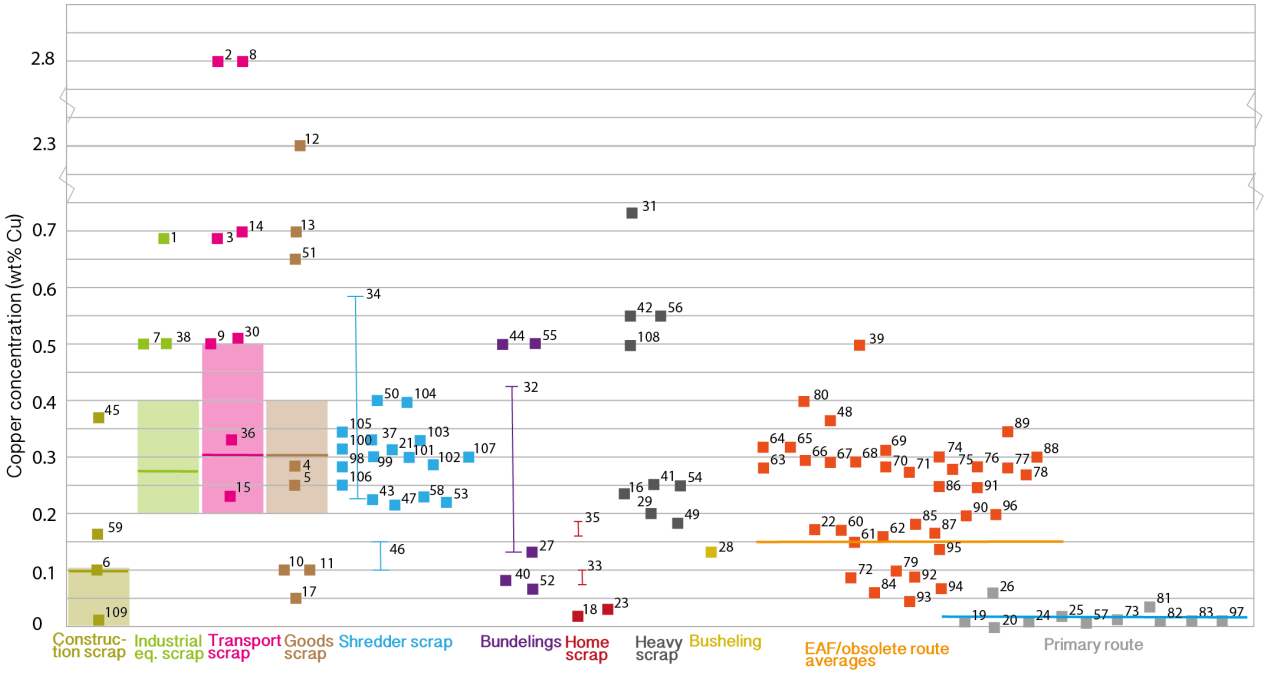

Figure 3.3: Plot of measured copper concentration values collected from the literature, colored by category and numbered to correspond with Table A1.1. The range of copper concentration assigned to construction, industrial equipment, transport and goods scrap are shown. The orange line is the calculated average EAF steel value and the blue line is the calculated average primary steel value.

The reported copper contents of EAF steel products can also be used to inform the copper concentration of the scrap categories. The copper concentration of EAF products reported in the literature is collated in Table A2.2. Again, these values are reported for different regions and years, but the majority of values are between 0.2 and 0.3wt% Cu. From this data, a copper concentration range (high, low and expected values) was assigned for each scrap category, shown in Table 3.3.

Table 3.3: Range of copper concentrations of scrap source categories decided for this analysis.

	Copper Concentration (wt %)		
Scrap Source	Expected	Low	High
Transport	0.3	0.2	0.5
Machinery	0.25	0.2	0.4
Construction	0.1	0	0.1
Goods	0.4	0.2	0.3

Scrap to products.

The next step is to understand how scrap may distribute to products. A vast range of steel compositions are produced in the primary and secondary routes. Here, the supply sources

entering the oxygen blown converter and EAF are summed to give an overall global average of copper concentration in these two routes, shown in Table 3.4. It was assumed that all end-of-life scrap was charged to the EAF (consistent with Nakamura et al., 2014), with only forming and fabrication scrap charged to the oxygen blown converter.

Table 3.4: Estimated copper concentrations and quantities of inputs into the primary and secondary routes.

Route	Supply Source	Estimated Cu Conc. (%)	Quantity (Mt)	Average Cu Conc. (%)
Primary	Iron Ore	0.01	826	0.02
	Primary Circulation Scrap	0.02	165	
	EAF Circulation Scrap	0.15	41	
EAF	Pig Iron	0.01	45	0.15
	DRI	0.01	66	
	Primary Circulation Scrap	0.02	50	
	EAF Circulation Scrap	0.15	12	
	Transport Scrap	0.3	107	
	Machinery Scrap	0.2	81	
	Construction Scrap	0.1	68	
	Goods Scrap	0.3	42	

The average copper concentration of 0.02% for primary steel is consistent with the values in Figure 3.3. The average concentration of 0.15% for EAF steel may be low compared to the values in Figure 3.3; however, the majority of data points comes from Japan, where end-of-life scrap is a high fraction of the material charged to the EAF. As reported by Daigo and Goto (2015), the bars made from EAF steel in China contain an average of 0.1wt% copper.

With the composition and quantities of inputs into the primary and secondary routes estimated, the next step is casting. Steel from the BOF and EAF is cast into semi-finished products: slabs, ingots, billets and blooms. Cullen et al. (2012) provide the quantities of each casting product. EAF steel is not widely cast into slabs (Schrade, 2006), but instead into billets and blooms that become long products. This is further supported by work from worldsteel (2016) which uses plant data to show that globally most BOF's produce flat products, and most EAF's produce long products. Some mini-mills in the U.S. cast EAF steel into thin slabs (dividing 2008 US finished steel production, 89.4 Mt, into flat products, 47 Mt, and long products, 42 Mt, and assuming all BOF steel, 39 Mt, is first used for long products, this means at least 8 Mt of EAF steel must cast into slabs for flat products in 2008 (USGS, 2010)). From casting, primary and secondary steel to intermediate products are

distributed on a pro-rota basis. The matrix by Cullen et al. (2012) then matches intermediate products to end-use products and sectors, to give the percentage of EAF steel used in these applications (Tables 3.5 and 3.6, respectively). There are yield losses at each process along the supply chain, as estimated by Cullen et al., which are illustrated by the dark gray lines pointed downwards in the Sankey diagram (Figure 3.6).

Table 3.5: Estimated percentage of EAF steel by pro-rota flow to each product.

End-Use Product	% EAF (%)
Cars	14
Trucks	25
Ships/Other	5
Mechanical Equipment	22
Electrical Equipment	21
Buildings	41
Infrastructure	40
Packaging	0
Appliances	7
Other	31

Table 3.6: Estimated percentage of EAF steel by pro-rota flow to each sector.

Sector	% EAF (%)
Construction	38
Vehicles	16
Industrial Equipment	22
Metal Goods	28

There is no data on the destination of secondary and primary steel to products or sectors at the global scale. However, the proportions above can be compared to the use patterns of Japanese steel use determined by Nakamura et al. (2012) using input-output analysis, showing 82.6% of old scrap goes to construction steel, with 16.4% of old scrap being used for machinery steel. The present results from the assumed pro-rota distribution have more generous proportions of EAF steel for use in industrial equipment and metal goods. The estimated flow of primary and secondary steel derives mainly from the casting routes, and the proportions thus reflect the amount of long products used by the sectors. The different copper tolerances of the intermediate products has not been accounted for, though this influences the proportion of old scrap that would be used. The copper tolerance of each intermediate

product is determined next, which further informs which streams are likely to have higher proportions of end-of-life scrap.

Copper tolerance of end-use products.

The flow of scrap to end-use products is determined partly by the casting routes, but also by the copper tolerance of the specific product stream. The copper tolerance of a product will determine if it is made from primary or EAF steel, and if made from EAF steel, the proportion of end-of-life scrap. Copper tolerances depend on both the product type/shape and its application. The literature was reviewed to determine typical quality requirements for steel products, and the collected information is presented in Tables A1.3 and A1.4. Table 3.7 presents the copper tolerance ranges assigned to each intermediate product flow. The flow was colored according to tolerance in the Sankey diagram, to illustrate the likely prevalence of end-of-life scrap in each flow.

Table 3.7: Copper tolerance ranges for each intermediate to end-use sector flow.

End-Use Sector	Product	Estimated Cu tolerance (wt%)	High (wt%)	Low (wt%)	Reason/Reference	Color
Vehicles	Wire Rod	0.1	0.2	0.1	Commercial quality, possible drawing	Blue
	Hot Rolled Bar	0.15	0.2	0.1	Commercial quality, shaped	Pale Orange
	Plate	0.15	0.2	0.1	Commercial quality, shaped	Pale Orange
	Hot Rolled Coil	0.15	0.2	0.1	Hatayama et al., 2014	Pale Orange
	Cold Rolled Coil Galvanized	0.06	0.1	0.06	Hatayama et al., 2014, deep drawing quality	Light Blue
	Welded Tube	0.15	0.2	0.1	Commercial quality, shaped	Pale Orange
	Seamless Tube	0.15	0.2	0.1	Commercial quality, shaped	Pale Orange
	Cast Iron	-	-	-		Green
Industrial equipment	Rail	0.15	0.2	0.1	Commercial quality, shaped	Pale Orange
	Wire Rod	0.1	0.2	0.1	Commercial quality, possible drawing	Blue
	Hot Rolled Bar	0.15	0.2	0.1	Commercial quality, shaped	Pale Orange
	Plate	0.15	0.2	0.1	Commercial quality, shaped	Pale Orange
	Hot Rolled Coil	0.1	0.15	0.06	Commercial quality, flat	Blue
	Cold Rolled Coil	0.06	0.1	0.06	Drawing quality	Light Blue
	Electrical Sheet	0.06	0.15	0.06	Drawing quality	Light Blue
	Welded Tube	0.15	0.2	0.1	Commercial quality, shaped	Pale Orange
	Seamless Tube	0.15	0.2	0.1	Commercial quality, shaped	Pale Orange
	Cast Iron	-	-	-		Green
	Cast Steel	-	-	-		Purple
Construc-tion	Light Section	0.3	0.3	0.2	Section	Orange
	Heavy Section	0.3	0.3	0.2	Section	Orange
	Rail	0.3	0.3	0.2	Section	Orange
	Rebar	0.4	0.5	0.4	Rebar	Dark Orange
	Wire Rod	0.15	0.2	0.1	Wire rod reference	Pale Orange
	Hot Rolled Bar	0.2	0.3	0.1	Construction quality	Light Orange
	Plate	0.15	0.2	0.1	Commercial quality, shaped	Pale Orange
	Hot Rolled Coil	0.2	0.2	0.06	Construction quality	Light Orange
	Hot Rolled Coil Galvanized	0.2	0.2	0.06	Construction quality	Light Orange
	Hot Rolled Narrow Strip	0.2	0.2	0.06	Construction quality	Light Orange

	Product	Estimated Cu tolerance (wt%)	High (wt%)	Low (wt%)	Reason/Reference	Color
Construc-tion	Cold Rolled Coil	0.1	0.2	0.06	Construction/drawing quality	Blue
	Welded Tube	0.15	0.2	0.1	Commercial quality, shaped	Pale Orange
	Seamless Tube	0.15	0.2	0.1	Commercial quality, shaped	Pale Orange
	Cast Iron	-	-	-		Green
	Wire Rod	0.1	0.2	0.06	Commercial/drawing quality	Blue
	Hot Rolled Bar	0.15	0.2	0.1	Commercial quality, shaped	Pale Orange
	Plate	0.15	0.2	0.1	Commercial quality, shaped	Pale Orange
	Hot Rolled Coil	0.1	0.15	0.06	Commercial quality, flat	Blue
	Hot Rolled Narrow Strip	0.1	0.15	0.06	Commercial quality, flat	Blue
	Cold Rolled Coil	0.06	0.15	0.06	Drawing quality	Light Blue
	Cold Rolled Coil Coated	0.06	0.06	0.04	Drawing quality	Light Blue
	Cold Rolled Coil Tinned	0.06	0.06	0.04	Drawing quality	Light Blue
	Welded Tube	0.15	0.2	0.1	Commercial quality, shaped	Pale Orange
	Cast Iron	-	-	-		Green
	Cast Steel	-	-	-		Purple

*Pale orange is more white in color than light orange

3.1.2 The future global steel system

With copper in the current steel system characterized, the future steel system is characterized to determine when copper might constrain steel recycling. The total amount of copper tolerated by demanded products, and the amount of copper entering the steel system in the scrap supply in the future is determined in this step, as summarized in Figure 3.4.

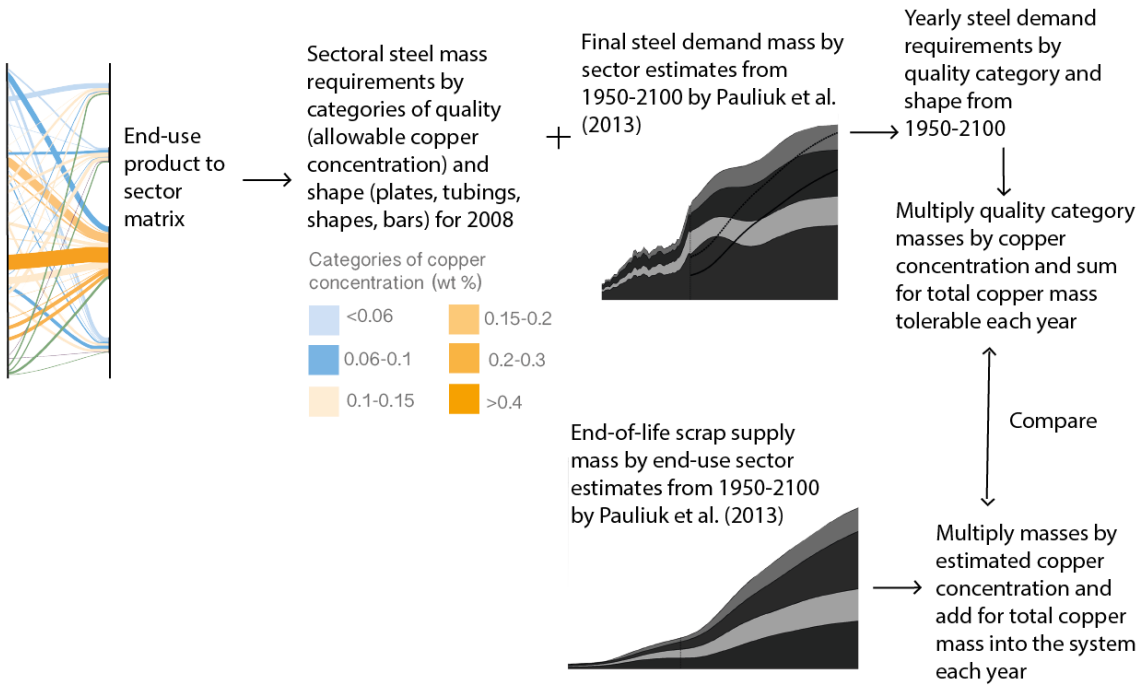

Figure 3.4: Summary of methodology for determining the role of copper in the future global steel system.

Future demand requirements.

To determine future steel demand, the estimates by Pauliuk et al. (2013b) by the four sectors from 1950 to 2100 are used. These sector quantities can then be correlated with intermediate products, using the intermediate product to sector matrix by Cullen et al. (2012). Table 3.8 compares the global steel sectoral division in 2008 between Cullen et al. (2012) and Pauliuk et al. (2013b). There is some mismatch, mostly between the division of goods and vehicles. However, since these sectors have similar steel requirements, the effect of this mismatch should not be significant. It should also be noted that the 2008 total finished steel demand is 1037 Mt from Pauliuk et al. (2013b), while the total from Cullen et al. (2012) is 1088 Mt, a difference of 5%.

Table 3.8: 2008 sectoral steel demand quantities by Pauliuk et al. (2013b) sectors and Cullen et al. (2012).

Source	Total (Mt)	Vehicles (Mt)	Vehicles (%)	Machinery (Mt)	Machinery (%)	Construction (Mt)	Construction (%)	Goods (Mt)	Goods (%)
Cullen	1088	139	13	176	16	596	55	177	16
Pauliuk	1037	200	19	165	16	543	52	129	12

To determine the quantities of product types required each year, the quantity of post-yield intermediate product used within a sector (as determined by the matrix from Cullen et al. (2012)), is divided by the total sector quantity. This fraction is then multiplied by the

sector demand quantity from Pauliuk et al. (2013b). Pauliuk et al. uses historic data for annual steel consumption from 1950 to 2009, so these reported yearly values are used here, directly from a spreadsheet provided by one of the co-authors. This spreadsheet did not include projections for sectoral demand from 2009 to 2100, so these values were measured directly from the published figure every ten years with a linear interpolation applied for the years not directly measured. The product quantities required each sector are summed to give a total quantity for each product type.

With the future quantities of intermediate products estimated, the quality requirements can be evaluated. Each intermediate product is assigned a copper tolerance range and an overall quality category, shown in Table 3.7. These steel categories by quality, as well as shape (flat/plate, tubing, shape, bar), can be summed. The quantity of the copper tolerated by each category can also be summed to give the total amount of copper tolerated by the system annually.

The sensitivity analysis by Pauliuk et al. (2013b) showed that future steel quantities can vary by +/-30% depending on input parameters. In this analysis a range of final steel demand quantities are therefore considered. Total final steel demand is varied +/-30%, applied across all sectors. To understand the effect of varying the proportions of the sectors, the demand from the construction sector is increased 30%, while the other sectors decrease by 30%, and vice versa.

Future scrap supply.

To estimate future scrap supply, estimates from Pauliuk et al. (2013b) by four end-use categories from 1950 to 2100 are also used. Pauliuk et al. (2013b) estimated these quantities using the stock-driven dynamic model with average product lifetimes and recovery rates. These values from 1950 to 2100 were measured directly from the published figure every 10 years using ImageJ, linearly interpolating for the years between. The objective of the analysis is to understand when copper arising from current scrap preparation practice can no longer be tolerated. So, the mass of end-of-life scrap supply by end-use category is multiplied by the expected concentrations arising from current scrap preparation practice, shown in Table 3.3. Copper formerly embedded into steel products is also a source of contamination. Most contaminated end-of-life scrap is used for construction products, which have a relatively long lifetime, of 75 years on average (Pauliuk et al., 2013b). Therefore, the influx of copper embedded in products 75 years ago, returning to the steel system for recycling, was modeled.

80% (consistent with the worldsteel (2010) recovery rate) of the quantity of copper entering the steel system in 1950 was added to the quantity of copper entering the system in 2025, increasing the average copper concentration of construction scrap to 0.17-0.18%. The same additions are done for 2026, by adding 80% of the copper in obsolete scrap in 1951, and so on.

A base case, or the best estimates of current practice extrapolated forward, for the total amount of future copper per annum is plotted. A similar sensitivity analysis was also performed with the scrap quantities, varying the total scrap supply quantity +/-30% and adjusting the proportion of the construction sector. Curves for high and low copper concentrations applied across all scrap categories are also plotted.

A version of material pinch analysis is presented per annum by the decades from 2008 to 2050 to show how categories of scrap and end-products could match, and the dilution that would be required for the best estimated case. The mass of primary steel required each year is calculated as the difference between demand and the supply of end-of-life scrap. Demand is calculated as the final steel in finished products plus losses in refining and processing: an overall average of 12%, consistent with the yields of the oxygen blown converter and EAF and losses in forming and fabrication that are not recovered in circulation scrap from the original Sankey diagram (Cullen et al., 2012), was added to each product category to cover these losses.

3.1.3 End-of-life vehicles in the global steel system

To understand the feasibility of closed-loop vehicle recycling, steel for vehicle production and end-of-life vehicles are traced through the global steel system, while considering copper concentration, as shown in Figure 3.5.

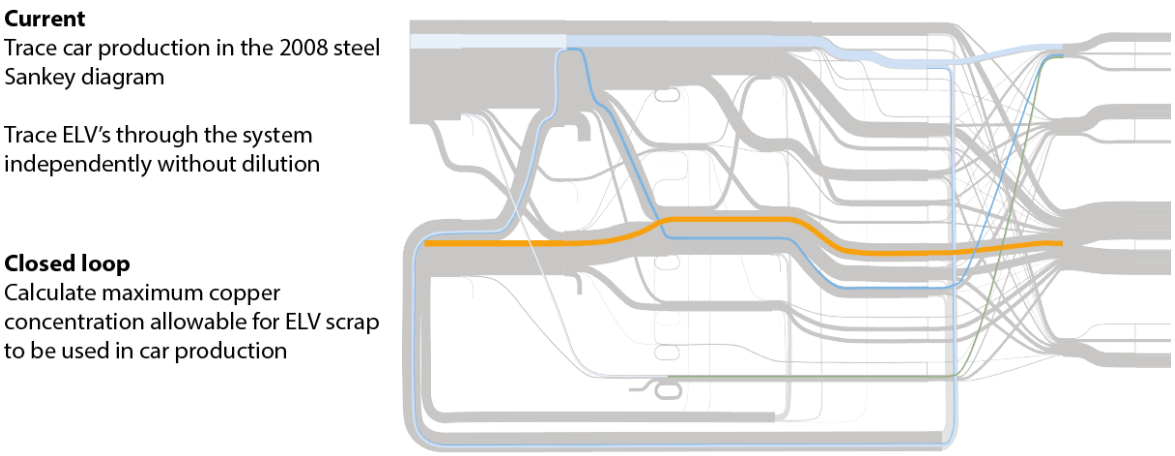

Figure 3.5: Summary of the methodology for analyzing end-of-life vehicles in the global steel system.

The mass of ELV's (in Mt) entering the system in 2008 was estimated from the global scrap breakdown by Hatayama et al. (2010), and applying the 80% recovery rate (worldsteel, 2010). Although ELV's are prepared for recycling in a variety of ways and are often combined with other scrap sources, they are examined independently here. Upon reviewing vehicle scrap preparation practice and literature values (Table 3.2), the global average copper concentration of ELV's was estimated as 0.4wt%. The flow of ELV's to end-use was determined by the copper tolerance of intermediate products. The only end-use to tolerate this level of copper contamination is reinforcing bar. 48 Mt of reinforcing bar can be made from the 58 Mt of ELV material, as determined by losses along the supply chain (Cullen et al., 2012).

The steel required to make new cars in 2008 is also traced. The steel used for vehicles is slightly simplified from the original Sankey diagram version (Cullen et al., 2012). Hot rolled bar, tube and wire rod are consolidated into one flow because they share the same copper concentration tolerance and a similar production route. 32 Mt of forming and fabrication scrap is generated in vehicle production and this is recirculated as a supply source. The amount of pig iron and iron ore required to make the 88 Mt of cars is calculated by taking the difference between the losses and demanded output, and the volume provided by the forming and fabrication scrap.

Lastly, a closed-loop scenario of ELV recycling is constructed. The amount of copper that must be removed is calculated and the resultant iron ore requirements.

3.2 Results

The results are presented in the same sequence as the methodology development

above.

3.2.1 Copper in the global steel system in 2008

Figure 3.6 shows global copper contamination, superimposed on the steel system in 2008. The gray box under "fabrication" shows the maximum copper tolerance of intermediate product streams. The gray box in the far right-hand side groups the tolerances of those streams by end-use products. The figure can then compare the likely flow of copper in the system with tolerance limits. For example, it can be seen in a zoom-in in Figure 3.7 that buildings are likely made from 40% secondary steel, at an average of 0.15 wt% copper while the box to the right shows the intermediate products making up buildings could (in 2008) tolerate a higher proportion of secondary steel at a higher copper concentration. Thus, comparing the proportion of flows of primary and secondary steel to the various sectors with the copper tolerances of final products, the main result is that contaminated scrap can be distributed to demanded products. The scope for absorbing more copper residing mostly in buildings and infrastructure. The total quantity of copper in the system is about 0.7 Mt, while 1.8 Mt could be tolerated. This total mass of copper is significant: over 3% of total global copper production in 2008 (USGS, 2008). Figure 3.6 (highlighted in Figure 3.8) also shows that end-of-life vehicles are the most potent contaminating source to the steel system, while new cars are the main end-use behind the demand for the highest quality steels, originating almost exclusively from the primary route.

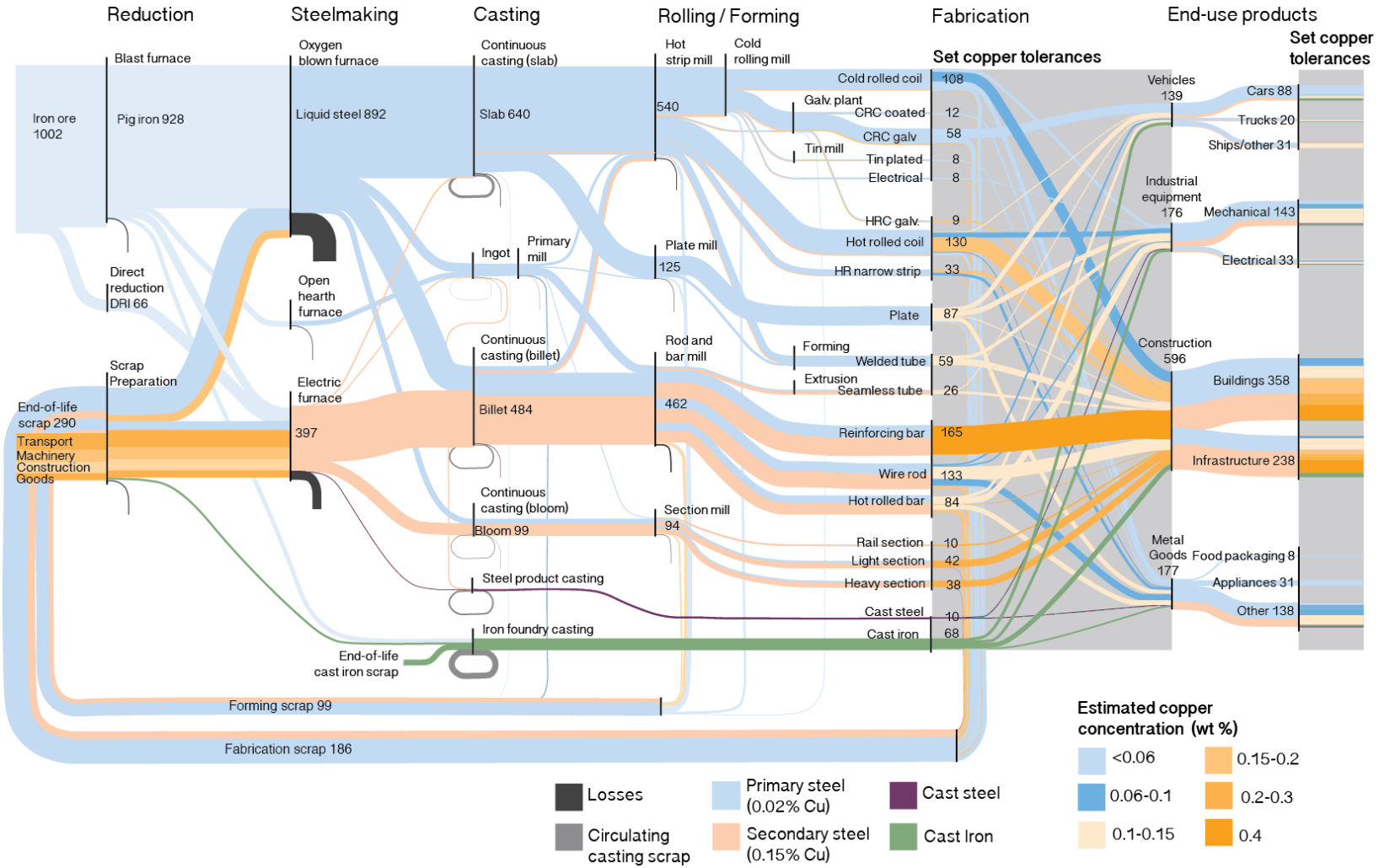

Figure 3.6: 2008 global steel flows (in Mt) with estimated copper concentrations of steel flows. The width of the flows corresponds to the mass processed per year. The gray boxes contain copper tolerance limits of intermediate and end-use products to compare copper in the system versus maximum tolerable.

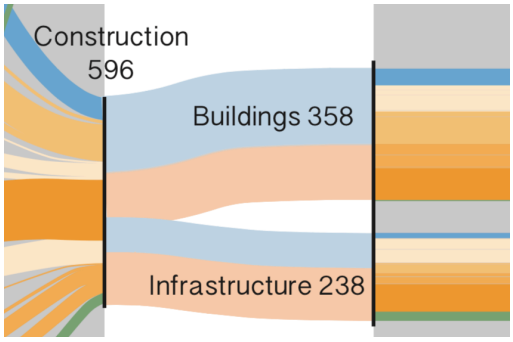

Figure 3.7: Zoom-in of the steel Sankey diagram in 3.6 showing the likely proportion and average copper concentration of EAF steel, used in the construction sector: buildings and infrastructure, as well as the copper tolerance of products (far right, with gray background). This reveals that there is capacity to tolerate yet more copper in the supply, particularly in this sector.

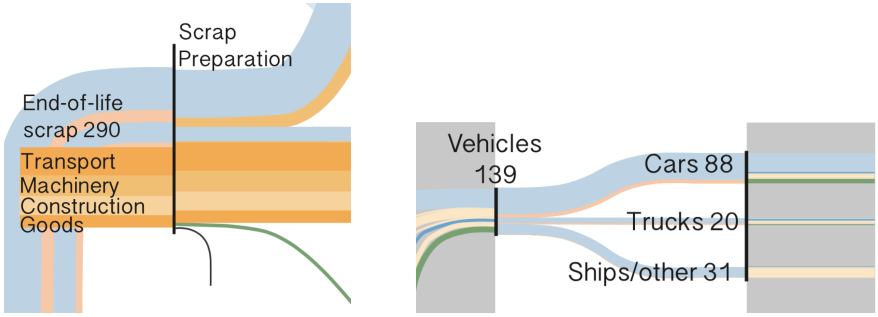

Figure 3.8: Zoom-in of the steel Sankey diagram in 3.6 showing the copper concentration of end-of-life scrap, specifically that transport scrap is the most significant source of copper (left). The right image is a zoom-in at the far-right of the Sankey diagram, showing vehicles are one of the most demanding applications, using mostly primary steel.

3.2.2 Copper in the future global steel system

Figure 3.9 shows the estimated mass of copper in the scrap supply and copper that can be tolerated by end-use products, as well as curves varying from this estimated case, from 1950 to 2100.

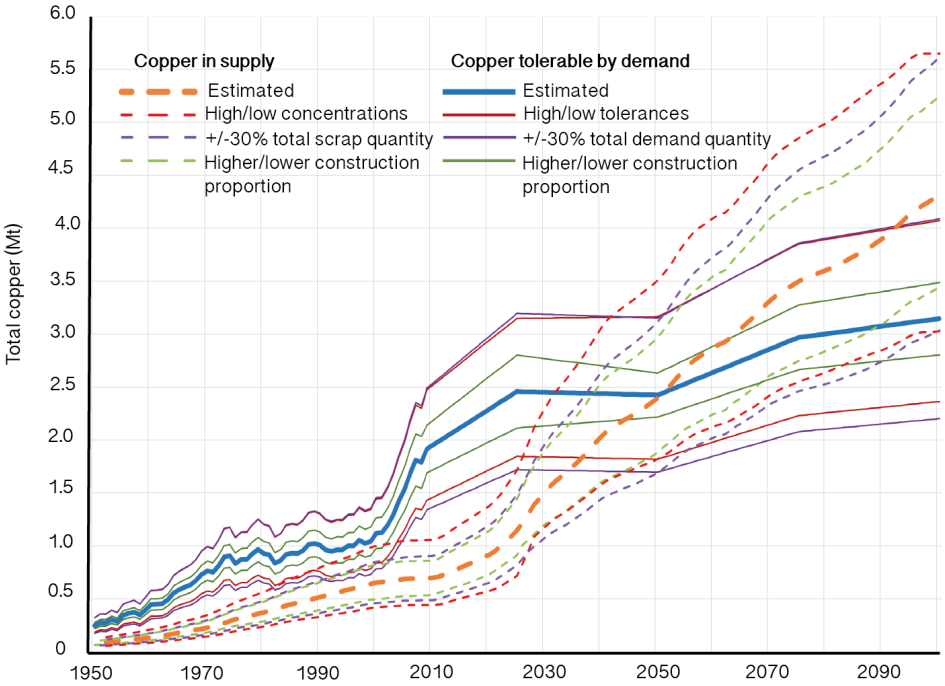

Figure 3.9: Mass of copper in the end-of-life scrap supply and copper tolerable by demanded products from 1950 to 2100. The estimated case uses sectoral final steel demand and scrap supply quantities as determined by Pauliuk et al. (2013b) and, the product to sector mapping by Cullen et al. (2012), and expected values of copper concentration for scrap categories and product tolerances as determined through a literature survey. Sensitivity curves apply high and low values for copper concentration across all categories, vary the total quantities of end-use steel demand and scrap supply across all sectors +/-30%, and vary the proportion of the construction sector by +/-30% (while other sectors decrease/increase by 30%, respectively).

There is a substantial range exhibited by the curves, such that the date when copper contamination will constrain global steel recycling cannot be defined, but best estimates indicate 2050. Applying low concentrations across scrap categories could effectively delay constraints to 2100, while assuming higher values could advance the cross-over to before 2030. There are combinations of curves that do not cross, for example if the scrap supply is reduced by 30% and final steel demand is increased by 30%. Even allowing these large uncertainty ranges, the trend is clear: there is a large difference between copper in the supply and copper tolerated by end-products today due to the substantial amount of primary steel, increasing since the early 2000's. The amount of copper tolerated by end-use products begins to plateau in 2025, while copper in the scrap supply invariably increases. The greater number of research projects to address copper contamination in the past can also be explained: the difference between the curves was smaller before 2000.

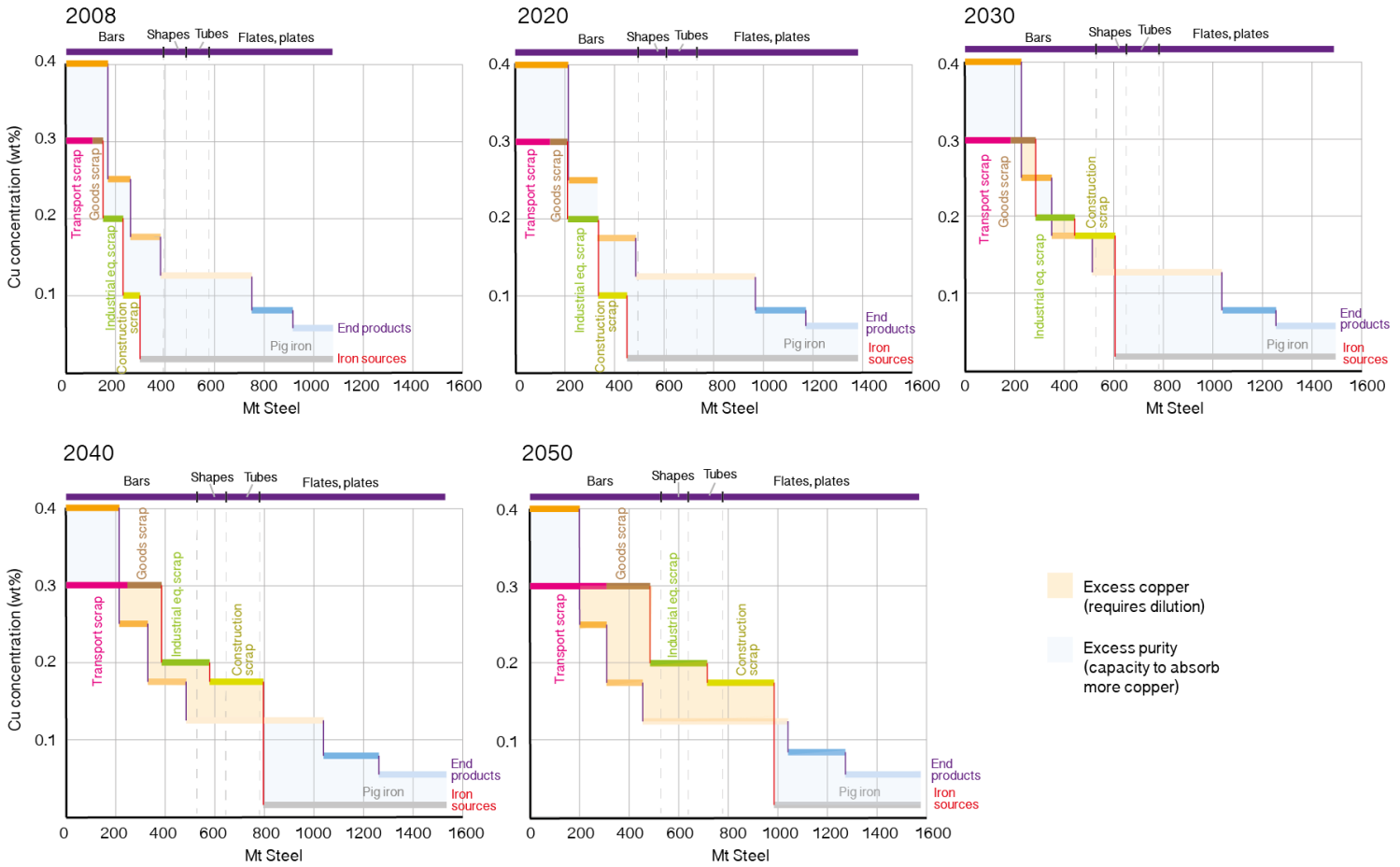

Figure 3.10: Projected masses of iron sources (end-of-life scrap and pig iron) and finished steel products in end-use, as determined from quantities by Pauliuk et al. (2013b) and the product to sector matrix by Cullen et al. (2012), plotted by expected copper concentration for 2008, 2020, 2030, 2040 and 2050. For end-products, the copper concentration is the expected tolerance. Gaps between the source and end product curves indicate either where dilution is required (orange), or where more copper could be tolerated by the end-use (blue). Masses of end products by shape are plotted above. An additional mass of 12% was added to each end product category to account for iron sources that would be lost (and not recovered in circulation scrap) in refining and processing.

Figure 3.10 provides snapshots of projected masses of iron sources (inputs into the steel system, left-hand side of the Sankey diagram) and end products (outputs of the steel system, right-hand of the Sankey diagram plus losses) per annum for the next few decades calculated from the best estimates scenario. The masses of steel in each category are plotted by copper concentration to visualize the possible destiny of scrap sources to meet demand. In 2008 and 2020, it can be seen that all end-of-life scrap can be used in products with tolerances greater than 0.15 wt% copper. By shape, all end-of-life scrap can be used for bars. By 2030 end-of-life scrap must be used for 0.1-0.15 wt% copper-tolerant products, and incoming construction scrap will have a higher concentration of copper due to past accumulation. In balancing copper in the sources over products, there exists capacity for accepting more copper in the 0.4 wt% category, which would mean further concentrating copper-containing sources, while the excess purity from pig iron would be utilized through dilution. 2030 marks the beginning of when dilution and distribution of scrap to the various product categories will be necessary on a global scale. By 2050 the total copper in the supply is forecast to be about the same as the maximum that can be tolerated across all products and to match supply with demand, scrap will have to be cast and rolled into flat and plate products.

Figure 3.11 plots the masses of several of the categories from Figure 3.10 to compare the relative growth rates. As the scrap volume grows the amount of primary material required to make up the difference between the scrap supply and demanded end products decreases. Concurrently, demand for the product categories best able to absorb copper (tolerances >0.4% Cu and bars) plateau or decrease slightly in mass, while categories least tolerant (tolerances <0.06% Cu and flats/plates) continue to expand to 2050.

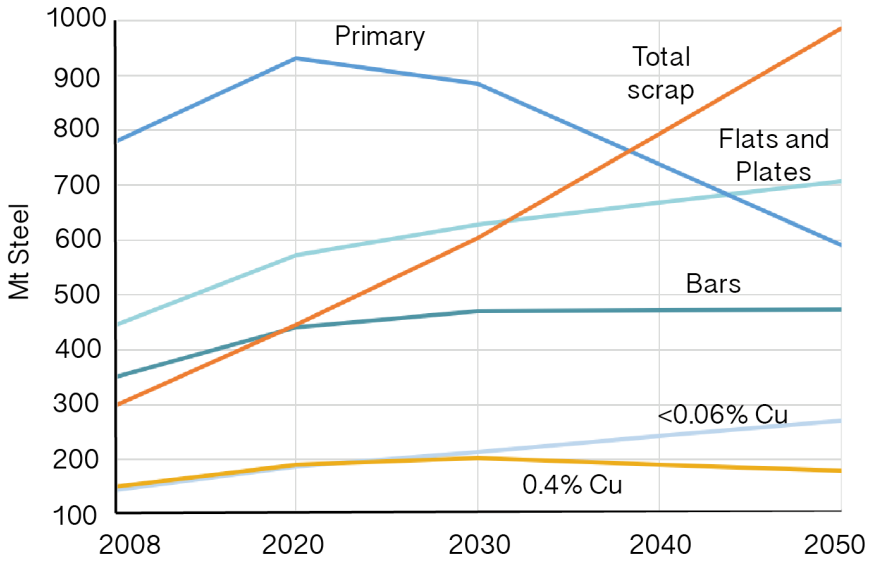

Figure 3.11: Trends in projected masses (Mt) of steel categories (required primary, total scrap, products requiring <0.06% copper and >0.4% copper) from 2008-2050.

3.2.3 End-of-life vehicles in the global steel system

Figure 3.12 shows steel flows involved in producing new cars and recycling end-of-life vehicles in 2008. In current practice, with an estimated copper concentration of 0.4%, reinforcing bars are the only viable use of ELV's without dilution. ELV's could be used to produce up to 48 Mt of the 165 Mt of reinforcing bar demanded globally in 2008.

A scenario for closed-loop end-of-life vehicle recycling is shown in Figure 3.13. Galvanized cold rolled coil requiring less than 0.06% copper, and bars, tubes and wire rods allowing up to 0.1% copper are the main intermediate products in cars. Therefore, to achieve a closed loop the material salvaged from ELV's should have a copper concentration of less than 0.08%, requiring removal of 0.19 Mt of copper. The interventions that could be implemented along the supply chain are shown in Figure 3.11. Using ELV scrap for the production of new vehicles would reduce the amount of iron ore required from 136 to 78 Mt, accounting for 32 Mt of fabrication scrap generated in car manufacturing. However, reinforcing bar is currently demanded, so iron ore may be used for this production if the flow of end-of-life vehicles is re-directed.

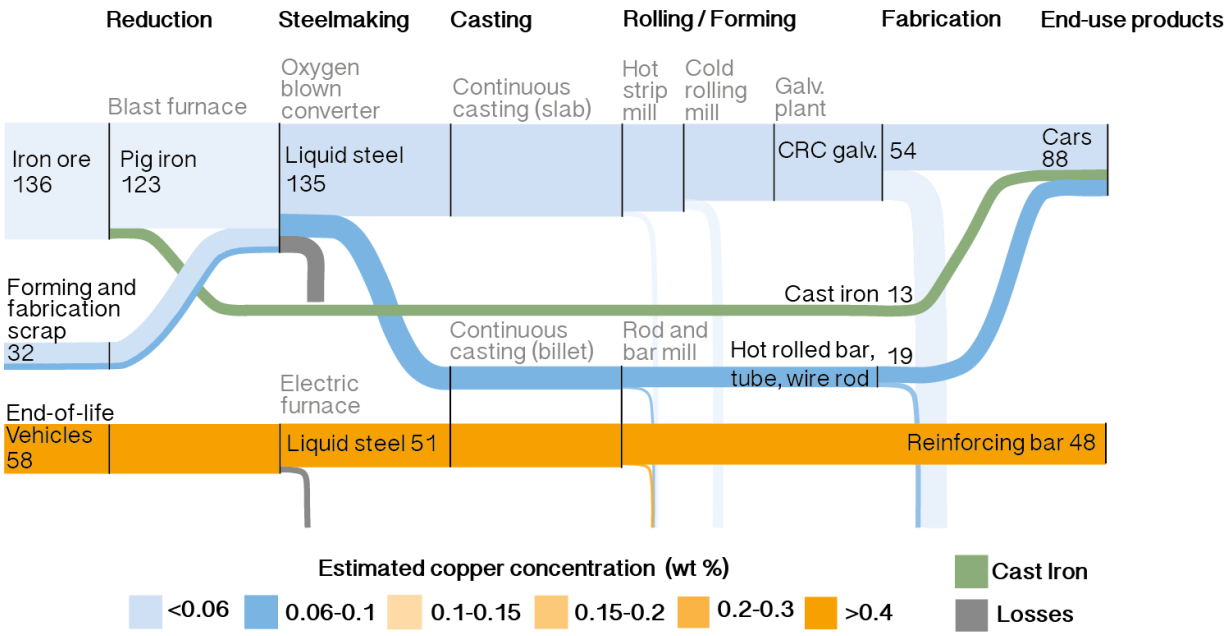

Figure 3.12: The steel mass flows (in Mt) corresponding to the production of cars and the recycling of end-of-life vehicles isolated from the 2008 global steel system.

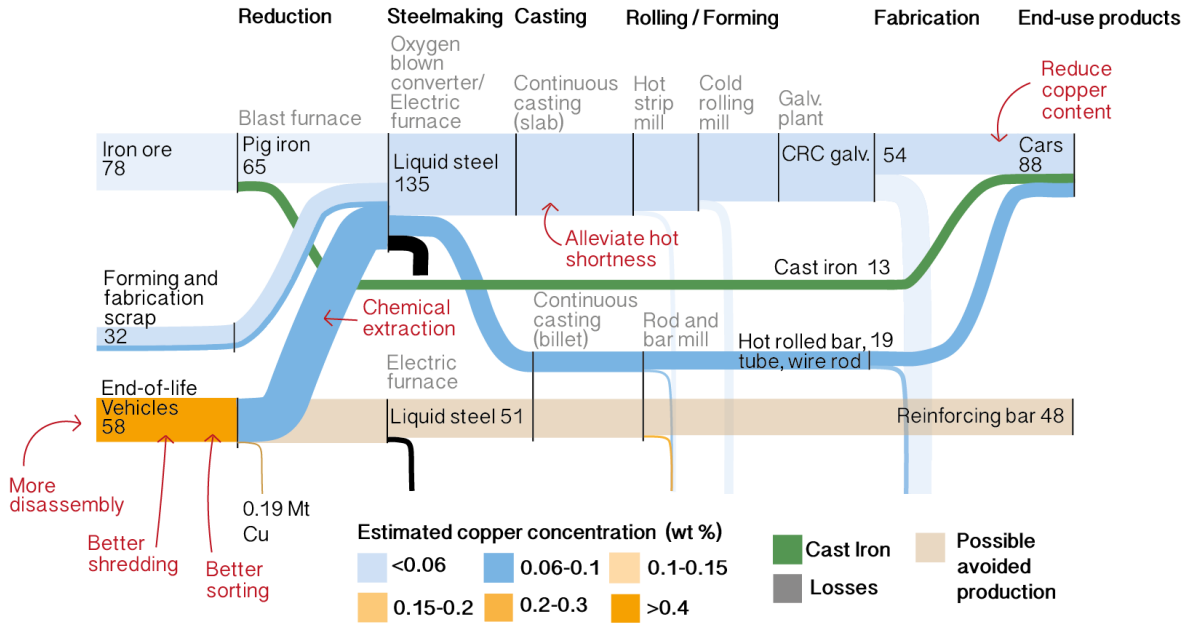

Figure 3.13: A hypothetical closed-loop of end-of-life vehicle recycling in the 2008 steel system. Steel mass flows in Mt. Technical interventions along the supply chain are shown in red text.

Figure 3.12 shows that the closed-loop recycling of automotive steel is currently unlikely. The retention of alloying elements unique to automotive steel, which are current dissipated when cars are recycled to structural steels, provides motivation to address current practice and close product loops before the global constraining point is met. A range of technical interventions if implemented now could create the basis for a more effective global steel recycling strategy over the next two decades. These opportunities for intervention have

been reviewed in Section 2.2.3.

3.3 Discussion

The results show that copper contamination constrains recycled steel to a segregated market, as illustrated in Figure 3.6, but current demand for steel products with high copper tolerance easily accommodates contaminated scrap. However, demand for tolerant products will not keep pace with the increased quantities of end-of-life scrap, and available primary steel will decrease. As the demand for copper-tolerant products (such as reinforcing bars) is likely to grow at a slower rate than demand for higher quality steels (such as those used in the production of cars) interventions will eventually be necessary to avoid accumulating stocks of unusable steel scrap. As shown in Figure 3.8, the 0.4% Cu category (reinforcing bar) cannot contain all transport scrap after 2040. Within this global context, strategically trading scrap to applications with sufficient demand has a limit. Best estimates show copper contamination could theoretically be managed until 2050, assuming perfect distribution of copper in the global steel system. However, in this case extensive dilution and careful allocation of scrap at a global scale would be required by 2030, as shown in Figure 3.8.

The analysis of the future steel system projects current scrap preparation practice forward. Exactly when copper contamination will prevent the utilization of end-of-life scrap cannot be determined, as assumptions must be made about future quantities of steel (scrap and demanded products) and their compositions. These sources of uncertainty and how each was resolved in the present analysis is summarized in Table 3.9.

Table 3.9: Identified sources of uncertainty and the resolution of each in the analysis of the future steel system.

Source of uncertainty			Resolution
Scrap	Quantity	Scrap supply by sector predictions	Use best available projections, from Pauliuk et al. (2013b) based on stock-based model. Vary total scrap quantity by +/-30% across all sectors, and the proportion of sectors (construction sector +30%, all other sectors -30% and vice versa), in sensitivity analysis.
	Composition	Copper concentration of scrap categories	A range of copper concentrations are assigned. Expected values are constant such that current scrap preparation practice is carried forward, while accounting for accumulation. Best/worst cases are presented by applying low and high values to all scrap categories.
Demand	Quantity	Sectoral steel requirements	Use best available global product to sector matrix, provided by Cullen et al. (2012). Error in extrapolating this matrix is discussed in Appendix, A1.
		Mismatch in defining sectors between Pauliuk et al. (2013b) and Cullen et al. (2012)	Varying sectors have similar steel requirements
		Extrapolating product to sector matrix beyond 2008	Assume steel requirements of sectors stays constant from 2008.
		Final steel demand by sector predictions	Use best available projections, from Pauliuk et al. (2013b) based on stock-based model. Vary total final steel demand quantity by +/-30% across all sectors, and the proportion of sectors (construction sector +30%, all other sectors -30% and vice versa), in sensitivity analysis.
	Composition	Compiled best available information	A range of copper tolerances are assigned. Best/worst cases are presented by applying low and high values to all end-products.

Uncertainty related to steel quantities is addressed by using the best available estimates, and varying the quantities by the error range noted in the study by Pauliuk et al. (2013b) in sensitivity analysis. To show the uncertainty arising from copper concentration assumptions, curves in Figure 3.6 were plotted with all high/low values of copper content representing extreme cases. However, it is unlikely all values will be exclusively low or high. Monte Carlo simulations can vary each value independently. Monte Carlo simulations of 2000 samples, with copper concentrations drawn from triangular distributions based on the low, expected and high concentrations in Tables 3.2 and 3.3 are shown in Figure 3.12. The range of uncertainty is much smaller when the distribution of concentrations is applied individually to scrap categories and end-products.

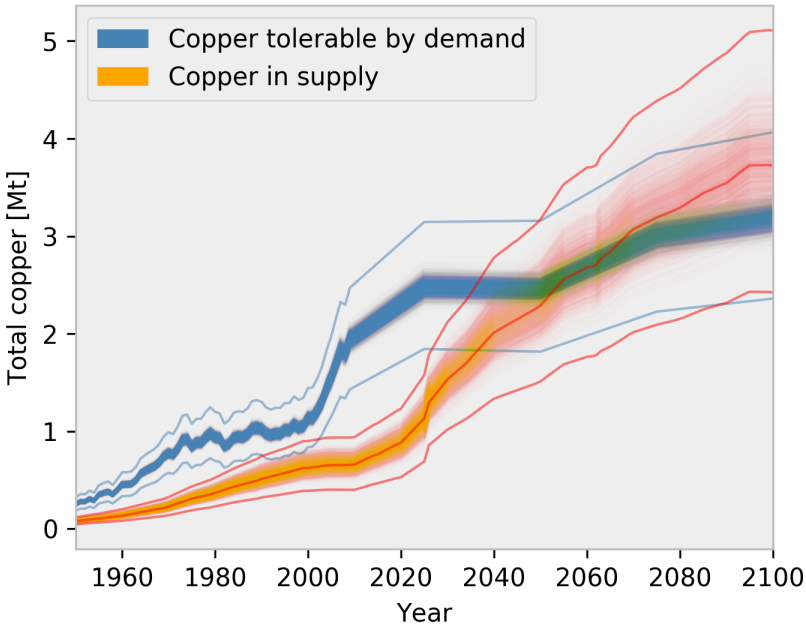

Figure 3.12: Copper tolerable by demand and copper in supply curves with the result of Monte Carlo simulations of 2000 samples, with copper concentrations drawn from triangular distributions based on the low, expected and high concentrations in Tables 3.2 and 3.3. The lines correspond to best, expected and worst cases where low, expected and high values are applied to all categories respectively.

Despite the uncertainty, characterizing current and future steel flows from a physical basis provides a new basis for qualitatively understanding what is most likely to happen in the future. Results must be interpreted at an aggregated, high level, but important long-term trends are revealed. As long as copper remains in the steel melt during refining, it will remain in the cycle once embedded in products, and many steel products have long lifetimes – thus current actions will have long-term consequences. Contextualizing the problem shows that the steel industry has been in a state of relative ease in tolerating copper contamination, but copper will cause increasingly greater inefficiencies, with a global effort in diluting and carefully distributing scrap sources most likely required by 2030. Forward-thinking and careful investment in the development and deployment of processes and policies to manage copper in the steel system will be necessary to avoid an accumulation of unusable scrap.

The constraining point for copper contamination depends on the balance of production between blast furnace and EAF routes. The analysis of this paper has assumed that all recovered scrap will be recycled, with blast furnace production supplying all other requirements, and that demand grows according to current stock saturation patterns. However, if concern about climate change leads to real action on limiting emissions and this

is applied across sectors, blast furnace production must be reduced. With a model of global mass flow and process emission intensities, Milford et al. (2013) concluded that currently legislated emissions abatement targets could only be achieved by an aggressive reduction in primary steel production to about 300 Mt/year by 2050. This is around half the anticipated figure in the demand forecast used in this paper and if implemented would greatly increase the urgency for action on copper contamination.

Chapter 4. Finding the most efficient way to extract residual copper from shredded steel scrap.

The content of is published in Metallurgical and Materials Transactions B as "Finding the most efficient way to extract residual copper from shredded steel scrap." My co-authors contributed the idea to plot specific energy versus reduction in copper concentration and provided feedback on iterations of the paper.

Chapter 3 shows that improved copper control is necessary. A strict global constraint will not arise for several decades, but extensively trading contaminating scrap and exporting it for dilution in countries with fast-growing demand will become increasingly unattractive and impractical. Regional constraints will arise now as primary plants are closed, and the overall global constraints may arise much sooner if emissions targets are taken seriously. Given this reality, options for more circular practices must be pursued now. Thus, this chapter returns to the technical interventions identified along the steel supply chain in Figure 3.11 to further investigate which options will be most applicable and effective.

Figure 4.1 provides a representation of the stakeholders involved in the steel cycle, considering the steps each is responsible for and the incentives each has to control copper. The makers of cars, appliances and equipment could use less copper (by challenging the trend of incorporating more electronic features (Leen et al., 2002), or using aluminum wiring instead (Oba, 2013)), or modify designs for easy disassembly at end-of-life (such as using detachable wiring harnesses (Toyota, 2015)). However, product re-designs must be motivated by consumer support, or regulation. A compromise in performance or price for enhanced recyclability may be unacceptable. Additionally, steel products have long lifetimes, so improvements at the product design stage would have a delay of at least 10 years before affecting the recycling process.

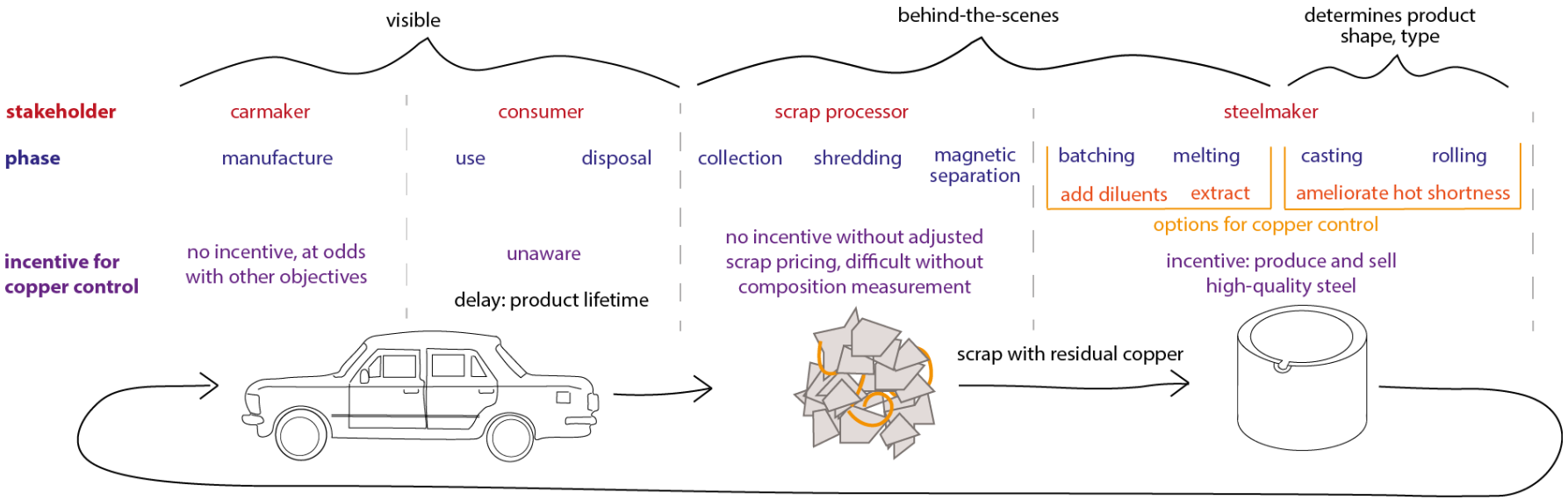

Figure 4.1: Stakeholders along the steel supply chain and incentives for improved copper control.

The scrap processor collects, dismantles and shreds steel products for recycling. Copper removal at this point would be highly energy-efficient. Separation is always more efficient before mixing – as the concentration of a component in a mixture decreases, the work to extract it increases (Gutowski, 2007). However, manual disassembly to remove copper before shredding is labor-intensive and cost-prohibitive in many regions.

Currently, the incentive to reduce the copper concentration of steel is to produce and sell high-value steel products. Thus, the steelmaker benefits from purer scrap. The steelmaker could incentivize the scrap processor to minimize contamination, but scrap is difficult to grade and price by copper concentration. The composition of scrap is known if it originates from production or manufacturing, but the copper concentration of end-of-life scrap cannot be measured until it is mixed with other raw materials and melted (unless neutron activation analysis technology is used, which is operating in at least 20 plants (Russo, 2014)). Although mutual agreements between the scrap merchant and steelmaker can be arranged, in scrap classifications (ISRI, 2016), (EUROFER, 2016), shredded scrap is nominally the same whether it contains 0.4 or 0.1wt% copper.

Policy could be formulated to re-structure the incentives along the supply chain. Incorporating quality measures into regulation and scrap pricing may motivate copper control during scrap processing. The European Union End-of-Life Vehicle Directive (2000) set targets for 2015 onwards that 95% of ELV material by mass must go for recovery, re-use and recycling, but these mass-based policies are counter-productive for impurity and alloying element control. A policy that prioritizes the recycling of the most environmentally-impactful parts of a vehicle and monitors for quality and dilution losses should be developed. For example, a recent Japanese law on the recycling of small waste electronic equipment that measures the recovery of specific scarce metals, as discussed by Nakamura et al. (2012).The EU ELV Directive has mandated the removal of fluids prior to shredding and has measurably improved the control of hazardous substances (Gerrard et al., 2007), so this regulation could also be extended to contaminating metals. To engage automakers in these solutions, policy could require that automakers use a certain portion of secondary steel.

The steelmaker has the responsibility and incentive to manage copper-contaminated scrap for the foreseeable future, until policy or market forces change the dynamics between stakeholders along the supply chain. Therefore, the scope of the current evaluation is limited to interventions the steelmaker could implement. These include either tolerating, or extracting copper. Additional alloying elements and adjusted atmospheres or heating/cooling

profiles during casting and rolling can alleviate hot shortness. However, the universal applicability of these techniques is uncertain. Such approaches prescribe the product composition and shape – for example the thickness of steel produced by direct strip casting is limited to 10-15 mm (Spitzer et al., 2003). Alternatively, extraction would be an effective, behind-the-scenes solution to enable the high-quality recycling of steel. The scope of this analysis is therefore on processes the steelmaker could employ to extract residual copper. Shredded end-of-life scrap typically has 0.4 wt% copper, but many flat steel products require less than 0.1 wt% copper. This analysis seeks to estimate the specific energy and material inputs needed to achieve this reduction in copper concentration across the full range of possible separation processes.

In 2.2.1, the existing forms of thermodynamic analysis were discussed: evaluating impurity removal independent of a process, and evaluating impurity removal during a specific, defined process. Thus far, process-dependent analyses have only assessed impurity removal during commercial refining. A new framework to define and evaluate potential separations is required, which is devised and then demonstrated in the methodology section, 4.1. The results – the specific energy and material inputs required in the potential processes – are presented in 4.2. The implications of these results are discussed in 4.3.

4.1 Applying the framework to copper in steel

A new framework to assess the space between process-independent theory and industrial practice is needed. Experimental work investigates this space, but each study evaluates copper removal under specific conditions. To provide an understanding of overall feasibility and give direction to these investigations, a framework is proposed in Figure 4.2. This framework links the two forms of analysis: theoretical separation principles serve as the basis for potential scaled-up processes. Once processes are defined, meaningful estimations of effectiveness and energy requirements can be made, using the thermodynamic and kinetic relationships revealed by the experimental work and data on metallurgical reactors. In such an analysis, the various separation options can be directly compared to identify the most efficient processes. By imparting an underlying logic to unify the various possible separations, and then evaluating the physical basis governing each separation, the "removability" of copper from iron can be understood from a more fundamental basis.

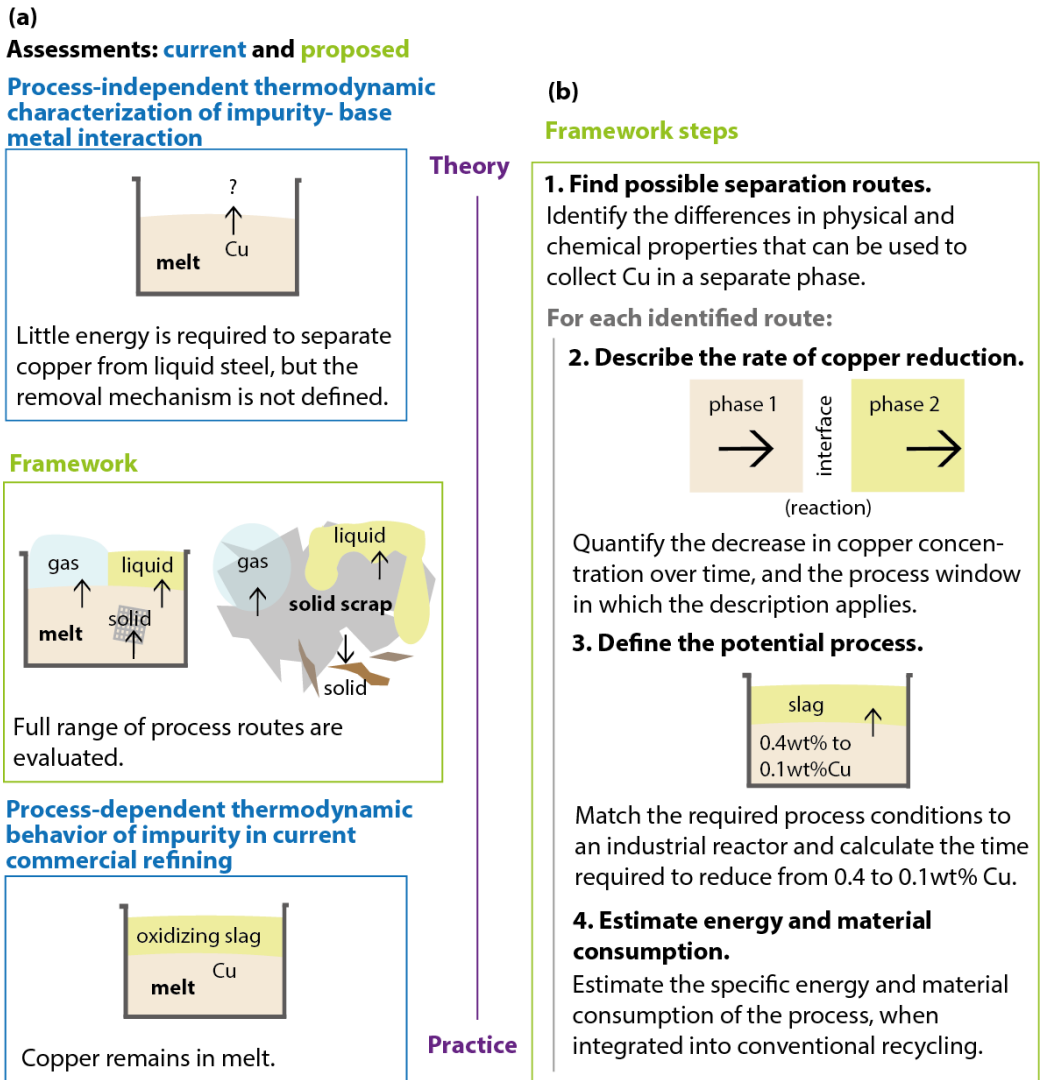

Figure 4.2: The current assessments and the proposed framework for evaluating the feasibility of removing copper from steel are shown in the left column (a). Steps of the framework are shown in the right-hand column, (b).The framework evaluates possible separations, from theoretical principles to the energy and material inputs required in practice, thus filling the gap between the process-independent and process-dependent assessments that evaluate current commercial practice.

The proposed framework identifies and assesses potential separation techniques in four steps: first, find the possible separation routes, and then for each route define the rate of copper reduction, define a potential process, and estimate the energy and material consumption. Applying these steps to the copper-steel system is described in 4.1.1-4.1.4.

4.1.1 Step 1: finding the possible separation routes.

A wide range of equilibrium and transport phenomena can be used in separation. In this step, in order to organize the different phenomena while covering the full range of

possible options, "separation routes" for a general impurity metal-base metal system are defined, and the applicability of each route to the copper-steel system is evaluated.

For a general impurity-base metal system, there are two main starting states: the impurity can be heterogeneously attached to solid scrap, or in the liquid phase as a homogeneous mixture which is formed upon melting. From these beginning states, a separation route can be defined for all possible separate phases to which the impurity can be moved and collected. Here, distinct routes are defined by the end state of the impurity. This scheme is shown in Figure 4.3. for solid scrap, and Figure 4.4 for the melt.

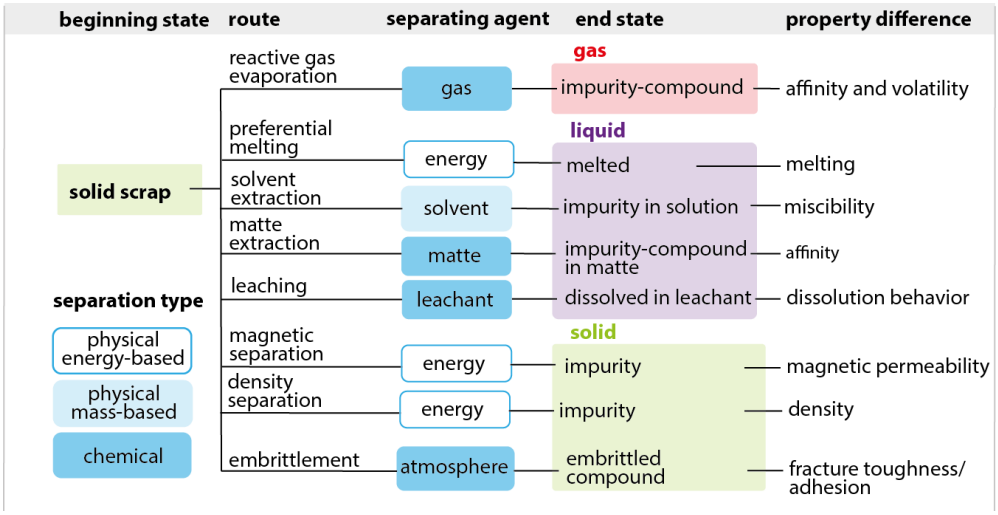

Figure 4.3: General routes to remove an impurity attached to solid scrap, showing the separating agent applied in each route and the property difference exploited.

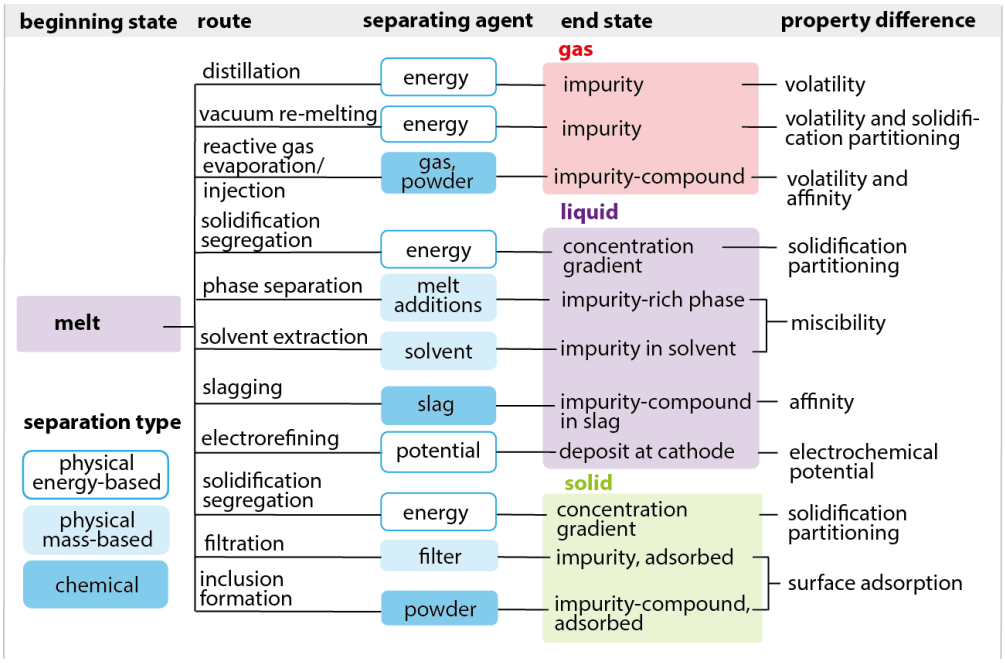

Figure 4.4: General routes to remove an impurity from the melt, showing the separating agent applied in each route and the property difference exploited.

The possible phase distributions envisioned for extracting copper from steel scrap are shown in graphical form in Figures 4.5 (solid scrap) and 4.6 (melt).

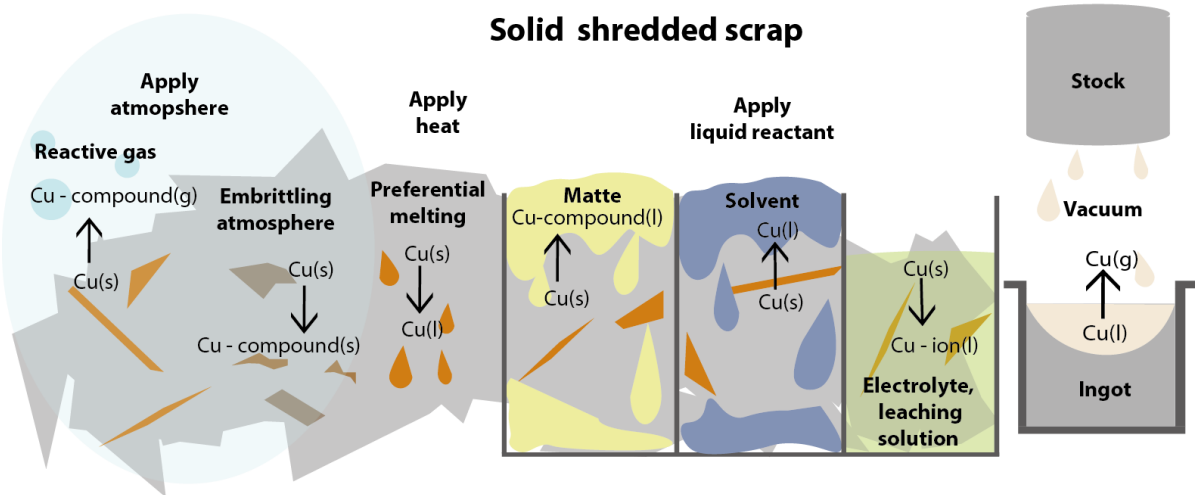

Figure 4.5: Possible phase distributions for extracting copper from solid scrap.

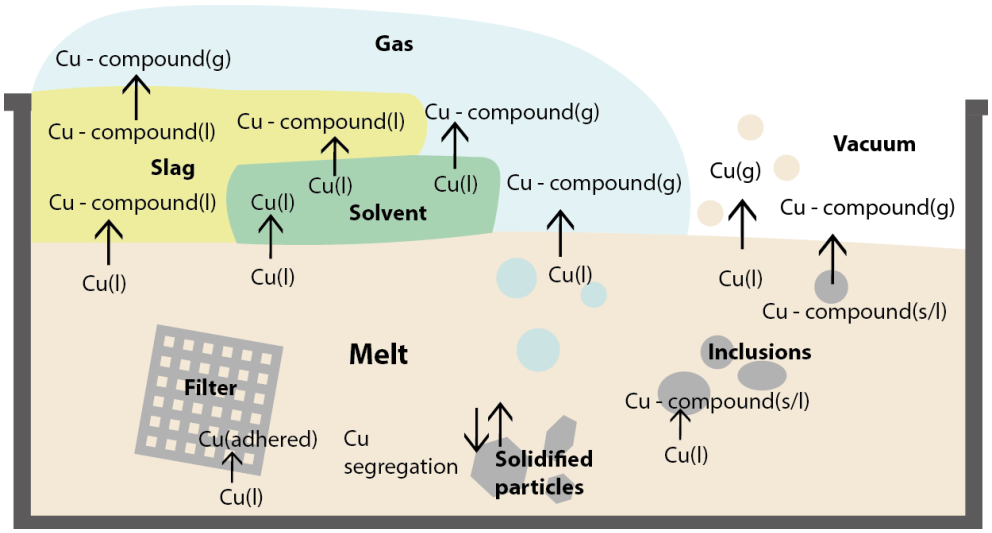

Figure 4.6: Possible phase distributions for extracting copper from the steel melt.

In all routes, separation is driven by a difference in properties between the impurity and base metal through the use of a separating agent, as reviewed in Section 2.2.1 and described by King (1987). King proposes a classification scheme to categorize these property differences and separating agents. Accordingly, here the separations are categorized into three distinct types, which are indicated by the coloring of the separating agent in Figures 4.3 and 4.4. The first is energy-based physical separations, in which energy is applied to exploit a difference in physical properties, such that the impurity changes phase. There are also mass-based physical separations, where material is added to the system to act as a collection site or

induce a phase change. Lastly, in chemical separations, a reactant is applied to preferentially react with the impurity, thus exploiting chemical property differences. In all cases, the magnitude of the exploited property difference is an a priori indication of feasibility. To apply this general scheme to the copper-steel system, the relevant property differences are identified and discussed, and are presented with references for all routes in Figures 4.7 (solid scrap) and 4.8 (melt).

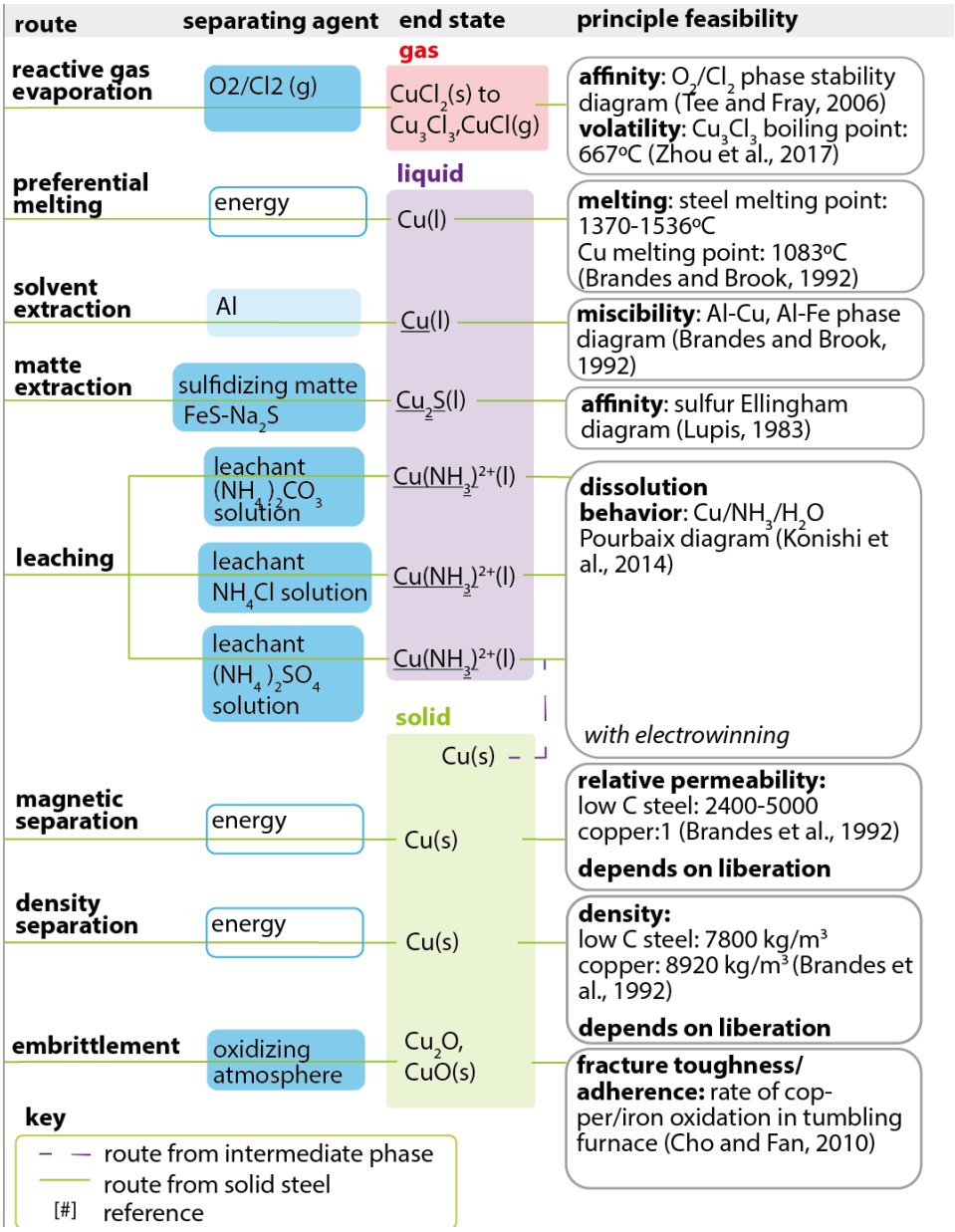

Figure 4.7: The possible copper separation routes with the associated measure of principle feasibility for solid steel scrap (summary of framework Step 1).

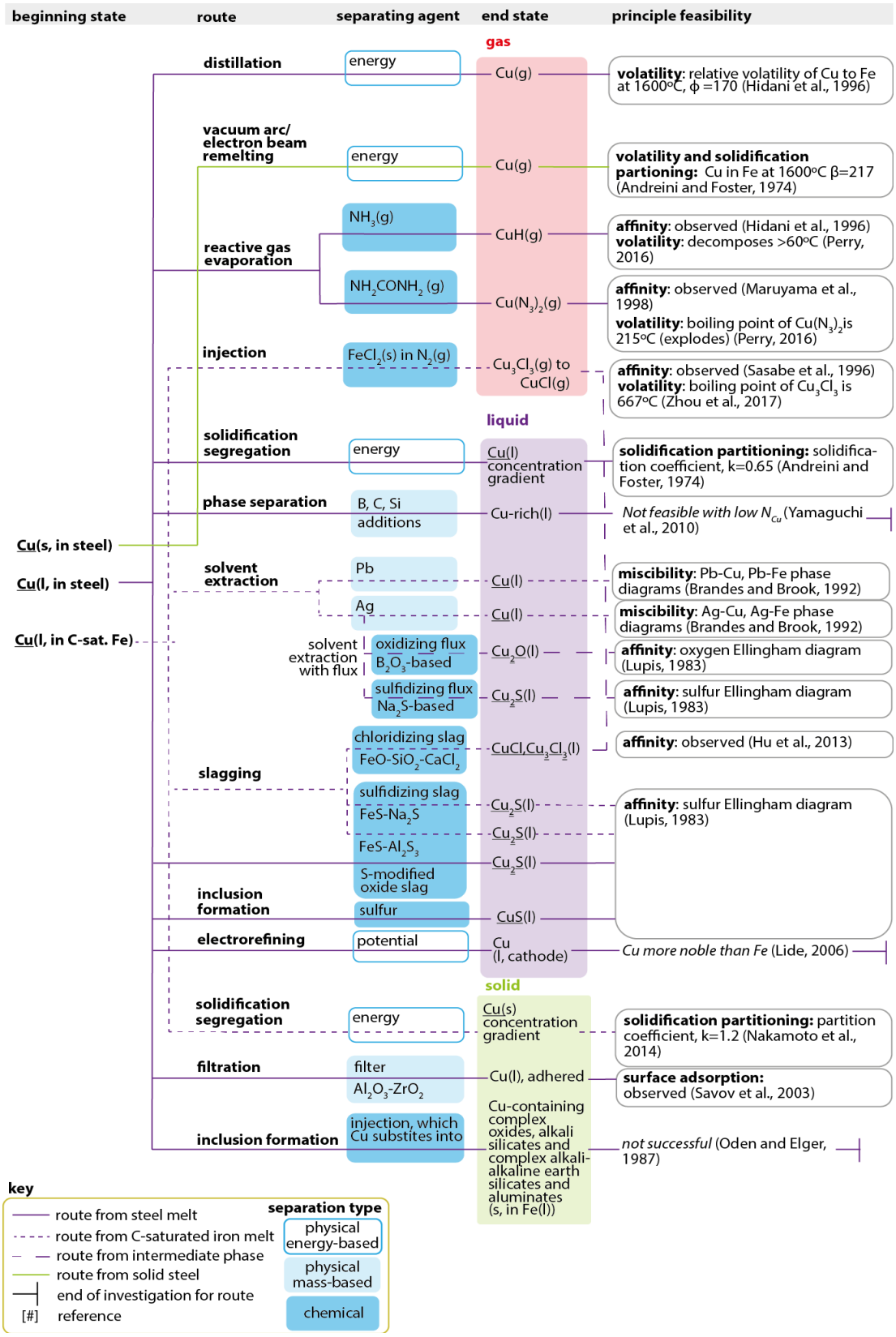

Figure 4.8: The possible copper separation routes with the associated measure of principle feasibility for the steel melt (summary of framework Step 1).

Energy-based separations for copper and steel exploit physical property differences in the solid state or during vaporization, melting and solidification. As solid scrap, copper can be separated from steel by magnetic permeability or density, and such processes are in standard

operation, but depend on the liberation achieved during shredding. Copper has a higher vapor pressure such that it can be distilled from a steel melt, and it has a lower melting point so that it can be melted while steel remains solid. Copper partitions to the liquid phase during solidification of iron, but to the solid phase during the solidification of carbon-saturated iron. In both cases, the partition coefficient is close to 1, indicating limited partitioning.

Physical mass-based separations include applying a solvent or filter to extract copper. Relevant solvents can be identified with phase diagrams, which reveal differences in miscibility. Iron is immiscible with lead and silver, while copper is miscible. A miscibility gap exists between iron and aluminum as well, but only at lower temperatures, so aluminum is a viable solvent when applied to solid scrap. Filtration has been cursorily investigated, with Savov et al. (2003) reporting that a ceramic filter or particles of Al_2O_3-ZrO_2 selectively absorb copper from an iron melt.

In chemical separations, copper undergoes a chemical reaction preferentially to steel. Sulfur is the only element that will react preferentially with copper, and this is the principle behind sulfide-based slags and mattes. However, researchers have identified viable chemical separations beyond sulfidation. Process windows exist to separate copper from steel through chlorination, oxidation and leaching. Chlorination is viable at certain ratios of oxygen and chlorine: copper chloridizes, while iron oxidizes to prevent its chlorination (Tee and Fray, 2006). To separate copper through oxidation, the lower fracture toughness of copper oxide is exploited. Brittle copper oxide can be collected by tumbling mixed scrap in an oxidizing atmosphere around 650^{o}C (Cho and Fan, 2010). In these conditions, iron forms adherent Fe_2O_3 at the surface, so iron loss is minimal. In leaching, copper dissolves in an electrolyte while iron remains inert or passivates. Ammonium-based leachants have the highest selectivity and have received the most attention (Gosh et al., 2015). Other chemical separations have been attempted experimentally, but the principles have not been confirmed. Ammonia-based gases were sprayed onto the steel melt to accelerate the evaporation of copper. Researchers hypothesize that volatile CuH(g) (Suzuke and Ono, 2000) or $Cu(N_3)_2$(g) (Maruyama et al., 1998) form. To form copper-containing inclusions, Oden et al. (1987) injected a range of complex alkali and alkaline earth compounds into the melt (chosen because of the stability of the associated copper-containing compounds), but the experiments were unsuccessful.

The above classification identifies the relevant physical property differences that can be exploited in energy-based separations, and the relevant solvents, filters and reactants that

can be applied in mass-based separations. The next steps evaluate the requirements and limitations of applying the identified principles in practice. This evaluation is dependent on the experimental results available in the literature, so all experimental work found in the literature was catalogued according to the distinct routes. This catalogue can be found in the Appendix. Information used directly in this analysis is cited in this chapter.

4.1.2 Step 2: describing the rate of copper reduction.

This step seeks to quantify the rate of reaction – the decrease in copper concentration over time – for the various routes shown in Figures 4.7 and 4.8. In all of these routes, copper collects in a separate end phase. The reaction happens at the interface between the beginning phase and end phase. The total reaction proceeds by three main steps: transport of the reactants to the interface, the reaction at the interface and transport of products away from the interface. Rate laws are experimentally determined and depend on process variables, such as temperature, chamber pressure and the extent of stirring. These variables determine which of the three kinetic steps is rate-determining (or the rate could be mixed-controlled by one or more of the steps). The catalogue of experimental results was used to identify the rate equation, and the process window in which this equation applies, for the routes in Figures 4.7 and 4.8. The kinetics of many routes have not been fully evaluated, so in these cases other experimental results are applied to estimate the rate at which copper is removed.

Rate equations have been determined for the reduction of copper concentration in distillation, reactive gas evaporation, leaching and vacuum arc refining. Distilling pure copper from an iron-based melt is governed by a first-order rate equation. A range of different process conditions can be employed, and there are several different rate-limiting regimes (Savov and Janke, 2000). Existing experimental work provides over 60 data points for the rate of copper concentration reduction in these regimes, which is presented in the appendix. First-order rate equations have been determined for the gaseous removal of copper when ammonia (Hidani et al., 1996), urea (Maruyama et al., 1998), or a chloridizing powder injection (Sasabe et al., 1996) is applied to an iron-based melt, but these equations apply only within the process window of the respective studies. The dissolution rate of copper in ammonium-based solutions has been studied extensively. Oden et al. (1973) investigate ammonium carbonate solutions, while Konishi et al. (2014) investigate the leaching rate of ammonium chloride and sulfate solutions while varying temperature and stirring rate. The maximum leaching rates,

and the associated process windows revealed by these studies are used here. The kinetics of solute removal during vacuum arc refining was investigated by Andreini and Foster (1974) and their proposed model is used here.

The remaining routes have not previously been characterized by a rate equation, so other information is used to estimate the rate of copper concentration reduction. To describe the removal of copper from the melt by a solvent or slag, the general rate equation for impurity removal during slag refining in steelmaking is used (Engh, 1992), with experimentally-determined distribution ratios for copper with the specific solvent and slag compositions. This assumes that transfer of copper through the melt phase is rate-limiting. There is no information available on the kinetics of copper removal by filtration, but Ghosh (2000) estimates the decrease in the flow rate if a ceramic filter were employed in steel tapping. With this set-up, the removal ratio reported by Savov et al. (2003) for an Al_2O_3-ZrO_2 ceramic is assumed. For unidirectional segregation, Nakamoto et al. (2014) describes the copper concentration gradient achieved in carbon-saturated iron with a specific cooling profile, and these results are used. For solid scrap treatments at elevated temperatures, namely applying a chloridizing gas (Tee and Fray, 2006) aluminum solvent (Iwase, 1996) or sulfidizing matte (Freuhan and Cramb, 1991), as well as preferential melting (Brown and Block, 1968) and oxygen embrittlement (Cho and Fan, 2010) experimental results provide the removal ratio of copper following a given treatment. These experiments show the chemical reaction is rapid, but the proportion of copper removed is limited by transport of reactants to, and products away from, the reaction site, which is dependent on the physical shape of the scrap. The physical presence of copper in typical shredded scrap, and the limitations this imposes for these techniques, has not been characterized, as experiments used simulated scrap. The rate of copper removal during magnetic separation and density separation similarly depends on prior shredding and fragmentation. However, copper removal during industrial magnetic separation as a function of shredded scrap density is reported by Newell (2017). Newell also describes how a copper-rich fraction of scrap could be isolated using a trommel system. Overall, the description for the rate of copper removal determined for each route and the conditions for which it applies is shown in Figures 4.9 and 4.10.

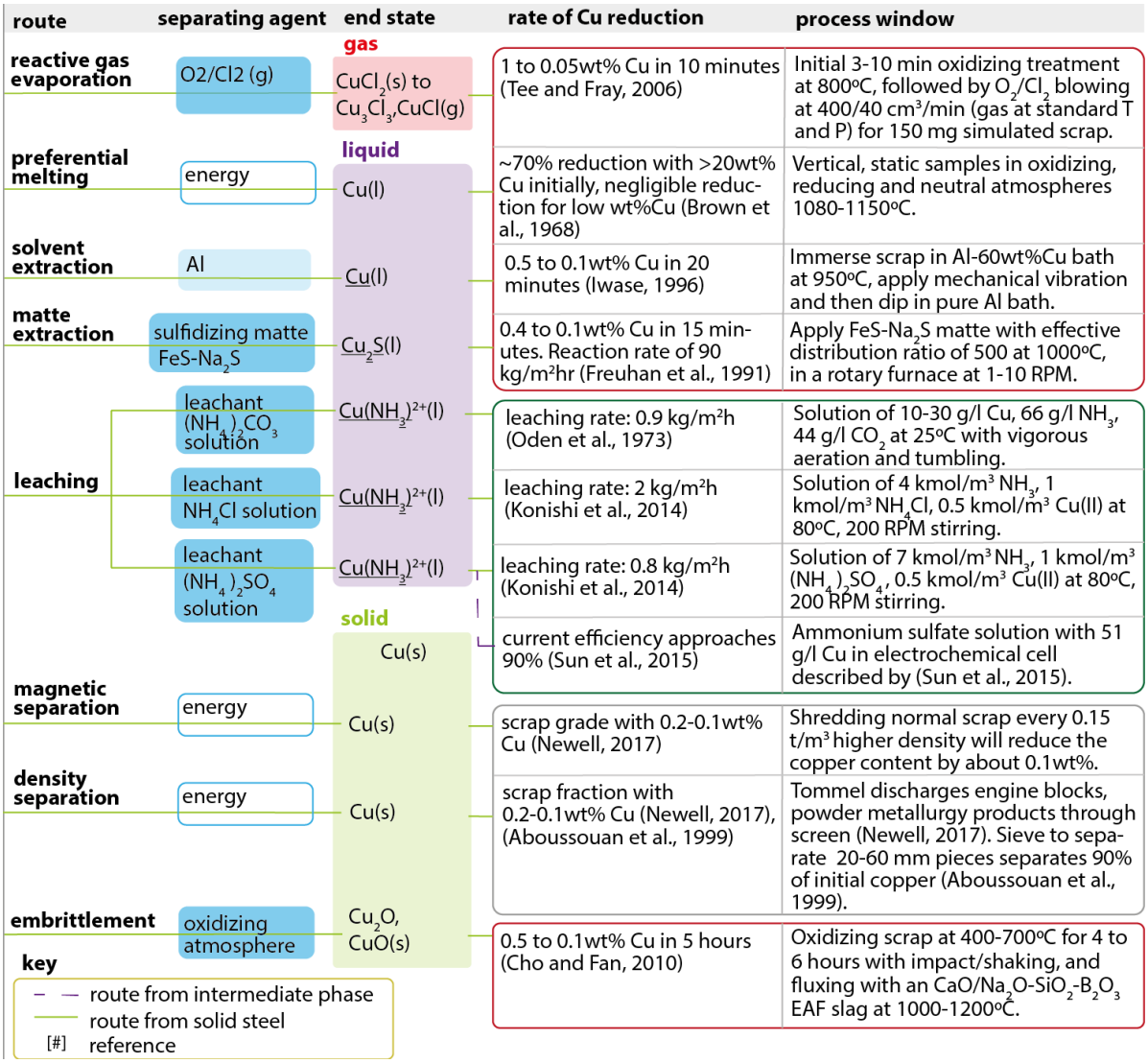

Figure 4.9: Routes for copper separation from solid scrap, with determined rates of copper reduction in the corresponding process window (summary of framework Step 2). The boxes surrounding the rate of copper reduction and process window information correspond with the process type: physical (gray), high-temperature treatments (red) and leaching (green).

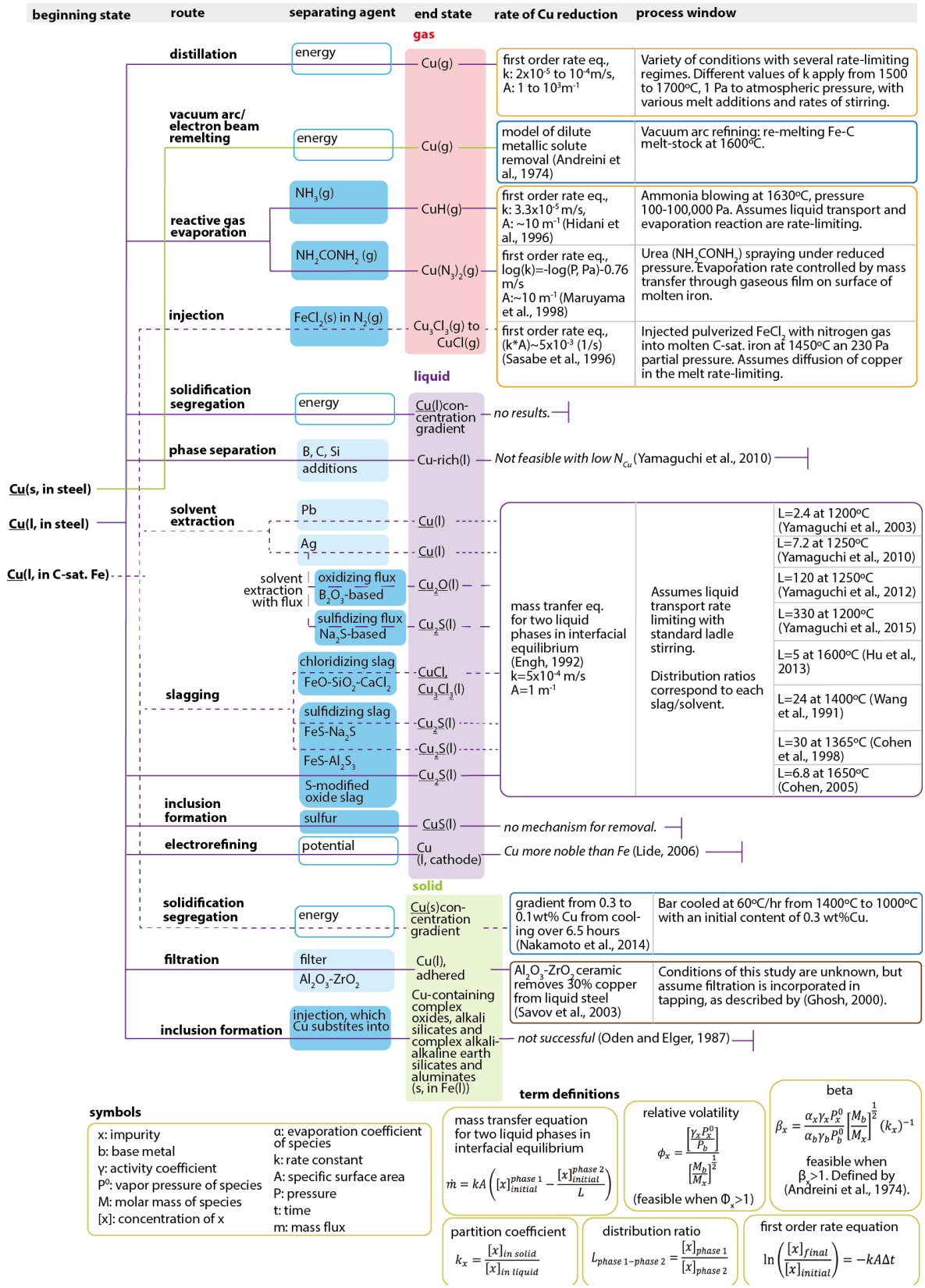

Figure 4.10: Routes for copper separation from the melt, with determined rates of copper reduction in the corresponding process window (summary of framework Step 2). The boxes surrounding the rate of copper reduction and process window information correspond to the process type: vacuum treatments (orange), slagging ladle treatments (purple), solidification segregation (blue), and filtration (brown).

4.1.3 Step 3: defining the potential processes.

This new framework aims to evaluate the feasibility of the various means to separate copper from steel, and this must account for the process requirements in practice. In the previous step, the rates of copper removal within certain process windows were evaluated. In practice, the required process conditions are delivered by industrial reactors. Therefore in this step, an industrial reactor, which could deliver the temperature, rates of stirring/agitation and contact with reactants as stipulated in the last column of Figures 4.9 and 4.10, was identified for each route. For distillation, a range of process conditions have been investigated so several potential processes are defined, including standard vacuum degassing. Scalable processes have been proposed in the academic literature or patents for the chloridizing gas treatment (Tee and Fray, 2006), oxygen embrittlement (Cho and Fan, 2010), leaching with ammonium-carbonate (Oden et al., 1973), vacuum distillation (Harris, 1988), (Warner, 2004), (Zaitsev et al., 2004), and slagging with FeS-Al_2S_3 (Cohen and Blander, 1998). Improved shredding and physical separation have already been demonstrated at scale (Newell, 2017).

The proposed reactor and process conditions for each route are shown in Figures 4.11 (solid scrap treatments) and 4.12 (melt treatments). The routes fall into the following types of processes: solid scrap physical separation, high temperature solid scrap treatments, leaching, vacuum treatments, slagging ladle treatments, filtration and solidification segregation. With an appropriate reactor and process conditions stipulated, treatment time can be estimated. The time to achieve 0.1wt% copper from an initial copper concentration of 0.4wt% was determined for all cases, using the relationships from Step 2. Some processes cannot achieve 0.1wt% copper, so the time to reach the greatest reduction in copper concentration possible is calculated. The estimated treatment time for each process is shown in Figures 4.11 and 4.12.

process route	reactant	reactor	T(°C)	time (min)	$[Cu_F]$ (wt%)	sources of energy consumption (per tonne steel)		secondary effects
improved shredding, magnetic separation		hammer shredder at lower process rate, or shredded in several passes, for 1.2-1.5 t/m^3 density.	25	varies	0.2-0.1	electricity for more intensive shredding or iterations (2-3 passes)	20-40 kWh/t (Lassesson, 2008)	improved yield, cleanliness in EAF
separate copper-rich fraction with sieve/trommel		trommel system described by (Newell, 2017)	25	varies	0.2-0.1	shaking/vibration	0.5 kWh/t	divert/further process copper-rich fraction.
						electricity for trommel system	0.5 kWh/t (Bianna Recycling, 2018)	
reactive gas evaporation	O_2/Cl_2	chlorination process described by (Tee and Fray, 2006)	800	10	0.1	total process energy consumption	27 kWh/t estimated by (Tee and Fray, 2006), assuming scrap at 800°C	Fe oxidation, external Zn, Sn also chloridize.
						transition into EAF	10-20 kWh/t	
preferential melting		continuous conveyor scrap heating in tunnel furnace (as demonstrated by Consteel: Jiemin et al., 2005) with vibration applied above 1083°C	1100	5-10	0.4-0.35	powering furnace during treatment	3-5 kWh/t	
						shaking/vibration	0.5 kWh/t	
						transition into EAF	10-20 kWh/t	
solvent extraction	Al	2 90t channel induction furnaces for Al baths with vibratory conveyor between	950	20	0.1	heating 20 kg Al to T	7-10 kWh/t	Al adherance, oxidizes in EAF (heat of formation: 172 kWh/t (Adolf et al., 2016))
						powering Al furnaces during treatment	20-30 kWh/t (Schmitz et al., 2014)	
						heated vibratory conveyor	4-6 kWh/t	
						transition into EAF	10-20 kWh/t	
matte extraction	FeS-Na_2S	rotary kiln (similar to (Zhang et al., 2008)) at 5RPM with matte as molten pool	1000	15	0.1	heating 10 kg matte to T	5-6 kWh/t (Matousek, 2008)	S contamination: desulfurization required, 20-30 kWh/t (Ghosh, 2000)
						powering furnace during treatment	4-6 kWh/t	
						tumbling	1-2 kWh/t	
						transition into EAF	10-20 kWh/t	
embrittlement	oxidizing atmosphere	oxidizing tunnel furnace with shaking	500	240	0.2-0.1	powering furnace during treatment	30-45 kWh/t	Fe oxidation
						shaking/vibration	1-2 kWh/t	
		subsequent fluxing in rotary kiln: (Zhang et al., 2000)	1000	15	0.1	fluxing treatment	20-35 kWh/t (similar to matte extraction above)	
leaching	$(NH_4)_2CO_3$ based	leaching reactor with stirring and aeration(Jung et al., 2016)	25	1440 (24 hr)	0.2-0.1	aeration	40-65 kWh/t	must be dry before EAF.
						stirring	30-40 kWh/t	
	NH_4Cl based	heated leaching reactor with stirring (Jung et al., 2016)	80	720 (12 hr)	0.2-0.1	heating scrap to T	15-25 kWh/t	
						maintaining T	15-25 kWh/t (Spirax, 2018)	
						stirring	15-20 kWh/t	
	$(NH_4)_2SO_4$ based	heated leaching reactor with stirring (Jung et al., 2016) followed by electrodeposition (Sun et al., 2015)	80	1440 (24 hr)	0.2-0.1	heating scrap to T	15-25 kWh/t	
						maintaining T	30-50 kWh/t (Spirax, 2018)	
						stirring	30-40 kWh/t	
						electrodeposition power	6-10 kWh/t (Sun et al., 2015)	
leaching with prior incineration	added to any leaching process above					heat scrap to 800°C	185-280 kWh/t	
						leaching process	45-125 kWh/t	

Figure 4.11: The reactor, conditions, sources of energy consumption and secondary effects of the physical solid scrap (gray), high temperature solid scrap (red), and leaching (green) potential processes.

process route	reactant	reactor	T(°C)	time (min)	$[Cu_f]$ (wt%)	sources of energy consumption (per tonne steel)		secondary effects
vacuum degassing (minimal)		tank degassing at 100 Pa, $A=0.5m^{-1}$, $k= 2x10^{-5}$ m/s (Savov et al., 2000)	1600	10	0.39	total process energy consumption	15 kWh/t (Winkler et al., 1971), (Ghosh, 2000)	other volatile impurities, inclusions, metallic elements simultaneously distilled
vacuum degassing (vigorous)		re-circulation degassing at 10 Pa, $A=2m^{-1}$, $k=6.5x10^{-5}$ m/s (Savov et al., 2000)	1600	30	0.32	total process energy consumption	50 kWh/t (Winkler et al., 1971), (Ghosh, 2000)	
extended vacuum distillation with bubbling		160 tonne ladle with argon bubbling at 50 Pa, model from (Zaitsev et al., 2004)	1600	130	0.1	heating during treatment	70-140 kWh/t (Ghosh, 2000)	
						applying vacuum	1-2 kWh/t (Kuznetsov et al, 2007)	
						increased pumping	10-20 kWh/t	
extended spray distillation in vacuum		1mm diameter drops in 10 Pa vacuum, $k=6.5x10^{5}$ m/s (Savov et al., 2000)	1600	4s	0.1	heating during treatment	125-220 kWh/t (Spirax, 2018)	
						applying vacuum	1-2 kWh/t (Kuznetsov et al, 2007)	
NH_3 gas evaporation	NH_3 gas	NH_3 blowing at 200 Pa, $A=10m^{-1}$, $k=3.3x10^{-5}$ m/s (Hidani et al., 1996)	1600	60	0.1	heat loss during treatment	45-115 kWh/t (Ghosh, 2000)	Nitrogen supersaturation
						increased pumping	10-20 kWh/t	
sulfide slagging (C-sat)	FeS-Al_2S_3	160 tonne ladle with stirring, $A=1m^{-1}$, $k=5x10^{-4}$ m/s. Scalable process described by (Cohen and Blander, 1998).	1365	50	0.1	heating 100kg slag to T	40-50 kWh/t (Matousek, 2008)	prior carburization, S contamination: desulfurization required (20-30 kWh/t (Ghosh, 2000))
						heat loss during treatment	4-5 kWh/t (Lange, 1988), (Alexis et al., 2000)	
						stirring	1 kWh/t	
						decarburization	+90-110 kWh/t (Madias, 2014)	
unidirectional solidification (C.-sat)		furnace at a cooling rate of 60°C/hr	1400 to 1000	400 (6.5 hr)	gradient 0.4-0.32	powering furnace during treatment	400-600 kWh/t (Margolis et al., 2000)	other elements present may also form a concentration gradient and effect how copper partitions
vacuum arc re-melting		melting 30t ingot at 9 kg/min in vacuum, described by Scholz	1600	720 (12 hr)	0.2-0.1	total process energy consumption	700-1100 kWh/t (Scholz et al., 2014), (Krüger et al., 2005)	
ceramic filtration	Al_2O_3-ZrO_2	filtration during tapping as described by (Ghosh, 2000)	1600	20-30	0.28	heat loss during treatment	20-30 kWh/t (Ghosh, 2000)	ceramic particle contamination

Figure 4.12: The reactor, conditions, sources of energy consumption and secondary effects of the vacuum treatments (orange), slagging ladle treatments (purple), solidification segregation (blue) and filtration (brown) potential processes.

4.1.4 Step 4: estimating specific energy and material consumption.

This last step evaluates the specific energy and material consumption of the processes defined in Step 3. It was assumed that each process would be integrated into the conventional steel recycling route, as shown in Figure 4.13. The energy – heat and mechanical – as well as material inputs required directly by the treatment, per tonne of steel treated, are estimated. Secondary effects of the treatment on the composition of steel, and additional energy and materials consumed as a consequence, are identified and added as well. A full breakdown of the sources of specific energy and material consumption for each process is explained in the Appendix, A3.

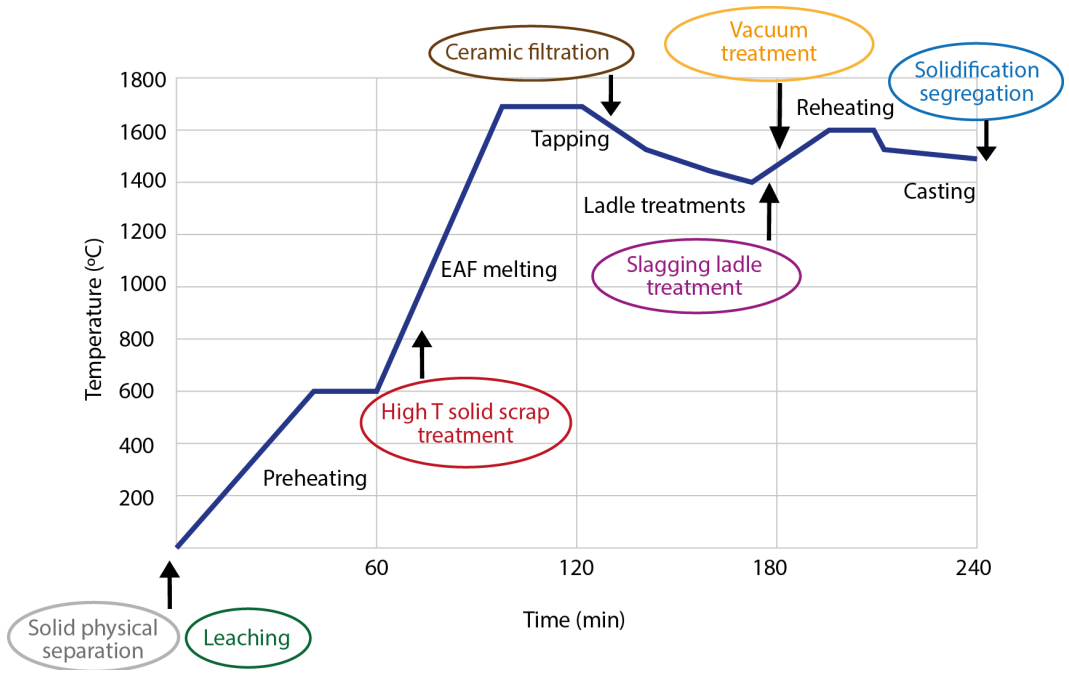

Figure 4.13: Temperature-time profile of the assumed EAF route informed by Yin (2009) with placement of potential processes.

The heat required for each process is estimated by calculating a heat balance. The assumptions behind the heat balance for each process type (melt treatments, high temperature solid scrap treatments, leaching and solidification segregation) are explained here. For melt treatments, heat is supplied by superheating in the EAF or arc heating in the ladle. The heat balance is estimated assuming the steel melt is initially at the required temperature, but that any additional reactants must be heated to temperature, and that energy of reaction and any energy losses from radiation and conduction must be included. Losses are highly dependent on the system and its geometry, so reported rates for vacuum degassing systems, ladles and tapping are used. To overcome these losses, liquid steel has a heat capacity of 0.22 kWh/tonne°C (Kor and Glaws, 1998) and an average efficiency of 50% for melt heating

methods is reported by Breus et al. (1999) while best practice could achieve 70% (Goodman et al., 2012), so a range of 50-70% is assumed here. The high temperature solid scrap treatments could be incorporated into scrap heating. Alternative designs exist for heating scrap with waste gases and direct combustion for energy savings compared to the EAF route (Zhang et al., 2008), (Jiemin et al., 2005). It is assumed that heating to the process temperature in the proposed furnace is as efficient as the conventional route, and that a continuous process to the EAF could be developed, but 10-20 kWh/tonne (Entec, 2006) is added to each high temperature solid scrap process to account for heat losses during the transition to the EAF. The process heat energy would be for powering the furnace during the treatment – i.e. maintaining 1000°C for an additional 10 minutes, and heating the additional reactants. These requirements are informed by the breakdown of heat outputs for a steel billet reheating furnace provided by Chen et al. (2005), and an assumed heating efficiency of 40-60%. For leaching, the process takes place at room temperature, or 80°C (in which case the energy to maintain the reactor at 80°C is calculated), but an additional heating step may be required before leaching. Sano et al. (1998) suggest prior incineration to remove enamel, so the specific energy consumption of raising scrap to 800°C is added in one version of the process. Lastly, the solidification processes take place during or after casting. Unidirectional solidification would replace the standard casting process, but requires slow cooling in a high-temperature furnace. Vacuum arc re-melting is a completely auxiliary re-melting step and reported rates of energy consumption for this process in practice are used here (Scholz et al., 2014), (Krüger, 2005).

Mechanical energy is required to improve mass transfer through tumbling, stirring, applying gas flow or reducing chamber pressure. The rate of energy consumption for these functions is dependent on process design, so data from representative equipment is used to inform the following power requirements per tonne of steel: 0.5-1 kW for shaking/vibrating scrap, 1-2 kW steel for rotating scrap, 2-3 kW for stirring during leaching, and 1.5-2 kW for electromagnetic stirring of the melt. These requirements are then multiplied by the process time and included as a source of energy consumption, as appropriate. For reducing chamber pressure, there is a wide range of metallurgical vacuum pump systems in use. Traditional steam ejector systems require about 50 kWh/tonne steel to achieve a vacuum, but commercially-available dry pumps can reduce chamber pressure to 50Pa with 1-2 kWh/tonne energy (Kuznetsov and Kats, 2007), so this figure is used here. Modern metal shredding uses approximately 20 kWh/tonne (Lassesson, 2008). This figure is used to estimate the energy

requirement of higher-density shredding. These sources of energy consumption for some of these processes are shown in Figures 4.11 and 4.12.

The material input required for the various processes may include a leachant, solvent, gas, or slag. Some of these materials may be re-circulated or re-used, so to enable a fair comparison of all processes only the amount of material directly consumed per tonne of steel processed is considered in this analysis. For leaching and solvent extraction, treatments require immersion (a typical liquid/solid ratio is 5ml/g, e.g. 5,000 l leachant/tonne steel, or 12 tonne liquid Al/tonne steel) in a leachant or solvent that can be re-used for further batches, so only the amount that must be replaced per tonne of steel treated is considered. For the leachant, the quantity of reactants consumed is calculated from the stoichiometric equation. Using aluminum as a solvent yields a valuable Al-Cu alloy, but aluminum adheres to the scrap and is effectively oxidized in the EAF, so this lost quantity is estimated. For chloridizing and oxygen embrittlement treatments, the amount of gas consumed is calculated from the stoichiometric reaction involving copper. The amount of slag, solvent or matte required is calculated from the distribution ratio at equilibrium. The associated embodied energy of these quantities of consumed material was calculated using values from the literature.

Secondary effects of the treatment, including iron oxidation, adherence of the reactant, carburization and melt contamination have implications for energy and material consumption, and must also be considered. The chloridizing gas and oxygen embrittlement treatments also result in steel oxidation, so the iron oxidized and the oxygen consumed is estimated. The slagging ladle treatments require carbon saturation (the activity of copper is increased and the melt temperature can be reduced, which progresses the reaction of copper to copper sulfide). However, EAF's typically process low carbon steel, so the additional energy and material required for prior carburization and subsequent decarburization is also attributed to these processes. The sulfidizing matte and slag treatments contaminate the melt with sulfur, so a desulfurization ladle treatment is required. Applying an ammonia gas during copper distillation supersaturates the melt with nitrogen, so a vacuum treatment is subsequently required. These considerations are summarized in Figure 4.11 and 4.12.

4.2 Results

The framework described in 4.1 allowed comparison of the additional energy and material required by all separation techniques for reducing copper concentration. In Figure

4.14, the final copper concentration achieved by each process in Figures 4.11 and 4.12 is plotted against the additional specific energy required by the process.

4.2.1 Specific energy consumption

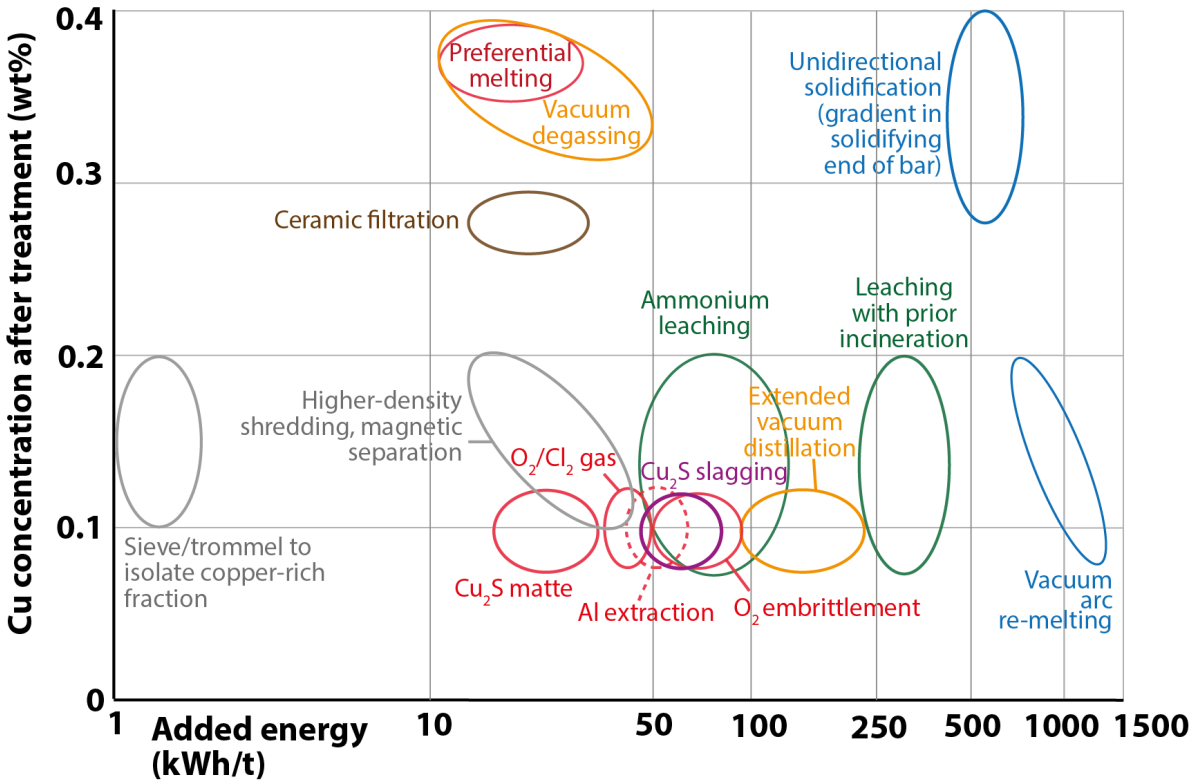

Figure 4.14: The copper concentration reduction from 0.4wt% and estimated specific energy consumption for the various processes defined in Figures 4.11 and 4.12.

The processes in Figure 4.14 span a wide range of specific energy consumption. Processes on the far-right require long treatment times at high temperatures, while processes on the left could be incorporated nearly seamlessly into the steelmaking route. Unidirectional solidification and vacuum arc re-melting exploit the segregation of copper from steel during solidification, but this requires slow and carefully controlled cooling, and leads to limited partitioning. Vacuum arc re-melting could reliably remove copper and is in commercial operation, but because it requires re-melting in a vacuum at extremely low process rates, its use is limited to high quality, low volume steels for which the high energy cost is justified. On the other end of the spectrum, improved physical separation of solid scrap can be efficient and effective. Abboussouan et al. (1999) show that the copper concentration in shredded scrap varies with the size of the steel fragments, so a sieve or trommel system could isolate the copper-rich fraction. Products could be shredded to a higher density to improve liberation for

magnetic separation. Preferential melting and ceramic filtration techniques appear less effective: copper adheres to scrap upon melting, and copper is absorbed from the melt onto the ceramic at a low rate.

A cluster of processes could remove copper to 0.1wt% with relatively low specific energy consumption (20 to 125 kWh/tonne). The most viable appear to be the high temperature solid scrap treatments: sulfide matte extraction, applying a chloridizing gas and aluminum extraction, which could be incorporated into scrap heating and have fast reactions. Another viable solid scrap process is ammonium leaching, but the rate is slow and its energy consumption comes from stirring the leachant over these long treatment times. The energy cost of ammonium leaching varies widely, as the type of leachant used has implications for the process requirements (an ammonia carbonate-based leachant requires vigorous aeration, while ammonium chloride does not). Prior incineration to remove enamel and allow contact between the leachant and copper has a high energy cost. Processes requiring immersion at elevated temperature (aluminum extraction and leaching) are only viable when running continuously. To maintain the temperature of the vat, an energy requirement of 20-40 kWh/tonne steel can be expected, but the energy cost to bring the entire quantity of solvent or leachant to treatment temperature for a batch is prohibitive (over 5,000 kWh/tonne steel for aluminum extraction at 950°C and over 800 kWh/tonne steel for leaching at 80°C).

Standard vacuum degassing has a similar energy requirement to the potential solid scrap treatments, but copper is only partially removed. Typically, melt vacuum treatments are designed to remove only gases and non-metallic inclusions. The most vigorous degassing process in operation would reduce copper concentration to about 0.32 wt%. To remove more copper the reaction rate, specific surface area, or treatment time must be increased. The reaction rate, k, is greatest at high temperatures and low pressures (or a high scavenging gas flow rate) and with certain additions to the melt, as shown in the supplementary information. However, k is limited by the rate of evaporation at the interface. The specific surface area can be increased by bubbling in a vat or spraying the melt. However, radiative heat loss is proportional to specific surface area multiplied by treatment time ($A^*\Delta t$), so there is a tradeoff between copper removed and the total energy required. Hidani et al. (1996) applied a gas to the melt in an attempt to form a more volatile copper-containing compound, but k was similar to the value in distillation and the reaction (and whether heat is added or further subtracted from the system) was not fully characterized. Overall, transferring copper from the melt to the gaseous phase is kinetically difficult.

Copper could be transferred from the melt to a liquid phase, which is kinetically easier in comparison to gaseous transfer. For sulfide slagging, k is higher, the reaction is exothermic and radiation heat losses are prevented by a thick slag during processing. However, carburization of the melt is required, which is difficult to incorporate into EAF steelmaking. Here, it is assumed that sulfide slagging would occur in a ladle process, but commercial ladles are not equipped for carburization and decarburization. Overall, melt treatments, whether gaseous or liquid may require more energy than solid scrap treatments, but have the advantage that they can remove copper in solution, not just that external to the steel scrap.

4.2.2 Specific material consumption

Figure 4.15 shows the quantity of material required to treat one tonne of steel from 0.4 to 0.1wt% copper concentration in the various processes, and the associated embodied energy of the required material. The secondary effects of the processes are shown in the right-hand side of Figure 4.15. Energy-based physical separations are not included as they require no direct material inputs. For the processes which require material inputs, a distinction in the amount of material required between melt and solid scrap treatments can be seen.

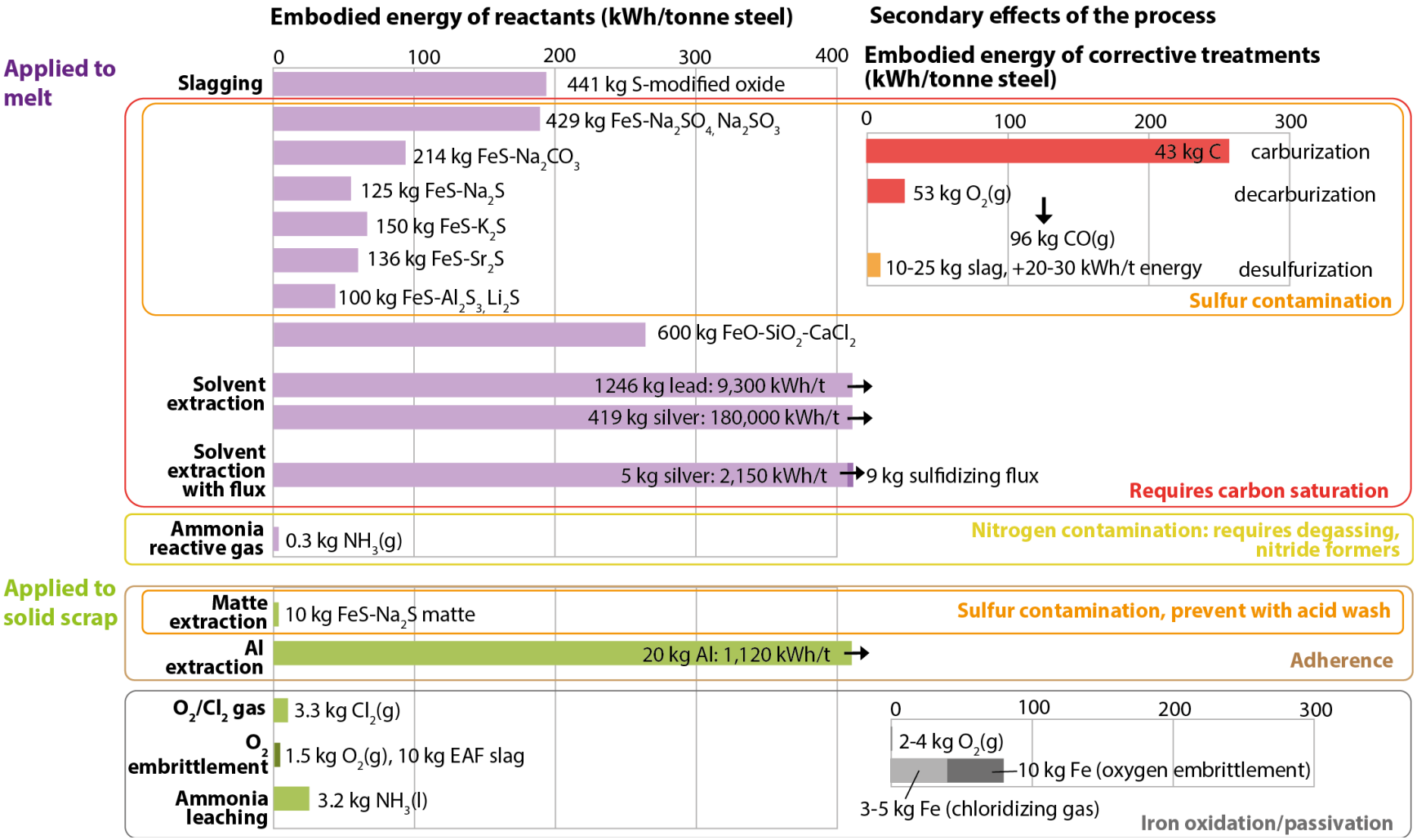

Figure 4.15: Mass of material reactants (kg/tonne steel treated, labeling the bars) and the calculated associated embodied energy (kWh/tonne steel treated, plotted) to reduce copper concentration from 0.4wt% to 0.1wt% in the various processes. Materials needed for corrective treatments, and other contamination problems caused by the treatment are shown to the right. All slag materials were calculated from the same embodied energy figure for a standard slag. The embodied energy values for metals are for the primary route.

Melt treatments have high specific material consumption, with a minimum slag requirement of 100 kg/tonne. Laboratory investigations attempted to reduce this amount by optimizing slag composition. Most experiments used sodium-based additions, but Wang et al. (1991) performed a systematic survey of alkaline and alkaline earth metal sulfide additions and determined Al_2S_3 to be the most favorable. This resulted in a distribution ratio of 30, but this is an order of magnitude lower than the distribution ratios achieved in conventional impurity slagging, which operate with approximately 10 kg slag/tonne. The amount of slag required could be further reduced by iterative applications or establishing a counter-flow. Cohen et al. (1998) describes this method, as well as a process to re-generate the Al_2S_3-based slag, but because this is operationally more difficult and would reduce the thermal efficiency of the process, it will probably not be practical for melts containing less than 1wt% copper.

Sulfur contamination of the melt also renders these slags impractical. Studies report contamination of the melt with 0.1 to 1wt%S – up to 100 times higher than levels typically encountered in refining. The sulfide-modified oxide slag designed by Cohen (2005) and the chloride slag designed by Hu et al. (2014) prevent sulfur contamination, but the distribution ratio of copper is much lower. Yamaguchi et al. (2010) demonstrated that metallic solvent layered between the melt and flux would prevent contamination while reducing the amount of flux required, but this is not practical because the relative densities do not allow layering in this way.

The processes applied to solid scrap generally require less material inputs than those applied to the melt, but the secondary effects of each process must be carefully considered. When applying a sulfide-based matte to solid scrap, copper is present pure, rather than dilute, so less matte is required, but sulfur contamination is still an issue – extended desulphurization, requiring an additional 20-30 kWh/tonne, would be necessary. For aluminum extraction, it was estimated that 20 kg/tonne steel of aluminum would adhere to scrap and oxidize in the EAF. This oxidation reaction would generate up to 265 kWh/tonne of chemical heat (Adolf and Socha, 2016), but this would not be energy-efficient considering the high embodied energy of aluminum. The chloridizing gas treatment appears feasible with a small amount of oxygen and chlorine consumed. Other impurities combined with steel – tin and zinc – would also chloridize, but some iron would be lost as iron oxide. Furthermore, chlorine gas is toxic and corrosive, which limits its use in practice. Alternatively, an ammonium-based leachant has a low toxicity, and Sun et al. (2015) demonstrate copper could be deposited, while re-generating the leachant with electrowinning.

4.3 Discussion

Figure 4.14 shows that processes could be developed to remove copper with relatively low energy consumption. Defining a process from a principle is complex, but the thermodynamic and kinetic constraints provided in Figures 4.7-4.10 define the space within which a process will operate. Figure 4.14 shows that improved physical separation, vacuum distillation, slagging and solid scrap pre-treatments can reduce copper concentration to 0.1wt% while adding only 5-20% to the melting energy of the EAF route. This discussion now considers how these four types of processes might be developed within the identified constraints to fit within steelmaking and further reduce the estimated energy and material inputs.

Physical separation in the solid-state is energy-efficient, but depends on prior shredding. The cheapest light scrap is often used in EAF steelmaking because scrap accounts for approximately 70% of costs (Toulouevski et al., 2010). Higher-density shredding may require at least twice as much specific energy as the conventional process. Whether this scrap can be directly priced according to copper content (perhaps enabled by real-time bulk composition analysis (Gamma-tech, 2018)), will determine the adoption of these practices by the scrap processor. A copper-rich fraction could be diverted by a trommel (Newell, 2017) or ballistic system (Steinert, 2018), (Shattuck et al., 2018). In this approach, the significant fraction (20-30%) of diverted scrap, could be directly used for products requiring copper as an alloying element (such as COR-TEN), or this step could concentrate copper before another extraction process.

Solid scrap pre-treatments also have potential for innovation. Melt processes require extended time at high temperature, but integrating a process into scrap heating might require little additional time and energy. Preferential melting appears limited by copper's adherence to steel scrap, but Leak et al. (1973) show that melting within a neutral molten salt medium, which also provides efficient heating and limits oxidation, could overcome this problem. Applying a sulfidizing matte to solid scrap appears particularly energy-efficient, but the efficiency decreases when accounting for the effects of sulfur contamination. Significant progress has been made on developing an efficient leachant and process design to electrowin copper from e-waste (Ghosh et al., 2015), and these same principles could be applied to steel scrap. In general, the irregular shape of end-of-life scrap and the heterogeneous distribution

of copper within it may hinder the deployment of solid scrap processes. Jimbo et al. (1988) report that 90% of contaminating copper is present at the surface of scrap feedstocks, but applying reactants to such a large surface area of fragmented scrap may not be practical. Additionally, copper in solution with steel from previous recycling will return in greater quantities, and these solid scrap techniques will not be effective.

The main limitation to vacuum distillation identified in this study is the radiative heat loss during an extended treatment. Previous research focused mainly on increasing the rate of copper evaporation at intermediate pressures, but low-pressure vacuums are increasingly used in metallurgy and theoretically require little energy – dry pumps significantly reduce energy and coolant water consumption compared to steam ejector systems (although have a higher capital cost) (Kuznetsov and Kats, 2007). Heat losses hinder prolonged melt vacuum treatments, but are dependent on reactor design. Therefore, opportunities exist to design optimized reactors, which shield radiation, while generating a high surface area to volume ratio and providing an efficient heat source. A reactive gas to evaporate a volatile copper compound may be beneficial if the reaction is exothermic and the gas does not contaminate the melt, but the gases proposed thus far are not suitable.

Removing copper through slagging is problematic. The only element that preferentially forms a compound with copper is sulfur, but this is a potent contaminant in steel. The carbon-saturation requirement and masses of slags are impractical, and given the extensive research on possible slag compositions, the space for improvement appears limited. A direction that has received little attention is applying electrolysis to displace the equilibrium of copper between the melt and slag. Rose (1981) used a cryolite-based slag containing cuprous sulfides. The current efficiency was small, but future work recommended exploring fluoride-based slags. Data on electrolytes for steel refining is lacking, as well as experimental work to support the design of a feasible cell.

This analysis focused on extraction processes, but there are many other supply chain interventions, as discussed in the introduction to this chapter. Hand-picking reduces copper concentration to less than 0.25wt%. The major factor limiting the efficient use of materials is the trade-off with labor, but automation could be a disruptive technology to change this dynamic (Material Economics, 2018). Intelligent sensing technologies, such as the system described by Shulman (2011), were not included in this analysis, as these are sorting techniques, not separation techniques rooted in physical and chemical properties. Down-cycling contaminated scrap to tolerant applications is viable now, but interventions for copper

control will be favorable when steel demand for these applications is saturated. Likewise, dilution is viable now due to abundant primary production. To dilute one tonne of steel from 0.4wt% copper to 0.1wt%, three tonnes of primary steel (with an average embodied energy of iron over 5,000 kWh/tonne) is required. As the global yearly scrap supply triples from present to 2050, primary production is projected to remain constant, so this ratio for dilution will not hold.

The analysis in this chapter evaluates potential processes from a physical basis, rather than economic. The principles governing separation are constant and universally applicable, while prices are volatile and vary greatly region to region. Developed countries with a growing end-of-life scrap supply, dwindling ore-based production and high-tech manufacturing industries will first confront the constraints caused by copper contamination. In these conditions, motivation to remove copper may exist, driven by the price differential between reinforcing bar and cold-rolled coil. In considering new processes, capital costs, equipment footprint and process time are important. These considerations can be compared amongst the proposed processes from the information in Figures 4.11 and 4.12. Capital costs may be significant, but the economics of EAF steelmaking are projected to only improve. Proper scrap management and the health of the industrial sector is in the national interest, so policies should support the transition to high-quality scrap-based production, and government-funded programs to spur innovation may be considered, as discussed by Allwood (2016b).

Many of the investigated processes would decrease productivity. The main focus of EAF innovations since the 1960's has been to increase productivity, because maintenance, labor, and overall plant expenditures decrease in turn (Toulouevski et al., 2010a). However, valuing systems and industry goals are sure to change as the urgency for reducing CO_2 emissions increases. Increasing productivity does not necessarily decrease environmental impacts. For example, the more intensive use of carbon and oxygen to decrease EAF time (Toulouevski et al., 2010a), directly increases CO_2 emissions. The energy and material implications of processing will be a principal deciding factor in the future.

Chapter 5. Preventing wetting between liquid copper and solid steel: a simple extraction technique

The content of this chapter is accepted for publication in Metallurgical and Materials Transactions B as "Preventing wetting between liquid copper and solid steel: a simple extraction technique." My co-authors contributed comments on draft versions of this paper. The experiments were performed at the Materials Processing Institute, where Dr. Adam Hunt provided training for the Misura heating microscope and assisted with technical questions. José Azevedo, a PhD student in the group, lathed my samples and Len Howlett's materials lab (Cambridge) was used for sample preparation and microscopy.

Chapter 4 shows that melt techniques such as sulfide slagging and vacuum distillation have received considerable investigation, but removing external copper before it is dilute within the melt requires less energy. Separations exploit a property difference, and the magnitude of the property difference is an a priori indication of the feasibility of separation. The difference in melting points between copper and steel is significant, and could be exploited to collect pure, liquid copper from solid steel. Melting is kinetically fast, and assuming the process is integrated into scrap heating, this step would require little additional energy. The analysis in Chapter 4 shows that physical density separation of solid scrap also uses very little specific energy (~1 kWh/t), and isolates a copper-rich fraction, so that the remaining stream contains 0.15wt% or less. Physical separation and preferential melting techniques could be used together: the copper-rich fraction could be treated with preferential melting to prevent external copper from entering the steel cycle.

Adherence of liquid copper to solid steel is the fundamental limitation. This chapter thus investigates whether a process window exists to prevent wetting between liquid copper and solid steel, by systematically observing the effects of key parameters: steel carbon content, initial surface oxidation and applied coatings. The methodology is described in 5.1, followed by results in 5.2 and a discussion on the mechanisms behind observed wetting behavior and the implications for future process development in 5.3.

5.1 Methodology

To observe the wetting behavior of copper in different conditions, copper was melted on various steel substrates and the droplet was observed with a heating microscope. Subsequent microscopy of the sample cross-sections revealed the character of the non-metallic surface layer, the interaction of copper with the surface layer and the distribution of copper across the substrate. Experimental procedures – the composition and surface preparations of the various steel substrates (5.1.1), the operating conditions of the heating microscope (5.1.2) and the preparation of the samples for microscopy (5.1.3) are detailed below.

5.1.1 Test matrix

Figure 5.1 illustrates the main variables of the wetting system, which determine the interaction at the liquid/solid interface:

- Environment: the environment could be gaseous or liquid, but the experimental apparatus limited observation to a gaseous environment. To maintain an oxide layer, but limit the growth of porous FeO, an inert atmosphere (argon) was chosen as a constant. Residual oxygen was present in the furnace, which reacted with the surface of the steel substrate.
- Steel composition: the composition of the steel varies widely in scrap, and this variability will influence iron oxidation and wetting behavior. Carbon content is the most important element because it can reduce the protective oxide layer. Unalloyed low and medium carbon steels, representative of the range of carbon contents encountered in practice were chosen to understand this effect.
- Surface condition: The surface condition of the steel scrap also varies in practice. Steel scrap may have no initial oxide layer (such as galvanized or coated steel, where the surface layer combusts around 800°C during pre-heating), or may exhibit a thick initial oxide layer of primarily magnetite from rusting during service. This range was investigated by preparing initially oxidized and initially ground sample surfaces. The surface condition may be further modified by applying a coating. Sodium metasilicate and sodium sulphate are widely available, cheap and non-toxic, so these coatings are applied to the various substrates to understand if they promote non-wetting behavior.

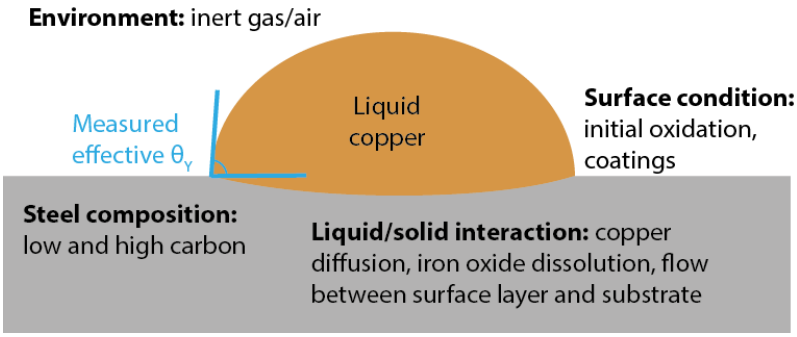

Figure 5.1: The copper/steel wetting system showing the variables at the focus of this study.

The test matrix is defined in Table 5.1. Each combination of steel composition, initial surface oxidation, and coating was tested, for a total of 12 distinct tests. Two additional tests were performed as well. To confirm the observations of other researchers, and understand the interaction of copper with the typically observed three-phase oxide layer, one test was performed with low carbon steel in air. To understand the wetting behavior of copper on a typical surface with no preparation, one test was performed on low carbon steel in the as-received condition.

Table 5.1: The characteristics varied between the different steel substrates. Each combination was tested in an inert atmosphere, for a total of 12 distinct tests.

Steel composition		Surface condition				
		Initial oxidation		Coating		
Low carbon	Medium carbon	Ground	Oxidized	None	Na_2SO_4	Na_2SiO_3

Commercially-available steels were used for the substrates. For a representative low carbon, unalloyed steel, CR4-grade was chosen. The CR4 steel was received in the black, cold-rolled condition as a 1mm-thick sheet, which was cut into 10x10mm square pieces. Key steel was chosen to represent an unalloyed medium-carbon steel used in general engineering applications, with a nominal carbon content of 0.35-0.45wt%. Steel with yet higher carbon content may be encountered in practice, but this medium-carbon steel represents the high-end of carbon content in wide-spread use. 10x10mm bar from RS Components UK was acquired, from which 1.5mm-thick sample pieces were cut (all pieces were then ground to a 2500 grit finish – therefore no samples for medium carbon steel were tested in the "as received" condition). Optical emission spectroscopy was performed on the CR4 and Key steel to determine their chemical composition beyond the nominal specifications. The composition as determined by the average of three sparks are shown in Table 5.2.

Table 5.2: Chemical composition of the low and medium carbon steel substrates.

Steel type	Element (wt%)									
	C	N	Si	Mn	P	S	Cr	Ni	Mo	Al
Low carbon	0.08	0.006	0.014	0.14	0.012	0.011	0.031	0.035	0.0058	0.039
Medium carbon	0.39	0.012	0.24	0.74	0.017	0.023	0.189	0.170	0.044	0.0012

To simulate steel scrap with a thick initial oxide layer, the samples were treated in a box furnace in air at 500°C for 24 hours. To simulate steel with a thin initial oxide layer, the samples were ground with sandpaper to 2500 grit and ultrasonically cleaned in water and rinsed with ethanol immediately before testing. Iron oxide forms on the surface of iron at room temperature rapidly after exposure to the atmosphere. Therefore, a thin initial oxide layer was present on the ground samples. To apply the coatings, sodium sulphate (Na_2SO_4 anhydrous, from Fisher Scientific UK) and sodium metasilicate (Na_2SiO_3, from Sigma Aldrich UK) solutions were prepared, as described in the patent by Leak and Fine (1973). 15 grams of Na_2SO_4/Na_2SiO_3 were mixed with 65 mL of water and the solution was stirred on a hot plate for about 10 minutes at 60°C to achieve dissolution. The steel samples were submerged into the solution and dried for about a minute under a hair dryer. The Na_2SO_4 coating left a white residue, while Na_2SiO_3 was present on the surface as a glassy gel.

Commercially-available copper wiring from wires.co.uk (99.95% purity) was used for the copper droplet. 2.64mm diameter bare copper wire was cut to 2.5mm length pieces, weighing 120-140 mg. All pieces were ultrasonically cleaned in water and rinsed with ethanol prior to testing to remove surface contaminants; however, a thin layer of copper oxide remained on the surface. Oxygen, either in solution with copper or in the form of copper oxide, effects the surface tension and wetting behavior of liquid copper, as characterized by Gallois and Lupis (1981). Copper wiring with a native surface oxide layer would be encountered in practice, so the condition studied here is relevant.

5.1.2 Droplet observation

The sessile drop technique is a standard experimental method to measure droplet shape – most commonly Young's contact angle. A Misura HSM2 heating microscope was used to observe the droplet, shown schematically in Figure 5.2. The steel substrates were

placed on the ends of two alumina sheaths, suspended within the furnace cavity. A thermocouple measured the temperature at the end of one of the alumina sheaths. The light source (a 50W halogen spotlight bulb) illuminated the sample on one end, while a camera imaged the droplet profile through a transparent quartz screen. Argon (from Air Products BIP N6.0 purity) flowing at a rate of 0.2 l/min was purged through the furnace cavity (200 x 18 mm diameter) and furnace inlet tube (40 x 3 mm diameter) for 60 minutes prior to testing, and flowed at the same rate during testing. A transparent quartz screen was secured at the end of the inlet tube, with a gap of 3mm between the screen and the tube. As the furnace cavity was not sealed, some oxygen was present in the system, which we estimate to be in the range of 10^{-4}-10^{-3} atm (Herring, 2009). A piece of metallurgical coke (approximately 12 x 12 x 3mm) was placed in the inlet tube, about 10 mm in front of the sample holder. Under flowing argon, the piece of coke had limited contact with oxygen for any substantial reaction, but CO(g) and CO_2(g) may have formed (Arthur, 1951), the ratio of which would have had a reducing or oxidizing effect (Linde Gas). These conditions were intended to approximate an inert industrial furnace. The atmosphere during testing remained oxidizing, evidenced by the surface oxide formed on all samples and decarburization of the medium carbon steel. Instrumentation or CO/CO_2 gas mixtures can be used to directly measure and control oxygen concentration. The present apparatus was not equipped with these capabilities, so this is recommended for future anlaysis.

The in-air test was run by flowing compressed air through the furnace, also at 0.2 l/min (the piece of metallurgical coke was removed for this test). The same heating profile was applied during each test. The sample was heated from 20 to 1,000°C at a rate of 50°C/min, and from 1,000 to 1,150°C at 5°C/min. The sample profile was illuminated and one snapshot was taken at each degree, from 1,000 to 1,150°C. The contact angles of both sides of the droplet were later measured manually using ImageJ software. In some cases, the copper wetting was rapid – the thermal cycles of the medium carbon tests were stopped early to prevent the sample from brazing to the thermocouple. After reaching the maximum temperature, the furnace was turned off and the samples were air cooled in the protective atmosphere of the furnace chamber.

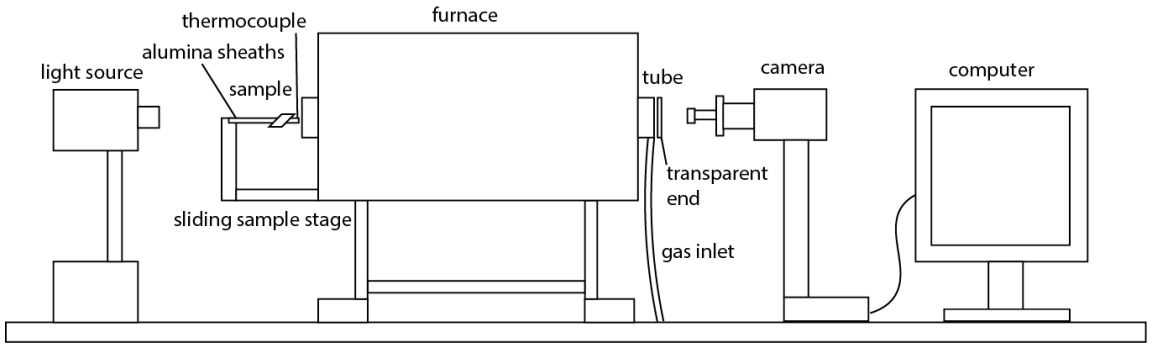

Figure 5.2: Schematic of the Misura HSM2 heating microscope.

5.1.3 Metallography

Upon cooling, samples were vacuum cold-mounted in epoxy and cross-sectioned through the center. Each sample was prepared using the standard grinding and polishing procedure, to 0.3μm with an alumina suspension. A Leica optical microscope as used to image the cross-section of each sample. All samples were imaged in the unetched condition. Later, a 2% Nital solution was applied to medium carbon substrates to reveal surface decarburization. Copper is easily distinguished in optical microscopy. Scanning electron microscopy (Desktop Phenom G2 Pro, 5kV working voltage of 5kV in back-scatter mode) was used to reveal the samples at higher resolution. Copper is distinguished as the lighter phase in these images. To determine the composition of the observed oxides and provide insight to the possible reactions resulting from the applied coatings, energy dispersive spectroscopy, EDS (Oxford instruments, x-act Penta FET Precision, 20 kV working voltage, IProbe=50pA) was performed at multiple points for several samples. To overcome difficulties with the non-conductive epoxy charging during EDS analysis, these samples were prepared with a gold coating and silver trace.

5.2 Results

Figure 5.3 shows snapshots of the copper droplet profiles on the low and medium carbon steel with different surface preparations at multiple temperatures upon melting, from 1060 to 1150°C. The most obvious distinction is between the low and medium carbon substrates: the droplets on low carbon steels are generally stable through to 1150°C, while the droplet disperses and spreads, on both the top and bottom surfaces, before the end of the heating cycle for the medium carbon steels. The copper droplet on the coated low carbon steels (with the exception of the oxidized-Na_2SO_4 sample) decreases in height and adopts a

non-symmetrical shape at the end of the thermal cycle. Amongst the various medium carbon substrates, the droplet on the oxidized sample was stable for the longest, and shows the highest temperature reached before complete spreading across the substrate. The coatings on the medium carbon substrates appear to accelerate wetting. The droplets on the Na_2SO_4-coated medium carbon samples show a textured, uneven surface developing on the droplet during spreading, while copper on the Na_2SiO_3-coated samples appears to flow rapidly under the lifted surface layer.

It should be noted that there is some variability on the left-hand side of the figure, in the temperature at which copper forms a droplet. The formation of a droplet prior to the melting point of copper (1083°C) can be explained by several factors. Commercially available copper wiring was used. Oxygen is the main impurity present in electrical copper, typically in the range of 250 to 400 ppm oxygen. The copper-oxygen phase diagram shows this level of oxygen decreases the melting point by 10-15°C. A discrepancy between the temperature of the sample and the temperature measured by the thermocouple is also present, which likely explains the different melting points observed between the tests. These factors should not affect the overall comparisons of droplet evolution between the different substrates.

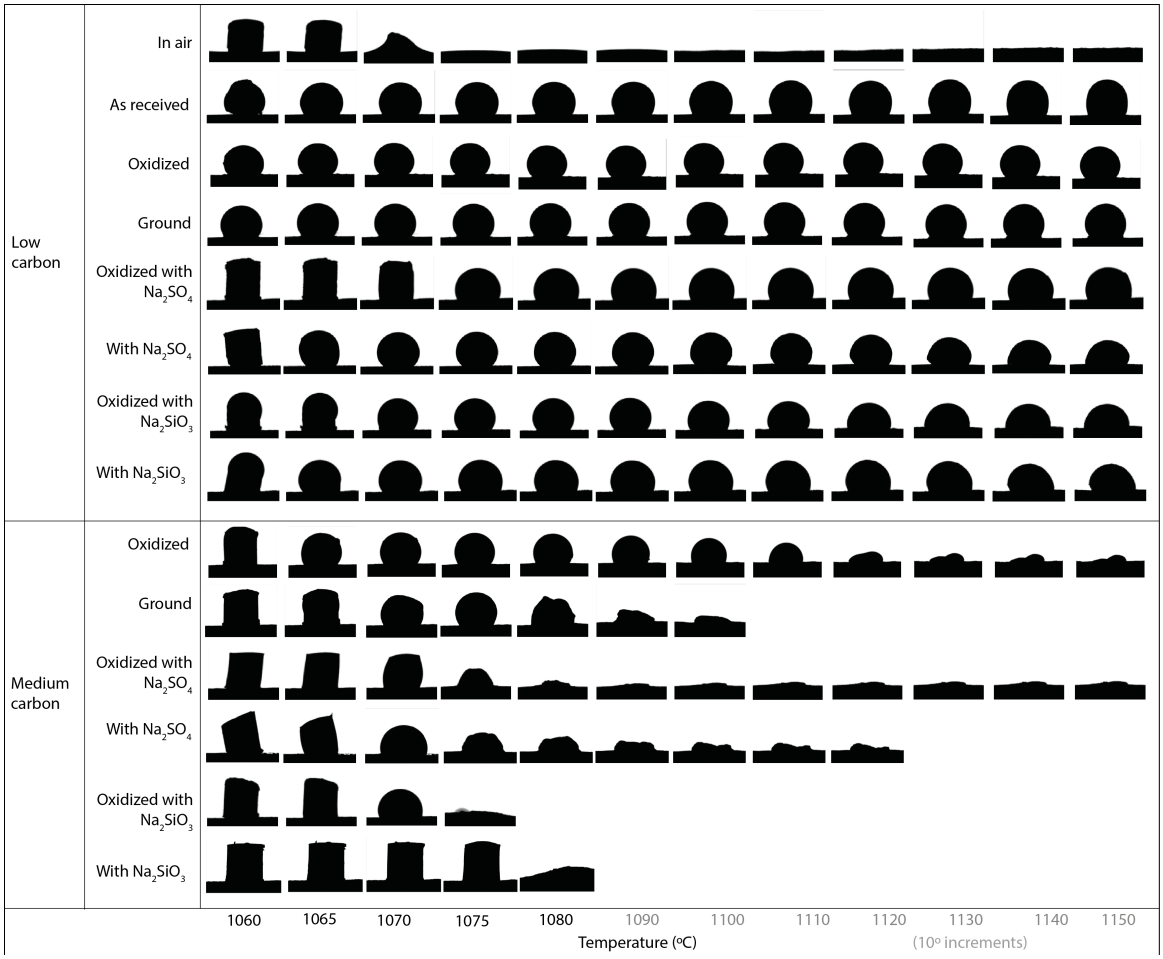

Figure 5.3: Profiles of copper droplets on low carbon and medium carbon steel with different surface preparations from 1060-1080°C at 5°C increments and 1080-1150°C at 10°C increments.

Figure 5.4 quantifies the contact angle (averaged between the left and right-hand side of the droplet) for the various substrates as temperature increases (at 5°C/min). The star-shaped marker denotes when the droplet forms, and an x-shaped marker shows when an asymmetric shape evolves (defined as when difference between the two sides is greater than 15°). Again, the main trend to note is the difference between the low and medium carbon substrates. The contact angle decreases to zero in all of the medium carbon cases, with the copper droplet on the oxidized medium carbon substrate maintaining a contact angle over 90° at the highest temperature. The droplets for the low carbon cases show a slight, gradual decrease in contact angle. The Na_2SiO_3 and Na_2SO_4-coated samples adopt an asymmetric shape at high temperature. The low carbon sample treated in air shows the most rapid wetting behavior of all cases, never forming a spherical droplet, but spreading immediately over the surface.

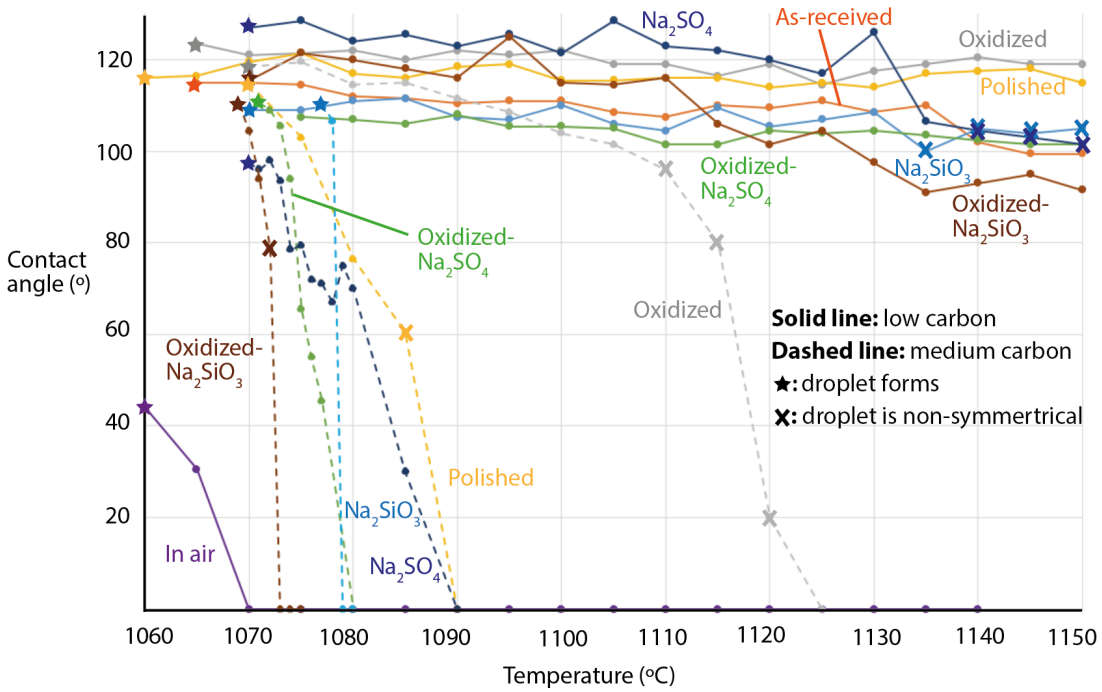

Figure 5.4: Droplet contact angle over temperature for all preparations. The heating rate in all cases is 5°C/min.

The cross-sections of the solidified copper on the substrates are compared side-by-side in Figure 5.5. The oxidized, ground and as-received low carbon steel samples show a spherical droplet with limited spreading. The reduced height and an assymetric shape of the droplets on the coated low carbon samples is explained by some copper flow between the surface scale and the substrate. The exception is the oxidized-Na_2SO_4 sample, which shows no copper flow between the surface layer and the substrate and negligible diffusion of copper into the substrate. The medium carbon substrates show copper spread sporadically over the top and bottom surfaces. In all cases, various pores, surface cracking and internal cavities of the copper droplet can be seen. This is a common observation for pure copper and high copper alloys, which are intrinsically susceptible to porosity (Konečná et al., 2012). The specific volume of copper decreases by 5% in the liquid-solid transition. Commercial copper casting uses a controlled, fine dispersion of oxygen to offset this decrease in volume. The sample cross-sections exhibit cracks and pores from uncontrolled shrinkage during solidification. Oxygen was present in the atmosphere and dissolution of the iron oxide in liquid copper. During cooling, oxygen solubility decreases. Excess oxygen can also react with hydrogen, resulting in water vapor porosity.

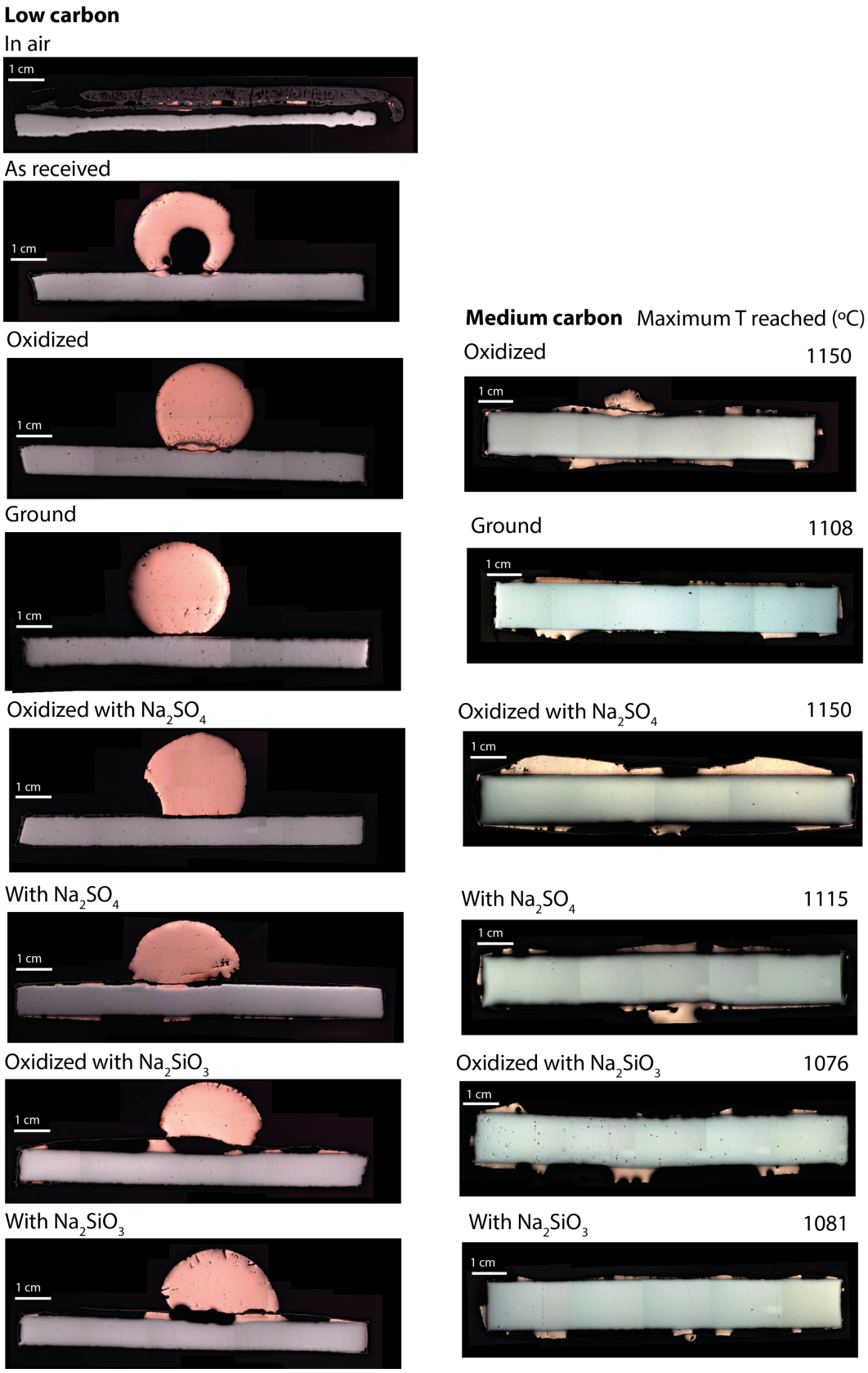

Figure 5.5: Cross-sections of solidified copper on all substrate preparations. All samples were air-cooled in the furnace chamber after the thermal cycle. All low carbon samples reached a maximum temperature of 1150°C, but to prevent brazing of liquid copper to the alumina sheaths the thermal cycle was stopped early for most medium carbon samples. The maximum temperature reached for the medium carbon samples is shown in the figure.

5.3 Discussion

The mechanisms controlling the observed wetting behavior must be determined. As discussed in the introduction, diffusion of liquid copper into the steel substrate, as well as chemical dissolution, reduction, and mechanical disruption of the oxide are known to promote wetting of copper to steel. Examining the varied substrates at higher magnification reveals evidence of these mechanisms. The implications for process development are then discussed.

5.3.1 Liquid copper wetting on steel in air

Figure 5.6 shows how copper distributes within the typical three-oxide layer scale that forms on low carbon steel when air is circulated through the furnace. The majority of the scale would be wüstite at high temperature, which transforms partially to magnetite upon cooling. Copper penetrates the pores in the wüstite, while the majority of copper appears to be present at a seam close to the substrate. This seam exhibits non-uniform features of oxides and pores. It appears iron oxide was delaminated from the surface by the flowing liquid copper, which exposed the surface to oxygen to allow further reaction. This result confirms that to enable copper separation, scale formation must be limited.

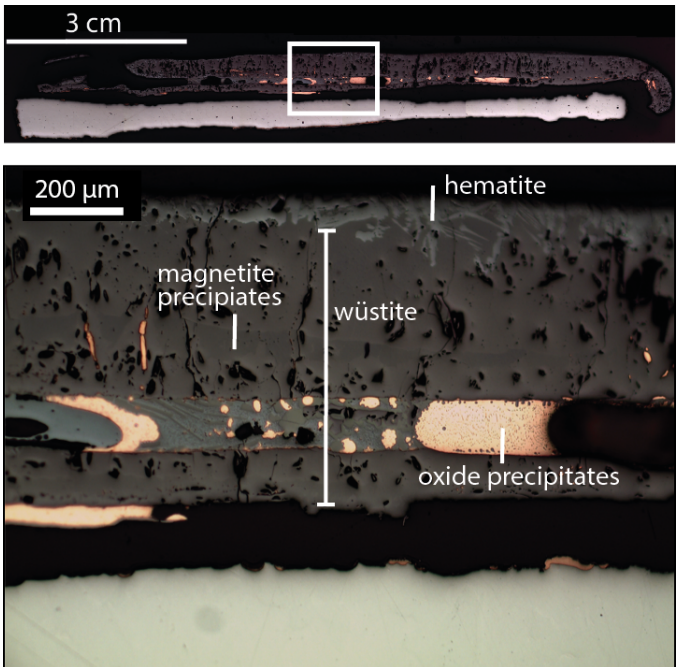

Figure 5.6: Iron oxide scale with liquid copper entrapment when low carbon steel was treated in air.

5.3.2 Liquid copper wetting on low carbon substrates

Figure 5.7 shows micrographs of the main features of the copper droplets on the low carbon substrates. For the uncoated low carbon samples with varying levels of initial oxidation, the main phenomena shown in these images are iron oxide dissolution and oxide precipitation on the surface of the copper droplet, copper diffusion into the substrate, and liquid copper flowing outwards in the gap between the oxide scale and substrate. The initially oxidized sample shows more oxide dissolution (and iron oxide precipitation) than the initially ground sample. EDS analysis reveals that iron oxide precipitated as a seam in the copper droplet. A thin copper oxide was formed on the surface of the droplet (EDS analysis shows the composition of this oxide varies and contains both iron and copper). For all of the uncoated samples, the iron oxide scale shows two layers distinguishable by color. The surface layer is a higher-oxygen oxide, Fe_3O_4 or Fe_2O_3. When contact of the scale with the substrate is disrupted, the transport of Fe ions is disrupted as well and the scale oxidizes further. The transformation of the iron oxide scale after a gap forms between the scale and substrate is described by Kim and Lee (2009). Thus, the proportion of the higher-oxygen oxide layer is an indication of when the scale was disrupted. The flow of liquid copper disrupted scale contact, especially for the as-received and ground conditions. Overall, it appears a non-wetting droplet with limited outward copper flow between the oxide layer and substrate can be achieved on uncoated low carbon steel whether there is a significant oxide layer initially present, or if the surface is ground or in the as-received condition. The oxygen in the furnace atmosphere reacts to form an adherent iron oxide layer on the initially ground sample. The oxygen also increases the surface tension of liquid copper and reacts to form surface oxides to impede droplet flow.

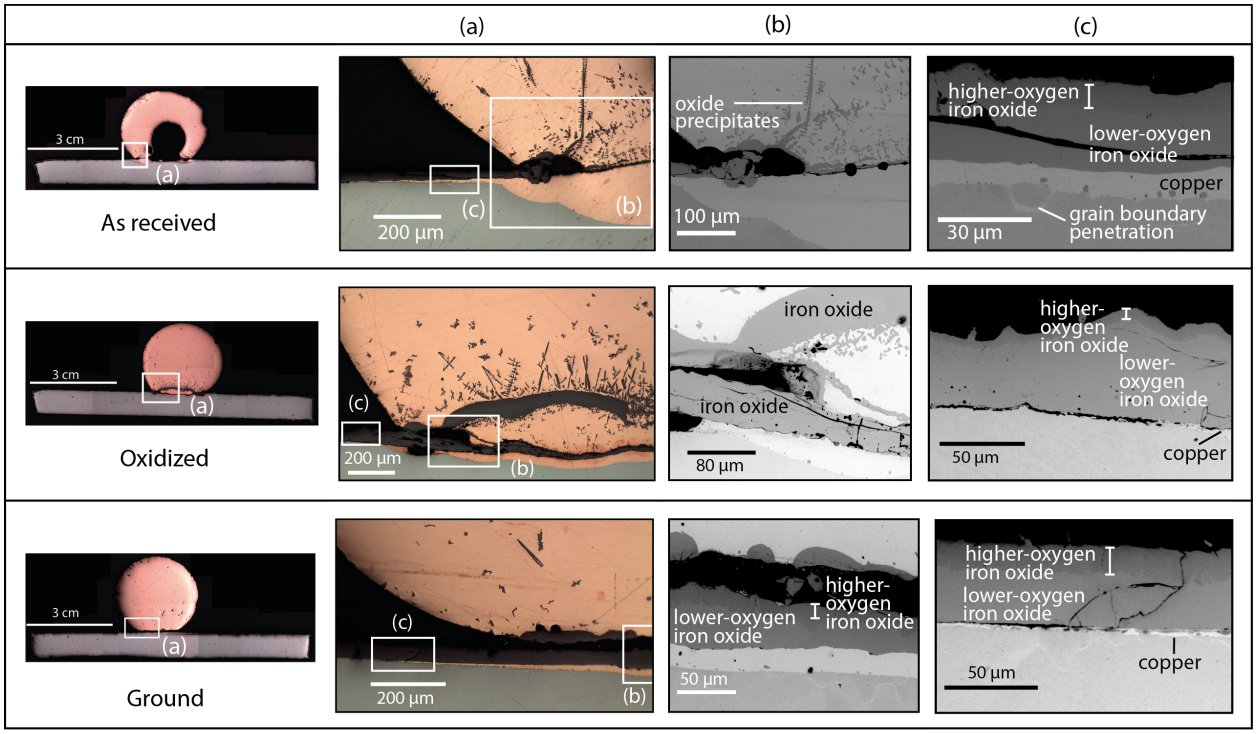

Figure 5.7: Optical micrographs of the copper droplet on low carbon steel substrates in the as received, oxidized and initially polished conditions (a). SEM images in (b) show the copper/oxide/steel interface. SEM images of the oxide layer are shown in (c).

Figure 5.8 shows the low carbon samples with an applied Na_2SO_4 coating. There is a significant difference in wetting behavior between the Na_2SO_4-coated initially oxidized and ground samples. Decohesion of the oxide with the substrate is observed in the initially ground sample, with copper flowing in this gap, while the scale on the oxidized-Na_2SO_4 sample appears to be the most resistant against disruption from the liquid copper. The difference between the two samples may be the reaction progression. Na_2SO_4 deposits on iron at high temperature cause an accelerated oxidation reaction known as "hot corrosion." Iron reacts with Na_2SO_4 to form iron sulfide and oxides. Shi (1993) shows that an Na_2SO_4-Na_2O eutectic melt forms, which maintains contact between the Na_2SO_4 deposit and substrate to progress the reaction. Fe_2O_3 dissolves in the melt and precipitates as discreet particles at the melt/solid interface. Once all the sulfate ions are reduced, only solid Na_2O and Fe_2O_3 are left. EDS analysis confirms that the scale of the Na_2SO_4-coated initially oxidized sample consists of iron oxide at all points tested. A sulfide-free oxide layer may then further develop beneath the Na_2O-Fe_2O_3 layer. With significant Fe_2O_3 initially present, the reaction may have progressed to completion in the oxidized case, such that the scale was solid and protective when the liquid copper melted. However, hot corrosion may have been in the propagation stage for the initially ground sample. The molten deposit destroys the protective reaction-product oxide scale (Birks et al., 2006), and the scale may have fractured at the molten layer, a

weak point. Overall, it appears that attaining a resilient, non-wetting scale with the Na_2SO_4 deposit depends on the initial oxidation condition. If the reaction is incomplete, the deposit may weaken the scale with a liquid reaction product.

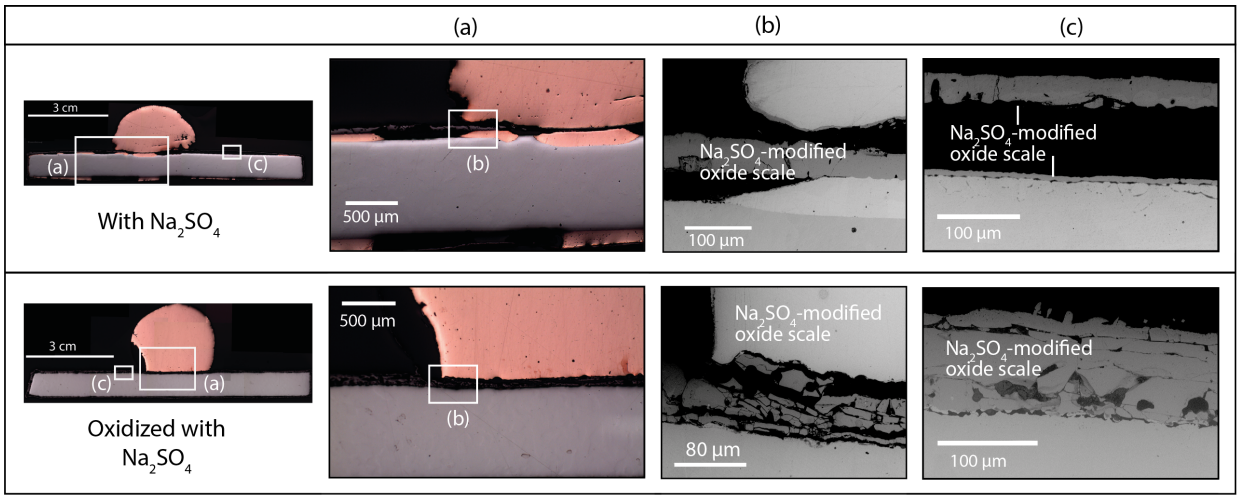

Figure 5.8: Optical micrographs of the copper droplet on initially ground and initially oxidized low carbon steel substrates with an applied Na_2SO_4 coating (a). SEM images in (b) show the copper/oxide/steel interface. SEM images of the oxide layer are shown in (c).

The cross-sections of the initially ground and oxidized surfaces coated with Na_2SiO_3 are shown in Figure 5.9. The coating appears to have caused decohesion between the iron oxide and steel substrate, which then provided a pathway for copper flow. Na_2SiO_3, also known as waterglass, is used in a wide range of high-temperature adhesion and repair applications. Excess water evaporates during heating to cure (Parashar et al., 2003) in a polymerization process (Slimak et al., 2001), leaving silicate compounds with glass-like properties. The glassy material can flow to fill cracks and act as a sealant. In this case, it appears the applied Na_2SiO_3 flowed through the oxide layer and the silicate compounds collected in the wüstite pores, shown by the darker phase at the base of the oxide scale. EDS analysis confirms that the scale consists of iron oxide and another phase, in which Na, Si and O are present, but could not be stoichiometrically identified. SiO_2 may have reacted with iron oxide to form fayalite, Fe_2SiO_4. Overall, the formation of a silicon-rich liquid phase may have compromised the connection between the oxide layer and the substrate, allowing copper flow. Silicates may have introduced additional stress and volume mis-match between the oxide and substrate so the oxide layer broke away from the substrate. The vaporization of water may have also contributed to the lack of adhesion. Matsumoto et al. (2009) studied the adhesive performance of waterglass and found the adhered film thickness decreased as temperature increased up to 1000°C, which the authors attributed to the formation of a vapor film. In any

case, Na_2SiO_3 did not act to seal the connection between the oxide in substrate. The mechanisms of iron oxide dissolution and copper oxide precipitation at the base of the droplet are not apparent.

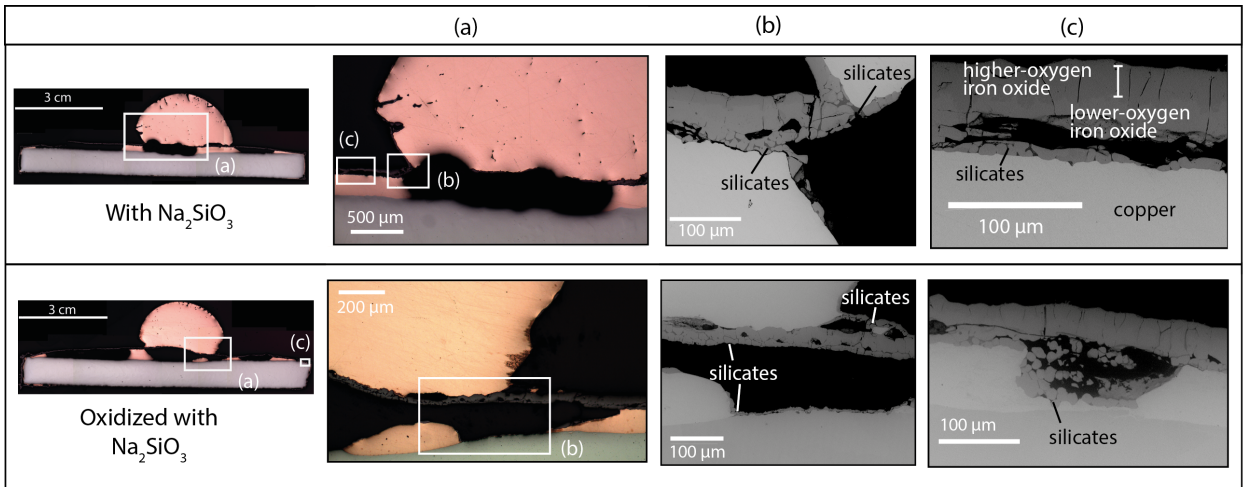

Figure 5.9: Optical micrographs of the copper droplet on initially ground and initially oxidized low carbon steel substrates with an applied Na_2SiO_3 coating (a). SEM images in (b) show the copper/oxide/steel interface. SEM images of the oxide layer are shown in (c).

5.3.3 Liquid copper wetting on medium carbon substrates

The images revealing the main characteristics of the medium carbon cross-sections are shown in Figure 5.10. Copper established a connection with the steel substrate and penetrated grain boundaries by flowing through the pathway between the oxide layer and substrate. The oxidized sample exhibited the slowest spreading of all the medium carbon substrates, and evidence of dissolution of iron oxide in copper and precipitation of a seam of iron oxide, similar to the low carbon cases, can be seen. In all cases, the spread of copper is sporadic. Pores and formation of an oxide, distinct from the iron scale, can be seen. The oxidation of the liquid copper surface during spreading may have contributed to the sporadic distribution, as copper oxide would act to intervene and prevent liquid flow. The iron oxide scale on the uncoated medium carbon samples is much thinner than the oxide scale observed in the uncoated low carbon samples.

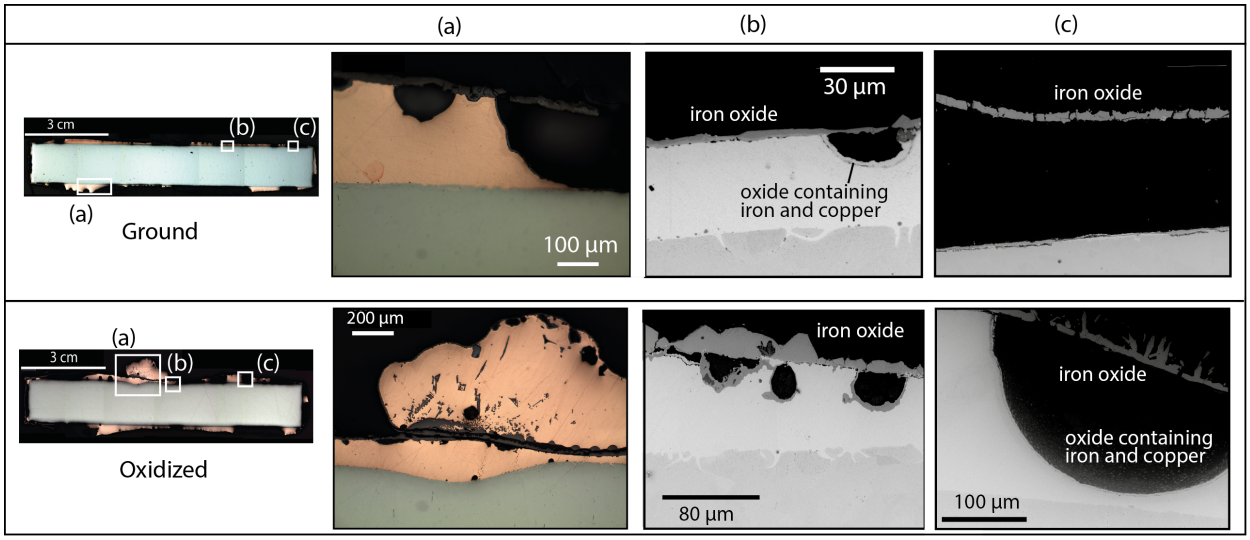

Figure 5.10: Optical micrographs of the copper spread on medium carbon steel substrates in the initially ground and initially oxidized condition (a). SEM images in (b) show the copper/oxide/steel interface. SEM images of the oxide layer are shown in (c).

The extensive wetting in the medium carbon cases cannot be attributed only to the lack of adherence between the oxide and substrate, as decohesion was observed for coated low carbon substrates, but the droplet remained intact. It is likely that the formation of CO(g) caused bulging and blistering of the scale to accelerate wetting. As reviewed by Chen et al. (2003), all steel types are susceptible to blistering above 800°C due to internal stresses during growth as iron ions diffuse outward and vacancies diffuse inward, as well as from the different thermal expansion coefficients of the scale and substrate. However, higher carbon steels are more susceptible to blistering due to the accumulation of gases. Carbon reacts with oxygen in wüstite to form CO(g), which fills pores and voids in the scale, or escapes through cracks and ruptures. CO(g) can also act as an additional reductant to produce CO_2(g). Figure 5.11 shows the initially oxidized medium carbon sample upon etching with Nital to reveal ferrite (α-Fe, the white phase) and cementite (Fe_3C, the dark phase). The decreased presence of cementite close to the surface confirms significant decarburization. The etched original medium carbon steel material is shown in image (c) in 5.11 for comparison.

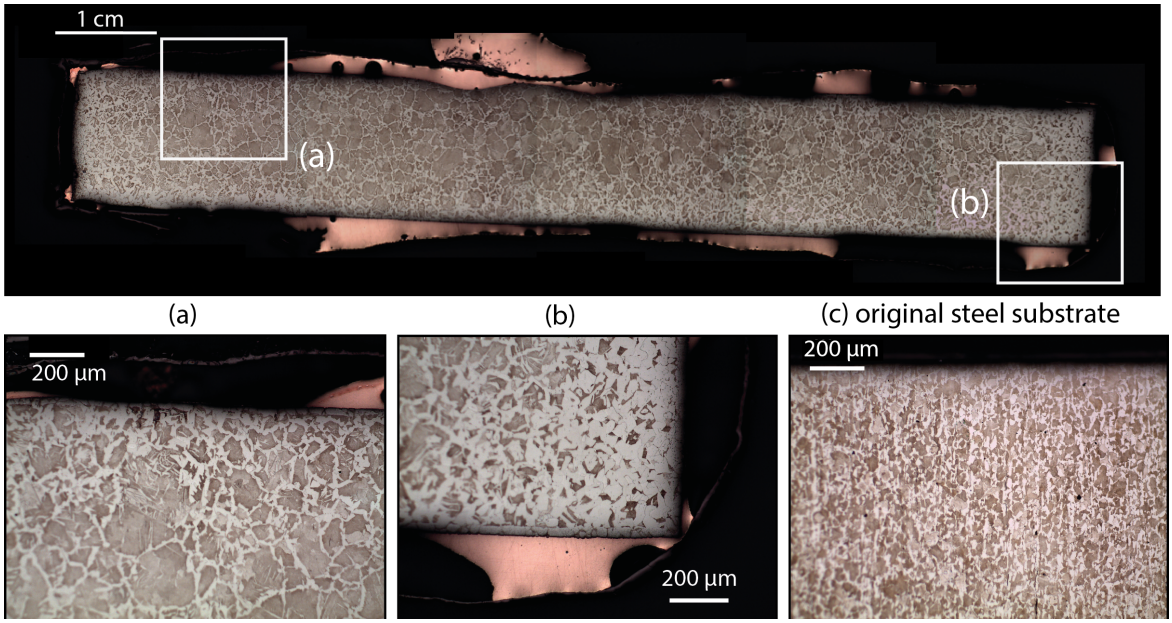

Figure 5.11: The initially oxidized medium carbon substrate with a 2% Nital etch to reveal decarburization, with higher magnification images shown in (a) and (b). The etched original medium carbon substrate is shown in image (c).

The scale on the medium carbon steel also appears to be intrinsically more irregular and less adherent, before testing. Figure 5.12 shows the initial oxide scales formed on the low and medium carbon steels after the oxidizing treatment, before testing. The oxide scale on low carbon steel was thick and adherent, while the scale on the medium carbon steel was thinner, and in places detached or exhibited pores at the interface. Carbon is known to cause a more erratic oxidation reaction (Marston et al., 2004), but the steels also had different processing histories. Medium carbon steels are typically in the form of bars, and may be hot rolled or annealed. Low carbon steels are more commonly cold-rolled into sheets. More adherent and thicker scales forms on cold-worked surfaces, while the scale adhesion on annealed/electropolished surface is poor, resulting in an irregular scale structure (Caplan et al., 1978).

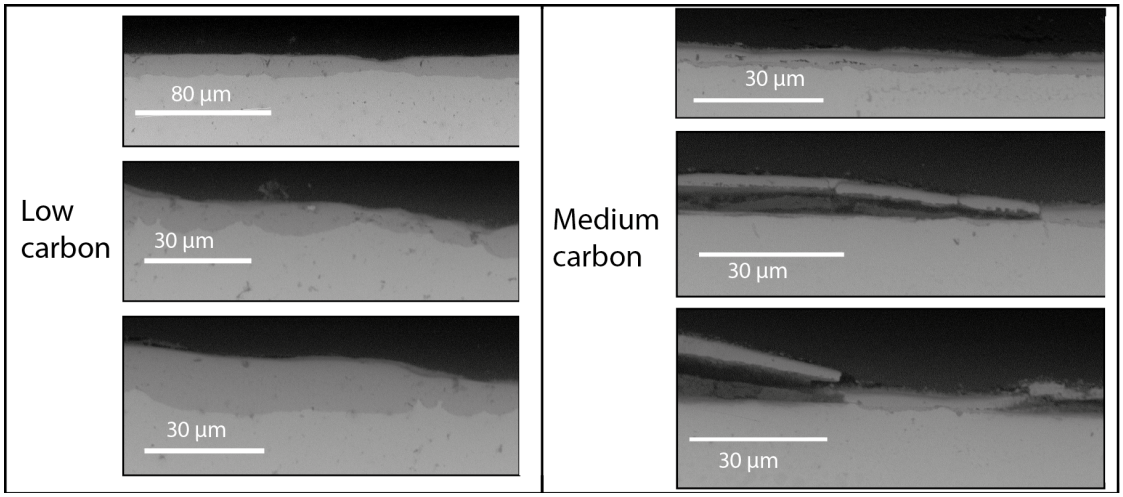

Figure 5.12: Initial oxide scales for medium and low carbon steel samples.

The cross-sections of the medium carbon substrates with coatings applied are shown in Figure 5.13. The coatings did modify the character of the oxide scale and wetting behavior, but not in favor of non-wetting. It again appears that the reaction for a solid, protective scale was incomplete for the Na_2SO_4-coated samples. The blistering of the scale would have disrupted contact between the substrate and Na_2SO_4 coating to terminate the hot corrosion reaction. EDS analysis shows that the majority of the scale is iron oxide, but an occluded darker phase contains significant quantities of Fe, Na, O, as well as Si (which would have oxidized from the Si-containing steel substrate and may have formed fayalite). It appears that Na_2SO_4 and Na_2S were then present to react with liquid copper. Voids in the scale close to the interface are apparent. Carbon from the steel, or CO(g), may have reduced the Na_2SO_4 deposit to form Na_2S and CO(g) or CO_2(g), respectively. The reaction of carbon with Na_2SO_4 is shown in equation 5.1.

$$Na_2SO_4 + 4C \rightarrow Na_2S + 4CO(g) \qquad (5.1)$$

The reaction of copper with Na_2S, shown below, is well-known to be favorable (Makar and Dunning, 1969). Precipitates are distributed throughout the solidified copper, which EDS analysis confirms is copper sulfide.

$$Na_2S + 2Cu \rightarrow Cu_2S + 2Na(g) \qquad (5.2)$$

The droplet profiles of the medium carbon Na_2SO_4-coated samples in Figure 5.2 show a textured reaction product enveloping the surface of the copper droplet as it spreads.

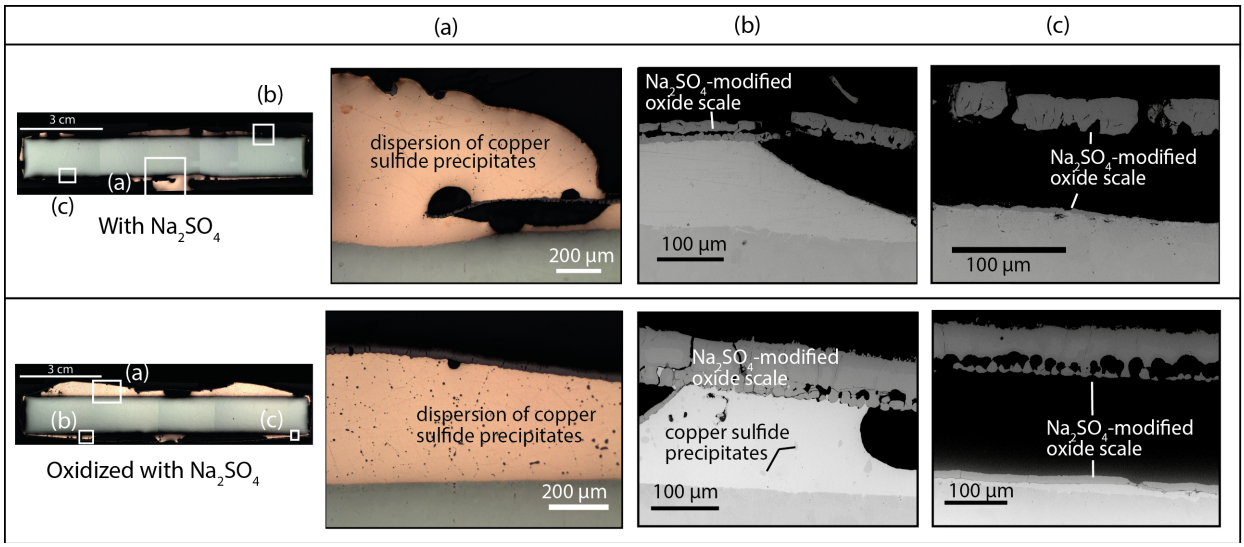

Figure 5.13: Optical micrographs of the copper spread on medium carbon steel substrates in the initially ground and initially oxidized condition with the Na_2SO_4 coating applied (a). SEM images in (b) show the copper/oxide/steel interface. SEM images of the oxide layer are shown in (c).

Figure 5.14 shows the features of the Na_2SiO_3 coated samples. Again, it appears silicates are present as a darker phase in the oxide, but this likely aided in decohesion. It appears the scale lifted and provided a pathway for copper flow. The spreading of liquid copper was most rapid for Na_2SiO_3-coated medium carbon samples.

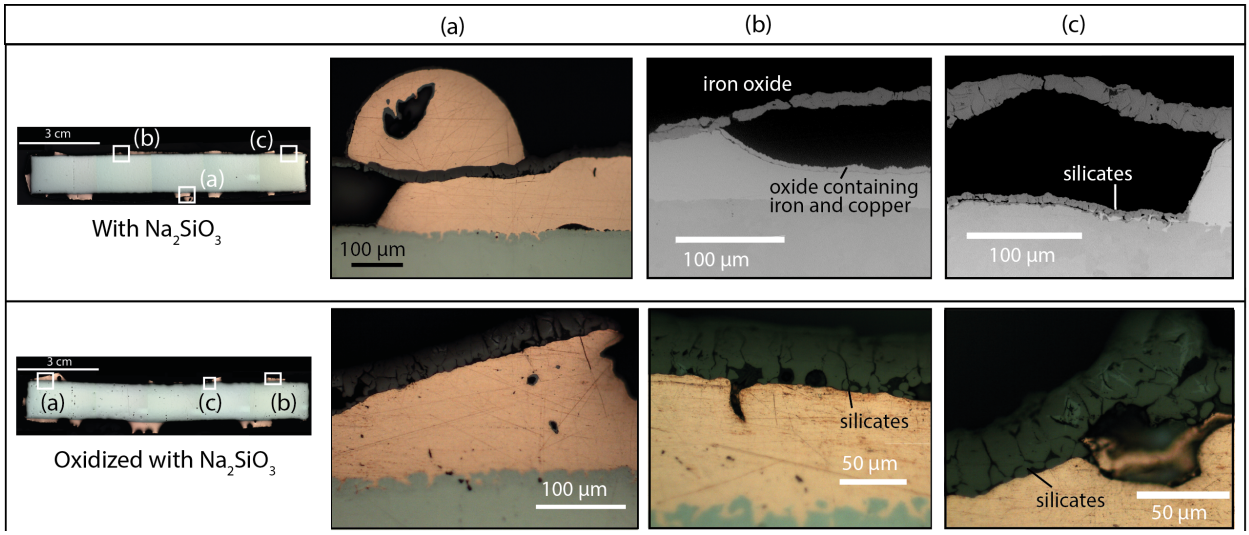

Figure 5.14: Optical micrographs of the copper spread on medium carbon steel substrates in the initially ground and initially oxidized condition with the Na_2SiO_3 coating applied (a). SEM images in (b) show the copper/oxide/steel interface. SEM (optical for the oxidized with Na_2SiO_3 sample due to issues with sample preparation) images of the oxide layer are shown in (c).

Overall, the coatings do not appear to be especially useful – the improved liquation aided by Na_2SO_4 and Na_2SiO_3 as described by Leak and Fine (1973) is not substantiated here. The difference in environments between this study and the study by Leak and Fine may explain this discrepancy. The molten salts employed in their tests, $BaCl_2$ and $CaCl_2$, may have dissolved the iron oxide scale present, such that the Na_2SO_4 and Na_2SiO_3 barriers were critical to prevent brazing. In a gaseous environment, the scale is present and the coatings weaken adherence between the scale and substrate to provide a pathway for copper flow.

5.3.4 Process development

These results provide a basis to begin defining a preferential melting process. The main requirement to prevent wetting is to maintain an adherent non-metallic surface layer for the duration of the treatment. The key parameter to affect rapid wetting appears to be carbon content. Blistering of the oxide scale provided a pathway for extensive copper flow between the scale and substrate. The sodium sulfate and sodium metasilicate coatings appeared to weaken the connection between iron and its oxide to allow liquid copper flow, to supersede the typical iron oxide dissolution and copper oxide precipitation behaviors observed in the non-coated samples. The exception was the oxidized-Na_2SO_4 surface on low carbon steel – the resultant scale was fully intact at the interface and prevented liquid copper penetration. The phases formed in the scale and at the interface with the application of these coatings could be further confirmed with compositional analysis. However, coatings should promote non-wetting behavior in a wider range of conditions, and the results show that Na_2SiO_3 and Na_2SO_4 can actually make wetting behavior more rapid, depending on initial oxidation and carbon content. Thus, these coatings may not warrant further investigation. Other further work, following from the present results, is discussed below to further develop the preferential melting process.

For energy-efficiency and industrial feasibility, the heat for preferentially melting copper must be retained to then melt the steel scrap, so the process conditions must be compatible with the conventional EAF route. The conditions of low carbon content and a lightly oxidizing atmosphere to achieve non-wetting do not present any significant scale-up obstacles. However, further work is required to determine the level of carbon concentration and oxygen partial pressure that cause liquid copper to transition from non-wetting to wetting behavior. Low-carbon sheet steel is used in cars, goods and equipment, which makes up the

shredded scrap contaminated by copper. However, these steels may contain up to 0.25wt%C. Decarburization can be prevented by adjusting the furnace atmosphere, specifically by increasing the carbon potential. The atmospheric conditions required to treat a range of carbon steels while avoiding decarburization are specified – such as by Herring (2009) and Linde Gas – so knowledge and expertise in downstream processing could be applied to scrap heating. Similarly, the oxygen potential of the atmosphere must be further investigated to determine the boundary between achieving a protective, thin oxide layer on both the droplet and substrate, and problematic entrapment of liquid in the scale must be further investigated. Industrially, the oxidizing potential of an environment can be controlled using the ratio of partial pressure of $CO/CO_2(g)$. Using off-gases from the EAF would reduce electrical energy consumption by up to 265 kWh/tonne (Toulouevski et al., 2010b), but the CO/CO_2 ratio must be carefully controlled.

The other key part of the process is applying a mechanical force to separate liquid copper from the steel surface. Dynamic flow behavior of a liquid metal on a solid substrate can generally be inferred from the evolution of a static droplet (Eustathopoulous et al., 1999). However, the goal of the process would be to minimize contact and avoid phenomena such as dissolution of the oxide layer and penetration into pores observed in these static tests. The time-scale of these behaviors and how liquid copper flows over the scale must be determined with further experimental testing.

Thus, future work is required to investigate promising directions for process development. Overall, a viable process must be designed through an iterative consideration of scientific and practical aspects: converging an understanding of the wetting behavior of copper on steel, with the industrial constraints of treating heterogeneous end-of-life scrap. The initial studies by the U.S. Bureau of Mines that concluded preferential melting would be ineffective due to liquid copper entrapment under the oxide scale may have used steel with a higher carbon content (steel composition was not reported), such that no atmosphere allowed for a "non-wetting" regime. For this technique and others, it is important to test the limits to controlling tramp elements.

Chapter 6. Conclusions

By evaluating copper contamination at the global level, and systematically evaluating possible separations by specific energy consumption, a set of experiments was performed to explore a potential process – to simply melt copper from scrap, with careful control of the oxide layer to act as a barrier to wetting. The present work provides a basis to develop a new strategy to manage copper in end-of-life steel recycling – and thus to enable high-quality recycling and reduce CO_2 emissions related to steel production. The contributions of this thesis are described in 6.1. The implications of this work for policy-makers, steelmakers, and researchers are discussed in 6.2. Many questions remain and given the potential for future development of this area, future work is recommended and outlined, in 6.3.

6.1 Main contributions of thesis

This thesis began with three distinct questions:

Q1. How does copper constrain steel recycling?

Q2. Can copper be removed, and what would be the energy and material requirements of extraction?

Q3. Is there space for further development in an extraction process?

The current literature provided partial answers to these questions, but the goal of Chapters 3, 4, and 5 was to address the most compelling gaps in knowledge. The new answers to these questions – the main contributions of this thesis – are presented below.

Q1

The metallurgical effects of copper on steel and the broader effects of down-cycling and dilution have been widely investigated in the existing literature. However, the future efficacy of steel recycling, i.e. the ability to produce demanded products from the available scrap supply, remained uncertain. Predictions of constraints from copper contamination at a regional level were limited to the assumed trade conditions. Scrap trade takes place at the

global level, and thus a model of global scope is needed to evaluate the future viability of steel recycling. Chapter 3 provides the first analysis of copper contamination in the global steel system. A range of literature data on the copper content of scrap and the copper tolerance of products is compiled and a visual representation of how copper flows through the steel system is presented for the first time. Most importantly, the first estimate of when copper contamination is likely to constrain steel recycling globally, if current scrap preparation continues, is presented: 2050. The increase in primary production temporarily reduced the urgency of managing copper in the steel system, but this analysis shows there will be a hard limit in the coming decades, when dilution and allocation to tolerant applications will no longer be effective. If primary production is cut as required to meet CO_2 emissions targets, this constraint will come sooner. This study serves as a comprehensive, quantitative basis to inform future steel recycling strategy.

Q2

Chapter 4 provides a novel framework, and estimates the specific energy and material requirements for the full range of copper extraction processes. Beyond initial conjectures that tramp element removal would be costly and energy-intensive, no figures existed for the energy consumption of copper removal. Before this investigation, it was unclear whether previous laboratory investigations explored all options for copper extraction, and in what direction to devote future efforts. Existing assessments were incomplete: evaluating the copper-steel system with process-independent thermodynamics, or evaluating the behavior of copper in the current commercial refining process. In the new framework, a scheme was derived from fundamental separation principles to identify possible separation routes, and dispersed experimental work was brought together to evaluate these routes. Rates of copper removal and the required process windows were used to estimate the energy and material requirements for a certain reduction in copper. It was shown that copper can be removed to 0.1wt% with energy consumption on the order of 5-20% of the melting energy required in the EAF. This provides an estimated amount of additional energy needed to return contaminated end-of-life steel scrap to the same quality as primary steel. The identified physical limits of the extraction processes can be further examined for improvements, and the most efficient options can be strategically pursued. The new framework can also be applied to evaluate the extraction options for other metal systems, which is vital as the scrap supply of all metals expands.

Q3

Chapter 5 demonstrates that the limits to copper removal can be further tested and explored. A separation technique that was previously deemed ineffective, preferential melting, was re-examined. The native oxide layer on metals is the bane of many metallurgical processes, particularly welding and joining, because it prevents true contact between the two metals. Here, this intrinsic property of the oxide layer to act as a barrier is used purposefully to prevent wetting between liquid copper and solid steel. Although there are many studies seeking to dissolve the surface oxide layer to improve wetting, Chapter 5 provides the first study to systematically evaluate the conditions required to maintain the oxide layer and prevent wetting. With this methodology, the importance of steel carbon content in determining wetting behavior is revealed. Coatings were found to be unnecessary and possibly detrimental, by impairing contact between the oxide and substrate. The study shows that a viable process window may exist to treat low carbon steel in a lightly oxidizing atmosphere, which is promising for future development. Such a process could require little additional energy if incorporated into scrap heating and melting, and would prevent copper from entering the steel cycle.

Cumulatively, this thesis combined three types of analyses: an evaluation of the systemic effects of contamination, an integrated energy assessment of possible separations, and the experimental determination of a viable process window. The results from the high-level analysis of the problem (Chapter 3) motivated the systematic evaluation of possible solutions (Chapter 4), and the overview of all possible separations led to a narrow experimental study (Chapter 5). This approach demonstrates the development of an effective strategy, that is widely applicable, yet pursues in-depth solutions. This multi-scale, interdisciplinary approach could be applied to other metal systems.

6.2 Implications for policy, industry, researchers

There are two main implications of the new answers above. The first is that constraints on steel recycling caused by copper are impending. The second implication is that there are opportunities for innovation, which have been investigated in Chapters 4 and 5. The

goal of this thesis was to develop a new plan for action, and so the present implications for policy-makers, steelmakers and researchers are explained below. These actors must increasingly work together in a coordinated fashion, so overall implications that apply to the interaction of all three, are discussed as well.

Policy-makers

Chapter 3 evaluates the constraints caused by copper in the global steel system. Further work is required to understand a given country's position within this global picture. The rise in scrap-based steelmaking and the stagnation of primary steelmaking is incorporated into the global model, but closures of integrated steelmaking plants will have an acute regional effect on the sourcing of diluent materials. Regions must consider the composition of the local scrap supply and the quality requirements of demanded products. Most of the developed world will face significant and near-term limitations due to copper. For example, in the EU nearly all available scrap could be utilized to meet over 80% of demand by 2030 to cut steelmaking emissions by more than half, but not until copper contamination is resolved. If the current levels of copper persist, around 50Mt of primary production would be required for dilution (Material Economics, 2018).

Beyond shifting production routes, political situations will also profoundly influence the urgency of copper contamination. The analysis in Chapter 3 assumes that scrap can be mixed with any diluent material and freely traded to any tolerant application in the global system. Extensive scrap trading is normal now (Gesing, 2004), but strict trade restrictions are coming into view. China has adopted banned imports of plastic and unsorted paper from January 1, 2018, onwards. This immediately instigated a crisis in Western countries, where bales of waste are piling up (Brooks et al., 2018). A protectionist "America first" stance is touted by the U.S. president, who aims to put this rhetoric into practice with tariffs on steel and aluminum. Cooper (2018) recommends utilizing the domestic scrap supply of steel and aluminum to drastically reduce dependence on foreign metals, but copper in steel scrap must be addressed. Brexit will profoundly alter import and export dynamics. Some view this as an opportunity for the UK to develop a self-sufficient circular economy (Loyd, 2018), but again copper in scrap places a limit on this possibility.

The assumption in Chapter 3 that contaminated scrap will be mixed with primary steel in developing countries with fast-growing demand is discordant with the historical

patterns of steel production, as industrialized countries have aimed to meet their steel demand with domestic production (Material Economics, 2018). Indeed, steel has traditionally been regarded as a resource of great strategic importance, and should continue to be treated as such. Steel connects sectors of the economy. The transformation of the steel industry could invigorate the transition to renewable electricity, and efficient manufacturing. Steel stocks embody CO_2 emissions, so careful stewardship of these materials is key for climate change mitigation.

Current markets have limited capacity to transition to high-quality steel recycling. Today's practices embed more copper in the steel system, but prioritizing solutions to this future problem is unrealistic in a dynamic and reactive industry. Material and energy prices are highly volatile, and scrap-based production is at a disadvantage because the raw material is less predictable, in quantity and composition. Eventually scrap-based production will enjoy economic favorability due to an increased scrap supply, depleted ore grades, and stricter CO_2 emissions mandates. However, the EAF infrastructure must be established now. Investment in new equipment and technologies is not possible while teetering on the edge of massive shutdowns. The government bears the costs of shutdowns and job losses, and could choose to alternatively invest in an industrial transformation. Allwood (2016b) presents a vision for a government project to support research and investment in new technology for high-quality steel recycling in the UK. Investing in productive solutions is likely to be far less costly compared to the consequences of tariffs.

There is already public and political will to increase recycling. In the last year, single-use plastic waste jumped to the top of the political agenda in the UK (Department for Environment, Food and Rural Affairs, 2018). However, the efficacy of recycling is nuanced. This thesis investigates an important phenomenon that is invisible to the public and cannot be described by a single metric. Tramp elements imperceptibly dissolve into metal and the impacts of contamination are difficult to determine. Blanket policies mandating a certain recycling quota, such as the EU-ELV directive that sets a goal to recycling 95% of the mass of vehicles (European Commission, 2000), actually hurt the management of contaminating elements (Reuter et al., 2006).

The flow and consequences of contaminating elements is complex and unclear even to those directly involved. The first step in supporting copper control is to survey and monitor the problem. In recycling, products are mixed in scrap grades, and scrap grades are mixed in melting, so it can be difficult to track the destiny of scrap. A first step could be for EAF

facilities to report the raw materials purchased and the product types sold. The copper concentration of scrap-based steel melts should be measured and reported to policy-makers.

As discussed in the beginning of Chapter 4, copper is most efficiently separated before shredding, but the incentives along the supply chain do not support this. Measuring the composition of a scrap stream before melting would allow for grading and pricing by copper concentration. Composition analysis equipment is available (Gamma-tech, 2018), and policies could support the adoption of this equipment, through tax breaks or low-interest loans. Policies could engage the makers of cars and appliances by providing incentives to incorporate more secondary steel into their products. This could then provide a motive for designers to prioritize recyclability. In all cases, regulation must navigate a fine-line. Strict regulation stipulating the handling of scrap or metal production may further burden scrap merchants and steelmakers, and inadvertently drive more scrap export and outsourcing.

Establishing circular practices is an ambitious undertaking at any level. However, copper contamination provides a concrete basis to start pursuing this abstract ideal. Material Economics, a consultancy that works to quantify natural resource debates, carried out a project to guide EU policy-makers and industry to transition to a circular economy. The project used the results of Chapter 3 to bring copper contamination to the forefront and provide actionable steps for the EU steel industry to increase scrap-based production (Material Economics, 2018).

Industry

As discussed above, industry alone cannot improve current scrap processing practice in the required timeframe. Government support in some form is key. Shifting to scrap-based production not only requires a pro-active strategy for copper contamination, but existing plants must be retro-fitted and infrastructure to collect, melt and cast more scrap to flat steel products must be built. This is difficult now, but in the long-term the EAF route will prove to be significantly more profitable than ore-based production, as explained by Toulouevski et al. (2010a). Additionally, the analysis in Chapters 4 and 5 shows that copper separation is not fundamentally costly or energy-intensive.

Thus, industry should adopt a renewed approach to the old problem of tramp elements. Rod et al. (2006) discuss how nominal residual element limits can be increased in some instances. The U.S. steel company, Nucor, has penetrated the automotive sheet market

with strict control over input materials and new casting and rolling techniques. For copper extraction, existing equipment, such as shredders, scrap-preheating systems, and ladles, can be used or slightly modified for new processes. Physically separating copper from solid scrap can be highly effective and requires relatively simple adjustments to current practice: another iteration of shredding, or passing scrap through a trommel system. The copper-rich fraction from the trommel could then be treated with preferential melting. EAF steelmakers should appreciate the capacity for innovation in the industry. Tremendous improvements in productivity have been achieved over the last several decades. Now attention must shift to other considerations, such as the energy and material intensity of processing. Essentially, these new initiatives derive more value from scrap, which benefits business. Recovering copper is a significant incentive, especially considering the increased use of electronic components. The use of alloying elements in high-strength steels is also increasing, and closing product loops will retain these elements and avoid the costly consumption of ferro-alloys.

The analysis in Chapter 4 shows that though copper separation is always theoretically possible, there are energy costs. Specifically, removal from the melt is energetically and practically difficult. Thus, it is imperative to prevent copper from entering the steel cycle. Newell (2017) reports that on average, steel in the U.S. contains 0.1wt% copper. There is abundant primary steel today, and this should be used strategically to dilute copper already embedded in steel.

Researchers

Unlike policy-makers and industry, researchers do not need to react to the cyclical market, or to unexpected political situations. Researchers must help to understand underlying fundamental trends, consider ideas that may not be politically or economically attractive in the present moment, and spur innovation.

Metallurgical research has delivered remarkable improvements in steel properties. Increasing strength has been a predominant objective (Weng et al., 2011), but most designs are stiffness-limited, and stiffness is a property of atomic bonding, unchanged by processing. Despite the advancements in more advanced processing and properties, steel is not used more efficiently (Allwood, 2018). There is a deficit of research dedicated to the stewardship of materials we have already produced – materials we are constantly surrounded by, that

contribute directly to climate change, and that everyone relies on for basic transport, shelter and infrastructure.

The industrial ecology community is growing. In further developing this field, research projects should be problem-led, rather than methodology-led. Contextualizing results in the original real-world problem forces researchers to reckon with and communicate uncertainty and limitations. For example, much research applies life-cycle assessment to various products or processes, but results are often inconsistent due to boundary selection, allocation assumptions and data availability. Results can then be misleading and difficult to translate to practical actions (Cullen et al., 2009). Maintaining focus on the problem will lead researchers to multi-disciplinary collaborations and new ways of thinking needed for the complex and urgent problems of climate change. Olivetti and Cullen (2018) argue that scientists and engineers should receive training to perform impact assessments and engage with stakeholders, and should be encouraged to perform "systems-based environmental analysis coupled with fundamental research."

Advanced methodologies and exhaustive databases are not necessary to begin addressing difficult questions. This thesis draws on existing literature to perform relatively simple calculations (summing total copper, or the main sources of energy consumption). In the end, an old process is re-investigated. Researchers may need to challenge the traditional conceptions of academic research and boundaries between disciplines to promote meaningful change (within reason). Accordingly, Sax (2018) recently challenged the popular definition of "innovation" in the New York Times, that is fitting for the reflective nature of this thesis:

> *"True innovation…is a continuing process of gradual improvement and assessment…Often that actually means adopting ideas and tools that already exist but make sense in a new context, or even returning to methods that worked in the past. Adapted to the challenges of today, these rearview innovations have proved to be as transformative as novel technologies… They are solutions firmly focused on the future — a human-centric future that reflects where we've been, what we've learned and how we actually want to live."*

For all

In order for policy-makers, steelmakers and researchers to make collective, informed decisions, more reporting of the composition of steel scrap is required. The worldsteel

association is a non-profit organization that represents steel producers internationally and reports detailed statistics on global steel production, to provide common information for steelmakers, politicians and researchers to make informed decisions. However, worldsteel does not report data on scrap types or composition beyond total scrap import and export quantities. Similarly, the Institute of Scrap Recycling Industries (ISRI) reports ferrous scrap imports and exports by country. These organizations could seek to provide more detailed statistics necessary to understand contamination and down-cycling.

Returning to the IPCC SR1.5 report discussed at the beginning of this thesis, the authors state that "limiting global warming to 1.5°C would require rapid, far-reaching and unprecedented changes in all aspects of society." Carefully planned and coordinated action is required. Copper contamination in end-of-life steel recycling is just one problem that must be addressed to meet emissions targets, but this problem exemplifies the level of cooperation required amongst the actors in policy, industry and research. Materials scientists must consider the wider implications of new technologies and industrial ecologists must understand the physical basis of the systems they study. Policy-makers must monitor the problems in industry and formulate productive solutions, and industry must be increasingly aware of future problems, and be open to changing today's practice in response. Short and long term strategies are needed, as well as both high-level, and deep, specific analyses.

6.3 Future work

Given the importance of the area, and the questions that remain, future work is described below by two categories: understanding contamination in metal systems and prioritizing action (6.3.1), and process development for the preferential melting technique (6.3.2).

6.3.1 Evaluating the effects of contamination in metal systems and prioritizing action

There are many opportunities to further investigate the steel system, including incorporating the effects of other contaminating elements, modeling shifts in future steel use, refining the estimates of copper concentration, and modeling copper in regional steel systems. To better understand potential technical interventions, the extraction processes could be

further characterized with experimental work, and the copper concentration of scrap could be varied in models of the future steel system to understand the effects of interventions. Lastly, the methodologies demonstrated in this thesis could be applied to recycling systems beyond steel.

Copper-steel system

This focus of this thesis was on copper contamination, but considering only the effect of copper in steel recycling is simplistic. In Section 2.1.1, the metallurgical effects of various elements on steel was discussed. These elements could be incorporated into additional analyses. The most interesting would be tin, nitrogen and valuable alloying elements such as vanadium, molybdenum and titanium. Some metallurgists point out that controlling tin should be the first priority because of the strong effects on hot shortness. The stringent limits on copper may be raised if the absence of tin can be assured, so a study of both copper and tin together in the steel system would be useful (Sridhar, 2016b). Nitrogen is often present at higher concentrations in EAF steel melts and has been cited as a deterrent to high-quality scrap-based steelmaking (Leroy et al., 1995), so an analysis could be performed to understand those limitations and techniques to reduce nitrogen content.

In the current analysis, the results for future steel demand by sector from Pauliuk et al. (2013b) were used, which extrapolate observed stock-saturation trends. The quality requirements of each sector were extrapolated from the matrix by Cullen et al. (2012). However, steel use will certainly be different in the future. The arrival of several disruptive technologies are much-discussed. Car-sharing is on the rise, with car ownership decreasing in some demographics (Higgins, 2017). Self-driving cars will further change the way cars are used, and the materials cars are made from. The proportion of steel in cars is decreasing, as materials such as aluminum and composites gain prevalence. Meanwhile, copper use is increasing, as more electronic elements are incorporated and as combustion engines are replaced with electric batteries (Copper Development Association). The increasing use of copper could in turn motivate better dismantling and collection, or the adoption of detachable wiring harnesses. As cars are the main source of copper contamination entering into the steel cycle, characteristics of the future fleet of cars are important to understand. Cabrera Serrenho et al. (2016) demonstrate how demographics can be applied to the fleet of UK cars to reveal broad trends in car use. Characterizing car stocks by the type and quantity of material would

allow the recycling infrastructure to prepare for when these products reach end-of-life. Incorporating possible new technologies, and the consequential shifts in steel use and steel requirements, into future steel recycling models would be useful.

The analysis in Chapter 3 was limited by the reported values of the copper concentration of steel scrap. All data from the publicly available literature (to the knowledge of the author) was collected and considered in the estimates, but the future creation of an association or regulation to require reporting may provide more data to refine the current estimates. Additionally, copper concentration will vary with time. In the analysis, the copper concentration of scrap in the future steel system remained constant to understand how long current practice would be viable for, but future analyses could vary copper concentration to model the implementation of different interventions – such as a process that could prevent external copper from entering the steel system, or a melt extraction process effective to 0.1wt%.

The global picture establishes the extent that free trade can delay the constraints caused by copper, but policy-makers and steelmakers must make decisions within regional bounds. Models of regional scope could be constructed following the same methodology in Chapter 3. As mentioned in 6.2, the implications of trade restrictions (future restrictions on ferrous scrap imports by China, or the effect of tariffs on steel in the U.S., or post-Brexit UK) could be modeled. Regional investigations could also evaluate how current facilities and infrastructure must respond to the increasing scrap supply. The closure of integrated steel plants will have an immediate impact on the economic feasibility of obtaining diluent materials. To maintain domestic primary steel and foster a smoother transition to scrap-based production, more scrap could be charged to Blast Oxygen Furnaces. Normally, about 20% of scrap is charged in the BOF, but the upper limits could be tested. Equipment and infrastructure considerations, and the possible steel product portfolio, must be considered simultaneously with the copper concentration of scrap.

In pursuing technical solutions, the integrated assessment provided in Chapter 4 can be further developed as the separation routes are further characterized, or as industry advances. Estimates are based on available experimental results and the rates of energy consumption reported for current reactors, with similar industrial processes serving as benchmarks. Pilot-scale work will be required to further define the processes, and more refined models will lead to more accurate estimates. The analysis assumed that current recycling infrastructure remains unchanged with new treatments for copper separation added,

but many of these treatments could be a part of larger modifications with auxiliary benefits. For example, higher-density shredded scrap improves yield in the EAF, extending vacuum treatments would refine other inclusions and metallic impurities, molten salts could provide an efficient heating and refining medium, and a treatment during heating could simultaneously remove other poorly-controlled external impurities such as tin and zinc.

Chapter 5 investigated preferential melting as a potential extraction technique, but research directions for further developing physical solid scrap separation, high-temperature solid scrap treatments, vacuum distillation and sulfide slagging were discussed in Chapter 4. Figures 4.7-4.10 compile the identified principles that can be used to separate copper from steel, as well as the physical constraints to copper removal for each route. This provides a structure for previous experimental work, but can also act as a guide for future experimental work. A researcher could further pinpoint uninvestigated process windows that might allow a greater rate of copper removal.

Other metal systems

Copper in steel is just one example of a metal system constrained by contamination. Across all the main metal industries the rate of end-of-life scrap recycling is increasing (Allwood et al., 2013). For example, aluminum recycling is particularly problematic. Aluminum oxidizes easily, so impurities cannot be collected in an oxidizing slag. Most elements are retained in the melt phase (Nakajima et al., 2010). Gaustad et al. (2012) explain that Si, Mg, Ni, Zn, Pb, Cr, Fe, Cu, V, and Mn are monitored in aluminum recycling currently and new processes for their control may be necessary. The extent of contaminant extraction in metal recycling is determined by the historical development of the infrastructure, rather than the impurity elements forming a strong interaction with the base metal. Innovation in the refining infrastructure is possible, but it is important to understand the energy and material impacts of the potential processes, and prioritize future development accordingly. The possible separations for other metal systems could also be assessed with the novel framework presented in Chapter 4. To understand when a given impurity element will limit the amount of metal that can be recycled, the methodology demonstrated in Chapter 3 could be employed.

6.3.2 Preferential melting process development

Future work is suggested to investigate the scientific principles governing preferential melting, as well as explore the viability of scale-up. Future areas for process development arising from the results of Chapter 5 were discussed in 5.3.4. Here, a yet wider process space is considered.

In determining the proper process conditions, it is important to further characterize the shape, surface condition, and composition of end-of-life scrap. End-of-life scrap is highly irregular, but further investigations following from the study by Aboussouan et al. (1999) could help to rigorously describe the presence of copper with scrap and the typical size and morphology of the pieces upon conventional shredding. The shape of scrap will determine the agitation needed to liberate liquid copper, and the surface condition and steel composition will determine wetting behavior. Copper present as dense "meatballs," from windings inside an electric motor will liquate and flow differently from dispersed, small copper pieces. Once the condition of end-of-life scrap is known in more detail, pre-processing steps to enhance the effectiveness of preferential melting may then be considered, for example using a trommel to concentrate a copper-rich fraction of scrap, or shredding to a different density. As discussed in 2.3.1, preferential melting is used to separate other metal systems so the scrap preparation and typical removal rates for these operating "sweating" processes could be used as reference.

The control of oxidation was shown to be essential in Chapter 5. Knowledge on scaling behavior during steel cooling and hot rolling could be applied to further explore this area. Scale formation and adhesion has been studied extensively (Yang, 2001). Increased H_2O or CO_2 in the atmosphere is known to increase the plasticity of the scale and improve adhesion (Chen et al., 2003). Precipitating a magnetite seam at the scale/steel interface with an appropriate heating profile is also shown to improve adhesion (Tanei and Kondo, 2016), and there are many coatings to control the iron scale proposed in patents (Ye et al., 2009), (Sheneider et al., 1965).

To aid in the separation of liquid copper from steel, a liquid environment, such as a chemically inert molten salt bath, might be especially helpful. The bath composition could be optimized to promote coalescence of the liquid copper, increase the thermal efficiency of heating (heating rates are 4 times as fast as atmospheric furnaces), and decrease the weight of the scrap by 25-60% due to buoyancy (Galopin et al., 1975), which would help with shaking and agitation. A chemically inert salt such as $CaCl_2$ is available virtually free in high purity as

a waste product from the chemical waste industry (Fray, 2002). The salt bath could also aid in controlling substances covering end-of-life steel scrap such as, zinc, paints and tin-coatings. The combustion of these substances during current EAF steelmaking is problematic, causing dust and pollution (de Buzin et al., 2017), and alternative processes for pre-heating scrap while simultaneously removing or treating the present coatings are being developed (Östman et al.), (Porzio et al., 2016). Molten salt baths are currently investigated at the pilot-scale as a more efficient and clean method to treat municipal waste (Yao et al., 2011). Such set-ups are scalable, as molten salts are also widely used in metallurgy, for aluminum melting and steel heat treating. The interaction of liquid copper with the steel surface in an inert molten salt must be explored.

Compatibility of the preferential melting step with EAF scrap charging may dictate the process conditions. Already, scrap pre-heating systems with continuous charging to the EAF are in operation, so a preferential melting process should be designed with these systems in mind. For example, in the BBS Brusa process a 13-m long rotary heating furnace continuously charges scrap into the EAF. Scrap is heated up to 1000^{o}C with gases along the furnace for 6-10 min. The furnace rotates to prevent the scrap pieces from brazing, and to transfer heat from the refractory lining (EPRI, 1997). Scrap pre-heating systems offer significant energy savings (120-265 kWh/tonne).

Incorporating solid scrap treatments to remove copper into the pre-heating systems, as they become more widespread, is promising. Preferential melting was investigated in more detail here, but the viability of applying an oxygen/chlorine gas or a sulfidizing matte to solid steel scrap have been demonstrated and could be performed in a rotary furnace or heated scrap vibratory conveyor. These processes were not economically justified in the past, but may make sense at some point in the future.

References

Aboussouan, L., Russo, P., Pons, M. N., Thomas, D., Birat, J. P., & Leclerc, D. (1999). Steel scrap fragmentation by shredders. *Powder Technology*, *105*(1-3), 288-294.

Adolf, Z. Socha, L. (2016). Ostrava Secondary Metallurgy http://katedry.fmmi.vsb.cz/Opory_FMMI_ENG/2_rocnik/MMT/Secondary%20Metallurgy.pdf. Accessed September 2018.

Afshar, S., Allaire, C., & Dajoux, E. (2004). Effect of Salt on Metal Oxidation and Refractory Corrosion Induced by Molten Aluminium Alloys. In *43rd Annual Conference of Metallurgists of CIM, Hamilton, Canada*.

Alexis, J., Jönsson, P., & Jonsson, L. (2000). Heating and electromagnetic stirring in a ladle furnace–a simulation model. *ISIJ international*, *40*(11), 1098-1104.

Allanore, A. (2015). Features and challenges of molten oxide electrolytes for metal extraction. *Journal of The Electrochemical Society*, *162*(1), E13-E22.

Allanore, A., Yin, L., & Sadoway, D. R. (2013). A new anode material for oxygen evolution in molten oxide electrolysis. *Nature*, *497*(7449), 353.

Allwood, J. (2013). *Squaring the circular economy: the role of recycling within a hierarchy of material management strategies*. In *Handbook of Recycling*; Worrell, E., Reuter, M., Eds.; Elsevier: Oxford, UK, pp 445–476.

Allwood, J. (2016a). The future of steel: time to wake up. *Materials World, 24* (1), 44–47.

Allwood, J. M. (2016b). A bright future for UK steel: A strategy for innovation and leadership through up-cycling and integration. Report, *University of Cambridge*.

Allwood, J. M. (2018). Unrealistic techno-optimism is holding back progress on resource efficiency. *Nature materials*, *17*(12), 1050.

Allwood, J. M., Ashby, M. F., Gutowski, T. G., & Worrell, E. (2011). Material efficiency: A white paper. *Resources, Conservation and Recycling*, *55*(3), 362-381.

Allwood, J. M., Cullen, J. M., & Milford, R. L. (2010). Options for achieving a 50% cut in industrial carbon emissions by 2050. *Environmental Science and Technology, 44*(6), 1888-1894.

Allwood, J. M., Cullen, J. M., Carruth, M. A., Cooper, D. R., McBrien, M., Milford, R. L., & Patel, A. C. (2012). *Sustainable materials: with both eyes open*. Cambridge: UIT Cambridge.

Andreini, R. J., & Foster, J. S. (1974). Kinetics of solute removal during electron-beam and vacuum-arc melting. *Journal of Vacuum Science and Technology*, *11*(6), 1055-1059.

Alonso, E., Gregory, J., Field, F., & Kirchain, R. (2007). Material availability and the supply chain: risks, effects, and responses. *Environmental Science and Technology, 41*(19), 6649-6656.

Arthur, J. R. (1951). Reactions between carbon and oxygen. *Transactions of the Faraday Society*, *47*, 164-178.

Ashby, M. F. (2013). *Materials and the Environment – Eco-Informed Material Choice*, 2nd ed., Butterworth-Heinemann.

Barnett, H. J., & Morse, C. (1962). Scarcity and growth: The economics of resource scarcity. *Baltimore MD: Johns Hopkins University Press.*

Bell, S., Davis, B., Javaid, A., & Essadiqi, E. (2006). *Final report on effect of impurities in steel* (No. 2005-41). Technical report by Natural Resources Canada. Retrieved at https://www.researchgate.net/publication/306293969_Final_Report_on_Effect_of_Impurities_in_Steel.

Bernardo, E., Oro, R., Campos, M., & Torralba, J. M. (2016). Wetting phenomena for liquid Cu and Cu alloys on Fe-base substrate. *Advanced Powder Technology*, *27*(3), 1027-1035.

Bianna Recycling (2018). Trommels, http://biannarecycling.com/en/trommel/.

Birks, N., Meier, G. H., & Pettit, F. S. (2006). *Introduction to the high temperature oxidation of metals*. Cambridge University Press.

Björkman, B.; Samuelsson, C. (2013) *Recycling of Steel*. In Handbook of Recycling; Worrell, E., Reuter, M., Eds.; Elsevier: Oxford, UK, 65–83.

Blacha, L., & Łabaj, J. (2011). Temperature impact on copper evaporation from liquid iron. *Science and Engineering*, *51*(2), 103-106.

Blacha, L., & Labaj, J. (2012). Factors determining the rate of the process of metal bath components evaporation. *Metalurgija/Metallurgy*, *51*(4), 529-533.

Bodsworth, C. (1963). *Physical chemistry of iron and steel manufacture*. Longmans.

Bondi, A. (1953). The Spreading of Liquid Metals on Solid Surfaces. Surface Chemistry of High-Energy Substances. *Chemical Reviews*, *52*(2), 417-458.

Brahmst, E. (2006). Copper in Vehicle Recycling. Center for Automotive Research. Retrieved at http://www.cargroup.org/wp-content/uploads/2017/02/Copper-in-End_of_Life-Vehicle-Recycling.pdf.

Brandes, E.A. & Brook, G.B. (1992). *Smithells Metals Reference Book,* 7th ed., Butterworth-Heinemann, Oxford.

Bratina, J. E., Kriech, A., & Wilson, S. (2013). U.S. Patent No. 8,518,147. *Washington, DC: U.S. Patent and Trademark Office.*

Breus, V. M., Kats, Y. L., & Klachkov, A. A. (1999). Optimizing the energy-heat regime in electric steelmaking. *Metallurgist*, *43*(3), 117-123.

Brooks, A. L., Wang, S., & Jambeck, J. R. (2018). The Chinese import ban and its impact on global plastic waste trade. *Science Advances*, *4*(6).

Brown, R. R., & Block, F. E. (1968). Copper removal from steel scrap by thermal treatment. Feasibility study. Report no. *7218, U.S. Dept of Interior, Bureau of Mines*.

Burbidge, E. M., Burbidge, G. R., Fowler, W. A., & Hoyle, F. (1957). Synthesis of the elements in stars. *Reviews of modern physics*, *29*(4), 547.

Burgmann, W., & Göhler, K. (2013). Modern vacuum pumps for the vacuum degassing of steel in small and large vacuum-degassing units. *Metallurgist*, *57*(5-6), 516-525.

Burke, J. (Ed.). (1968). *Surfaces and Interfaces II: Physical and Mechanical Properties*. Syracuse University Press, Syracuse, New York.

Burn, D. L. (1961). *The economic history of steelmaking, 1867-1939: a study in competition*. Cambridge University Press.

Cabrera Serrenho, A., & Allwood, J. M. (2016). Material stock demographics: cars in Great Britain. *Environmental science & technology*, *50*(6), 3002-3009.

Caplan, D., Sproule, G. I., Hussey, R. J., & Graham, M. J. (1978). Oxidation of Fe-C alloys at 500° C. *Oxidation of Metals*, *12*(1), 67-82.

Carlson, O.N. and Schmidt, F.A. (1974). 103rd Annual AIME Meeting, Dallas, Texas, Feb 24-27, Ames Laboratory, USAEC, Iowa State University.

Castro, M. B. G., Remmerswaal, J. A. M., Brezet, J. C., & Reuter, M. A. (2007). Exergy losses during recycling and the resource efficiency of product systems. *Resources, Conservation and Recycling*, *52*(2), 219-233.

Castro, M. B., Remmerswaal, J., Reuter, M., & Boin, U. (2004). A thermodynamic approach to the compatibility of materials combinations for recycling. *Resources, Conservation and Recycling*, *43*(1), 1-19.

Chapman, P.F. and Roberts, F. (1983). *Metal Resources and Energy*, Butterworth and Co. Ltd., London.

Chen, R. Y., & Yeun, W. Y. D. (2003). Review of the high-temperature oxidation of iron and carbon steels in air or oxygen. *Oxidation of metals*, *59*(5-6), 433-468.

Chen, W. H., Chung, Y. C., & Liu, J. L. (2005). Analysis on energy consumption and performance of reheating furnaces in a hot strip mill. *International Communications in Heat and Mass Transfer*, *32*(5), 695-706.

Chin, D. T. (1977). Electrochemical extraction of copper from scrap steel. *AIChE Journal*, *23*(4), 434-440.

China Energy Statistical Yearbook (2013). National Bureau of Statistics of the People's Republic of China, China Statistics Press: Beijing, China.

Cho, W. D., & Fan, P. (2010). U.S. Patent No. 7,789,936. *Washington, DC: U.S. Patent and Trademark Office.*

Cho, W. D., Fan, P., Han, G., & Rhee, K. (2004). A new approach for the removal of copper from solid ferrous scrap. In *AIS Tech- Conference Proceedings*, 861.

Coates, G., & Rahimifard, S. (2007). Assessing the economics of pre-fragmentation material recovery within the UK. *Resources, Conservation and Recycling*, *52*(2), 286–302.

Coburn, S. K. (1969). Weathering steel favored by architects. Metal Progress, 96(2), 77–78.

Cohen, A. (1997). Removal of copper from iron-based metal with aluminum sulfide/ferrous sulfide matte, PhD thesis, Northwestern University.

Cohen, A., & Blander, M. (1998). Removal of copper from carbon-saturated iron with an aluminum sulfide/ferrous sulfide flux. *Metallurgical and Materials Transactions B*, *29*(2), 493-495.

Conejo, A.N., Lara, F.R., Marcias-Hernandez, Morales, R.D. (2007). Kinetic model of steel refining in a ladle furnace. *Steel Research International, 78*(2), 141-150.

Connelly, L., & Koshland, C. P. (1997). Two aspects of consumption: Using an exergy-based measure of degradation to advance the theory and implementation of industrial ecology. *Resources, Conservation and Recycling*, 19(3), 199–217.

Cooper-Searle, S., Livesey, F., & Allwood, J. M. (2018). Why are Material Efficiency Solutions a Limited Part of the Climate Policy Agenda? An application of the Multiple Streams Framework to UK policy on CO2 emissions from cars. *Environmental Policy and Governance*, *28*(1), 51-64.

Cooper, D. (2018, June 15). How recycling more steel and aluminum could slash imports without a trade war. *The Conversation,* Retrieved from: https://theconversation.com/how-recycling-more-steel-and-aluminum-could-slash-imports-without-a-trade-war-97766

Cooper, D. R., & Allwood, J. M. (2012). Reusing steel and aluminum components at end of product life. *Environmental science & technology*, *46*(18), 10334-10340.

Cooper, D. R., & Allwood, J. M. (2012). Reusing steel and aluminum components at end of product life. *Environmental science & technology*, *46*(18), 10334-10340.

Copper Development Association (2018). Copper drives electric vehicles. Retrieved from: https://www.copper.org/publications/pub_list/pdf/A6191-ElectricVehicles-Factsheet.pdf

Copper Development Association. Copper Facts. Retrieved from https://www.copper.org/education/c-facts/facts-print.html

Cottrell, A. H., & Bilby, B. A. (1949). Dislocation theory of yielding and strain ageing of iron. *Proceedings of the Physical Society. Section A*, *62*(1), 49.

Cramb, A. W., & Fruehan, R. J. (1991). A new low temperature process for copper removal from ferrous scrap. *Iron and Steelmaker*, *18*(11), 61-68.

Cullen, J. M. (2017). Circular economy: theoretical benchmark or perpetual motion machine?. *Journal of Industrial Ecology*, *21*(3), 483-486.

Cullen, J. M., & Allwood, J. M. (2009). The role of washing machines in life cycle assessment studies: the dangers of using LCA for prioritization. *Journal of Industrial Ecology*, *13*(1), 27-37.

Cullen, J. M., Allwood, J. M., & Bambach, M. D. (2012). Mapping the global flow of steel: from steelmaking to end-use goods. *Environmental science & technology*, *46*(24), 13048-13055.

Cullen, J. M., Allwood, J. M., McBrien, M., Milford, R. L., Carruth, M. A., Patel, A. C. H., & Cooper, D. R. (2011). Taking our metal temperature: energy and carbon savings by managing heat in steel and aluminium supply chains. Technical Report.

Daigo, I., Fujimaki, D., Matsuno, Y., & Adachi, Y. (2005). Development of a dynamic model for assessing environmental impact associated with cyclic use of steel. *Tetsu-to-Hagané*, *91*(1), 171-178.

Dalmijn, W. L., & de Jong, T. P. (2007). The development of vehicle recycling in Europe: Sorting, shredding, and separation. *Journal of the Minerals, Metals and Materials Society*, 59(11), 52–56.

Das, S., Curlee, T. R., Rizy, C. G., & Schexnayder, S. M. (1995). Automobile recycling in the United States: energy impacts and waste generation. *Resources, Conservation and Recycling*, *14*(3-4), 265-284.

David, R. G., & Gaskell, D. R. (1995). Introduction to the Thermodynamics of Materials. *Taylor & Francis*.

de Buzin, P. J. W. K., Heck, N. C., & Vilela, A. C. F. (2017). EAF dust: An overview on the influences of physical, chemical and mineral features in its recycling and waste incorporation routes. *Journal of materials research and technology*, *6*(2), 194-202.

Department for Environment, Food and Rural Affairs, UK government (2018, October 22). Government launches plan to ban plastic straws, cotton-buds, and strirrers. Retrieved from: https://www.gov.uk/government/news/government-launches-plan-to-ban-plastic-straws-cotton-buds-and-stirrers

Diegmann, W., Adam, F., Tiedeck, R., and Hoffmanns, W. (2000). Profitable Recycling of Automotive Wiring Harnesses, SAE Technical Paper 2000-01-0736.

Diener, D. L., & Tillman, A. M. (2015). Component end-of-life management: Exploring opportunities and related benefits of remanufacturing and functional recycling. *Resources, Conservation and Recycling*, *102*, 80-93.

Dunant, C. F., Drewniok, M. P., Sansom, M., Corbey, S., Cullen, J. M., & Allwood, J. M. (2018). Options to make steel reuse profitable: An analysis of cost and risk distribution across the UK construction value chain. *Journal of Cleaner Production*, *183*, 102-111.

Ekvall, T., Fråne, A., Hallgren, F., & Holmgren, K. (2014). Material pinch analysis: a pilot study on global steel flows. *Revue de Métallurgie–International Journal of Metallurgy*, *111*(6), 359-367.

Elger, G. W., Hunter, W.L., and Armantrout, C.E. (1968). Removal of nonferrous metals from synthetic automobile scrap on heating in a rotary kiln. *U.S. Dept. of the Interior, Bureau of Mines.*

Emi, T., & Wijk, O. (1996). Residuals in steel products--Impacts on properties and measures to minimize them. *Iron and Steel Society, Warrendale, PA (United States).*

Energy Consumption of Tanks and Vats (Spirax Sarco Limited, 2018), *http://www.spiraxsarco.com/Resources/Pages/Steam-Engineering-Tutorials/steam-engineering-principles-and-heat-transfer/energy-consumption-of-tanks-and-vats.aspx*. Accessed September 2018.

Engh, T. (1992). Principles of metal refining. *Oxford University Press.*

Entec (2006). Iron and Steel – Electric Arc Furnace steelmaking. https://webarchive.nationalarchives.gov.uk/20060716035729/http://www.dti.gov.uk/files/file28605.pdf

EPRI Center for Materials Production (1997). Electric arc furnace scrap preheating. Retrieved from https://p2infohouse.org/ref/10/09048.pdf.

EUROFER (2016). European Steel Scrap Specification. Retrieved at www.eurofer.org/facts&figures/ws.res/eursteelscrapspec.pdf

European Commission (2000). 2000/53/EC of the European Parliament and the council of 18 September 2000 on end of life vehicles, *Official Journal of the European Communities*, 21-10-2000.

European Commission. (2012). Critical raw materials for the EU - Annex V to the Report of the Ad-hoc Working Group on defining critical raw materials, 2012.

Eustathopoulos, N. (2015). Wetting by liquid metals—application in materials processing: the contribution of the Grenoble group. *Metals*, *5*(1), 350-370.

Eustathopoulos, N., & Drevet, B. (1994). Interfacial bonding, wettability and reactivity in metal/oxide systems. *Journal de Physique III*, *4*(10), 1865-1881.

Eustathopoulos, N., Nicholas, M. G., & Drevet, B. (Eds.). (1999). *Wettability at high temperatures* (Vol. 3). Elsevier.

Fernando, J. J. (1950). U.S. Patent No. 2,512,578. *Washington, DC: U.S. Patent and Trademark Office.*

Fischer, W. A., & Derenbach, M. (1964). Beitrag zur Frage der Verdampfung beim Schmelzen von Eisenlegierungen im Vakuum Teil I. Theoretische Ableitungen und Untersuchungen an Zweistofflegierungen von Eisen mit Arsen, Mangan, Kupfer und Zinn. *Archiv für das Eisenhüttenwesen*, *35*(4), 307-316.

Fray, D. J. (2002). Anodic and cathodic reactions in molten calcium chloride. *Canadian metallurgical quarterly*, *41*(4), 433-439.

Fredriksson, H., Hansson, K., & Olsson, A. (2001). On the mechanism of liquid copper penetration into iron grain boundaries. *Scandinavian journal of metallurgy*, *30*(1), 41-50.

Froschauer, L., & Fulrath, R. M. (1975). Direct observation of liquid-phase sintering in the system iron-copper. *Journal of Materials Science*, *10*(12), 2146-2155.

Fruehan, R., Cramb, A. (1991). Copper Removal from Steel Scrap Using a Sulfur Matte. CMP Report Number 91-6.

Gallois, B., & Lupis, C. H. P. (1981). Effect of oxygen on the surface tension of liquid copper. *Metallurgical Transactions B*, *12*(3), 549-557.

Galopin, M., & Daniel, J. S. (1975). Molten salts in metal treating: Present uses and future trends. *Electrodeposition and Surface Treatment*, *3*(1), 1-31.

Gamma-tech Analyzer. (2018). http://www.gammatech.us.

Gaustad, G., Li, P., & Kirchain, R. (2007). Modeling methods for managing raw material compositional uncertainty in alloy production. *Resources, Conservation and Recycling, 52*(2), 180–207.

Gaustad, G., Olivetti, E., & Kirchain, R. (2012). Improving aluminum recycling: A survey of sorting and impurity removal technologies. *Resources, Conservation and Recycling, 58*, 79–87.

Gerrard, J., & Kandlikar, M. (2007). Is European end-of-life vehicle legislation living up to expectations? Assessing the impact of the ELV Directive on "green" innovation and vehicle recovery. *Journal of Cleaner Production, 15*(1), 17–27.

Gesing, A. (2004). Assuring the continued recycling of light metals in end-of-life vehicles: A global perspective. *Journal of the Minerals, Metals and Materials Society*, *56*(8), 18-27.

Ghosh, A. (2000). *Secondary steelmaking: principles and applications*. CRC Press.

Ghosh, A., & Chatterjee, A. (2008). *Iron making and steelmaking: theory and practice*. PHI Learning Pvt. Ltd.

Ghosh, B., Ghosh, M. K., Parhi, P., Mukherjee, P. S., & Mishra, B. K. (2015). Waste printed circuit boards recycling: an extensive assessment of current status. *Journal of Cleaner Production*, *94*, 5-19.

Gibbs, J. W., & Bumstead, H. A. (1906). *Thermodynamics* (Vol. 1). Longmans, Green and Company.

Giddings, J. C. (1991). *Unified separation science*. New York: Wiley.

Gill, G. M., Ineson, E., & Austin, G. W. (1959). The behaviour of various elements in vacuum steelmaking. *Journal of the Iron & Steel Institute*, *191*, 172-175.

Ginsel, D. & Vandenbroeck, F. (2011). Purification of post-consumer steel scrap. *Euromat*, *39*(7), 1–2.

Glöser, S., Soulier, M., & Tercero Espinoza, L. A. (2013). Dynamic analysis of global copper flows. Global stocks, postconsumer material flows, recycling indicators, and uncertainty evaluation. *Environmental science & technology*, *47*(12), 6564-6572.

Goodman, P., Robertson, C., Skarstein, A., Lyonas, L., & Pahal, S. (2012). Industrial and Laboratory Furnaces and Ovens, *ERA Technology*, Report No. 2012-0230. https://www.eup-network.de/fileadmin/user_upload/ENTR_Lot_4_Final_Report_Appendices.pdf

Gurell, J., Bengtson, Falkenström, M., & Hansson, B. M. (2012). Laser induced breakdown spectroscopy for fast elemental analysis and sorting of metallic scrap pieces using certified reference materials. *Spectrochimica Acta Part B: Atomic Spectroscopy, 74–75*(0), 46–50.

Gutowski, T. G. (2007). Thermodynamics and Recycling. *IEEE International Symposium on Electronics and the Environment*, 19–21 May, San Francisco, CA.

Gutowski, T. G., Suh, N. P., Cangialose, C., & Berube, G. M. (1983). A low-energy solvent separation method. *Polymer Engineering & Science*, *23*(4), 230-237.

Gutowski, T.G. (2005) Materials Separation and Recycling. In *Thermodynamics and the Destruction of Resources,* Bakshi, B.R., Gutowski, T.G., & Sekulic, D.P., Cambridge University Press.

Hara, S. 'Fundamental Study on the Removing Residual Elements from Steel Scrap', (1996), *ISIJ,* 105.

Harald, P. (1925). U.S. Patent No. 1,562,472. *Washington, DC: U.S. Patent and Trademark Office.*

Harris, R. (1988). Numerical Simulation of Vacuum Refining of Liquid Metal. *Canadian Metallurgical Quarterly*, *27*(3), 169-178.

Harris, R., & Davenport, W. G. (1979). Pilot Plant Scale Vacuum Distillation of Liquid Steel to Remove Copper. *Canadian Metallurgical Quarterly*, *18*(3), 303-311.

Harris, R., & Davenport, W. G. (1984). U.S. Patent No. 4,456,479. *Washington, DC: U.S. Patent and Trademark Office.*

Harris, R., & Davenport, W. G. (1992a). Vacuum distillation of liquid metals: Part I. Theory and experimental study. *Journal of Electronic Materials*, *21*(1), 581-588.

Harris, R., & Davenport, W. G. (1992b). Vacuum distillation of liquid metals: Part II. Photographic study. *Journal of Electronic Materials*, *21*(1), 589-591.

Harris, R.L. (1980). Vacuum refining of molten steel. PhD thesis, McGill University.

Hartman, A. D., Oden, L. L., & Davis, D. L. (1994). Copper removal from solid ferrous scrap by a solid/gas reaction. *Iron Steelmaker*, *21*(5), 59-62.

Hartman, A.D., Williamson, C.A., and Davis, D.S. (1996). *Iron & steelmaker*, *23*(8), 43-45.

Hatayama, H., Daigo, I., & Tahara, K. (2014). Tracking effective measures for closed-loop recycling of automobile steel in China. *Resources, Conservation and Recycling*, *87*, 65-71.

Hatayama, H., Daigo, I., Matsuno, Y., & Adachi, Y. (2010). Outlook of the world steel cycle based on the stock and flow dynamics. *Environmental science & technology*, *44*(16), 6457-6463.

Hatayama, H., Daigo, I., Matsuno, Y., & Adachi, Y. (2012). Evolution of aluminum recycling initiated by the introduction of next-generation vehicles and scrap sorting technology. *Resources, Conservation and Recycling*, *66*, 8-14.

Hatayama, H., Yamada, H., Daigo, I., Matsuno, Y., & Adachi, Y. (2007). Dynamic substance flow analysis of aluminum and its alloying elements. *Materials transactions*, *48*(9), 2518-2524.

Hayes, P. C. (1985). *Process selection in extractive metallurgy*. Hayes Publishing Co., Brisbane, Australia.

Hernandez, A. G., Lupton, R. C., Williams, C., & Cullen, J. M. (2018). Control data, Sankey diagrams, and exergy: Assessing the resource efficiency of industrial plants. *Applied energy*, *218*, 232-245.

Herring, D.H. (2009). Considerations in heat treatment, part one: furnace atmospheres. *IndustrialHeating.com*, October 2009, pp. 45-48.

Herter, Carl J. "Method for preparing a low residual alloy steel charge from scrap metal." U.S. Patent No. 4,517,016. 14 May 1985.

Hidani, T., Takemura, K., Suzuki, R. O., & Ono, K. (1996). Elimination of copper from molten steel by ammonia gas blowing. *Tetsu-to-Hagané*, *82*(2), 135-140.

Higgins, T. (2017, June 20). The end of car ownership. The Wall Street Journal. Retrieved from: https://www.wsj.com/articles/the-end-of-car-ownership-1498011001

Holappa, L. (2010). Towards sustainability in ferroalloy production. *Journal of the Southern African Institute of Mining and Metallurgy*, *110*(12), 703-710.

Horton, P. M., & Allwood, J. M. (2017). Yield improvement opportunities for manufacturing automotive sheet metal components. *Journal of Materials Processing Technology*, *249*, 78-88.

Hu, X. Jiang, P., Yan, Z., Zhu, L., Chou, K., Matsuura, H. and Tsukihashi, F. (2013a). *ISIJ international, 53*, 541.

Hu, X., Yan, Z., Jiang, P., Zhu, L., Chou, K., Matsuura, H., & Tsukihashi, F. (2013b). Removal of Copper from Molten Steel using FeO–SiO2–CaCl2 Flux. *ISIJ international*, *53*(5), 920-922.

Hui, K., JianJun, W., Shangxing, G., Li, Z., & Jie, L. (2009). Copper Removal from Molten Steel with FeS-Na2S Slag. *High Temperature Materials and Processes*, *28*(1-2), 67-72.

ICE Database (Circular Ecology, 2018), http://www.circularecology.com/embodied-energy-and-carbon-footprint-database.html#.W5Jf5i-ZOb9. Accessed September 2018.

IEA (2017), Energy Technology Perspectives 2017: Catalysing Energy Technology Transformations, Paris, France.

Igarashi, Y., Daigo, I., Matsuno, Y., & Adachi, Y. (2007). Estimation of the change in quality of domestic steel production affected by steel scrap exports. *ISIJ international*, *47*(5), 753-757.

Imai, N., Komatsubara, N., and Kunishige, K. (1997). Effect of Cu, Sn and Ni on hot workability of hot-rolled mild steel. *ISIJ International, 37*, 217- 223.

Imai, T. and Sano, N. (1988). Copper partition between Na2S fluxes and carbon-saturated iron melts. *Tetsu-to-Hagane, 74*, 640.

Institute of Scrap Recycling Industries (ISRI) (2016). Scrap Specifications Circular. Retrieved at http://www.isri.org/docs/default-source/commodities/specsupdate.pdf

Intergovernmental Panel on Climate Change (2014). Climate Change 2014: Mitigation of Climate Change. Working Group III Contribution to the IPCC 5th Assessment Report: Technical Summary.

International Energy Agency (2009). World Energy Model – Methodology and Assumptions. Paris, France: International Energy Agency (IEA).

International Iron and Steel Institute Committee on Technology (1983). *The Electric Arc Furnace*. International Iron and Steel Institute; 2nd edition.

IPCC (2018). Global warming of 1.5°C. [V. Masson-Delmotte, P. Zhai, H. O. Pörtner, D. Roberts, J. Skea, P.R. Shukla, A. Pirani, W. Moufouma-Okia, C. Péan, R. Pidcock, S. Connors, J. B. R. Matthews, Y. Chen, X. Zhou, M. I. Gomis, E. Lonnoy, T. Maycock, M. Tignor, T. Waterfield (eds.)]. In Press.

Iwase, M. (1996). Refining of solid ferrous scrap intermingled with copper by using molten aluminum. *Iron and Steel Society, Warrendale, PA (United States).*

Iwase, M., & Ohshita, H. (1994). Further studies of the removal of copper from solid ferrous scrap. *Steel Research*, *65*(9), 362-367.

Iwase, M., & Tokinori, K. (1991). A feasibility study for the removal of copper from solid ferrous scrap. *Steel research*, *62*(6), 235-239.

Janke, D., Savov, L., Weddige, H.-J., & Schulz, E. (2000). Scrap-based steel production and recycling of steel. Materials Tech. 34(6), 387-399.

Japanese Ferrous Raw Materials Association (2008). Uniform Standards of Ferrous Scraps, Retrieved at http://www.tetsugen.gol.com/kikaku/uniform%20standards(2008).pdf.

Javaid, A. and Essadiqi, E. (2003). Final Report on Scrap Management, Sorting and Classification of Steel. Government of Canada Report No. 2003-23(CF). Retrieved from https://www.nrcan.gc.ca/sites/www.nrcan.gc.ca/files/mineralsmetals/pdf/mms-smm/busi-indu/rad-rad/pdf/2003-23(cf)cc-eng.pdf

Jiemin, T., Xuefeng, W., Ferri, M. B., & Argenta, P. (2006). Charging hot metal to the EAF using Consteel. *Millennium Steel*, pg. 79-86.

Jimbo, I., Sulsky, M. S., & Fruehan, R. J. (1988). The Refining of Copper From Ferrous Scrap. *Iron and Steelmaker*, *15*(8), 20-23.

Jindal Steel and Power. Wire Rods. Retrieved from http://www.jindalsteelpower.com/product_broucher/wire_rod_mailable.pdf

Johnson, J. X., McMillan, C. A., & Keoleian, G. A. (2013). Evaluation of life cycle assessment recycling allocation methods: The case study of aluminum. *Journal of Industrial Ecology*, *17*(5), 700-711.

Jung, J., & Keller, W. (2016). Process and cost optimized agitator solutions for hydrometallurgical base metals processing. *World of Metallurgy – ERZMETALL 69*, 2, 108-118.

Jung, S. H., & Kang, Y. B. (2016). Evaporation Mechanism of Cu from Liquid Fe Containing C and S. *Metallurgical and Materials Transactions B*, *47*(4), 2164-2176.

Jung, S. H., & Kang, Y. B. (2016). Simultaneous Evaporation of Cu and Sn from Liquid Steel. *Metallurgical and Materials Transactions B*, *47*(4), 2564-2570.

Kakudate, K., Adachi, Y., & Suzuki, T. (2000). A macro model for usage and recycling pattern of steel in Japan using the population balance model. *Science and Technology of Advanced Materials*, *1*(2), 105.

Karimi, H. J., & Saidi, M. H. (2010). Heat transfer and energy analysis of a pusher type reheating furnace using oxygen enhanced air for combustion. *Journal of Iron and Steel Research, International*, *17*(4), 12-17.

Katayama, H.; Sano, N.; Sasabe, M.; Matsuoka, S. (1997). Research Activities on Residual Element Removal Japan Iron and Steel – Today, Yesterday, and Tomorrow. *Stockholm 11–14 June Conference Proceedings, 1*, 15–26.

Keeling, C. D., Piper, S. C., Bacastow, R. B., Wahlen, M., Whorf, T. P., Heimann, M., & Meijer, H. A. (2005). Atmospheric CO2 and CO2 exchange with the terrestrial biosphere and oceans from 1978 to 2000: observations and carbon cycle implications. In *A history of atmospheric CO2 and its effects on plants, animals, and ecosystems* (pp. 83-113). Springer, New York, NY.

Kim, S. H., & Fruehan, R. J. (1987). Physical modeling of liquid/liquid mass transfer in gas stirred ladles. *Metallurgical transactions B*, *18*(2), 381-390.

Kim, S. W., & Lee, H. G. (2009). Effect of Oxide Scale Formation on the Behaviour of Cu in Steel during High Temperature Oxidation in O2-N2 and H2O-N2 atmospheres. *steel research international*, *80*(2), 121-129.

King, C.J. (1987). *Separation and Purification: Critical Needs and Opportunities*; National Research Council, National Academy Press, Washington D.C.

Klempner, D., Frisch, K. C., Pokorski, B., Sendijarevic, V. (1999). Characterization of Various ASR Streams. *CPAPER, SAE International.*

Klöpffer, W. (1997). Life cycle assessment. *Environmental Science and Pollution Research*, *4*(4), 223-228.

Komolafe, B., & Medraj, M. (2014). Progress in wettability study of reactive systems. *Journal of Metallurgy*, Article ID 387046.

Kondo, Y. (2011). Suppression of Surface Hot Shortness Caused by Copper during Hot Rolling. In *Materials Science Forum*, *696*, 183-188.

Konečná, R., & Fintová, S. (2012). Copper and copper alloys: casting, classification and characteristic microstructures. In *Copper Alloys-Early Applications and Current Performance-Enhancing Processes*. InTech.

Konishi, H., Bitoh, T., Ono, H., Oishi, T., Koyama, K., & Tanaka, M. (2014). Behavior of Copper Dissolution in an Ammonia Solution Containing Ammonium Chloride or Sulfate. *Journal of the Japanese Society for Experimental Mechanics*, *14*(Special Issue), 205-209.

Kor, G. J. W., & Glaws, P. C. (1998). Ladle refining and vacuum degassing. In *The making, shaping and treating of steel*, *2,* Fruehan, R.J., The AISE Steel Foundation.

Kostetsky, Y., Troyansky, A., & Samborsky, M. (2013). Removal of Copper From Carbon-Iron Melts. *22nd International Conference on Metallurgy and Materials*

Koyama, K., Tanaka, M., & Lee, J. C. (2006). Copper leaching behavior from waste printed circuit board in ammoniacal alkaline solution. *Materials transactions*, *47*(7), 1788-1792.

Krüger, M. Reuter, C. Kögler, T. Probst (2005). *Metallurgical Furnaces (Chap. 5),* Wiley, Weinheim.

Kuznetsov, V. A., & Kats, Y. L. (2007). Economical vacuum degassing of steel with the use of mechanical pumps. *Metallurgist*, *51*(3-4), 220-225.

Łabaj, J., Oleksiak, B., & Siwiec, G. (2011). Study of copper removal from liquid iron. *Metalurgija*, *50*(4), 265-268.

Lange, K. W. (1988). Thermodynamic and kinetic aspects of secondary steelmaking processes. *International materials reviews*, *33*(1), 53-89.

Langenberg, F. C., & Lindsay, R. W. (1954). Removal of Copper from Iron-Copper-Carbon Alloys. *AIME TRANS, 200,* 967-968.

Leak, V. G., Fine, M. M., & Dolezal, H. (1973). Separating Copper From Scrap by Preferential Melting. *GOVT REP, BUREAU OF MINES*, (48).

Leak, V., & Fine, M. (1973). U.S. Patent No. 3,776,718. *Washington, DC: U.S. Patent and Trademark Office.*

Leary, R. J. (1965). Removing copper from copper-clad steel by oxidation. *GOVT REP, BUREAU OF MINES.*

Lee, H. S., & Harris, R. (1997). Characterization of the surface area of overflow droplets generated by a gas-lift pump under reduced pressure. *The Canadian Journal of Chemical Engineering*, *75*(1), 256-263.

Leen, G., & Heffernan, D. (2002). Expanding automotive electronic systems. *Computer*, *35*(1), 88-93.

Leroy, V., D'Haeyer, R., Defourny, J., Hoogendoorn, T., Birat, J.P, Grabke, H.J., Morrison, W.B., Henderson, N.G., Longbottom, R.D., Laux, T., Les, I. (1995). Effect of tramp elements in flat and long products. *European Commission.*

Li, L. S., Xiang, C. X., Cao, J., Li, S. Q., & Ichise, E. J. (1998). Copper elimination from the molten steel by addition of hydronitrogens. *Journal of University of Science and Technology Beijing*, *5*(2), 93-96.

Li, L.X., Zhao, C., Wang, P., Tian, C., Hangyan, L.S. (1998). Decopperization of steel melt through filtration. *Journal of Iron and Steel Research*, 3.

Li, S.Q., Yu, B.J., Li, S. Li, L.S. (1999). A basic study of decopperization in molten steel by ammonium salt. *Journal of Baotou University of Iron and Steel Technology*, 3.

Liansheng, L., Shiqi, L., Changxiang, X., Jie, C., Keming, L., & Suqin, L. (1999). Copper Removal from Molten Steel by Gasification. *Journal of Iron and Steel Research International*, *6*(2), 10-13.

Lide, D.R. (2006). *CRC Handbook of Chemistry and Physics*, 87th ed. CRC Press, Boca Raton, FL.

Lim, Y., Kwon, O. H., Lee, J., & Yoo, K. (2013). The ammonia leaching of alloy produced from waste printed circuit boards smelting process. *Geosystem Engineering*, *16*(3), 216-224.

Linde Gas. Furnace atmospheres No. 2. Neutral hardening and annealing. https://www.linde-gas.com/en/legacy/attachment?files=tcm:g.17-460205,tcm:.17-460205,tcm:17-460205. Accessed March 2019.

Lindner, K. A. (1936). U.S. Patent No. 2,041,844. *Washington, DC: U.S. Patent and Trademark Office.*

Lindsay, R., & Simkovich, A. (1960). Results of Treating Iron with Sodium Sulphite to Remove Copper. *Trans Metall Soc AIME*, *218*(3), 569-570.

Liu, X., & Jeffes, J. H. E. (1985). Effect of Sodium Sulphide on Removal of Copper and Tin From Molten Iron. *Ironmaking & Steelmaking*, *12*(6), 293-294.

Liu, X., & Jeffes, J. H. E. (1989). Decopperization of molten steel by various slags. *Ironmaking & Steelmaking*, *16*(5), 331-334.

Loyd, A. (2018, July 31). The implications of Brexit on circular economy initiatives. *Wast Management World.* Retrieved from: https://waste-management-world.com/a/blog-the-implications-of-brexit-on-circular-economy-initiatives

Lupis, C.H.P. (1983). *Chemical Thermodynamics of Materials,* North-Holland, New York.

Lüthi, D., Le Floch, M., Bereiter, B., Blunier, T., Barnola, J. M., Siegenthaler, U., Raynaud, D., Fischer, H., Kawamura, K. & Stocker, T. F. (2008). High-resolution carbon dioxide concentration record 650,000–800,000 years before present. *Nature*, *453*(7193), 379.

Ma, Z., Savov, L., & Janke, D. (1999). Chemical activities of the solute elements Cu and Sn in scrap-based iron melts. *Metall*, *53*(1-2), 61-67.

Machlin, E. S. (1960). Kinetics of vacuum induction refining-theory. *Transactions of the American Institute of Mining and Metallurgical Engineers*, *218*(2), 314-326.

Madias, J. (2014). Electric furnace steelmaking. In *Treatise on Process Metallurgy: Industrial Processes* (pp. 271-300).

Majima, H., Nigo, S., Hirato, T., Awakura, Y. and Iwai, M.: Shigen-to-Sozai, 109 (1993), 191-194.

Makar, H. V., & Brown, R. E. (1974). Copper Removal From Molten Ferrous Scrap--A Pilot Plant Study. *U.S. Bureau of Mines, Rep. Invest.*, (7914).

Makar, H. V., & Dunning, B. W. (1969). Use of sodium sulfate for copper removal from molten iron. *Journal of the Minerals, Metals and Materials Society*, *21*(7), 19-22.

Makar, H. V., Dunning, B., & Caldwell, H. (1968). Laboratory Studies on the Use of Sodium Sulfate for Removing Copper From Molten Iron. *U.S. Bureau of Mines.*

Manning, C. P., & Fruehan, R. J. (2001). Emerging technologies for iron and steelmaking. *Journal of the Minerals, Metals and Materials Society*, *53*(10), 36-43.

Manouchehri, H. R. (2006). Mapping and development of shredding product streams: four shredding plants in Sweden. *Jernkontorets Forskning, Report 2006-06-30.*

Marique, C. (1996). Recycling of scrap for high quality products. *Rev. Met. Paris*, *93* (11), 1377-1385.

Marston, H. F., Bolt, P. H., Leprince, G., Röder, M., Klima, R., Niska, J., & Jarl, M. (2004). Challenges in the modelling of scale formation and decarburisation of high carbon, special and general steels. *Ironmaking & steelmaking*, *31*(1), 57-65.

Maruyama, T., Katayama, H. G., Momono, T., Tayu, Y., & Takenouchi, T. (1998). Evaporation rate of copper from molten iron by urea spraying under reduced pressure. *Tetsu-to-Hagane*, *84*(4), 243-248.

Material Economics Sverige (2018). The circular economy – a powerful force for climate mitigation, Stockholm, http://materialeconomics.com/publications/publication/the-circular-economy-a-powerful-force-for-climate-mitigation

Matousek, J. W. (2008). The thermodynamic properties of slags. *Journal of the Minerals, Metals and Materials Society*, *60*(2), 62-64.

Matsubae, K., Nakajima, K., Nakamura, S., & Nagasaka, T. (2011). Impact of the recovery of secondary ferrous materials from alternative ELV treatment methods on CO2 emission: A waste input output analysis. *ISIJ international*, *51*(1), 151-157.

Matsumaru, K., Susa, M., & Nagata, K. (1996). Removal of Copper from Iron-based Scraps by O2-Cl2 Gas Mixtures. *Tetsu-to-Hagane*, *82*(10), 799-804.

Matsumoto, K., Izawa, M., Nakanishi, T., & Tsubouchi, K. (2009). Tribological properties of water glass lubricant for hot metalworking. *Tribology Transactions*, *52*(4), 553-559.

Matsuo, T. (1988). Removal of Copper and Tin with Plasma. *Transactions of the Iron and Steel Institute of Japan*, *28*(4), 319-324.

Matsuo, T. (2000). Acceleration of copper and tin removal from molten steel by decarburization under reduced pressure. *Tetsu-to-hagane*, *86*(11), 741-747.

Matsuo, T., Maya, K., Nishi, T., Shinme, K., Ueno, A., & Anezaki, S. (1996). Removal of copper and tin in molten iron with decarburization under reduced pressure. *ISIJ international*, *36*(Suppl), S62-S65.

Melford, D. A. (1980). The influence of residual and trace elements on hot shortness and high temperature embrittlement. *Phil. Trans. R. Soc. Lond. A*, *295*(1413), 89-103.

Memoli, F., Giavani, C., & Malfa, E. (2012). Melting/Forming/Joining-Consteel Evolution—The Second Generation of Consteel Technology. *Industrial Heating*, *80*(8), 59.

Meng, X., & Han, K. N. (1996). The principles and applications of ammonia leaching of metals—a review. *Mineral Processing and Extractive Metallurgy Review*, *16*(1), 23-61.

Metz, B. (Ed.). (2007). *Climate change 2007: mitigation: contribution of working group III to the fourth assessment report of the intergovernmental panel on climate change*. Intergovernmental Panel on Climate Change.

Michaelis, B. M., Dunn-Rankin, D., Smith Jr, R. F., & Bobrow, J. E. (2007). In-flight thermal control of molten metal droplet streams. *International Journal of Heat and Mass Transfer*, *50*(23-24), 4554-4558.

Milford, R. L., Pauliuk, S., Allwood, J. M., & Müller, D. B. (2013). The roles of energy and material efficiency in meeting steel industry CO2 targets. *Environmental science & technology*, *47*(7), 3455-3462.

Moore, J. J. (1981). Chemical Metallurgy. London: Butterworths, Print.

Morales, D. (1982). Alloying effect on vaporization rate of copper and tin from molten iron alloys. *Ironmaking Steelmaking*, *9*(2), 64-76.

Moynihan, M. C., & Allwood, J. M. (2014). Utilization of structural steel in buildings. *Proc. R. Soc. A*, *470*(2168), 20140170.

Müller, D. B., Wang, T., Duval, B., & Graedel, T. E. (2006). Exploring the engine of anthropogenic iron cycles. *Proceedings of the National Academy of Sciences*, *103*(44), 16111-16116.

Murphy, J. J., & Shaddix, C. R. (2006). Combustion kinetics of coal chars in oxygen-enriched environments. *Combustion and flame*, *144*(4), 710-729.

Nafziger, R.H.; Hartman, A.D.; Farrell, R.F. (1990). Trends in Iron Casting Compositions as Related to Ferrous Scrap Quality and Other Variables, 1981-86, *Bureau of Mines, United States Department of the Interior, Washington DC.*

Nakajima, K., Takeda, O., Miki, T., Matsubae, K., & Nagasaka, T. (2011). Thermodynamic analysis for the controllability of elements in the recycling process of metals. *Environmental science & technology*, *45*(11), 4929-4936.

Nakajima, K., Takeda, O., Miki, T., Matsubae, K., Nakamura, S., & Nagasaka, T. (2010). Thermodynamic analysis of contamination by alloying elements in aluminum recycling. *Environmental Science & Technology, 44*(14), 5594–600.

Nakamoto, M., Okumura, Y., Tanaka, T., & Yamamoto, T. (1975). Segregation of Cu by Unidirectional Solidification in Molten Fe-C-Cu Alloy. *Tetsu-to-Hagané*, *100*, 761-768.

Nakamura, S., Kondo, Y., Kagawa, S., Matsubae, K., Nakajima, K., & Nagasaka, T. (2014). MaTrace: Tracing the fate of materials over time and across products in open-loop recycling. *Environmental science & technology*, *48*(13), 7207-7214.

Nakamura, S., Kondo, Y., Matsubae, K., Nakajima, K., Tasaki, T., & Nagasaka, T. (2012). Quality-and dilution losses in the recycling of ferrous materials from end-of-life passenger cars: input-output analysis under explicit consideration of scrap quality. *Environmental science & technology*, *46*(17), 9266-9273.

Nakamura, S., Nakajima, K., Kondo, Y., & Nagasaka, T. (2007). The waste input-output approach to materials flow analysis. *Journal of Industrial Ecology*, *11*(4), 50-63.

Nelson, H. R. (1937). The primary oxide film on iron. *The Journal of Chemical Physics*, *5*(4), 252-259.

Newell, S. (2017). The true value of shredded steel when used in EAF steel production. Presentation to UK Electric Steel Makers, Darlington UK.

Newell, S. (1996). Production of low copper residual shredded steel scrap. *International Conference on Recycling in the Iron & Steel Industry, Oct 27-30*. Retrieved from newellequip.com/wp-content/uploads/2017/05/LRCU-30oct96.doc

Nippon Steel and Sumitomo Metal. (2012). Cold Rolled Steel Sheets and Coils. Retrieved from https://www.nssmc.com/product/catalog_download/pdf/U003en.pdf.

Nishi, T., Fukagawa, S., Shinme, K., & Matsuo, T. (1999). Removal of copper and tin in molten iron with combination of plasma heating and powder blowing decarburization under reduced pressure. *ISIJ international*, *39*(9), 905-912.

Noll, R., Bette, H., Brysch, A., Kraushaar, M., Mönch, I., Peter, L., Sturm, V. (2001). Laser-induced breakdown spectrometry — applications for production control and quality assurance in the steel industry. *Spectrochimica Acta Part B: Atomic Spectroscopy*, *56*(6), 637–649.

Non-Integrated Steel Producers' Association. (2008). Electric Furnace Reinforcing Steel Bar Quality Inspection Report, Tokyo.

Noro, K., Takeuchi, M., & Mizukami, Y. (1997). Necessity of scrap reclamation technologies and present conditions of technical development. *ISIJ international*, *37*(3), 198-206.

Oba, K. (2013). Wiring Harnesses for Next Generation Automobiles. *Fujikura Tech Rev, 42*, 77–80.

Oda, J., Akimoto, K., Tomoda, T. (2013). Long-term global availability of steel scrap. *Resources, Conservation and Recycling, 81*, 81–91.

Oden, L. L., & Elger, G. W. (1987). Removal of copper from molten ferrous scrap: results of laboratory investigations. *US Department of the Interior, Bureau of Mines.*

Oden, L. L., Adams, A., & Fugate, A. D. (1973). Reducing copper and tin impurities in ferrous scrap recovered from incinerated municipal refuse (No. BM-RI-7776). *Bureau of Mines, Washington, DC (USA).*

Oelsen, W., Schürmann, E., & Heinrichs, G. (1959). Die Verteilung von Kupfer, Zinn, Arsen, Antimon, Silber und Gold zwischen Bleischmelzen und kohlenstoffgesättigten Eisenschmelzen. *Archiv für das Eisenhüttenwesen*, *30*(11), 649-654.

Ogawa (1950). Japan Patent, 16, Jan 11.

Ohno, H., Matsubae, K., Nakajima, K., Kondo, Y., Nakamura, S., & Nagasaka, T. (2015). Toward the efficient recycling of alloying elements from end of life vehicle steel scrap. *Resources, Conservation and Recycling*, *100*, 11-20.

Ohno, H., Matsubae, K., Nakajima, K., Nakamura, S., & Nagasaka, T. (2014). Unintentional flow of alloying elements in steel during recycling of end-of-life vehicles. *Journal of Industrial Ecology*, *18*(2), 242-253.

Ohno, R., & Ishida, T. (1969). Rate of Evaporation of Manganese, Copper, Tin, Chromium, and Sulphur from Molten Iron under Vacuum. *Science reports of the Research Institutes, Tohoku University. Ser. A, Physics, chemistry and metallurgy*, *21*, 130.

Okazaki, T., & Robertson, D. G. C. (1985). Removal of tramp elements: mathematical modeling. *Ironmaking and Steelmaking*, *12*(6), 295-298

Olivetti, E. A., & Cullen, J. M. (2018). Toward a sustainable materials system. *Science*, *360*(6396), 1396-1398.

Ollette, M. (1959). Vacuum Distillation of Minor Elements from Liquid Ferrous Alloys. *Inst. de Recherches de Siderurgié*, *111*.

Ono-Nakazato, H., Taguchi, K., Seike, Y., & Usui, T. (2003). Effect of silicon and carbon on the evaporation rate of copper in molten iron. *ISIJ international*, *43*(11), 1691-1697.

Ono, K., Ichise, E., Suzuki, R. O., & Hidani, T. (1995). Elimination of copper from the molten steel by NH3 blowing under reduced pressure. *Steel research*, *66*(9), 372-376.

Östman, M., Lundkvist, K., & Larsson, M. (2011). Environmental system effects when including scrap preheating and surface cleaning in steel making routes. In *World Renewable Energy Congress-Sweden*, no. 57, 1684-1691.

Parashar, G., Bajpayee, M., & Kamani, P. K. (2003). Water-borne non-toxic high-performance inorganic silicate coatings. *Surface Coatings International Part B: Coatings Transactions*, *86*(3), 209-216.

Pauliuk, S., Milford, R. L., Müller, D. B., & Allwood, J. M. (2013b). The steel scrap age. *Environmental science & technology*, *47*(7), 3448-3454.

Pauliuk, S., Wang, T., & Müller, D. B. (2011). Moving toward the circular economy: The role of stocks in the Chinese steel cycle. *Environmental science & technology*, *46*(1), 148-154.

Pauliuk, S., Wang, T., & Müller, D. B. (2013a). Steel all over the world: Estimating in-use stocks of iron for 200 countries. *Resources, Conservation and Recycling*, *71*, 22-30.

Perry, D.L. (2016). *Handbook of Inorganic Compounds,* 2nd ed., CRC Press.

Phillips, W. G. B., & Edwards, D. P. (1976). Metal prices as a function of ore grade. *Resources policy, 2*(3), 167-178.

Porzio, G. F., Colla, V., Fornai, B., Vannucci, M., Larsson, M., & Stripple, H. (2016). Process integration analysis and some economic-environmental implications for an innovative environmentally friendly recovery and pre-treatment of steel scrap. *Applied Energy*, *161*, 656-672.

Prausnitz, J.M. (1994). Thermodynamics and Separation of Mixtures. *Phys. Chem. 98*, 1461-1470.

Pretorius, E., Oltmann, H., & Jones, J. (2010). *EAF fundamentals*. New York, LWB Refractories.

Protsenko, P., & Eustathopoulos, N. (2005). Surface and grain boundary wetting of Fe based solids by molten Pb and Pb-Bi eutectic. *Journal of materials science*, *40*(9-10), 2383-2387.

Rackham, H. (1952). Pliny: natural history (English trans.), Loeb Classical ser. W. Heinemann, London

Ramadan, A., Shash, A. Y., El-Mahallawi, I. S., Senk, D., & Mattar, T. (2015). Effect of Tempcore processing on mitigating problems of tramp elements in low C steel produced from recycled material. *Journal of Iron and Steel Research, International*, *22*(7), 582-589.

Ramström, E. (2009). Mass transfer and slag-metal reaction in ladle refining: a CFD approach, Doctoral dissertation, KTH Royal Institute of Technology.

Rankin, W.J. (2011). Minerals, metals and sustainability meeting future material needs an introduction to sustainability. In: *Minerals, Metals and Sustainability: Meeting Future Material Needs*., pp. 41–61.

Reck, B. K., & Graedel, T. E. (2012). Challenges in Metal Recycling. *Science, 337*(2011), 690–695.

Recycling Today (2001). Shredder Guide – high speed machinery https://www.recyclingtoday.com/article/shredder-guide----high-speed-machinery-/.

Reiichi, O. (1979). Kinetics of Evaporation of Manganese, Copper and Sulfur from Iron Alloys in Vacuum Induction Melting (Metallurgy). *Science reports of the Research Institutes, Tohoku University. Ser. A, Physics, chemistry and metallurgy*, *27*, 86-87.

Reijnders, L. (2016). Conserving functionality of relatively rare metals associated with steel life cycles: a review. *Journal of cleaner production*, *131*, 76-96.

Reuter, M. A., Van Schaik, A., Ignatenko, O., & De Haan, G. J. (2006). Fundamental limits for the recycling of end-of-life vehicles. *Minerals Engineering*, *19*(5), 433-449.

Rod, O.; Becker, C.; & Nylén, M. (2006). Opportunities and dangers of using residual elements in steels: a literature survey. *Jernkontorets Forskning*, D819, 1–59. Retrieved at https://www.jernkontoret.se/globalassets/publicerat/forskning/d-rapporter/d819.pdf.

Rose, A. (1981). The extraction of copper from steel by molten electrolysis. PhD thesis, University of Cambridge.

Rotary Electric Vibrators (Cleveland Vibrator): https://www.clevelandvibrator.com/images/Documents/Full%20RE%20Manual.pdf. Accessed September 2018.

Rousseau, E. R. W. (2009). *Handbook of separation process technology*. John Wiley & Sons.

Rudnik, E. (2017). Application of Ammoniacal Solutions for Leaching and Electrochemical Dissolution of Metals from Alloys Produced from Low-Grade E-Scrap. *Archives of Metallurgy and Materials*, *62*(3), 1681-1688.

Russo, P. (2014). Quality control of scrap and chemical analysis needs at ArcelorMittal. Jernkontoret scrap seminar in Hofors, Sweden.

Safiah, A. A., and F. R. Sale. (1972). Influence of Carbon on the Removal of Copper From Iron Melts With Sulfide Slags. *J. Iron and Steel Inst., 210*(1), 52-56.

Salomon-de-Friedberg, H., & Davenport, W. G. (1977). Vacuum Removal of Copper from Melted Steel Scrap. *Canadian Metallurgical Quarterly*, *16*(1), 225-231.

Sampson, E., & Sridhar, S. (2013). Effect of Silicon on Hot Shortness in Fe-Cu-Ni-Sn-Si Alloys During Isothermal Oxidation in Air. *Metallurgical and Materials Transactions B*, 44(5), 1124–1136.

Sano, N., Katayama, H., Sasabe, M., & Matsuoka, S. (1998). Research activities on removal of residual elements from steel scrap in Japan. *Scandinavian journal of metallurgy*, *27*(1), 24-30.

Sasabe, M., Harada, E., & Yamashita, S. (1996). Removal of copper from carbon saturated molten iron by using FeCl2. *Tetsu-to-Hagané*, *82*(2), 129-134.

Sato, S., Takeuchi, M., Mizukami, Y., & Birat, J. P. (1996). The shinseiko project : A new environment friendly steelmaking route based on scrap. Revue de Metallurgie. *Cahiers D'Informations Techniques, 93*(4), 473–483.

Savov, L, Volkova, E., & Janke, D. (2003). Copper and tin in steel scrap recycling. *Materials Geoenvironment*, *50*(3), 627-640.

Savov, L., & Janke, D. (1998). Recycling of scrap in steelmaking in view of the tramp element problem. *Metall, 52*(6), 374-383.

Savov, L., & Janke, D. (2000). Evaporation of Cu and Sn from induction-stirred iron-based melts treated at reduced pressure. *ISIJ international*, *40*(2), 95-104.

Sawyer, J. (1974). Automotive Scrap Recycling: Processes, Prices and Prospects. Resources for the Future, Inc.

Sax, D. (2018, December 7). End the innovation obsession. *New York Times.* Retrieved from: https://www.nytimes.com/2018/12/07/opinion/sunday/end-the-innovation-obsession.html

Schenck, H., & Perbix, G. (1962). Entfernung von Kupfer aus Roheisen und Blei mit Natriumsulfidschlacken. *Archiv für das Eisenhüttenwesen*, *33*(7), 417-420.

Schenck, H., Roth, H., & Steinmetz, E. (1970). Der Stoffumsatz des Kupfers zwischen flüssigem Eisen im Bereich der Kohlenstoffsättigung und Natriumsulfidschlacken. *Archiv für das Eisenhüttenwesen*, *41*(7), 595-603.

Schmidt, M. (2008). The Sankey diagram in energy and material flow management Part II: methodology and current applications. *Journal of Industrial Ecology, 12*(2), 173-185.

Scholz, H., Biebricher, U., Franz, H., Paderni, A., and Bettoni, P. State of the art in VAR and ESR processes - a comparison (ASO Group Steel). http://www.asogroupsteel.com/wp-content/uploads/2014/05/var-and-esr-processes.pdf

Schrade, C., Huellen, M., Wilhelm, U., Zulhan, Z. (2006). EAF-Based Flat-Steel Production Applying Secondary Metallurgical Processes. Linz/Austria October Secondary Steelmaking Session, Paper No. 7.1.103 (10).

Seetharaman, S. (2013). Treatise on Process Metallurgy, Volume 1: Process Fundamentals. ELSEVIER, Print.

Seetharaman, S., Andersson, G., & Teng, L. D. (2013). Retainment, Recovery and Recycling: A Swedish Success Story of ECO-Steelmaking. *Transactions of the Indian Institute of Metals*, *66*(5-6), 567-575.

Seetharaman, S., Worsley, D., Pleydell-Pearce, C., & Edy, M. B. (2016). The sun has risen over steel town. Report, *Swansea University*.

Serrenho, A. C., Mourão, Z. S., Norman, J., Cullen, J. M., & Allwood, J. M. (2016). The influence of UK emissions reduction targets on the emissions of the global steel industry. *Resources, Conservation and Recycling*, *107*, 174-184.

Shattuck, M. & Ramsdell, C. (2018). The case for producing low-copper steel with ballistic separators, Waste Advantage. Retrieved from https://wasteadvantagemag.com/the-case-for-producing-low-copper-steel-with-ballistic-separators/.

Shen, P., Gu, Y., Yang, N. N., Zheng, R. P., & Ren, L. H. (2015). Influences of electric current on the wettability and interfacial microstructure in Sn/Fe system. *Applied Surface Science*, *328*, 380-386.

Sheng, Y.Y. and Irons. (1992). Measurements of the internal structure of gas-liquid plumes., *Metallurgical Transactions B*, 23(6), 779-788.

Sherwood, Y.K. (1959). Mass Transfer between Phases. Phi Lambda Upsilon, Pennsylvania State University, University Park, PA.

Shi, L. (1993). Accelerated oxidation of iron induced by Na 2 SO 4 deposits in oxygen at 750° C—A new type low-temperature hot corrosion. *Oxidation of metals*, *40*(1-2), 197-211.

Shibata, K., Seo, S. J., Kaga, M., Uchino, H., Sasanuma, A., Asakura, K., & Nagasaki, C. (2002). Suppression of surface hot shortness due to Cu in recycled steels. *Materials Transactions*, *43*(3), 292-300.

Shimpo, R., Ogawa, O., Fukaya, Y., & Ishikawa, T. (1997). Copper removal from carbon-saturated molten iron with Al 2 S 3-FeS flux. *Metallurgical and Materials Transactions B*, *28*(6), 1029-1037.

Shulman, A. D. (2011). U.S. Patent No. 7,886,915. *Washington, DC: U.S. Patent and Trademark Office.*

Sicon (2018). Sicon PrimeScrap, https://sicontechnology.com/en/sicon-primescrap/.

Skelton, A. C., & Allwood, J. M. (2013). The incentives for supply chain collaboration to improve material efficiency in the use of steel: an analysis using input output techniques. *Ecological economics*, *89*, 33-42.

Slimak, K. M., & Slimak, R. A. (2001). U.S. Patent No. 6,303,234. *Washington, DC: U.S. Patent and Trademark Office.*

Smith, P. N., & Ward, R. G. (1966). The Evaporation of Liquid Iron Alloys Under Vacuum. *Canadian Metallurgical Quarterly*, *5*(2), 77-92.

Söderholm, P., & Ejdemo, T. (2008). Steel scrap markets in Europe and the USA. *Minerals & Energy-Raw Materials Report*, *23*(2), 57-73.

Spitzer, K. H., Rüppel, F., Viščorová, R., Scholz, R., Kroos, J., & Flaxa, V. (2003). Direct Strip Casting (DSC)-an Option for the Production of New Steel Grades. *Steel research international*, *74*(11-12), 724-731.

Sridhar, S. (2016a). Circular Economy – Can there be a Sunrise in Steel Town? April 29th presentation to VDEh, 3rd European Scientific Steel Panel.

Sridhar, S. (2016b). University of Warwick Tata Steel/RAEng Chair in Low C Materials Manufacturing, telephone communication.

Stahel, W. R. (2016). The circular economy. *Nature News*, *531*(7595), 435.

Staker, W. L., Chindgren, C. J., & Dean, K. C. (1971). Improved Cupric Ammonium Carbonate Leaching of Copper Scrap. *U.S. Bureau of Mines.*

steeluniversity (2016). Electric Arc Furnace. World Steel Association, Retrieved from: http://steeluniversity.org/learn/

Steinert (2018). Steinert SteelMaster, https://steinertglobal.com/us/magnets-sensor-sorting-units/magnetic-separation/magnetic-head-pulleys/steinert-steelmaster/.

Strassert, G. (2002). Physical input-output accounting. In *A handbook of industrial ecology*, edited by R. Ayres and L. Ayres. Cheltenham, UK: Elgar.

Stubbles, J. (2000). Energy use in the US steel industry: a historical perspective and future opportunities. Energetics, Inc., Columbia, MD (US).

Sun, Z. H. I., Guo, M., Vleugels, J., Van der Biest, O., & Blanpain, B. (2012). Strong static magnetic field processing of metallic materials: A review. *Current Opinion in Solid State and Materials Science*, *16*(5), 254-267.

Sun, Z., Xiao, Y., Sietsma, J., Agterhuis, H., & Yang, Y. (2015). A cleaner process for selective recovery of valuable metals from electronic waste of complex mixtures of end-of-life electronic products. *Environmental science & technology*, *49*(13), 7981-7988.

Suzuki, R. O., & Ono, K. (2000). Enhanched Evaporation of Copper by NH3 Gas Blowing. In *Proceedings of 10th International Conference on High Temperature Materials Chemistry (HTMC-X), Jülich, Germany, 10–14 April 2000* (pp. 491-494). International Union of Pure and Applied Chemistry.

Swaan Arons, J. D., Kooi, H. V. D., & Sankaranarayanan, K. (2004). *Efficiency and sustainability in the energy and chemical industries*. CRC Press, Boca Raton.

Szargut, J. (2005). *Exergy method: technical and ecological applications* (Vol. 18). WIT press.

Taguchi, K., Ono-Nakazato, H., & Usui, T. (2004). Enhancement of Evaporation Removal Rate of Copper in Molten Iron by the Silicon and/or Carbon Addition. *Resources Processing*, *51*(3), 158-162.

Takahira, N., Tanaka, T., Hara, S., & Lee, J. (2005). Unusual wetting of liquid metals on iron substrate with oxidized surface in reduced atmosphere. *Materials transactions*, *46*(12), 3008-3014.

Tayeb, M. A., Spooner, S., & Sridhar, S. (2014). Phosphorus: the noose of sustainability and renewability in steelmaking. *Journal of the Minerals, Metals and Materials Society*, *66*(9), 1565-1571.

Tee, J. K. S., & Fray, D. J. (1999). Removing impurities from steel scrap using air and chlorine mixtures. *Journal of the Minerals, Metals and Materials Society*, *51*(8), 24-27.

Tee, J. K. S., & Fray, D. J. (2006). Separation of copper from steel. *Ironmaking & steelmaking*, *33*(1), 19-23.

Tee, J. K. S., and D. J. Fray. (2004). Reaction of zinc, copper and iron in air and chlorine mixtures. *Mineral Processing and Extractive Metallurgy, 113*(3), 129-138.

Tilting Rotary Furnace (Melting Solutions), https://www.aluminium-messe.com/local/php/productpdf.php?id=6527&ext=.pdf. Accessed September 2018.

Tokumitsu, N., and Hirata, H. (1990). *CAMP-ISIJ, 3*(4), 1184.

Topkaya, Y. A., Lu, W. K., & —K. (1975). Metal-Slag-Gas Reaction and Processes, ed. by ZA Foroulis and WW Smeltzer. *Electrochem. Soc., Princeton*, *111*.

Toulouevski, Y. N., & Zinurov, I. Y. (2010a). Innovation in electric arc furnaces. Nova Iorque: Springer, 1-23.

Toulouevski, Y. N., & Zinurov, I. Y. (2010b). Preheating of Scrap by Burners and Off-Gases. In *Innovation in Electric Arc Furnaces* (pp. 93-113). Springer, Berlin, Heidelberg.

Toyota (2015). Toyota's Environmental Initiatives: Contribution to a Recycling-Based Socieity, pg. 32. Retrieved from: http://www.toyota-global.com/sustainability/report/er/pdf/er15_04_en.pdf

Turkdogan, E. T., Grieveson, P., & Darken, L. S. (1963). Enhancement of diffusion-limited rates of vaporization of metals. *The Journal of Physical Chemistry*, *67*(8), 1647-1654.

U.S. Department of Energy, Office of Industrial Technologies (2000). Energy and Environmental Profile of the U.S. Chemical Industry, <www1.eere.energy.gov/manufacturing/resources/chemicals/pdfs/profile_full.pdf>

U.S. Environmental Protection Agency. Secondary Aluminum. Retrieved from: https://www3.epa.gov/ttn/chief/ap42/ch12/bgdocs/b12s08.pdf

Uchida, Y. I., Matsui, A., Kishimoto, Y., & Miki, Y. (2015). Fundamental Investigation on Removal of Copper from Molten Iron with Na2CO3–FeS Fluxes. *ISIJ International*, *55*(8), 1549-1557.

USGS, *2008 Minerals Yearbook: Copper*. United States Geological Survey Annual Publications; https://minerals.usgs.gov/minerals/pubs/commodity/copper/myb1-2008-coppe.pdf

USGS, *Iron and Steel Scrap 2010*. United States Geological Survey Annual Publications; http://minerals.usgs.gov/minerals/pubs/commodity/iron_&_steel_scrap/

Van Hecke, M. C., & Fontainas, L. M. (1984). *U.S. Patent No. 4,451,289*. Washington, DC: U.S. Patent and Trademark Office.

Vignes, Alain. (2011) Extractive Metallurgy 1: Basic Thermodynamics and Kinetics. Wiley-ISTE, Print.

W. Schmitz and D. Trauzeddel. The melting, holding and pouring process – energy and process-related aspects (Otto Junker): http://www.hossl.com/archivos/201605/articulo-junker.pdf?1. Accessed September 2018.

Wang, C., Nagasaka, T., Hino, M., & Ban-Ya, S. (1991a). Copper distribution between molten FeS-NaS0. 5 flux and carbon saturated iron melt. *ISIJ international*, *31*(11), 1300-1308.

Wang, C., Nagasaka, T., Hino, M., & Ban-Ya, S. (1991b). Copper distribution between FeS-alkaline or-alkaline earth metal sulfide fluxes and carbon saturated iron melt. *ISIJ international*, *31*(11), 1309-1315.

Wang, T., Müller, D. B., & Graedel, T. E. (2007). Forging the anthropogenic iron cycle. *Environmental science & technology*, *41*(14), 5120-5129.

Ward, R. G. (1963). Evaporative losses during vacuum induction melting of steel. *J. Iron & Steel Inst.*, *1963*, 11-15.

Ward, R. G., & Aurini, T. D. (1966). Mechanism of Alloying Elements Evaporation During the Vacuum Induction Melting of Steel. *IRON STEEL INST*, *204*(9).

Warner, N. A. (2004). Continuous oxygen steelmaking with copper-, tin-, and zinc-contaminated scrap. *Metallurgical and Materials Transactions B*, *35*(4), 663-674.

Webler, B. A. (2008). *A study of the processes during high temperature oxidation that control surface hot shortness in copper-containing low carbon steels*, Doctoral dissertation, Carnegie Mellon University.

Webler, B. A., & Sridhar, S. (2008). Evolution and Distribution of the Copper-rich Phase during Oxidation of an Iron–0.3 wt% Copper Alloy at 1150° C. *ISIJ international*, *48*(10), 1345-1353.

Weng, Y., Dong, H., & Gan, Y. (Eds.). (2011). *Advanced Steels: The Recent Scenario in Steel Science and Technology*. Springer Science & Business Media.

Whalen, T.J. & Humenik, M. (1967). Sintering and Related Phenomena, edited by Kuczynski, G., Hooton, N.A. & Gibbon, C.F. Gordon and Breach, New York, 715-746.

Winkler, O., & Bakish, R. (Eds.). (1971). *Vacuum metallurgy*. Amsterdam: Elsevier.

worldsteel (2001-2018), Steel Statistical Yearbook, Brussels, Belgium.

worldsteel (2010). Steel and Raw Materials Fact Sheet; worldsteel Association, https://www.worldsteel.org/publications/fact-sheets.html.

worldsteel Association (2016). Future of ferrous scrap availability and demand. IOM3 Steel Strategy Seminar Series 2–4, London.

Worrell, E., D. Phylipsen, D. Einstein and N. Martin (2000). Energy Use and Energy Intensity of the U.S. Chemical Industry, University of California Berkeley, <www.energystar.gov/ia/business/industry/industrial_LBNL-44314.pdf>

Xiao-Wei, Z., Bai-Ling, A., De-Yang, H., Lin, Z., & En-Gang, W. (2016). Migration and alignment of Fe-rich particles in Cu melt under high magnetic field. *Acta Physica Sinica*, *65*(13).

Yamaguchi, K., & Ono, H. (2012). Oxidative Removal of Cu from Carbon-saturated Iron via Ag Phase into B2O3 Flux. *ISIJ international*, *52*(1), 18-25.

Yamaguchi, K., & Takeda, Y. (2003). Impurity removal from carbon saturated liquid iron using lead solvent. *Materials transactions*, *44*(12), 2452-2455.

Yamaguchi, K., Ono, H., & Takeuchi, E. (2015). Removal of Cu in Carbon Saturated Iron by Sulfurization via Ag Phase. *Tetsu-to-Hagané*, *101*(12), 10-18.

Yamaguchi, K., Ono, H., & Usui, T. (2010). Oxidation removal of cu from carbon saturated iron via Ag phase. *Tetsu-to-Hagané*, *96*(9), 531-535.

Yamaguchi, K., Ono, H., & Usui, T. (2010). The Equilibrium Relation of Immiscibility in an Fe-Cu-B System at 1873 K. *Materials transactions*, *51*(7), 1222-1226.

Yamamoto, K., Shibata, H., & Mizoguchi, S. (2005). Defective or effective? Tramp elements in steels. Transactions of the Indian Institute of Metals, *58*(4), 695-702.

Yamamoto, M., & Kato, E. (1980). The Effect of Surface Movement on the Evaporation Rates of Alloying Elements from Liquid Iron under Vacuum. *Tetsu-to-Hagané*, *66*(6), 608-617.

Yang, W. (2001). *The structure and properties of mill scale in relation to easy removal*, Doctoral dissertation, University of Sheffield.

Yao, Z., Li, J., & Zhao, X. (2011). Molten salt oxidation: A versatile and promising technology for the destruction of organic-containing wastes. *Chemosphere*, *84*(9), 1167-1174.

Yellishetty, M., Ranjith, P. G., & Tharumarajah, A. (2010). Iron ore and steel production trends and material flows in the world: Is this really sustainable?. *Resources, conservation and recycling*, *54*(12), 1084-1094.

Yi, H., Xu, G., Cheng, H., Wang, J., Wan, Y., & Chen, H. (2012). An overview of utilization of steel slag. *Procedia Environmental Sciences*, *16*, 791-801.

Yin, L., Sampson, E., Nakano, J., & Sridhar, S. (2011). The effects of nickel/tin ratio on Cu induced surface hot shortness in Fe. *Oxidation of metals*, *76*(5-6), 367-383.

Yin, R. (2011). *Metallurgical process engineering*. Springer Science & Business Media.

Young, T. (1805). III. An essay on the cohesion of fluids. *Philosophical transactions of the royal society of London*, *95*, 65-87.

Yuan, Y., Sassa, K., Iwai, K., Wang, Q., He, J., & Asai, S. (2008). Copper distribution in Fe–Cu and Fe–C–Cu alloys under imposition of an intense magnetic field. *ISIJ international*, *48*(7), 901-905.

Zaitsev, A. I., Shelkova, N. Y. E. E., Litvina, A. D., Shakhpazov, E. K., & Mogutnov, B. M. (2001). An investigation of evaporation of liquid alloys of iron with copper. *High Temperature*, *39*(3), 388-394.

Zaitsev, A. I., Zaitseva, N. E., Shakhpazov, E. K., & Mogutnov, B. M. (2004). Evaporation of copper from iron melts. *ISIJ international*, *44*(4), 639-646.

Zaitsev, A.I., Zaitseva, N.E., Shakhpazov, E. K., & Mogutnuv, B.M. (2004). Potentialities of simultaneous removal of tin and copper from molten iron through evaporation. *ISIJ international*, *44*(6), 957-964.

Zhang, Y., Barr, P. V., & Meadowcroft, T. R. (2008). Continuous scrap melting in a short rotary furnace. *Minerals Engineering*, *21*(2), 178-189.

Zhou, K., Shinme, K., & Anezaki, S. (1995). Removal of copper from ferrous scrap with ammonia leaching method. I. Dissolution rate of copper in aqueous ammonia solution. *Journal of the Mining and Materials Processing Institute of Japan*, *111*(1), 49-53.

Zhou, S., Shen, S., Zhao, D., Zhang, Z., & Yan, S. (2017). Evaporation and decomposition of eutectics of cupric chloride and sodium chloride. *Journal of Thermal Analysis and Calorimetry*, *129*(3), 1445-1452.

Zigalo, I.N., Baptizmanskii, V.I, Vyatkin, Y.F, Velichko, A.G., Shakhpazov, K., and Grishchenko, Y.N. (1991): Steel USSR, 21, July, 299.

Appendix. A1 – copper in global steel recycling

Table A1.1: References corresponding to the numbered points in Figure 3.3.

Point	Description	Reference
1	EAF route obsolete ordinary machines	Daigo et al, 2005
2	EAF route obsolete ordinary pressed autos	Daigo et al, 2005
3	EAF route obsolete ordinary shredded autos	Daigo et al, 2005
4	EAF route obsolete ordinary containers	Daigo et al, 2005
5	EAF route obsolete ordinary other	Daigo et al, 2005
6	EAF route obsolete special construction	Daigo et al, 2005
7	EAF route obsolete special machines	Daigo et al, 2005
8	EAF route obsolete special pressed autos	Daigo et al, 2005
9	EAF route obsolete special shredded autos	Daigo et al, 2005
10	EAF route obsolete special containers	Daigo et al, 2005
11	EAF route obsolete special other	Daigo et al, 2005
12	Waste electronic equipment	Daigo et al, 2005
13	Incinerator bottom ash	Ginsel et al, 2011
14	ELV's	Ginsel et al, 2011
15	Car shredded scrap	Schrade et al, 2006
16	Heavy scrap	Schrade et al, 2006
17	Can scrap	Schrade et al, 2006
18	Home scrap	Schrade et al, 2006
19	Hot metal/pig iron	Schrade et al, 2006
20	DRI/HBI	Schrade et al, 2006
21	Shredder	Savov et al, 2003
22	Obsolete	Savov et al, 2003
23	Home scrap	Savov et al, 2003

Point	Description	Reference
51	MSWI scrap	Haupt et al, 2016
52	USA 1992 #1 Bundles	Leroy et al, 1995
53	USA 1992 Shredded	Leroy et al, 1995
54	USA 1992 #1 HMS	Leroy et al, 1995
55	USA 1992 #2 Bundles	Leroy et al, 1995
56	USA 1992 #2 HMS	Leroy et al, 1995
57	USA 1992 DRI	Leroy et al, 1995
58	France 1985 shredded	Leroy et al, 1995
59	UK 1982 OA/OB	Leroy et al, 1995
60	1954 US EAF steel, cold scrap shop	Nafziger et al, 1990
61	1962 US EAF steel, cold scrap shop	Nafziger et al, 1990
62	1977 US EAF steel, cold scrap shop	Nafziger et al, 1990
63	1987 Japan EAF steel bar	Non-Integrated Steel Producers' Association, 2008
64	1989 Japan EAF steel bar	Non-Integrated Steel Producers' Association, 2008
65	1991 Japan EAF steel bar	Non-Integrated Steel Producers' Association, 2008
66	1996 Japan EAF steel scrap	Igarashi et al, 2007
67	1997 Japan EAF steel bar	Non-Integrated Steel Producers' Association, 2008
68	2001 Japan EAF steel bar	Non-Integrated Steel Producers' Association, 2008
69	2004 Japan steel bar	Non-Integrated Steel Producers' Association, 2008
70	2007 Japan steel bar	Non-Integrated Steel Producers' Association, 2008
71	Average Japanese steel bar	Daigo et al, 2015
72	Average Chinese steel bar	Daigo et al, 2015
73	Converter products in 2000 in Japan	Daigo et al, 2005

Point	Description	Reference
24	Hot metal	Savov et al, 2003
25	DRI (total impurity content)	Björkman et al, 2013
26	Pig iron (total impurity content)	Björkman et al, 2013
27	Number 1 factor bundles (total impurity content)	Björkman et al, 2013
28	Busheling (total impurity content)	Björkman et al, 2013
29	Number 1 heavy melting (total impurity content)	Björkman et al, 2013
30	Shredded auto scrap (total impurity content)	Björkman et al, 2013
31	Number 2 heavy melting (total impurity content)	Björkman et al, 2013
32	Obsolescent scrap and electric-furnace bundles	Kostetskey et al, 2013
33	Heavy home scrap	Kostetskey et al, 2013
34	Waste chips	Kostetskey et al, 2013
35	Miscellaneous home scrap (scrap, tedges, pours, deadheads)	Kostetskey et al, 2013
36	Shredded scrap	Ohno et al, 2014
37	Shredded autos	Igarashi et al, 2007
38	Machine scrap	Igarashi et al, 2007
39	Low quality EAF scrap	Igarashi et al, 2007
40	#1 Bundles	Pretorius et al
41	#1 HMS	Pretorius et al
42	#2 HMS	Pretorius et al
43	Shredded	Pretorius et al
44	#2 Bundles	Pretorius et al

Point	Description	Reference
74	Ordinary EAF construction product in Japan in 2000	Daigo et al, 2005
75	Ordinary EAF machine product in Japan in 2000	Daigo et al, 2005
76	Ordinary EAF auto product in Japan in 2000	Daigo et al, 2005
77	Ordinary EAF container product in Japan in 2000	Daigo et al, 2005
78	Ordinary EAF other product in Japan in 2000	Daigo et al, 2005
79	Special EAF steel in Japan in 2000	Daigo et al, 2005
80	EAF steel for construction and buildings	Igarashi et al, 2007
81	Converter steel for construction	Igarashi et al, 2007
82	Canada 1985 integrated steel	Leroy et al, 1995
83	USA 1984 integrated steel	Leroy et al, 1995
84	EAF scrap mix #3	Leroy et al, 1995
85	EAF scrap mix #3	Leroy et al, 1995
86	Finland 1985 EAF steelshop, long products	Leroy et al, 1995
87	Canada 1985 EAF steelshop, long products	Leroy et al, 1995
88	UK 1982 EAF steelshop, long products	Leroy et al, 1995
89	France 1993 EAF steelshop, long products	Leroy et al, 1995
90	Canada 1993 EAF steelshop, long products	Leroy et al, 1995
91	Italy 1993 EAF steelshop, long products	Leroy et al, 1995
92	1984 Bethelehem Johnstown flat EAF shop mean	Leroy et al, 1995
93	1984 Rouge Steel flat EAF shop mean	Leroy et al, 1995
94	1984 National Great Lakes flat EAF shop mean	Leroy et al, 1995

Point	Description	Reference
45	Plate and structural	Pretorius et al
46	#1 shredded	Brahmst, 2006
47	#2 shredded	Brahmst, 2006
48	Internal returns	Haupt et al, 2016
49	Sheared heavy	Haupt et al, 2016
50	Shredded	Haupt et al, 2016

Point	Description	Reference
95	1993 mini-mill B flat EAF shop mean	Leroy et al, 1995
96	100% EAF scrap based process	Burin, 2016
97	Steel sheets from primary route	Hatayama et al, 2014
98	1999 E40 (shredded) average	Data from internal industry presentation
99	2000 E40 (shredded) average	Data from internal industry presentation
100	2001 E40 (shredded) average	Data from internal industry presentation
101	2002 E40 (shredded) average	Data from internal industry presentation
102	2003 E40 (shredded) average	Data from internal industry presentation
103	2004 E40 (shredded) average	Data from internal industry presentation
104	2005 E40 (shredded) average	Data from internal industry presentation
105	2006 E40 (shredded) average	Data from internal industry presentation
106	2007 E40 (shredded) average	Data from internal industry presentation
107	2016 shredded average	Data from internal industry presentation
108	2016 HMS #1 and 2 average	Data from internal industry presentation
109	2016 OA scrap average	Data from internal industry presentation

Table A1.2: Reported copper concentrations of EAF steel products.

Year	Country	Cu Conc. (wt%)	Steel Type	Source
2012, 2013	China	0.098	EAF steel bar	Daigo and Goto, 2015
2011	Japan	0.278	EAF steel bar	Daigo and Goto, 2015
2007	Japan	0.281	EAF steel bar	Non-Integrated Steel Producers' Association, 2008
2004	Japan	0.318	EAF steel bar	Non-Integrated Steel Producers' Association, 2008
2001	Japan	0.288	EAF steel bar	Non-Integrated Steel Producers' Association, 2008
2000	Japan	0.304	Construction EAF steel	Daigo et al., 2005
2000	Japan	0.285	Machine EAF steel	Daigo et al., 2005
2000	Japan	0.27	Auto EAF steel	Daigo et al., 2005
2000	Japan	0.287	Container EAF steel	Daigo et al., 2005
2000	Japan	0.274	Other EAF steel	Daigo et al., 2005
2000	Japan	0.274	Export EAF steel	Daigo et al., 2005
2000	Japan	0.105	Special EAF steel	Daigo et al., 2005
1997	Japan	0.289	EAF steel bar	Non-Integrated Steel Producers' Association, 2008
1996	Japan	0.297	EAF steel scrap	Igarashi et al., 2007
1993	France	0.35	EAF carbon and low alloy steels	Leroy et al., 1995
1993	Canada	0.2	EAF carbon and low alloy steels	Leroy et al., 1995
1993	Italy	0.25	EAF carbon and low alloy steels	Leroy et al., 1995
1993	USA	0.14	hot-rolled coils	Leroy et al., 1995
1992	USA	0.048	AISI 1008	Leroy et al., 1995
1991	Japan	0.325	EAF steel bar	Non-Integrated Steel Producers' Association, 2008
1991	USA	0.07	AISI 1006	Leroy et al., 1995
1990	USA	0.09	AISI 1008	Leroy et al., 1995
1989	Japan	0.327	EAF steel bar	Non-Integrated Steel Producers' Association, 2008
1985	Finland	0.25	EAF carbon and low alloy steels	Leroy et al., 1995
1985	Canada	0.16	EAF carbon and low alloy steels	Leroy et al., 1995
1984	USA	0.08	carbon steels	Leroy et al., 1995
1984	USA	0.2	low-carbon flats	Leroy et al., 1995
1984	USA	0.048	DDQ HSLA	Leroy et al., 1995
1984	USA	0.069	hot-rolled coils	Leroy et al., 1995
1982	Japan	0.22	EAF carbon and low alloy steels	Leroy et al., 1995
1982	UK	0.3	EAF carbon and low alloy steels	Leroy et al., 1995
1977	US	0.162	Cold scrap shop only	Nafziger et al., 1990

Year	Country	Cu Conc. (wt%)	Steel Type	Source
1977	USA	0.162	EAF carbon and low alloy steels	Leroy et al., 1995
1972-1977	Japan	0.23	EAF carbon and low alloy steels	Leroy et al., 1995
1962	US	0.151	Cold scrap shop only	Nafziger et al., 1990
1962	USA	0.151	EAF carbon and low alloy steels	Leroy et al., 1995
1954	US	0.17	Cold scrap shop only	Nafziger et al., 1990
1954	USA	0.17	EAF carbon and low alloy steels	Leroy et al., 1995

Table A1.3: Reported copper tolerances of steel products.

Steel grade	Copper tolerance (wt%Cu)	Reference
Tin plate for draw and iron cans	**0.12**	Björkman et al., 2013
Extra deep drawing quality sheet	**0.14**	Björkman et al., 2014
Drawing quality and enameling steels	**0.16**	Björkman et al., 2015
Commercial quality sheet	**0.22**	Björkman et al., 2016
Fine wire grades	**0.25**	Björkman et al., 2017
Special bar quality	**0.35**	Björkman et al., 2018
Merchant bar quality	**0.5**	Björkman et al., 2019
Steel sheets for deep drawing	<0.06	Nakamura et al., 2012
Hot and Cold Rolled Steel	<0.1	Nakamura et al., 2013
Sections	<0.3	Nakamura et al., 2014
Steel Bars	<0.4	Nakamura et al., 2015
Interstitial Free	0.03	Schrade et al., 2006
Deep Drawing Quality	0.04	Schrade et al., 2007
Drawing	0.06	Schrade et al., 2008
Commercial	0.1	Schrade et al., 2009
Structural	0.12	Schrade et al., 2010
Fine Wire	0.07	Schrade et al., 2011
Rebar	0.4	Schrade et al., 2012
LC fine wire	0.1	Pretorius et al.
Cold heading	0.1	Pretorius et al.
Forging grades	0.15	Pretorius et al.
Plating quality	0.2	Pretorius et al.
IQ	0.3	Pretorius et al.
Structural	0.4	Pretorius et al.
Deep drawing	0.06	Pretorius et al.
Drawing quality	0.1	Pretorius et al.
Cold-rolled	0.1-0.15	Hatayama et al., 2014
Cold-rolled galvanized	0.1-0.15	Hatayama et al., 2015
Hot-rolled	0.15-0.2	Hatayama et al., 2016
Hot-rolled galvanized	0.2	Hatayama et al., 2017
Wire Rod for Welding Wire	0.2-0.25	Severstal
Rod for Ropes and Structures	0.1-0.15	Severstal
Telegraph Wire	0.2	Severstal
Copper Telegraph Wire	0.2-0.4	Severstal

*Values in bold denote total impurity content, (wt%, sum of Cu+Sn+Ni+Cr+Mo)

Table A1.4: Qualitative requirements of steel products.

Product Category	Requirement	Reference
Low carbon and mild steel	Very low content of tramp elements	Jindal Steel and Power
Medium and high carbon	Very low content of tramp elements	Jindal Steel and Power
Low carbon wire rods for stick electrodes	Very low content of tramp elements	Jindal Steel and Power
Wire rods for continuous electrodes	Control of chemical composition within a very close band	Jindal Steel and Power
Cold heading quality wire rods	Very low content of tramp elements	Jindal Steel and Power
Alloy steel	Very low content of tramp elements	Jindal Steel and Power
Refrigerators, cabinets, power distributing boards and drums (greatest demand)	Commercial Quality	Nippon steel
Automobile floor and roof panels	Drawing Quality	Nippon steel
Automobile fenders and quarter panels	Deep-Drawing Quality	Nippon steel
Automobile interior panels and deep drawn parts	Extra Deep Drawing	Nippon steel

Error in extrapolating the intermediate product to end-use matrix

As the intermediate product to end-use matrix was already imperfect in 2008 due to limited and conflicting data sources, this error is undoubtedly compounded when extrapolating to 2050. This matrix is used as the best available proxy. Future work could entail following trends in steel use in more detail and more thoroughly predicting the steel needs of the sectors. Here, the goal is to acknowledge the error and understand its likely magnitude.

Worldsteel provides statistics dating back to 1990 for annual global intermediate product production. Not all products have statistics – for example hot rolled coil and hot rolled narrow strip. To understand the validity of extrapolating from the product to end-use matrix by Cullen et al. (2012), available historic data for intermediate product production was summed from 1990 to 2014 and compared to the summed estimated production. The results and percent error are shown in Table A1.5.

Table A1.5: Comparison of annual historic worldsteel data from 1990-2014 to production estimated by extrapolating the intermediate product to sector matrix by Cullen et al. (2012) (pre-yield values).

Intermediate Product	Estimated Production (Mt)	Historic Production (Mt)	% Error
Light Sections	770	1029	-25.2
Heavy Sections	696	1122	-38
Rail	185	208	-11.1
Rebar	3025	3110	-2.7
Wire Rod	2588	2722	-4.9
Hot Rolled Bar	2126	2154	-1.3
Plate (2004 to present)	1224	1138	7.6
CRC Galv.	2973	2001	48.6
CRC Coated	214	237	-9.7
CRC Tinned	153	343	-55.4
Electrical Sheet	185	210	-11.9
Welded Tube	1094	1278	-14.4
Seamless Tube	556	627	-11.3
Total	15789	16179	-2.4
		Product Average % Error	-10

Some products are more problematic than others. For example, CRC galvanized is overestimated by approximately 50%, while CRC tinned is underestimated by 55%. This is partly due to the mismatch in sector definition between Pauliuk et al. (2013b) and Cullen et al. (2012). As CRC galvanized and CRC tinned, CRC coated and electrical sheet have the same quality requirements, aggregating to quality categories helps to correct this error. Averaging the percent errors of the products gives -10%, while totaling the estimated production and the historic production gives a percent error of -2.4%. This indicates the magnitude of error in extrapolating the 2008 matrix over a 24-year period. Thus, extrapolating forward this range of error can be expected. Extrapolating this matrix forward to 2050 could result in errors on the order of 20%.

A2 – catalogue for copper extraction experimental work

Table A2.1: Catalogue of studies for improved shredding and magnetic separation.

Author	Year	Title	Alternative processing	Main results
Newell	1996	Production of low copper residual shredded steel scrap	Describes several strategies for the scrap processor to employ: careful control of the input materials, hand-picking, and higher-density shredding.	Density has a large effect on the amount of copper removed. Higher density means lower copper residual range. Increasing the density from 65 lb/cubic ft to 85 lb/cubic ft adds $2-$4/ton (due to additional electrical power, more time in the shredder and more labor), and reduces Cu to 0.09 to 0.12 wt%.
Katayama, Sano, Sasabe, Matsuoka	1997	Research activities in Japan on removal of residual elements from ferrous scrap	Cryogenic shredding at -100 to -200ºC for brittle fracture instead of plastic shearing Reiterating shredding and magnetic separation	95% of copper can be removed, but costs of this process are prohibitive and there has been little further development of this idea. 0.15wt% Cu can be achieved with three passes through the shredding and magnetic separation
Newell	2017	The true value of shredded steel when used in EAF steel production	High-density shredding	Shredding normal scrap (70 lb/cubic ft) to 10-15 lb/cubic ft higher density will reduce the copper content by about 0.1 points.

Table A2.2: Catalogue for density separation to isolate copper-rich fraction.

Author	Year	Title	Alternative processing	Main results
Aboussouan et al.	1999	Steel scrap fragmentation by shredders	Use sieve meshes to separate scrap stream by different sizes.	Most copper was found between mesh sizes 20 and 60 mm. Simply sieving and separating fraction for other sizes would reduce the initial copper by up to 90%. However, a use for this large fraction of high-copper scrap is required.
Shulman	2011	US Patent: Method for bulk sorting of shredded scrap metal	A stream of shredded scrap is sorted by copper content using bulk composition analysis, such as neutron activation	Author claims this technique could generate grades of scrap with specific copper concentration values, such as 0.2 and 0.1wt% Cu.
Russo	2014	Quality control of scrap and chemical analysis needs at ArcelorMittal	Use neutron activation analysis (by Gamma Tech) to measure scrap copper content before it is charged and melted.	Statistical analysis of the composition of steel melts can provide overall trends on copper concentration, but it is difficult to trace to specific scrap supplies. Bulk composition analysis can be used for real-time control over copper concentration.
Newell	2017	The true value of shredded steel when used in EAF steel production	Trommel sorting	Engine blocks, powder metallurgy products fall through screen while sheet passes to produce scrap with 0.12-0.15 wt% Cu.
SICON	2018	SICON PrimeScrap: low-copper shredded scrap	Scrap is transported from a vibrating feeder to a chute, where it is accelerated to 20 ft/s. A head drum with a magnet system ejects copper-rich pieces.	Copper “meatballs” are ejected. 75% of material is clean ferrous scrap, and the copper-rich fraction (25%) goes to further sorting/handpicking.
STEINERT	2018	SteelMaster: Separate your heavy ferrous parts	Combines magnetic field forces and ballistic effects to concentrate copper impurities in 20-30% of the overall mass stream	Less magnetically permeable material is separated with ballistic forces. 110t scrap/hour.
Shattuck and Ramsdell	2018	The case for ballistic metal separators	A ballistic separator uses a fast belt, high magnetic attraction and a charged trajectory method.	A ballistic separator can ensure 0.16 to 0.17wt%Cu. Reports that it offers low operating costs, requires no air and uses very little electricity. Process rates of 100 t/hr.

Table A2.3: Catalogue of studies for reactive gas applied to solid scrap.

Author	Year	Title	T (ºC)	Main results	Information provided by
Hartman, Oden and Davis	1994		650 to 800	Reported the deposition of copper on iron when oxide film is not formed. The rate of copper removal is a function of time, and an increase in temperature from 650 to 800ºC reduces the amount of copper deposited on iron. Recommended 800ºC to ensure a good oxide bond and obtain reasonable vapor pressure for copper chloride volatilization.	Tee and Fray (2006)
Hartman, Williamson and Davis	1996		800	Used 11% HCl and 89% air at 800ºC. The condensed products, copper and zinc chlorides, were treated by solvent extraction and electrowinning to obtain copper and zinc. 74% of copper was removed from 3.5 kg of scrap in 90 minutes.	Savov and Janke
Matsumaru, Susa and Nagata	1996	Removal of copper from iron-based scraps by O_2-Cl_2 gas mixtures	827	Determined evaporation rate limited by the transport of chlorides across the boundary layer. Using thermodynamic and kinetic considerations proposed the optimal condition of 827ºC and O_2-10%Cl_2 gas. In Japanese.	
Katayama, Sano and Sasabe	1998	Research activities on residual element removal in Japan		Reported chloridization and vaporization of copper as a feasible technique, but noted practical application would call for protection of the apparatus against corrosion and the treatment of waste gas.	
Tee and Fray	1999	Removing impurities from steel scrap using air and chlorine mixtures	800	Presented process conditions for large scale dezincing of steel scrap with chlorination, with an economic evaluation and market analysis. Discussed how copper could also be chlorinated.	
Tee and Fray	2004	Reaction of zinc, copper and iron in air and chlorine mixtures	800	Showed copper can be separated from iron via chlorination, forming volatile copper chloride. All copper chlorinated in 10 min. However, if iron did not have a cohesive oxide film, copper could deposit onto iron, and thus not separate.	
Tee and Fray	2006	Separation of copper from steel	800	Recommended optimum conditions of air/chlorine ratio of 10:1, flow rate: 400/40 cm^3/min and 800ºC with an initial oxidizing treatment to form the protective layer of iron oxide. Experiments were performed with Fe and windings of copper wire from 60wt%, 13wt% and 1wt%, the latter of which could be reduced to 0.05wt% in 10 minutes.	

Table A2.4: Catalogue of studies for preferential melting.

Authors	Year	Title	T (°C)	Set up	Main results
Brown and Block	1968	Copper removal form steel scrap by thermal treatment, U.S. Bureau of Mines Report No. 7218	600 to 1150	Furnace in various oxidizing, reducing and neutral atmospheres. Recommended a traveling grate system over a rotary kiln.	Treated automotive scrap, but copper was not successfully removed with raised temperatures. Liquation varied considerably and the surface area between copper and iron must be kept to a minimum to prevent wetting.
Elger, Hunter and Armantrout	1968	Removal of non-ferrous metals from synthetic automobile scrap on heating in a rotary kiln	450 to 1150	Rotary kiln under oxidizing and reducing atmosphere	Copper was most successfully removed when it was embrittled. Otherwise, copper wetted the steel with heavy oxidation. High metal loss, high fuel cost and excessive refractory wear were noted.
Leak, Fine and Dolezal	1973	Separation of copper from scrap by preferential melting	1150 to 1250	Various combinations of sweating media and pre-coatings	Achieved ~0.15wt% Cu with sodium silicate pre-coating in $BaCl_2$ molten salt bath.
Katayama, Sano, Sasabe, Matsuoka	1997	Research activities in Japan on removal of residual elements from ferrous scrap	1100	Measured work of adhesion of liquid copper on various steel oxide films	The flow-off of copper droplets from the steel surface was investigated as a function of oxygen partial pressure. Copper easily flows down magnetite and iron-silica surfaces, but the adherence between copper droplets and wüstite is high.
Cramb and Fruehan	1991	Copper removal from steel using sulfur matte			Reviewed preferential melting as unsuccessful due to copper wetting solid iron.
Savov, Volkova, Janke	2003	Copper and tin in steel scrap recycling			Reviewed preferential melting and concluded poor separation due to liquid copper entrapping in cavities, and disadvantages of iron oxidation and high fuel costs, unless integrated into scrap pre-heating.

Table A2.5: Catalogue of studies for solvent extraction applied to solid scrap.

Author	Year	Title	T (ºC)	Set up	Main results
Iwase, Masanori, Tokinori, Kenji	1991	Feasibility study for the removal of copper from solid ferrous scrap	745	Al bath	Pilot study. Claimed scrap is clean of copper contamination after immersion for 5 to 10 minutes.
Iwase, Ohshita	1994	Further studies of the removal of copper from solid ferrous scrap	690 to 950	2-step Al bath process	Proposed solution to Al-Cu alloy adhering to scrap with 2-step process
Iwase	1996	Refining of solid ferrous scrap intermingled with copper by using molten aluminum	690 to 950	2-step Al bath process, with vibration	Intermingled scrap was immersed for 5 to 30 minutes into an Al-Cu bath, followed by mechanical shaking and immersed in a pure Al bath to achieve as low as 0.04wt% Cu.
Katayama, Sano, Sasabe, Matsuoka	1998	Research activities in Japan on removal of residual elements from ferrous scrap			Reviewed Al extraction, noting Al is the most viable solvent as it is easy to handle and copper can be readily separated from Al.

Table A2.6: Catalogue of studies for matte extraction applied to solid scrap.

Author	Year	Title	Slag system	T(ºC)	Main results
Jimbo, Sulsky and Freuhan	1988	The refining of copper from ferrous scrap	FeS - (19-25wt%) Na_2S	800, 900, 1000	Experiments on 100g of scrap confirmed that the reaction is more favorable in the solid state. L~500. Planned a larger scale experiment.
Cramb and Fruehan	1991	Copper removal from steel using sulfur matte	FeS – 18wt% Na_2S	1000	10 kg matte/tonne scrap to decrease from 0.4wt% to 0.1wt%. Demonstrated process in a rotary kiln at 1-10RPM with 100 kg scrap. The treated scrap needed desulfurizing because matte adhered to the scrap. One suggestion was to use hot acid, but hydrogen sulphide would be produced as a result.

Table A2.7: Catalogue of studies for copper embrittlement.

Author	Year	Title	T (C)	Atmosphere	Set up	Main results
Leary	1965	Removal of copper from copper-clad steel by oxidation	650 to 1040	Various flow rates of oxidizing gas	Horizontal muffled furnace, treatments of 15 to 120 minutes	All copper oxidized and the copper oxide scale could be easily separated from underlying steel during cooling, while steel oxidation was limited. Light-gage copper coatings could be removed in an incineration process.
Brown and Block	1968	Copper removal from steel scrap by thermal treatment	800 to 900	Oxidizing, neutral and reducing	Furnace treatment followed by 15 minutes of tumbling	Major compounds in the scale were 1-10% $CuO•Fe_2O_3$ and $Cu_2O•Fe_2O_3$, CuO, Cu_2O, FeO, Fe_2O_3, and Fe_3O_4. Scale formation was more effective with insulated wire than bare, possibly due to the presence of lead. Experiments with a lead wire showed lead oxide is likely involved in copper's embrittlement. Tried various chemical pretreatments and $Na_2Si_4O_9$ may embrittle copper.
Elger, Hunter, Armantrout	1968	Removal of nonferrous metals from synthetic automobile scrap on heating in a rotary kiln	450 to 1160	Oxidizing, neutral and reducing	Rotary kiln	In some cases, copper wiring was embrittled and mechanically removed by fragmentation. Authors thought the insulation of the wire might have embrittled the copper. In an oxidizing atmosphere, the percent of copper removed increased with temperature.
Herter	1985	Method for preparing a low residual alloy steel charge from scrap metal	930 to 1040	Oxidizing, neutral to reducing	Rotary kiln	Scrap enters the kiln in the oxidizing condition, then the atmosphere changes to neutral and reducing as the temperature increases to form a brittle scale of external impurities. Rates of 50% copper removal were reported.
Cho and Fan	2004	A new approach for the removal of copper from solid ferrous scrap	400 to 700	Oxidizing	Oxidizing treatment for 4 to 6 hours with thermal cycling, followed by mechanical impacting and a fluxing process from 1000 to 1200ºC	Over 90% of copper can be removed from scrap containing initially 3 to 5 wt% by utilizing the preferential oxidation of copper.

Table A2.8: Catalogue of studies for leaching.

Authors	Year	Title	Leach solution	T (°C)	Main results
Staker, Chindgren, Dean	1971	Improved cupric ammonium carbonate leaching of copper scrap	Ammonium carbonate	25 to 40	Showed leaching with ammonium carbonate to be very effective. Used entrained air bubbles to increase the copper dissolution rate to 1.5 g/in^2/hr. Also proposed using powdered sulfur to precipitate copper from solution.
Oden, Adams and Fugate	1972	Reducing copper and tin impurities in ferrous scrap recovered from incinerated municipal refuse	Ammonium carbonate	25	Achieved 0.1-inch penetration per 24-hour period, sufficient to dissolve thickest copper pieces and reduce from 0.6 to 0.5wt% Cu to 0.1 to 0.2wt% Cu. Suggested a tumbling reactor, with vigorous aeration and excess ammonia.
Chin	1977	Electrochemical extraction of copper from scrap steel	Ammonium sulfate and carbonate, pyrophosphate, alkaline cynaide	25	Tested four electrolytes in an electrochemical packed bed cell. Achieved less than 0.06% Cu with alkaline cyanide, but did not yet achieve copper deposition on the cathode.
Majima, Nigo, Hirato, Awakura and Iwai	1993		Ammonium sulfate		Leaching speed increased with increasing NH_3 up to 7 kmol/m^3 and optimum $(NH_4)SO_4$ concentration existed corresponding to NH_3 concentration. Referenced by Konishi.
Zhou, Shinme and Anezaki	1995	Removal of copper from ferrous scrap with ammonia leaching method	Ammonium carbonate	40	Leaching speed increased with increasing Cu(II) concentration, O2 gas flow rate and bath temperature. Tested with 200-liter tank and argued ammonia leaching with air injection in a closed circuit system is effective to remove copper from automobile scrap.
Meng and Han	1996	The principles and applications of ammonia leaching of metals - a review			Reviews the thermodynamics of the Cu-NH_3-H_2O system, as well as the kinetics of copper dissolution. When air is the oxidant, oxygen and ammonia determine the overall rate.
Katayama, Sano, Sasabe	1998	Research activities on residual element removal in Japan	Ammonium, concentrated nitric acid, sulfuric acid		Reviewed several possible leachants and concluded an amine ion solution with oxygen blowing dissolved copper with the greatest stability and relatively high rate. Noted motors must be heated to remove enamel before dissolving copper.

Authors	Year	Title	Leach solution	T (ºC)	Main results
Koyama, Tanaka, Lee	2006	Copper leaching behavior from wasted printed circuit board in ammoniacal alkaline solution	Ammonium alkaline solution	25 to 55	Studied leaching rate of copper from crushed PCB's to understand feasibility of electrowinning set-up, with $Cu(NH_3)_4$ as the oxidizing agent instead of oxygen. 200 RPM stirring, temperature effects insignificant, used 0.3 kmol/m^3 $CuSO_4$, 5 kmol/m^3 NH_3, 1 kmol/m^3 $(NH_4)_2SO_4$ solution to achieve 80% leaching from 3.5 mm diameter particles in 4 hours.
Lim, Kwon, Lee, Yoo	2013	The ammonia leaching of alloy produced from waste printed circuit boards smelting process		30	Suggested 2 kmol/m^3 NH_4Cl and 5 kmol/m^3 NH_3 with 0.1 kmol/m^3 $CuCl_2$ at 200 RPM and 30ºC for 3 kg/m^2hr leaching rate.
Konishi, Bitoh, Ono, Oishi, Koyama, Tanaka	2014	Behavior of copper dissolution in an ammonia solution containing ammonium chloride or sulfate	Ammonium chloride and ammonium sulfate solutions	25 to 80	Found ammonium chloride solutions to be superior to ammonium sulfate solutions. Reported relationship between stirring speed and leaching rate. Achieved maximum leaching speed of 3.98 kg/m^2hr at 80ºC with 600 RPM stirring with 4kmol/m^3 NH_3 and 1 kmol/m^3 NH_4Cl with 0.5 kmol/m^3 Cu(II).
Sun, Xiao, Sietsma, Agterhuis, Yang	2015	A cleaner process for selective recovery of valuable metals from electronic waste of complex mixtures of end-of-life electronic products	Ammonium carbonate, sulfuric acid and salt-aluminum chloride solutions	20 (ammonia solutions), 80 (other)	Describes a two-step hydrometallurgy process to extract metals from e-waste. Leached copper with an ammonia-based leachant, then proved electrodeposition from an ammonium sulfate solution containing 51 g/l Cu with a current efficiency of 90%. The cell design is very important for achieving a high current efficiency.
Ghosh, Ghosh, Parhi, Mukherjee, Mishra	2015	Waste Printed Circuit Boards recycling: an extensive assessment of current status			Reviewed hydrometallurgical routes for copper extraction and concluded ammonium leaching to be superior for selectivity. Reported that the effect of temperature on leaching rate is insignificant, but the concentration of the Cu(II)-amine complex enhances leaching rate, while Cu(I)-amine complex depresses it.
Rudnik	2017	Application of ammoniacal solutions for leaching and electrochemical dissolution of metals from alloys produced from low-grade e-scrap	Sulfate, chloride and carbonate ammonium solutions	20	Anodically dissolving the metals was achieved, but the cathodic current efficiency of depositing of copper was low, below 1%.

Table A2.9: Catalogue of studies for distillation.

Authors	Year	Title	Pressure regime /atmosphere	T (ºC)	Main result	Information provided by
Gill, Inveson, Wesley-Austin	1959	The behavior of various elements in vacuum steelmaking	vacuum		0.32 to 0.01% in 90 min from 0.1 kg of steel, A/V=50m^{-1}.	Data from Harris
Olette	1959	Vacuum distillation of minor elements from liquid ferrous alloys	vacuum		0.12 to 0.001% in 40 min from 0.5 kg Fe, A/V=10m^{-1}. Defined relative volatility.	Data from Harris
Ward	1963	Evaporative losses during vacuum induction melting	vacuum		1.0 to 0.1% in 120 min from 12 kg Fe, A/V=8m^{-1}.	Data from Harris
Turkdogan, Grieveson, Darken	1963	Enhancement of diffusion-limited rates of vaporization of metals	atmospheric		Showed that the rate of vaporization of metals in a stream of neutral atmosphere can be increased by increasing the partial pressure of a reacting gas, until a critical value, at which point a surface film forms.	
Fischer and Derenbach	1964	Contribution to the question of evaporation in melts of iron alloys in a vacuum: Part 1. Theoretical investigations on binary alloys of iron with arsenic, manganese, copper and tin	vacuum	1627	0.17 to <0.001% in <60 min from 0.03 kg Fe, A/V=50m^{-1}.	Data from Harris
Smith and Ward	1966	The evaporation of liquid iron alloys under vacuum	vacuum, ~0.1 Pa	1700 to 1760	0.55 to 0.1% in 0.2 min from 0.001 kg Fe, A/V=500m^{-1}. Rate of evaporation of copper from levitated droplets was 50-70% of the theoretical value, suggesting liquid diffusion of copper is a rate-limiting step.	
Ward and Aurini	1966	Mechanism of alloying elements evaporation during the vacuum induction melting of steel	vacuum, below 100 Pa		Found both mass transfer in the liquid and evaporation at the surface to be rate limiting.	Referenced in Nishi, et al.
Ohno and Ishida	1968	Rate of evaporation of manganese, copper, tin, chromium and sulphur from molten iron under vacuum	vacuum	1600	1.0 to 0.1% in 15 min from 0.15 kg Fe, A/V=60 m^{-1}.	Only abstract found. Data from Harris

Authors	Year	Title	Pressure regime /atmosphere	T (ºC)	Main result	Information provided by
Olette	1974		vacuum, below 10 Pa			Cited as pioneering study
Fischer, Janke and Stahlschmidt	1974	The evaporation of copper, manganese and chromium from melts of steel X5 Cr Ni 18 9 under reduced pressure	vacuum		1.9 to 0.1% in 50 min from 5 kg X5 Cr Ni 18 9 steel, A/V=11m^{-1}.	Data from Harris
Salomon De-Friedberg and Davenport	1977	Vacuum removal of copper from melted steel scrap	vacuum		0.5 to 0.1% in 150 min from 26 kg steel, A/V=8 m^{-1}.	Only abstract found. Data from Harris
Reiichi	1977	Kinetics of evaporation of manganese, copper and sulphur from iron alloys in vacuum induction melting	vacuum	1415 to 1600	2.1 to 0.3% in 15 min from 0.15 kg steel, A/V=60m^{-1}.	Only abstract found. Data from Harris
Harris and Davenport	1979	Pilot plant scale vacuum distillation of liquid steel to remove copper	vacuum, 3 to 20 Pa	1587 to 1617	2.0 to 0.1% in 180 min from 22 kg A36 steel, A/V=10m^{-1}. Found removal efficiency is reduced in large systems and concluded slow evaporation rates are caused by the presence of a thin surface film from air leakage.	
Yamamoto and Kato	1980	The effect of surface movement on the evaporation rates of alloying elements from liquid iron under vacuum	vacuum		Both the evaporation step and the diffusion step through the liquid boundary layer are rate-controlling.	
Harris	1980	Vacuum refining of molten steel, dissertation	vacuum, 3 to 2000 Pa	1507 to 1757	Developed a theoretical model to describe vacuum distillation and validated with experimental work. Found most favorable refining with high T, no surface films, low chamber pressure and induction mixing of the liquid.	

Authors	Year	Title	Pressure regime /atmosphere	T (ºC)	Main result	Information provided by
Morales and Sano	1982	Alloying effect on vaporization rate of copper and tin from molten iron alloys		1800	C, Cr and Si were found to enhance the vaporization of Cu. K_{Cu} data point.	Only abstract accessed. Data from Ono-Nakazato, et al.
Harris and Davenport	1984	Vacuum purification of liquid metals: United States Patent	vacuum to atmospheric, with gas flow		Proposed using a scavenging gas to develop bulk flow at higher pressures, with a lifting gas to produce a spray.	
Harris	1988	Numerical simulation of vacuum refining of liquid metal	vacuum to atmospheric		Proposed a mathematical model to simulate vacuum refining and applied it to the design constraints described in the "LSV" patent.	
Matsuo	1988	Removal of copper and tin with plasma	2x10^4 Pa, with Ar flow		Applied argon-hydrogen and argon plasma flames under 2x10^4 Pa pressure at a laboratory scale. Found hot spot of plasma increased removal rate.	Matsuo, Maya, et al.
Tokumitsu and Hirata	1990		10 to 100 Pa	1560	K_{Cu} data point.	Data found in Ono-Nakazato, et al.
Harris and Davenport	1992a	Vacuum distillation of liquid metals: Part I. Theory and experimental study	3 to 20 Pa	1577 to 1777	Presented the kinetics of evaporating copper, as given in transport equations below. Confirmed with experimental results.	
Harris and Davenport	1992b	Vacuum distillation of liquid metals: Part II. Photographic study	5 to 25 Pa	1677	Photographs confirm the different vapor behavior as chamber pressure varies (bulk flow for low P, decaying to diffusive transport as the chamber pressure exceeds the melt vapor pressure) and the importance of surface cleanliness and avoiding condensate refluxing.	
Emi and Wijk	1996	Residuals in steel products - impacts on properties and measures to minimize them			Concluded that removal of copper under vacuum is not practicable on a commercial scale	Warner

Authors	Year	Title	Pressure regime /atmosphere	T (°C)	Main result
Matsuo, Maya, Nishi, Shinme, Ueno, Anezaki	1996	Removal of copper and tin in molten iron with decarburization under reduced pressure	130 Pa	1650	Evaluated different oxidizing agents to generate fine CO bubbles in a 1-1.5 tonne vat and found SiO2 to be most effective.
Lee and Harris	1997	Characterization of the surface area of overflow droplets generated by a gas-lift pump under reduced pressure	Reduced, with gas flow		Used water-modelling experiments to characterize droplets under varying operating conditions to predict molten metal refining.
Zaitsev, Shelkova, Litvina, Shakhpazov, Mogutnov	1999	An investigation of evaporation of liquid alloys of iron with copper		1167 to 1643	Determined thermodynamic characteristics of liquid alloys of iron with copper, including sublimation enthalpies.
Ma, Savov and Janke	1999	Chemical activities of the solute elements Cu and Sn in scrap-based iron melts		1600	Found evaporation of Cu and Sn can be enhanced by C and Si, but at quantities not practical in steelmaking. Recommended charging scrap with ferrosilicon grades, where high Si contents and C contents are desired.
Savov and Janke	2000	Evaporation of Cu and Sn from induction-stirred iron-based melts treated at reduced pressure	1 to 100 Pa	1400 to 1600	Presented experimental results on 20 kg, A/V=6m^{-1} set up, quantifying the effects of chamber pressure, melt temperature, melt composition and stirring intensity on evaporation rate. Recommended pressures less than 10Pa, high melt temperatures and induction stirring.
Matsuo	2000	Acceleration of copper and tin removal from molten steel by decarburization	130 Pa	1600 to 1700	Measured effective removal with different decarburization powders and found MgO>SiO_2 >O_2. The rate of decopperization was 1.5-3 times higher than without decarburization. Low oxygen was favorable as it is a surface-active element that can retard the reaction.

Authors	Year	Title	Pressure regime /atmosphere	T (ºC)	Main result	
Ono-Nakazato, Taguchi, Seike, Usui	2003	Effect of silicon and carbon on the evaporation rate of copper in molten iron	133 to 10^5 Pa with hydrogen flowing	1650 to 1700	Found C and So additions to increase the rate constant by 1.7 and 1.4 times respectively, and achieved a rate equivalent to chemical-reaction limiting at 133 Pa.	
Taguchi, Ono-Nakazato, Usui	2004	Enhancement of evaporation removal rate of copper in molten iron by the silicon and/or carbon addition	133 Pa	1650	Found the optimum composition for enhanced removal rate to be Fe-1.5Si-3C.	
Zaitsev, Zaitseva, Mogutnov	2004	Evaporation of copper from iron melts	10 Pa, 100 Pa and 0.1MPa, with and without gas blowing	1600	Modeling analysis of a 160-tonne vat with conditions ranging from an undisturbed surface, to high vacuum with high velocity gas stream blowing. Found blowing of the melt raises the rate of copper transfer to the gaseous phase by a factor of 1.7. Decarburizing with SiO_2 increased transfer by a factor of 2.2-2.6, and MgO by 2.8-3.1.	
Zaitsev, Zaitseva, Mogutnov	2004	Potentialities of simultaneous removal of tin and copper from molten iron through evaporation	100 Pa with gas blowing	1550	Modeling analysis of a 160-tonne vat with argon blowing found 0.01 to 0.6wt% tin additions did not affect the rate of evaporation of Cu.	
Warner	2004	Continuous oxygen steelmaking with copper, tin and zinc-contaminated scrap	250 Pa with desorption gas	1780	Kinetic analysis showed a typical RD-KTB vacuum pumping system could refine 0.6 Mtpa liquid scrap from 0.5% to 0.05% Cu.	
Blacha, Labaj	2011	Temperature impact on copper evaporation from liquid iron	0.06 to 101 Pa	1650 to 1725	Measured activation energy of Cu evaporation under various conditions to determine the rate determining step. At low pressures the copper evaporation process is determined by mass transfer in the liquid phase.	Only abstract accessed
Labaj, Oleksiak, Siwiec	2011	Study of copper removal from liquid iron	0.06 to 101 Pa	1377	Found liquid mass transfer and gaseous transfer to be rate-limiting between 10 and 100 Pa. Concluded vacuum distillation should be conducted at 10 Pa, for the maximum rate.	

Authors	Year	Title	Pressure regime /atmosphere	T (ºC)	Main result
Blacha, Labaj	2012	Factors determining the rate of the process of metal bath components evaporation			Review paper on the effect of pressure, gaseous atmosphere, rate of bath mixing and melt composition on the rate of impurity evaporation.
Jung and Kang	2016	Evaporation mechanism of Cu from Liquid Fe containing C and S	Atmospheric, with 0-2 L/min Ar-4%H_2 and Ar-5%NH_3 gas mixture flowing	1600	Decopperization experiments were conducted with inert and reactive gas flows on Fe levitated droplets with C and S additions. S was found to accelerate the rate of Cu evaporation by forming CuS(g), but simultaneously decelerates by blocking evaporation sites. Found the rate constant of the CuS reaction.
Jung and Kang	2016	Simultaneous evaporation of Cu and Sn from liquid steel	Atmospheric with 1L/min Ar-4%H2 gas mixture flowing	1600	Considering the mechanisms of Cu evaporation with C, S and Sn present in levitated droplets, found Cu evaporation could be increased at most to 2.2 times with 5%C and 0%S.

Table A2.10: Catalogue of studies for vacuum arc re-melting.

Authors	Year	Title	Melt composition	T(ºC)	Melting rate (kg/hr)	Main results
Carlson and Schmidt	1974	Paper presented at the 103rd Annual AIME Meeting	Automotive steel	1600 and 1750	1 to 4	Conducted experiments on the solute removal from automotive scrap steel using electron-beam-refining techniques
Andreini and Foster	1974	Kinetics of solute removal during electron-beam and vacuum-arc melting	Fe-Cu	1600	1 to 4	Presented a model to describe the kinetics of dilute metallic-solute removal from molten alloys using electron beam or vacuum arc refining techniques. Applied model to refining of copper from automotive steel scrap and compared results to data in study above. Can predict the solute concentration in the final ingot for a given melt rate.
Scholz, Biebricher, Franz		State of the art in VAR and ESR processes - a comparison	Fe-Cu	1600	540	Reviewed the methods and recent trends in process technology and provided rates of energy consumption.

Table A2.11: Catalogue of studies for reactive gas applied to the melt.

Authors	Year	Title	Main results	Referenced by
Turkdogan, Grieveson, Darken	1963	Enhancement of diffusion-limited rates of vaporization of metals	Provides theory of reactive gas evaporation	
Ono, Ichise, Suzuki, Hidani	1995	Elimination of copper from molten steel by NH3 blowing under reduced pressure	Pilot study	Hidani et al.
Hidani, Takemura, Suzuki and Ono	1996	Elimination of copper from molten steel by ammonia gas blowing	Blew NH3 gas onto molten steel under low pressure. Noted boiling, splashing and violent slopping and observed copper smoke from the surface. The mechanism of de-copperization was considered that gaseous CuH was produced and enhanced surface area.	
Liansheng, Shiqi, Changxiang	1999	Copper removal from molten steel by gasification	Ammonium salts or urea were added into 400g of molten steel under normal pressure at 1600C. Noted copper reduction of about 0.5 to 0.3 wt%Cu with about 0.5 g of NH_4C and $(NH_4)_2C_2O_4$.	
Suzuki, Ono	2000	Enhanced evaporation of copper by NH_3 gas blowing	Observed copper smoke from top-blowing NH_3 onto the melt and hypothesized that an unstable and volatile compound such as CuN_x or CuH was formed. Also noted the cooling effect due to the endothermal decomposition of NH_3. Also investigated the nitrogen solubility of the melt under application of the NH_3 gas.	
Maruyama, Katayama, Momono, Tayu, Takenouchi	1998	Evaporation rate of copper from molten iron by urea spraying under reduced pressure	Sprayed urea onto molten iron with 0.4wt% Cu at 1600ºC under reduced pressure. Noted splashing and reported the rate constant of copper evaporation as a function of pressure. Concluded that acceleration of copper evaporation by urea was mainly due to the evaporation of $Cu(N_3)_2$, which has a higher vapor pressure than metallic copper.	
Li, Xiang, Cao, Ichise	1998	Copper elimination from the molten steel by addition of hydronitrogens	Compounds of hydrogen and nitrogen (NH_4Cl and NH_2CONH_2) were added to the steel melt at normal pressure at 1600C. Noted copper reduction and that the technique was worthy of further study.	

Authors	Year	Title	Main results
Li, Yu, Li, Li	1999	A basic study of decopperization in molten steel by ammonium salt	Agents of NH_4Cl, $(NH_4)_2C_2O_4$ and $CO(NH_2)_2$ by feeding wires. NH_4Cl has the best result, efficiency of removing copper is 36%. The content of copper can be reduced from 0.6 to 0.3% with 4.5 kg/t agents
Jung, Kang, Seo, Park, Choi	2014	Evaporation mechanism of Cu from liquid Fe containing C and S	Investigated the evaporation mechanism of Cu under argon and NH_3, but observed no appreciable difference in evaporation rate.

Table A2.12: Catalogue of studies for melt injection.

Authors	Year	Title	Main results
Sasabe, Harada, Yamashita	1996	Removal of copper from carbon saturated molten iron by using $FeCl_2$	Injected pulverized $FeCl_2$ with nitrogen gas into carbon-saturated molten iron. Iron chloride vaporized first, but noted decrease in copper content due to copper reacting with chlorine. Described with first order rate equation and estimated 18.5 kg of $FeCl_2$/t iron would be required to reduce Cu from 0.5 to 0.1wt%.

Table A2.13: Catalogue of studies for solidification segregation.

Authors	Year	Title	Melt composition	Cooling profile	Main results
Andreini and Foster	1974	Kinetics of solute removal during electron-beam and vacuum-arc remelting	Fe-Cu	Presented model for different melt rates	Presented model for kinetics of solute removal during electron-beam and vacuum-arc re-melting, which incorporates segregation behavior. Segregation coefficient for Fe-Cu, k=0.65.
Yuan, Sassa, Iwai, Wang, He, Asai	2008	Copper distribution in Fe-Cu and Fe-C-Cu alloys under imposition of intense magnetic field	Fe with 0.4% Cu and Fe-3.95C-0.4 Cu	Held above liquidus 10-15 min, cooled to below the solidus over 60 min then quenched	Applying a 10T magnetic field makes a uniform micro distribution of Cu in the Fe-C-Cu alloy, but not the Fe-Cu alloy.
Sun, Guo, Vleugels, Van der Biest, Blanpain	2012	Strong magnetic field processing of metallic materials: a review			Review of the principles and progress behind materials processing using strong magnetic fields.
Nakamota, Okumura, Tanaka, Yamamoto	2014	Segregation of Cu by unidirectional solidification in molten Fe-C-Cu alloy	C-saturated iron with 0.5-3.7mass%Cu	Cooling rates 600 K/hr to 20 K/hr	Segregation coefficient, k=1.2. Starting with 0.3%Cu, could be reduced to 0.1%Cu by the end of the bar.
Xiao-Wei, Bai-Ling, De-Yang, Lin, En-Gang	2016	Migration and alignment of Fe-rich particles in Cu under high magnetic field	Cu-30wt% Fe alloy		Applied a static 0.1 and 12 T and magnetic field and a field with a gradient of 92.1 T^2/m. Fe-rich particles can migrate upwards in the direction opposite gravity and tend to align along the direction of high magnetic field. The degree of alignment is related to external magnetic field strength, resistance force, effective time, initial condition of particles, etc.

Table A2.14: Catalogue of studies for phase separation.

Authors	Year	Title	Main results
Yamaguchi, Ono, Usui	2010	The equilibrium relation of immiscibility in an Fe-Cu-B system at 1873K	Investigated the Fe-Cu-B system for potential application in steel recycling. Confirmed separation between Fe-rich and Cu-rich phases, but the minimum mass%Cu in the Fe-rich phase was 20.

Table A2.15: Catalogue of studies for solvent extraction applied to the melt.

Reference			Experimental details as available					Main results	Referenced by
Authors	Year	Title	Solvent	Melt composition	T (ºC)	Contacting phases	Displacing equilibrium		
Harald	1925	Process for the treatment of alloys containing copper and iron, US Patent 1,562,472.	Lead					Pioneering study.	
Ogawa	1950	Japan Patent, 16(1950). Jan 11, 1950						Pioneering study. L=2.	Jimbo and Freuhan
Langenberg and Lindsay	1954	Removal of copper from iron-copper-carbon alloys			1600			Evaporation of lead noted as a significant issue. L=1.2-2.3.	
Oelsen, Schuermann and Heinrichs	1959				1250 to 1450			L=1.5-1.1, decreasing with increasing temperature.	Jimbo and Freuhan
Schenck and Perbix	1962	Removal of copper from pig iron with lead and sodium sulphide slag		Pig iron	1400 to 1600	Droplets through the melt		Found L as a function of temperature from 1400 to 1600ºC: $\log(L_{Cu}) = \frac{1415}{T} - 0.552$	
Imai and Sano	1988	Copper partition between Na_2S fluxes and carbon-saturated iron melts		C-saturated iron	1150	Immiscible layers		L=2.4	

Authors	Year	Title	Solvent	Melt composition	T (ºC)	Contacting layers	Displacing equilibrium	Main results
Yamaguchi and Takeda	2003	Impurity removal from carbon saturated liquid iron using lead solvent	Lead	C-saturated iron	1150	Immiscible layers	Recommended repetition or counter flow	L=2.2. By adding the same amount of lead to iron scrap, 70% of copper can be eliminated.
Yamaguchi, Ono and Usui	2010	Oxidation removal of Cu from carbon-saturated iron via Ag phase	Silver	C-saturated iron	1250	Immiscible layers	1 atm oxygen atmosphere over Ag phase to promote oxidation of Cu	L between Fe-$C_{sat.}$ and Ag=7.15. Showed the Cu content of Fe-$C_{sat.}$ can be reduced from 4 wt% to 0.3-0.6wt% by oxidative removal via an Ag phase.
Yamaguchi and Ono	2012	Oxidative removal of Cu from carbon-saturated via Ag phase into B2O3 flux		C-saturated iron	1250	Immiscible layers	B_2O_3-Al_2O_3-Ag_2O fluxes to promote oxidation of Cu	Greatest L between flux and Ag was 17 at 0.6 atm O and mole fraction B_2O_3 =0.42. Also performed numerical calculations for diffusion of the reactants and products.
Yamaguchi, Ono and Takeuchi	2015	Removal of Cu in carbon saturated iron by sulfurization via Ag phase		C-saturated iron	1200	Immiscible layers	Na_2S-Cu_2S-Ag_2S fluxes to promote sulfidization of Cu	Greatest distribution ratio between flux and Ag was 42 with mole fraction Na_2S =0.4. Ag layer can prevent sulfidization of melt.
Rose	1981	The extraction of copper from steel by molten electrolysis	Thorium					Noted possibility, but also noted impracticality with high melting point (1750ºC) and its radioactivity.

Table A2.16: Catalogue of studies for slagging.

Author	Year	Title	Slag system	T (ºC)	Main results	Referenced by
Fernando	1950	Method for desulfurizing and copperizing ferrous metals, US Patent	FeS-Na_2S		Pioneering study.	Jimbo and Freuhan
Langenberg and Lindsay	1954	Removal of copper from iron-copper-carbon alloys	FeS-Na_2S			Jimbo and Freuhan
Simkovich and Lindsay	1960	Results of treating iron with sodium sulphite to remove copper	FeS-Na_2SO_3 with carbon additions		Removed between 30 and 50% of copper. Carbon additions were needed for formation of slag from sulphite.	Rose
Schenck and Perbix	1962	Removal of copper from pig iron with lead and sodium sulphide slag	FeS-Na_2S	1200 to 1500	Investigated the mechanism of the reaction and sulfur content of metal. L=7-8.	
Markar, Dunning and Caldwell	1968	Laboratory studies on the use of sodium sulfate for removing copper from molten iron	FeS-Na_2SO_4	Up to 1550	Investigated the efficiency of Na_2SO_4 slags. Found used slags were almost as effective as fresh Na_2SO_4 slags. Lump additions were more effective than powder. L=1.2-7.9. High temperatures and long slag reaction times tended to induce Cu and S reversion from the slag. Na_2SO_4 treatments were effective up to 1550ºC with reaction times of less than seven minutes.	Rose
Markar and Dunning	1969	Use of sodium sulfate for copper removal from molten iron	Li_2SO_4, Na_2SO_4, K_2SO_4 , $MgSO_4$	1354 to 1649	Studied the quantitative relationship between copper removal and slag treatment using sodium sulphate additions. Also investigated other types of sulphates, but found Na_2SO_4 to be most effective. Increased efficiency by using lance injection and upgraded the scale to 0.5, 1 and 4 ton ladles.	Rose
Schenck, Roth and Steinmetz	1970		FeS-Na_2S	1260 to 1550	L=7-8	Jimbo and Freuhan

Author	Year	Title	Slag system	T (°C)	Main results	Referenced by
Safiah and Sale	1972	Influence of carbon on the removal of copper from iron melts with sulfide slags	Na_2SO_4	1550	Investigated mechanism of Cu removal, sulfur pickup and Na vaporization. Cu removal was 1.5 to 1.4% when C=0.01%, and 1.5 to 0.8% for C-saturated. Concluded sulfide slags are not effective at removing Cu from melts with low C. C is needed for the reaction with the sulfate.	
Markar and Brown	1974	Copper removal from molten ferrous scrap: a pilot plant study				
Topkaya and Lu	1974	Metal-slag-gas reaction and processes	Na_2S		Found gas/slag and metal/slag reactions and diffusion of Na in the gas phase to be rate controlling. L=24.	
Rose	1981	The extraction of copper from steel by molten electrolysis	Cryolite with Cu_2S		Demonstrated electrolysis could be used to modify a ferrous melt beneath a sulfide-bearing slag, but modifications are needed for better current efficiency.	
Van Hecke, Fontainas	1984	Process for extracting non-ferrous metals from iron-bearing scraps	Oxide-based		Scraps are heated a slagging agent for iron separates the iron contained in scraps.	
Liu and Jeffes	1985	Effect of sodium sulfide on removal of copper and tin from molten iron	Na_2S-FeS and CaO additions	1200 to 1350	Concluded that 70 wt%Na_2S-30 wt%FeS was the best composition and the addition of CaO improved the transfer of Cu to the slag while impeding the transfer of S to the metal. Found mass transport to be an important controlling step.	
Okazaki and Robertson	1985	Removal of tramp elements: mathematical modeling	Na_2S-FeS	1250	Modelled copper removal assuming mass transfer in the boundary layer to be rate controlling. L=25. 0.2FeS-0.8Na_2S has maximum copper removal.	
Oden and Elger	1987	Removal of copper from molten ferrous scrap: Results of laboratory investigations	Na_2S-FeS-K_2O		Partitioned Cu into alkali or alkaline earth silicate slags or oxide-moderated sulfides. Unsatisfactory Cu removal.	

Author	Year	Title	Slag system	T (ºC)	Main results	
Imai and Sano	1988	The copper partition between Na_2S-bearing fluxes and carbon-saturated iron melts	Na_2S-FeS, as well as Li_2S , BaS, K_2S and CaS-FeS		Found favorable order as Na_2S>Li_2S>BaS>K_2S>CaS. 13%Na_2S resulted in L=21.5.	
Jimbo, Sulsky, Freuhan	1988	Refining of copper from ferrous scrap	FeS-Na_2S and Na_2S-FeS-Cu_2S-Cu systems	1400	Na_2S-FeS-Cu_2S-Cu systems can contain up to 36 wt% Cu_2S. 30%Na_2S resulted in L=20.	
Liu and Jeffes	1989	Decopperization of molten steel by various slags	Na2S, FeS, CaS, CaO, MgS and MgO based slags	1600	20-30% of initial copper was removed in 5 min.	
Wang, Nagasaka, Hino, Ban-Ya	1991a	Copper Distribution between Molten FeS-NaS0.5 Flux and Carbon Saturated Iron Melt.	FeS-Na2S	1400	FeS flux, L=9. Na2S=0.4, L=24. Addition of 0.8 Na2S decreases melt S content to 0.04%.	
Wang, Nagasaka, Hino, Ban-Ya	1991b	Copper Distribution between FeS-Alkaline or -Alkaline Earth Metal Sulfide Fluxes and Carbon Saturated Iron Melt	Li2S, K2S, Sr2S and BaS-FeS	1400	Li2S-FeS flux, L=30. K2S-FeS flux, L=20. SrS-FeS flux, L=22. BaS-FeS flux, L=19. Sulfur content decreases with addition of other sulfides to FeS.	
КАШИН, et al	1991		Na_2CO_3 soda		Achieved copper percentages lower than 0.03% from 0.23-0.38%. Soda reacts with sulfur in melt to produce Na2S, but the reaction was difficult to control.	Kostetsky et al.
Katayama, Sano, Sasabe	1998	Fundamental studies on removing residual elements from steel scrap	Na_2S and Na_2SO_4		Showed that flux could be recycled by leaching with water. The Na_2S and Na_2SO_4 components could be separated from the water.	

Author	Year	Title	Slag system	T (ºC)	Main results
Shimpo, Fukaya, Ishikawa, Ogawa	1997	Copper removal from carbon-saturated molten iron with Al_2S_3-FeS flux	Al_2S_3-FeS	1200	L=28. Proposed a counter-flow method with recycling of the flux.
Cohen and Blander	1998	Removal of copper from carbon-saturated iron with aluminum sulfide/ferrous sulfide flux	Al_2S_3-FeS	1365	L=30.
Kostetsky, Troyansky, Samborsky		Removal of copper from carbon-iron melts	Fused soda block, soda and sulfur powders, mixtures of soda, sulfur and carbon powders	1250	Found at most 24% reduction in Cu from 0.64% Cu, but did not achieve consistent results.
Cohen	2005	Removal of copper from iron-based metal with aluminum sulfide/ferrous sulfide matte	FeS-Al2S3 and sulfide-modified oxide fluxes	1365 and 1650	Al2S3 fluxes, L=30 but sulfur pickup was high. A sulfide-moderated oxide flux resulted in less sulfur transfer and could operate at 0.1wt% C for L=6.8, but it was thought this could be further optimized.
Hui, Jianjun, Shangxing et al	2009	Copper removal from molten steel with FeS-Na2S slag	FeS-Na2S-	1580	Found improved copper removal with increasing carbon, due to the increase in copper's activity.
Uchida, Matsui, Kishimoto, Miki	2015	Fundamental investigation on removal of copper from molten iron with FeS-Na2CO3 fluxes	Na2CO3-FeS	1234 to 1404	Highest L=13.9, but high sulfur of 0.34%. Difference in distribution with Na2CO3 and Na2S as starting materials attributed to difference in optical basicities.
Sasabe, Harada, Yamashita	1996	Removal of copper from carbon saturated molten iron by using FeCl2	FeCl2 injections	1450	Injected FeCl2 into molten iron. Iron chloride was vaporized in liquid iron and reacted with copper. Cu reduced from 0.7% to 0.5%. Calculated 18.5 kg FeCl2 to reduce 1t from 0.5% to 0.1% and presented a rate equation for copper removal.

Author	Year	Title	Slag system	T (ºC)	Main results
Hu, Yan, Jiang et al	2013a		CaCl2	1600	Investigated the selective chlorination of copper for Cu2O-FeO by CaCl2. Thermodynamic calculations showed copper could be selectively chlorinated by CaCl2 and removed from the system.
Hu, Yan, Jiang et al	2013b	Removal of copper from molten steel using FeO-SiO2-CaCl2 flux	FeO-SiO2-CaCl2	1600	Based on previous studies. Copper is partly oxidized and transferred to the flux as Cu2O, then chlorinated by CaCl2. Copper chlorides, CuCl or Cu3Cl3, evaporate. Acidic SiO2 thought to promote chlorination and evaporation. Cu reduced from 1.29 to 0.74%.

Table A2.17: Catalogue of studies for inclusion formation.

Authors	Year	Title	Main results
Oden and Elger	1987	Removal of copper from molten ferrous scrap: results of laboratory investigations	Injected mixed oxides (copper-containing complex oxides, alkali silicates and complex alkali and alkaline-earth silicates and aluminates) with the purpose of forming copper-containing complex oxide inclusions, but was unsuccessful.

Table A2.18: Catalogue of studies for filtration.

Authors	Year	Title	Main results
Zigalo et al.	1991		
Li et al.	1997		
Savov, Volkova and Janke	2000	Copper and tin in steel scrap recycling	The above publications were not found, but this review reports that an Al_2O_3-ZrO_2 ceramic filter removes copper at a rate of 30%, as found by Zigalo et al. and Xiang et al.

A3 – energy and material consumption estimates for each process route

The rate of copper reduction, scale-up reactor, and estimations for energy and material consumption are explained for each process route shown in Figures 4.10 and 4.11.

Improved shredding and magnetic separation

Rate of copper reduction

Newell (2017): 0.1wt% Cu reduction with every 10-15lb/cubic ft (0.15 to 0.25 tonne/cubic m) higher-density shred from conventional shredded scrap (40-60 lb/cubic ft, 0.6-0.9 tonne/cubic m), which normally contains 0.4wt%Cu.

Scale-up reactor

A conventional hammer shredder could be used, operating at a lower process rate. Katayama et al. (1997) show that repeating shredding and magnetic separation reduces copper content from 0.2 to about 0.14 wt% Cu. This could be repeated a third time to reduce to the range of 0.1wt% Cu. A dedicated high-density shredder could be developed as well, to process scrap in one pass. Shredder outputs depend on horsepower, which could vary from 5 to 10,000. A typical shredding plant may process 100 t/hr, but rates vary from 25 to 250 t/hr (Recycling Today Shredder Guide). Higher density comes with a slower process rate (Newell, 1996).

Energy consumption

Lassesson (2008) reports that a modern Swedish shredding facility, which processes 70% iron, uses 15-20 kWh/ton input. Das et al. (1995) report that 21 kWh/t is consumed in shredding vehicles. A more intensive shredding process with a slower rate, would use more energy. Here, we assume an additional pass through the shredder consumes an additional 20 kWh-t for 0.2wt%Cu, and a third pass would reduce copper content to 0.1wt% (but require a total additional 40kWh/t).

Material consumption

None directly.

Separate copper-rich fraction with sieve/trommel/ballistic separator

Rate of copper reduction

A range of copper concentrations are possible. Aboussouan et al. (1999) report that 90% of copper initially present can be isolated by separating a certain size range of pieces from a conventional shredder. Newell (2017) explain that their trommel system produces a scrap grade with 0.12-0.15wt%Cu. SICON (2018) report that a "clean" ferrous fraction can be obtained with their ballistic separator to divert copper meatballs. Shattuck and Ramsdell (2018) report 0.16 to 0.17wt% Cu can be achieved with their ballistic system.

Scale-up reactor

Above, Aboussouan et al. (1999), Newell (2017), SICON (2018) and Shattuck and Ramsdell (2018) describe varying methods for separating scrap streams by size, magnetic permeability or density. Schulman (2011) also describes sorting scrap streams by copper concentration using real-time bulk composition analysis. Industrial equipment is available, and could be operated by scrap processors or steelmakers.

Energy consumption

In general, trommels that separate scrap metal in a rotating cylindrical sieve or screen are highly energy efficient. Bianna Recycling (2018) provide specifications for a range of trommels, which can process at most 210 m^3/hr with a power requirement of 30kW. Therefore, such a process should require on the order of 1kWh/t. More advanced technologies employing ballistics may not require significantly more energy. Shattuck and Ramsdell (2018) report that their ballistic separator requires little electricity consumption and no air.

Sieves require

Material consumption

None directly.

O_2/Cl_2 applied to solid scrap

Rate of copper reduction

Tee and Fray (2006) experimental results are used: copper reduction from 1wt% to below 0.05wt% in 10 minutes. The samples were 150 mg Fe, with copper winding, and the flow rate was 400/40 cm^3/min O_2/Cl_2 (at normal temperature and pressure) with the iron and copper sample at 800°C. An initial oxidizing treatment (O_2 blowing only) for 3 to 10 minutes at 800°C was recommended.

Scale-up reactor

Tee and Fray (2006) describe a continuous dezincing plant by chlorination with a proposed capacity of 100,000 t/y. This process employs the same process conditions required for copper chlorination.

Energy consumption

Tee and Fray (2006) estimate energy consumption of 27 kWh/tonne for the above chlorination plant, which assumes ferrous scrap initially at 800°C. An extra 10-20 kWh/tonne is added to account for heat losses during the transition from the process furnace to the EAF.

Material consumption

$$Cu(s) + Cl_2(g) \rightarrow CuCl_2(g)$$

To form $CuCl_2$ to eliminate 3kg of Cu/tonne steel, 3.3 kg $Cl_2(g)$ is required.

Embodied energy of Cl_2: 3.1 kWh/kg (US Department of Energy, 2000).

Embodied energy of Cl_2 consumed: 10.3 kWh/tonne steel.

For the amount of oxygen and iron consumed by oxidation, Tee and Fray (2006) show iron weight gain of approximately 0.01 g/cm^2, and that primarily Fe_2O_3 is formed. Assuming shredding produces scrap pieces about the size of a fist, the average shredded scrap piece was estimated as a sphere with a 5cm diameter, weighing 0.5 kg. With this average surface area, approximately 3 to 5 kg Fe/tonne steel would be lost, with 2 kg O_2/tonne steel consumed.

Embodied energy of O_2: 0.5 kWh/kg (Worrell, 2000)

Embodied energy of O_2 consumed: 1 kWh/tonne steel.

Embodied energy of low-carbon steel: 7-8 kWh/kg (Ashby, 2013)

Embodied energy of low-carbon steel consumed: 21-40 kWh/tonne steel.

The quantity of gas directly consumed is calculated, but a gas flow of 400/40 cm^3/min $O_2/Cl_2(g)$ was required in experiments, and a high gas flow would be required in the process.

Preferential melting

Rate of copper reduction

Brown and Block (1968) experimental results were used, which showed negligible reduction in copper concentration due to adherence of liquid copper to the solid steel substrate, even as atmosphere varied from reducing, to inert and oxidizing conditions (unless liquation was achieved with a high initial copper concentration, >20wt%). Sano et al. reported that the work of adhesion of liquid copper was minimized on magnetite and hematite, and this route could be theoretically feasible. Work has not been done to demonstrate a significant reduction in copper from typical scrap at low concentrations. Leak and Fine (1973) demonstrate that an inert molten sweating medium and pre-coatings could prevent intimate contact between liquid copper and the steel substrate, but their experiments used samples with high initial concentrations of copper to achieve liquation.

Scale up reactor

Scrap heating with rotation, vibration or shaking applied at temperatures above 1083°C. A continuous scrap heating system in a tunnel furnace, such as the one demonstrated by Consteel (Memoli et al., 2012), could be developed.

Energy consumption

Alternative heating designs are shown to be at least as efficient as conventional heating in the EAF (and oftentimes more). This treatment requires 10 additional minutes above

1083°C to collect liquefied copper. It is assumed that a tunnel furnace with a scrap conveyor is used. A conventional design is 2x2x20m (Memoli et al., 2012), to contain 220 tonnes of steel scrap. Karimi and Saidi (2010) report an overall heat transfer coefficient of 4 W/m^2K from the furnace walls of a pusher type reheating furnace for steel billets. Chen et al. (2005) give a break-down of the sources of heat output of a reheating furnace for steel billets. Roughly 18% of heat is lost from furnace walls, while 32% is lost as hot flue gas. Therefore, for a ten-minutes at 1100°C, it is calculated that 120 kWh is lost from the furnace walls, and 240 kWh is lost as hot flue gas. To overcome this loss at 40-60% efficiency, an energy input of 3 to 5 kWh/tonne steel is calculated. This treatment could be made continuous into the EAF, but an additional 10-20 kWh/t is accounted for the transition from the process furnace to the EAF.

Shaking: The documentation on rotary electric vibrators by Cleveland Vibratory reports that the three phase 900 RPM model RE 185-8 max force 40,700 lbs. draws 43 A at 230 V = 10 kW. If 2 of these motors are used, 20 kW. For 10 minutes, less than 0.5 kWh/tonne steel is required.

Material consumption

No direct inputs.

Solvent extraction applied to solid scrap

Rate of copper reduction

Iwase (1996) experimental results are used: reduction from 0.5wt% to 0.1wt% copper at 950°C with an Al-60 wt% Cu bath, followed by a second dip in a pure Al bath and mechanical vibration in between.

Scale up reactor

Two 90-tonne baths with liquid Al at 950°C, with a heated vibratory conveyor in between.

Energy consumption

Assuming the process is integrated into scrap heating and melting, such that scrap would be entering treatment at 950°C, sources of energy consumption are to heat Al added to the bath for each treatment, to maintain the Al baths at 950°C, to power the vibratory

conveyor and compensate heat losses while scrap is transitioned from the process to the EAF.

Around 20 kg Al/tonne steel treated is lost for each treatment (see below). To heat the 20kg of Al added to the bath each treatment from 25 to 950°C, 7 to 10 kWh would be required (assuming 50-70% melt heating efficiency).

The Al baths are assumed to be 90-tonne channel furnaces for holding molten metal, as described by Schmitz and Trauzeddel. For immersion, a liquid/solid ratio of 5 ml/g is assumed. With this ratio, approximately 7 tonnes of steel scrap could be treated in the 90-tonne Al bath. These furnaces consume 4 kW/tonne liquid metal to maintain temperature, so this totals 15 to 20 kWh/tonne steel for two ten-minute bath immersions. However, heat is lost when the furnace lid opens when steel scrap enters and leaves the bath. Schmitz and Trauzeddel report 10kWh/tonne liquid metal is lost for having the lid open for 20 minutes, so 5 to 10 kWh/tonne steel is added.

The heated vibratory conveyor between Al baths is assumed to require 4 to 6 kWh/tonne steel (similar to heat and vibration requirements of preferential melting).

Total energy consumption is 42 to 60 kWh/tonne steel.

Material consumption

For scrap immersion, a liquid/solid ratio of 5 ml/g is assumed, which is a ratio of about 12 tonnes of Al/tonne steel scrap. The Al-Cu alloy generated from treatment is a valuable product, and thus is not considered as material consumption. However, the amount of Al adhering, and lost to oxidation in steelmaking, is considered as material consumption. Iwase did not quantify the amount of Al adhering. Assuming shredding produces scrap pieces about the size of a fist, an average shredded scrap piece was estimated as a sphere with a 2.5cm radius, weighing 0.5 kg. If 0.5mm of Al adhered to the surface of each scrap piece, this would correlate to a loss of 20 kg Al/tonne steel treated.

Embodied energy of Al (primary): 56 kWh/kg (Ashby, 2013).

Embodied energy of Al consumed: 1120 kWh/tonne steel.

Al oxidation in the EAF at 1600°C (Adolf and Socha, 2016):

$$2Al + \frac{3}{2}O_2(g) = (Al_2O_3), \Delta H = -31000 \frac{kJ}{kg\ Al}$$

Heat generated: 172 kWh/tonne steel.

Matte extraction applied to solid scrap

Rate of copper reduction

Cramb and Fruehan (1991) experimental results for 100 kg scrap were used, proving that copper concentration could be reduced from 0.4 to 0.1wt% Cu in a rotary kiln at 1-6 RPM after about 15 minutes.

Scale-up reactor

Rotary furnace, such as the continuous melting furnace described by Zhang, et al. (2008).

Energy consumption

Assuming the scrap heating is at least as efficient as the conventional route, the initial temperature of the scrap is assumed to be 1000°C. The sources of energy consumption would be to heat the matte to 1000°C (heat content of industrial slag at 1000°C is 1 MJ/kg from Matousek, 2008), assuming heating efficiency of 40-60%, for 10kg matte/t steel, this equates to 5 to 6 kWh/tonne steel), maintain the scrap and matte at 1000°C for the 15 minute treatment (4 to 6 kWh/tonne, similar to preferential melting furnace requirements), rotate the scrap (1-2 kWh/tonne. The documentation on tilting rotary furnaces from Melting Solutions shows a power requirement of 125 kW for motors to rotate 1 to 6RPM for 25t of scrap) and overcome any heat losses from the transition of scrap from the furnace to the EAF (10 kWh/tonne). Altogether, 20 to 26 kWh/tonne.

Material consumption

With an effective distribution ratio of 500, 10 kg of 82wt%FeS – 18wt%Na2S matte would be required for a reduction from 0.4 to 0.1wt% Cu.

Embodied energy of matte (general slag): 0.38 kWh/kg (ICE Database).

Embodied energy of matte consumed: 3.8 kWh/tonne steel.

Sulfur contamination of the scrap is noted, so a desulfurization treatment of the melt is required. Ghosh (2000) provides a detailed report of desulfurization practice in secondary steelmaking. It is common to apply 10-25 kg slag/tonne steel. Sarna (2013) reports a temperature loss of 30°C can be expected. With powder injection and stirring, the total energy consumption is estimated as 20-30 kWh/tonne. Alternatively, Cramb and Fruehan (1991) state that an acid wash following the matte extraction could prevent sulfur contamination, but this would not allow heat retention in the EAF route.

Embrittlement

Rate of copper reduction

Cho et al. (2010) describes a system for removing copper from ferrous scrap by oxidation, mechanical impact and fluxing with an EAF slag while the ferrous scrap remains solid. There are various embodiments to the idea, described in the patent, but the above steps are reported to remove 99.5 to 99.9wt% copper in scrap initially containing 3 to 5 wt% copper. Therefore, it is assumed the final copper concentration is below 0.1wt%.

Scale-up reactor

The process requires a furnace for oxidizing scrap for 4 to 6 hours at 400 to 700°C. Thermal cycling or impact, such as vibrating or shaking, is required to aid in copper oxide spallation. Afterwards, the solid scrap is fluxed with an EAF slag at 1000 to 1200°C. For this step, a rotary furnace, such as the one described by Zhang et al. (2008) is assumed.

Energy consumption

For the oxidizing step, a 2x2x20m tunnel furnace for 220t scrap with an overall heat transfer coefficient of 4 W/m^2K from the furnace walls is assumed (similar to the tunnel furnace assumed in preferential melting). For a 4 hour treatment at 500°C, heat losses from the furnace walls amount to 1280 kWh, with 2560 kWh for losses from hot flue gases (assuming similar heat output proportions to those reported by Chen et al.(2005)). With an efficiency of 40-60%, this results in heat requirements of 30 to 45 kWh/tonne steel.

It is assumed that scrap would be shook by a conveyor in the tunnel furnace periodically throughout the oxidation treatment. Assuming that in total the scrap is shaken for one hour, this amounts to 1 to 2 kWh/t.

For the fluxing treatment, a 15 minute treatment in a rotary kiln at 1000°C with 10 kg slag/tonne steel is assumed. This step is thus identical to the matte extraction process, so 20-25 kWh/t is attributed to this step.

Material consumption

Both CuO(s) and Cu_2O(s) form in the oxidizing step.

$$2Cu(s) + \frac{1}{2}O_2(g) \rightarrow Cu_2O(s)$$

$$Cu(s) + \frac{1}{2}O_2(g) \rightarrow CuO(s)$$

For 3kg Cu/tonne steel, this requires between 0.8 kg O_2(g) (assuming only Cu_2O forms) and 1.5 kg O_2(g) (assuming only CuO forms).

Embodied energy of O_2 consumed: 0.4 to 0.75 kWh/tonne steel (Worrell, 2000).

For the fluxing step, it is assumed 10 kg slag/tonne steel would be consumed: 3.8 kWh/t (ICE Database).

Cho reports that around 1% of iron would be lost to oxidation, e.g. 10 kg/tonne steel.

Embodied energy of O_2 consumed: 2 kWh/tonne steel.

Embodied energy of low-carbon steel: 7-8 kWh/kg (Ashby, 2013)

Embodied energy of low-carbon steel consumed: 70-80 kWh/tonne steel.

Leaching

Rate of copper reduction

With ammonium carbonate solution

Oden, Adams and Fugate (1973) explain that to dissolve metallic copper in ammonium carbonate solution, ammonium carbonate and metallic copper react to oxidize copper and form cuprous ammonium carbonate:

$$Cu^o + Cu(NH_3)_4^{2+} \rightarrow 2Cu(NH_3)_2^+$$

$$2Cu(NH_3)_2^+ + (NH_4)_2CO_3 + 2NH_4OH + \frac{1}{2}O_2 \rightarrow 2Cu(NH_3)_4^{2+} + 3H_2O + CO_2$$

The first equation does not proceed unless excess ammonia is present. Cupric ammonium complex is the active species. Re-oxidation of the cuprous species is a critical step, so oxygen must be supplied by vigorous aeration.

A well-aerated solution containing 10 to 30 g/l Cu, 68 g/l NH_3 and 44 g/l CO_2 achieved dissolution rates of 0.00156 g/cm^2/min. This rate is equivalent to 0.1-inch penetration per 24 hour period, sufficient to dissolve in 24 hours the thickest copper pieces observed in scrap. The treatment was followed by an ammoniacal rinse solution (1 hour with air agitation) and a water rinse. The solution was analyzed daily to maintain the necessary water, ammonia and CO_2. The ammoniacal rinse solution was regenerated daily by electrodepositing the copper. 0.3wt% was removed by the total treatment. Insufficient circulation of the leaching solution or incomplete removal of the leach solution during rinsing account for incomplete removal.

With ammonium chloride solution

Konishi et al. (2014) explain that $Cu(NH_3)_4^{2+}$ can oxidize metallic copper, which is present in $CuCl_2$-NH_3-NH_4Cl solution. Konishi et al. (2014) compared the leaching speed of copper in various concentrations of NH_3 and NH_4Cl and found leaching speed increased increasing NH_3 and NH_4Cl concentration, and proposed 4 kmol/m^3 NH_3 and 1 kmol/m^3 NH_4Cl and 0.5 kmol/m^3 Cu(II) as an optimum concentration. Leaching speed increased with stirring speed, described by the following equation.

$$R = k[Cu(NH_3)_4{}^{2+}]^{\frac{1}{2}} V^{\frac{2}{3}}$$

Industrially, stirring speeds of 200 RPM can be achieved, so the leaching speed of 2kg/m^2hr at 80^{o}C is used here. The authors found the leaching rate in chloride-based solutions to be superior to sulfate-based.

With ammonium sulfate solution

Konishi et al. (2014) compared ammonium chloride and sulfate solutions, and found the chloride solutions to have a higher leaching speed. However, Sun et al. (2015) demonstrated that copper can be electrodeposited from an ammonium sulfate solution containing 51 g/l at a current efficiency of 89%. Sun et al. (2015) did not report the leaching rate of the sulfate solution used, so the results by Konishi et al. (2014) are used. For a solution with 7 kmol/m^3 NH_3, 1 kmol/m^3 $(NH_4)_2SO_4$, 0.5 kmol/m^3 Cu(II) a leaching speed of 0.8 kg/m^2hr at 80^{o}C and 200 RPM was reported.

Scale-up reactor

Oden, Adams and Fugate (1973) performed experiments on 100 kg scrap and recommended a tumbling reactor for scale-up. Jung and Keller (2016) describe the dimensions and operating costs for hydrometallurgical processing of metals in gassed continuously stirred tank reactors on the order of 1000 m^3.

With electrowinning

Sun et al. (2015) describe an electrochemical cell that can electrodeposit copper leached into solution (concentration greater than 50 g/l) with 90% current efficiency. This was demonstrated at a laboratory scale, so scale-up design is needed.

Energy consumption

With ammonium carbonate solution

The ammonium carbonate solution requires aeration and stirring. Jung and Keller (2016) report that the power requirements of gassed continuously stirred tank reactors are driven by the agitator and compressor motor. Primary bioleaching reactors and vessels of 1000 m^3 typically require 250 to 315 kW for agitation and up to 300 to 500 kW for the compressor motor.

Assuming a ratio of 5ml leachant/g scrap in a 1000 m^3 tank, 180 tonne steel could be treated with 0.9 ML leachant. With the given leaching rate, 24 hours would be needed. Given the above power consumption, this would amount to 30-40 kWh/tonne for agitation and 40-65 kWh/tonne for aeration.

With ammonium carbonate solution

The ammonium chloride solution requires stirring and a higher temperature (80^oC) to achieve the reported leaching rate. To raise the scrap to 80^oC, 15-25 kWh/t is required. It is assumed that the process runs continuously, so the energy to heat the leachant to 80^oC is not included. To calculate the energy to maintain the reactor at 80^oC during the treatment, the heat loss is estimated. Documentation from Spirax Sacro (2018) reports heat transfer coefficients from a steel surface to the atmosphere. A value of 12 W/$m^2$$^oC$ is used for a surface of 725m^2 (sides and top of a 10m diameter, 13 m high vessel treating 180 tonnes steel), amounting to 6,300 kWh for the treatment. With a heating efficiency of 40-60%, this accounts for 70-120 kWh/tonne steel. However, with 25 mm of insulation, this value would be reduced by 80%, to 15-25 kWh/tonne, and this case is used here. Stirring for 12 hours would require 15-20 kWh/tonne.

With ammonium sulfate solution and electrowinning

The ammonium sulfate solution has similar requirements to the ammonium carbonate solution above, but the treatment requires 24 hours.

For electrodeposition, Sun et al. (2015) report that 2.1 kWh/kg Cu power is required with their set-up. With 3 kg Cu/tonne steel, this amounts to 6.3 kWh/tonne steel.

Prior incineration

The heat capacity of steel is 0.5 kJ/kg^{o}C. Assuming an efficiency of 40-60%, raising the temperature to 800^{o}C would require 185-280 kWh/t.

Material consumption

Assuming that dissolved copper is in the form of $Cu(NH_3)_4^{2+}$, 3.2 kg ammonia would be consumed per tonne of steel.

Embodied energy of ammonia: 7.9 kWh/kg (US Dept of Energy, 2000)

Embodied energy of ammonia: 25.3 kWh/tonne steel.

The reactions above do not proceed unless excess ammonia is present. For the ammonium carbonate solution, there will be ammonia losses due to aeration. These losses are not accounted.

Distillation

Rate of copper reduction

Most studies on copper distillation have focused on understanding and optimizing the kinetics of the process. Harris (1980) concluded that the 3 steps (transport from the melt to the reaction site, the reaction and transport away from the reaction site) fully describe the mechanism of vacuum distillation. These steps will be summarized here.

Liquid phase transport follows the same description used in the ladle treatment, so please refer to that section. For surface vaporization, the reaction at the interface and is described by the Hertz-Knudsen-Langmuir equation, which gives the rate of evaporation of solute atoms in a perfect vacuum. The rate constant, k^v, of this step is given below.

$$k^v = \frac{a_{Cu}\gamma_{Cu}^0 M_{Fe} P_{Cu}^0}{\rho(2\pi RTM_{Cu})^{\frac{1}{2}}}$$

The gaseous transport of copper atoms involves a combination of diffusion and convection, depending on the chamber pressure and surrounding gas flow. There are three main regimes:

1. Bulk flow of evaporating vapors is established with convection being the main transport mechanism. It is achieved when the melt vapor pressure is higher than chamber pressure or there is a flow of scavenging gas carrying away evaporating vapors. The rate constant, k^g, of this step in this regime was determined by Harris et al. (1992) as the equation below, with n_i being the flux of evaporating atoms in the gas phase (kg/m^2s), Z the total number of species in solution, and P_{ch} the chamber pressure (Pa).

$$k^g = \sum_{i=1}^{Z} n_i / P_{ch}$$

2. An intermediate regime exists when the chamber pressure is less than the total melt vapor pressure but more than that of the pure solvent. Here, both bulk flow convection and diffusion mechanisms are significant. Savov and Janke (2000) found this regime to operate when the chamber pressure is 10-100 Pa and proposed the following empirical equation to determine k^g.

$$\log(k^g) = -0.45 \log(P_{ch}) - 3.79$$

3. When the chamber pressure is greater than the melt vapor pressure there is significant resistance to transport and diffusion is the operating mechanism. Many studies have concluded refining in this regime to be entirely impractical.

Thus, since copper has a relatively low vapor pressure resistance in the gas phase is significant unless very low chamber pressures are achieved. When the total pressure is less than 10Pa, resistance is minimal, k^g approaches zero and atoms collide with cold walls to be removed by condensation. Ward found that experimental k_{Cu} values from levitated droplets are on average 65% of the theoretical maximum value predicted by the Hertz-Knudsen-Langmuir equation due to liquid-phase resistance. The overall rate constant, which is used in the first order rate equation, is determined by combining the rate constants of the steps above as shown below.

$$k_{Cu} = \left(\frac{1}{k^l} + \frac{1}{k^v} + \frac{1}{k^g}\right)^{-1}$$

The overall rate constant is not constant with respect to time because the gas phase transport coefficient is a function of the total flux evaporating from the steel surface and the total pressure of the vacuum chamber, which changes throughout the reaction. Harris recommends using a numerical solution, but most researchers measure and report the overall k_{Cu} value. The figure below compiles these results, with the corresponding source of the data shown in the table.

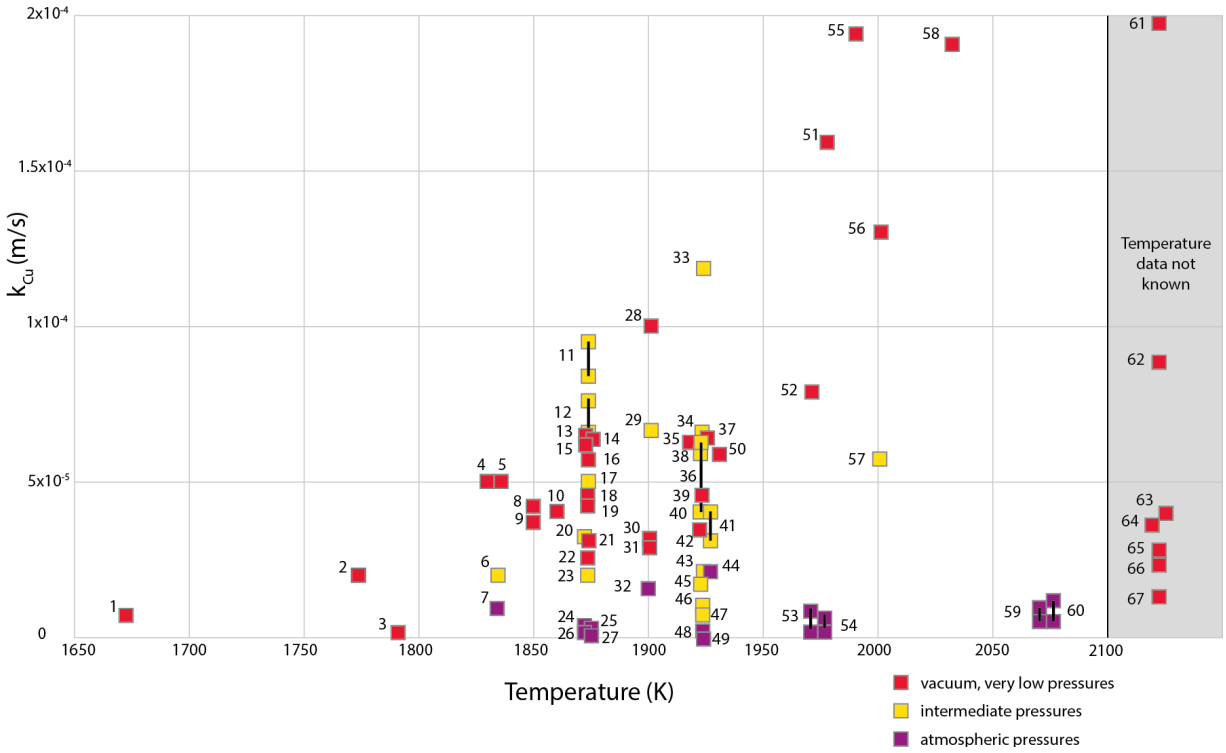

Figure A3.1: k_{Cu} values in the literature plotted by temperature and pressure regime.

Table A3.1: Experimental parameters, pressure (Pa) and melt additions, corresponding to the measured points in Figure A3.1 and the corresponding reference.

#	Pressure (Pa)	Additions	Reference	#	Pressure (Pa)	Additions	Reference
1	10		Savov and Janke	35	8		Harris
2	10		Savov and Janke	36	133	with C	Ono-Nakazato et al
3	9	Sn, Mn, S additions to A36 steel	Harris	37	0.2		Nakajima et al
4	2.00E-02		Tokumitsu and Hirata	38	133	Fe-1.5Si-3C	Taguchi et al
5	10		Tokumitsu and Hirata	39	0.1, 1		Blacha and Labaj
6	20		Tokumitsu and Hirata	40	50		Nakajima et al
7	100		Tokumitsu and Hirata	41	133	with Si	Ono-Nakazato et al
8	vacuum	with induction stirring	Yamamoto and Kato	42	10		Blacha and Labaj
9	vacuum	without stirring	Yamamoto and Kato	43	100		Nakajima et al
10	10		Savov and Janke	44	1000	with Si	Ono-Nakazato et al
11	100	with MgO powder	Zaitsev et al	45	50		Blacha and Labaj
12	100	with SiO2 powder	Zaitsev et al	46	200		Nakajima et al
13	1		Savov and Janke	47	100		Blacha and Labaj
14	10	with 4% C	Savov and Janke	48	2000		Nakajima et al
15	1		Zaitsev et al	49	1000		Blacha and Labaj
16	10		Savov and Janke	50	7		Harris
17	100	with argon blowing	Zaitsev et al	51	0.01		Smith and Ward
18	0.1, 10		Zaitsev et al	52	11		Harris
19	vacuum		Ohno and Ishida	53	10000	with Si	Morales and Sano
20	50		Savov and Janke	54	10000	with C	Morales and Sano
21	10	Fe-Cr-Ni alloy	Savov and Janke	55	0.01		Smith and Ward
22	10	Reduced stirring	Savov and Janke	56	12		Harris
23	100		Savov and Janke, Zaitsev et al	57	20		Harris
24	10000	4% C with 1L/min Ar-H_2 flow	Jung and Kang	58	0.01		Smith and Ward
25	1000		Zaitsev et al	59	10000	with Si	Morales and Sano
26	10000	with 1L/min Ar-H_2 flow	Jung and Kang	60	10000	with C	Morales and Sano
27	100000		Zaitsev et al	61	vacuum		Ollette
28	10		Fischer et al	62	vacuum		Fischer, Janke and Stahlschmidt

#	Pressure (Pa)	Additions	Reference	#	Pressure (Pa)	Additions	Reference
29	100		Fischer et al	63	vacuum		Ward
30	7		Harris	64	vacuum		Ohno and Reiichi
31	vacuum		Fischer et al	65	vacuum		Harris and Davenport
32	1000		Fischer et al	66	vacuum		Salomon De-Friedberg and Davenport
33	100	with Ar gas flow, 4g/s SiO_2 and 340 kW plasma flame	Nishi et al	67	vacuum		Gill, Inveson, Wesley-Austin
34	130	with SiO_2 powder	Matsuo, Maya et al				

The highest values of k_{Cu} are achieved at very high temperatures and very low pressures. Increased temperature increases the vapor pressure of copper, which is 105 Pa at 1600°C, but increases to 430 Pa at 1730°C. These conditions are difficult to maintain at industrial scales, so significant work has been done to study k_{Cu} at intermediate pressures, around 100 Pa, to find favorable treatment times in a less demanding operating space. Parameters that could be varied to enhance the reaction in this regime include:

- Gaseous atmosphere type: The chamber is flushed with an inert gas, typically argon. Blacha et al. (2011) explain that the type of gaseous atmosphere does have an effect on the diffusivity of evaporating vapors, but when the pressure is reduced below 1000 Pa, the impact drops significantly and ultimately fades out.

- Use of a scavenging gas: a scavenging gas can be used to dilute the vapors at the liquid/gas interface and establish a bulk flow of evaporating gases to a condensing surface.

- Additions to the melt: Blacha et al. (2011) explain that evaporation rate depends on phenomena occurring on the interface and the key factors are the presence of a group of surfactants: oxygen, sulfur, selenium and tellurium. It is possible that a surface-active bath component causes the evaporation rate to increase. Additions to the melt may increase the activity of copper, to increase the partial pressure above the melt (see equation below). Carbon increases the activity of copper, with Jung observing that the evaporation rate increased by about 2 times when liquid Fe was saturated by carbon, but within the normal carbon concentration range, 0.05 to 0.58wt%, Zaitsev et al. (2004) noted that there was no perceptible effect on evaporation rate. Jung (2016) investigated the evaporation rate of

copper in the presence of sulfur, but found the highest rate to be achieved with an initial sulfur concentration of zero.

$$P_{Cu} = \gamma_{Cu} X_{Cu} P^0_{Cu}$$

Savov and Janke (2000) concluded in order to apply vacuum distillation on a large scale, it will be necessary to optimize the thermodynamic conditions. They gathered thermodynamic data on activities of Cu and Sn in ternary and more complex iron-based melts and calculated the activity of Cu in the Fe-Si-Cu system. The most favorable conditions were realized at 15% Si in the melt. They suggested a process of recycling contaminated scrap in ferrosilicon production, but the results are not immediately relevant for typical low-carbon steel production.

The parameters above can increase k_{Cu}, but the specific surface area (A/V) is equally important in determining the refining time. A/V is determined by the reactor type, of which there are three main categories:

1. The liquid/gas interface exists only at the top surface, such as in a vat, but dimensions could range to a thin film.
2. Dispersing a gas through the melt.
3. Spraying the melt through the gaseous atmosphere/vacuum.

Therefore, in this analysis these three types of set-up's are defined as potential processes: vat with some recirculation (standard vacuum degassing), vat with bubbling and spraying

Scale-up reactor

Standard vacuum degassing

Adolf and Socha (2016) describe the types of vacuum degassing: in the ladle, degassing in a stream and by lifting (Dortmund- Hüttenunion, DH and Ruhrstal-Heraeus, RH). The vat and lifting processes typically require 15 to 20 minutes. There are a range of chamber pressures typically achieved. 100 Pa is reported as typical, but 50 Pa or lower is possible. Because of this range, we define a minimal and a vigorous vacuum degassing process which should span the range of degassing processes currently in operation.

Minimal

The melt is stirred in the 160 tonne ladle described by Zaitsev et al. (2004) (3.2m inner diameter, 2.9m height). Morales et al. (2015) state that stirring increases the nominal surface area by a factor of 1.5 so the specific surface area, A, is set to $0.5m^{-1}$. The chamber pressure is 100Pa and the total time is 10 minutes. Corresponding to 100Pa and 1600°C, $k=2x10^{-5}$ m/s (Savov and Janke, 2000). The final copper concentration was calculated to be 0.39wt%.

Vigorous

The melt is stirred re-circulated in a lifting process. Ostrava state that typically the melt is circulated three to five times. Therefore, we estimate the effective specific surface area as $2m^{-1}$. The pressure of the vacuum chamber is reduced to 50 Pa ($k=3x10^{-5}$ m/s, Savov and Janke, 2000). The process time is 30 minutes. The final copper concentration was calculated to be 0.35wt%.

Extended vacuum distillation with bubbling:

The model proposed by Zaitsev et al. (2004) is used, with the equation for the flux of copper under a vacuum accounting for argon blowing shown below.

$$J = \frac{p^0(Cu)\gamma(Cu)x(Cu)U\left(1+\left(\frac{\rho gH}{p_{atm.}}\right)\right)}{RT} + \frac{p^0(Cu)\gamma(Cu)x(Cu)}{\sqrt{2\pi RTM(Cu)}}k_{turb.}\left(\frac{\pi D^2}{4}\right)$$

Here, we set the chamber pressure, $p_{atm.}$, as 50 Pa. Zaitsev et al. (2004) set $k_{turb.}=3$ for 100 Pa chamber pressure. Here, $k_{turb.}$ was set to 4 to correspond with the reduced pressure. U=0.14 m^3/s (gas-stream velocity), H=2.9m (height of metal column), D=3.2m (ladle internal diameter), $\gamma(Cu)$=10, T=1600°C (R is the universal gas constant and x(Cu) is molar concentration). The time to reduce to 0.1wt% Cu was calculated to be 130 minutes.

Bubbles could also be generated by a decarburization reaction. Nishi et al. (1999) proposed applying SiO_2 powder to react with carbon in the melt and create CO(g) bubbles to increase the interfacial area. It was noted that this reaction is endothermic, so plasma heating was also applied to the surface to supply the heat needed for copper's vaporization.

With this approach, k_{Cu} values similar to those attained at very low pressures could be attained at 130 Pa. Zaitsev et al. (2004) also calculated that decarburizing the melt accelerates the process of copper extraction, as compared to evaporation from undisturbed surface, by a factor of 2.2-2.6 with SiO_2 and 2.8-3.1 times when MgO was used. However, because of the high carbon content required for the melt and simultaneous heating needed to overcome the endothermic reaction, this method of bubbling is difficult to incorporate into the conventional route and is not further considered in this analysis.

Extended spray distillation in vacuum:

Winkler and Bakish (1971) describe stream degassing for a 120 ton plant: typical treatment time is about 0.5s, but depends on the initial flow rate and height of the drop. Upon release into the vacuum, the melt disperses into drop sizes typically 1 to 5mm in radius.

Here, we set the vacuum pressure to the lowest possible reported by Winkler and Bakish (1971) for ladles: 10 Pa. At this pressure, $k=6.5x10^{-5}$ m/s. With this low chamber pressure, a droplet diameter of 1mm is assumed for a specific surface area of 6,000m^{-1}, so the time to reduce to 0.1wt% Cu was calculated to be 4s. The reactor would need to be adjusted to allow for this extended treatment time, either with a greatly increased falling distance, or multiple circulations of the melt.

Energy consumption

Standard vacuum degassing

The most significant source of energy consumption for vacuum treatments is overcoming the heat losses during treatment. Lange (1988) provides the change in temperature for RH-type, DH-type and tank degassing processes, reporting that there is a temperature drop of at least 50°C. This requires 16-22 kWh/t of heat to overcome.

Ghosh (2000) provides rates of temperature loss for different ladle (200t) treatments. For circulation degassing, the rate is 0.7-1.5 °C/min, and for ladle holding the rate is 0.5-1°C/min. Assuming it takes 10 minutes to reach the chamber pressure, about 5 kWh/t of heat would be needed for holding during this time. The temperature drop could be as low as 10°C during the minimal treatment, requiring 5 kWh/tonne steel. Ghosh (2000) notes that temperature losses in prolonged treatments of the melt can be as high as 100°C. For

the more vigorous treatment, a temperature loss of 70°C is assumed, requiring 25-40 kWh/tonne steel of heat.

To generate a vacuum, Kustenov and Kats (2007) show the energy consumption for mechanical pumps is about 1 kWh/ton liquid steel for a 90t vacuum degassing unit. An energy requirement of 1-2 kWh/tonne steel is assumed here.

Overall, it was estimated that standard vacuum degassing treatments require 15-50 kWh/tonne steel.

Extended vacuum distillation with bubbling
Ghosh (2000) reports that the temperature loss for a 200t ladle during gas purging is 1-2°C/min. With this rate, the total temperature loss would be 130-260°C. Heat would need to be delivered during treatment: 70-140 kWh/tonne steel (roughly estimated from the constant heat loss rate).

With the extended treatment, the vacuum would need to be maintained and the argon flow rate increases the pumping requirement. However, Burgmann and Göhler (2013) state that the mechanical pumping system is well-suited for compensating for constant volume flow rates. The energy requirement for argon blowing within the vacuum system is estimated as an additional 10-20 kWh/tonne steel.

Extended spray distillation in vacuum: The heat loss of a liquid metal stream is difficult to model as surrounding droplets can shield radiation losses. Michaelis et al. (2007) describe this "caravan effect" – that each droplet experiences a unique cooling profile dependent on its position and the character of the stream. Most models are for the cooling of a single droplet. Here, we use the observed heat losses from a 120 ton plant during 0.5s stream degassing reported by Winkler and Bakish (1971), below:

T loss due to heat absorbed in tap ladle: 24°C
T loss due to heat absorbed in vacuum ladle: 28°C
T loss due to heat absorbed in limiter, nozzle, etc: 3°C
T loss due to heat lost by radiation: 50°C

The heat lost by radiation is proportional to the effective time for radiation to take place and the area from which it is radiating, and the nature and temperature of the receiving surface. Heat loss is dependent on the geometry of the system, but radiation heat losses are expected to be proportional to time and the relative radiating and receiving areas.

Extending the treatment from 0.5s to 4s and decreasing the droplet size from 2-10mm to 1mm in diameter, results in ($A^*\Delta t$) effectively increasing by a factor of 14. Applying this factor to the radiation heat loss, particles would certainly solidify, so heat must be supplied during treatment. Winkler and Bakish (1971) noted that their system could be further optimized with the use of a heat shield. Here, we estimate that heat would need to be supplied to overcome an equivalent temperature drop of 400-500^{o}C. With the assumed efficiency of 50-70%, this equates to 125-220 kWh/tonne steel.

Material consumption

None directly.

Reactive gas evaporation

Rate of copper reduction

Hidani et al. (1996) provide the average rate constant of $3.3x10^{-5}$ m/s at 1600^{o}C for intermediate pressures 100-100,000 Pa when NH_3 is blown on the melt at 2L/min. The authors note that boiling occurred, so the specific surface area increases. Tayeb et al. (2014) notes that intense reactions in the ladle can increase the specific surface area by 3 to 14 times the nominal value, but Ghosh (2000) reports a factor of 100 for emulsification. A value of $10m^{-1}$ is used here.

Scale-up reactor

NH_3 is blown onto the melt under reduced chamber pressure, assumed to be 200Pa. With $k=3.3x10^{-5}$ m/s and $A=10m^{-1}$, the time to reduce to 0.1wt%Cu was calculated to be 60 min.

Energy consumption

The reactions occurring have not been confirmed, so the heat generated/absorbed is unknown. As the reaction generates a large surface area, heat loss would be greater from the exposed surface area. Ghosh (2000) states that powder injection in a 200t ladle results in a temperature loss rate of 2-3.5°C/min. Assuming a similar heat loss rate, this process results in a temperature drop of 120-210°C, requiring 45-115 kWh/tonne steel heat to compensate.

Similar to argon blowing, the chamber pressure must be maintained with increased pumping requirements for blowing NH_3. 10-20 kWh/tonne is allocated.

The melt supersaturates with nitrogen. Hidani et al. (1996) note that a 30 minute vacuum degassing treatment would be required afterwards. Above, it was determined that such a treatment requires ~50 kWh/tonne.

Material consumption

The reaction proposed by Hidani et al. is:

$$\underline{Cu}(l) + \frac{1}{2}H_2(g) \rightarrow CuH(g)$$

Where hydrogen is provided by NH_3(g) dissociating into nitrogen and hydrogen gas:

$$NH_3(g) \rightarrow \frac{1}{2}N_2(g) + \frac{3}{2}H_2(g)$$

0.3 kg of NH_3 would be consumed per tonne of steel.

Embodied energy of ammonia: 7.9 kWh/kg (US Dept of Energy, 2000)

Embodied energy of NH_3 consumed: 2.4 kWh/tonne steel.

Ladle melt treatment

Rate of copper reduction

In the absence of kinetic data, we assume this liquid-liquid process would be similar to other liquid-liquid steel refining reactions. Bodsworth (1963) states that steelmaking interface reactions are transport-controlled within a few minutes of the start of the reaction, when a concentration gradient has been established.

The mass transfer of a solute between two liquid phases in interfacial equilibrium is given by the equation below.

$$\dot{m} = kA\left([x]_i^{phase\ 1} - \frac{[x]_i^{phase\ 2}}{L}\right)$$

The rate constant, k, is usually determined by transport in the melt, k_m (Kim and Fruehan, 1987). The rate constant in slag, k_s, is usually of similar magnitude (Morales et al., 2015). Therefore, here we estimate k_m. Several approaches exist.

Machlin's model

If the liquid metal is being mixed, mass transfer of the solute element can be described by the model developed by Machlin (1960) using surface renewal theory. The following equation gives the rate constant, k_m, of copper to the surface, where v is the surface velocity of the melt (m/s) and r is the radius of the crucible (m). Melt velocity is difficult to determine. Sheng and Irons (1992) found this value to be 0.2 m/s in induction melting furnaces. The values for melt velocity with new induction stirring in ladle furnaces was found to be 0.5 to 1 m/s. Ovako steel reported a melt velocity of 0.7 m/s (Ramström, 2010).

$$\mathrm{k}_m = \left(\frac{8D_l v}{\pi r}\right)^{\frac{1}{2}}$$

Higbie and Danckwerts' model

Higbie's surface renewal theory is applicable when the flow at the interface is laminar. In a slag-metal system, the slag would tend to flow like a rigid body. Mass transfer at the interface in the high viscosity phase would be exclusively by molecular diffusion. Since the surface gets renewed continuously it was derived that, where t_e is the time of exposure of the rigid body:

$$k_m = 2\left(\frac{D_l}{\pi t_e}\right)^{\frac{1}{2}}$$

In turbulent flow, Danckwerts derived that:

$$k_m = (D_l S)^{\frac{1}{2}}$$

S varies between 5 to 25 per second for mild turbulence, and up to 500 per second for violent turbulence (Ghosh, 2000).

k_mA/k_m and mixing power density

In stirred systems it is difficult to measure the contact surface area, A, so a total k_mA parameter is experimentally determined as gas flow rate, Q, or mixing power density, ε, is varied. There are many results available which relate rate constants for slag-metal reactions with stirring gas flow rate. The relationship below has been found to be generally useful, as provided by Lange (1988), where k_p is in (1/min) and specific stirring power, ε (kW/t).

$$k_p = 0.14\varepsilon^{0.68}$$

Electromagnetic stirring is reported to have a stirring intensity of 0.05 W/kg (Engh, 1992), while modern Argon practice has a stirring intensity of 0.006 W/kg (Ghosh, 2000).

Diffusivities

In the above models, the diffusivity value, D_l, of copper in the melt is important. The values in the table below are diffusion coefficients relevant to the copper-iron system found in the literature.

Table A3.2: Diffusivities of copper in liquid iron found in the literature.

D_{Cu} (m^2/s)	Reference	Notes
$2x10^{-8}$	Davenport, Bradshaw and Richardson	Most liquid metals
10^{-8}	Harris	
$4.15x10^{-8}$	Ono and Ishiboti	carbon-saturated iron from 1623-1823K
$5x10^{-8}$	Iida and Guthrie	
$D_{Cu}=14.6x10^{-8}$ exp(-9700/RT)	Blacha and Labaj	Darken equation for binary solutions
$5x10^{-9}$	Lange	

Overall range

The values in the table below were calculated by the different models. The Iron and Steel Institute provided a range of values as well, saying the mass transfer coefficient of should

is at least 10^{-4} m/s, and at most 10^{-2} m/s. Morales (2015) calculated k_m to be 1 to 53x10^{-4} m/s. Engh (1992) showed k_m variations of 3 to 50x10^{-4} m/s.

Table A3.3: Range of variables used to calculate k_m.

Variable	D_{Cu} (m^2/s)	Melt velocity (m/s)	S (1/s)	Stirring power density (W/kg)
min	5x10^{-9}	0.2	10	0.006
max	4.15x10^{-8}	1	100	0.05

Table A3.4: Range of values calculated for k_m.

Calculated k_m from range of variables (m/s)	Machlin's model (furnace radius 1.5m)	Danckwert's model	k and stirring density	Individual mass transfer coefficient	Iron and Steel Institute range
Min	4.12x10^{-5}	2.24x10^{-4}	1.83x10^{-4}	7.00x10^{-4}	1.00x10^{-4}
Max	2.65x10^{-4}	2.04x10^{-3}	4.32x10^{-3}	3.70x10^{-3}	1.00x10^{-2}

Here, we assume the value of k_m to be 5x10^{-4} m/s.

For specific surface area, the interfacial area with stirring is typically 1.5 times (Morales, 2015) or 3 to 14 times (Tayeb, 2014) the nominal surface area. Here, we use a value of 1m^{-1}, which is typical for ladles with intense stirring.

The values of L, distribution ratio, have been determined for copper between the melt and the various slag/solvent compositions. The distribution ratios for most of the compositions in Figure 4.7 are too low to use industrially. Here, we use the most optimized slag composition, FeS-Al_2S_3 with L=30 (Cohen et al., 1998).

To reach 0.1wt%Cu in the melt, a treatment time of 50 minutes was calculated.

Scale-up reactor

This treatment would be an additional step in the ladle. The ladle would have similar dimensions to the 160 tonne ladle described by Zaitsev et al. (2014) (3.2m inner diameter, 2.9m height). It would be stirred with argon (typical rates of 0.14 m^3/s), or electromagnetically.

Energy consumption

The process requires that the melt is carburized and subsequently decarburized. It is assumed that the melt is initially at 1600°C, and during carburization the temperature is

decreased to 1365°C. The main sources of energy consumption would be heating the quantity of slag, maintaining treatment temperature, stirring and returning to 1600°C after treatment.

Heating 100 kg slag to 1365°C: heat content of industrial slag at 1000°C is 1 MJ/kg (Matousek, 2008). With heating efficiency of 50-70%, for 100kg slag/t steel, this equates to 40-50 kWh/tonne steel.

Heat loss during treatment: The main source of heat loss would be conduction through the ladle sides and bottom, as a thick slag layer often radiation from the top, such that radiation heat losses are negligible (Lange, 1988). Alexis et al. (2000) report the measured conduction heat loss rate from the sides and bottom of a 100 ton ladle furnace to be 12.5 kW/m^2. With the dimensions above, the ladle sides and bottom have a surface area of 40 m^2. Therefore, the heat loss during treatment is around 500 kWh, requiring 4-5 kWh/tonne steel.

Stirring: Thrum compares induction and gas stirring in ladle furnaces. The power consumption of electromagnetic stirring is about 1kW/tonne steel, so roughly 1 kWh/t is required in this treatment.

Decarburization: The melt would be carburized before treatment. To continue in the EAF route, the melt would be decarburized following treatment. The melt must also be heated to 1600°C following the 1365°C treatment temperature. During decarburization, heat is supplied:

$$\underline{C} + \frac{1}{2}O_2(g) \rightarrow CO(g), 2.55\frac{kWh}{kg\ C}$$ (Madias, 2014)

With 43 kg C/tonne steel, this generates 109 kWh/tonne. 75-100 kWh/tonne heat is required to raise the temperature of the melt from 1365 to 1600°C, so the heat generated by the decarburization reaction should be sufficient.

Material consumption

The treatment requires a significant quantity of slag. From the equilibrium distribution ratios in Figure 4.7, the following quantities were calculated per tonne steel in Table A3.5 below.

Table A3.5: Calculated quantities of solvents and slags needed to treat one tonne of steel from 0.4 to 0.1wt% from the reported equilibrium ratios.

Solvent/slag	kg/tonne
Lead solvent	1246
Silver solvent	419
0.6 FeS-0.4 Na_2S slag	125
0.8 FeS-0.2 K_2S slag	150
0.7 FeS-0.3 Sr_2S slag	136
0.2 FeS-0.8 Al_2S_3 slag	100
S-modified oxide slag	441
FeO-SiO_2-$CaCl_2$ slag	600

To calculate the embodied energy, the ICE Database reports slag has an embodied energy of 0.44 kWh/kg. The above slags have different compositions and would have different embodied energies, but in the absence of this data this general figure is applied to all slags. For the lead and silver solvents, an embodied energy of 7.5 and 430 kWh/kg (primary) is reported (Ashby, 2013).

The above distribution ratios were achieved with carbon-saturated melts. Carbon-saturation increases the activity of copper and the temperature of the melt can be reduced, such that the exothermic reaction of copper to copper sulfide progresses further. To saturate the melt, 43 kg C/tonne steel is required. Coal has an embodied energy of which has an embodied energy of 5.8 kWh/kg (China Statistical yearbook, 2013), assuming a similar value for metallurgical coal, this corresponds to 250 kWh/tonne steel.

In decarburization, assuming CO(g) is formed, 53 kg O_2(g) is required, with an embodied energy of 0.5 kWh/kg (Worrell, 2000), which totals 27 kWh/tonne steel. This reaction produces 96 kg CO(g)/tonne steel.

The melt is contaminated with sulfur by the FeS-Al_2S_3 slag. A desulfurization treatment would be requires, which typically requires 10-25 kg slag and 20-30 kWh/tonne steel

energy (Ghosh (2000) and Sarna (2013)). However, the sulfur concentrations from the contamination are much higher than amounts typically encountered in steel refining, so a more intensive treatment may be required.

Unidirectional solidification

Rate of copper reduction

Nakamoto et al. (1975) show that the partition coefficient, k, of copper in carbon-saturated iron is 1.2. The cooling rate that resulted in the greatest gradient was 60°C/hour in their experimental work. With the given partition coefficient, the gradient would decrease from 0.4wt% Cu to about 0.32wt% during solidification.

(Note that the catalogue shows some preliminary investigations which use a magnetic field during solidification to migrate copper within an Fe-C-Cu alloy. Applying a magnetic field is not included in this analysis as a scalable reactor does not exist in steelmaking).

Scale-up reactor

A slow cooling rate would be required during casting and solidification. The furnace could be similar to an in-line tunnel furnace used for keeping billets at high-temperature from casting to rolling.

Energy consumption

The US Dept of Energy document (2013) reports that in-line tunnel furnaces consume about 200 kWh/tonne steel. These furnaces hold steel over 1000°C for several hours. This treatment requires 6.5 hours, so this requirement is multiplied by 2-3, for 400 to 600 kWh/tonne.

Material consumption

None directly.

Vacuum arc re-melting

Rate of copper reduction

Andreini and Foster (1974) developed a model of the process to predict the degree of refining of solute elements and applied it to automotive scrap and compared it to experimental results.

The authors introduced a dimensionless constant, β. When β>1, the magnitude of β can indicate the extent to which refining will occur during the process. The equation below gives the formula for β, where k_i is the distribution coefficient of the species, α_i is the evaporation coefficient of the species, P_i^0 is the vapor pressure of the pure species and γ_i is the activity coefficient, and j denotes the melt species.

$$\beta_i = \frac{\alpha_i \gamma_i P_i^0}{\alpha_j \gamma_j P_j^0} \left[\frac{M_j}{M_i}\right]^{\frac{1}{2}} (k_i)^{-1}$$

Scale-up reactor

Scholz et al. reviewed the technology and equipment available for vacuum arc re-melting. They report that tramp elements such as Pb, Sn, Bi, Te, As and Cu will be removed, and their level can be adjusted with the vacuum pressure.

Scholz et al. provide the key operating parameters for VAR, given in the table below. The ingots may be up to 1300mm in diameter and 30t in weight.

Table A3.6: Representative operating parameters in VAR.

Stock diameter (m)	0.9
Energy consumption during re-melting (kWh/t)	700
Melting rate (kg/min)	9

Applying these parameters to the model presented by Andreini and Foster (1974) and an initial concentration of 0.4wt%, a treatment would lead to a final concentration in the range of 0.2wt%. The treatment could be repeated, or a slower melting rate or lower chamber pressure could be employed to further reduce the final copper concentration.

Energy consumption

Scholz et al. state that the power consumption of the process depends mainly on the alloy to be remelted, with the specific heat of the material to be the most important factor as it determines the arc formation. Minor influences are the gas load of the material and the suction capacity of the pumping system and electrical efficiency.

Therefore, the energy consumption is close to the re-melting energy, 700kWh/t. Krüger (2005) reports that the electroslag refining steel can consume up to 1300 kWh/tonne. For a more intensive process which reduces copper concentration to 0.1wt%, this higher end of energy consumption is assumed.

Material consumption

None directly.

Ceramic filtration

Rate of copper reduction

The original publications could not be found, but Savov and Janke (2000) report that an Al_2O_3-ZrO_2 ceramic filter removes copper at a rate of 30%, as found by Zigalo et al. (1991) and Li et al. (1998).

Scale-up reactor

Ghosh (2000) discusses that ceramic filters have been used to remove inclusions from the melt for low-melting nonferrous metals such as aluminum. For steel melts, active research and development work is being pursued. Ghosh (2000) reports that the mass flow of steel with a filter is slowed by 0.25 to 0.6.

Here, we assume a filter is incorporated into tapping such that the time for tapping doubles.

Energy consumption

Yin (2009) reports a temperature drop of around 70°C during tapping. Assuming that the slower tapping due to filtration causes an additional 70°C temperature drop, this would require 20-30 kWh/tonne steel heat to recover.

Material consumption

None directly, but contamination of the melt by ceramic particles is possible. Filters would need regular replacement.